

Activities and Microstructure of Co/SiO₂ Catalysts for FT Synthesis

Guozhu Bian, Takehisa Mochizuki, Norimasa Fujishita, Hiderou Nomoto, Muneyoshi Yamada

Department of Applied Chemistry, Graduate School of Engineering, Tohoku University, Aoba 07, Aramaki, Aoba-ku, Sendai 980-8579, Japan

Introduction

The activities of cobalt based catalysts for FT synthesis are closely related to the cobalt dispersion values. For Co/SiO₂ catalysts prepared by impregnation method, weak interactions between cobalt precursors and silica support may result in aggregation of the cobalt species during calcinations of the samples in air. On the other hand, strong interactions between cobalt precursors and support result in high dispersion of the cobalt species. However, such highly dispersed cobalt species are difficult to be reduced to cobalt metal [1].

It has been reported that Co/SiO₂ catalysts prepared with impregnation method using different cobalt salts as precursors show quite different catalytic activities for FT synthesis. On the oxidized Co/SiO₂ samples with cobalt nitrate as precursor (denoted as Co(N)/SiO₂), large particles of cobalt oxide are formed, which can be easily reduced. On the other hand, on the oxidized Co/SiO₂ catalysts with cobalt acetate as precursor (denoted as Co(A)/SiO₂), small particles of cobalt oxide are formed, which are difficult to be reduced. Both the Co(N)/SiO₂ and the Co(A)/SiO₂ samples show low activities for FT synthesis after reduction by H₂ at 400°C. However, the Co/SiO₂ catalysts prepared from the mixture of cobalt nitrate and cobalt acetate (denoted as Co(A+N)/SiO₂), on which cobalt species show middle sizes, show significantly higher activities for FT synthesis after H₂ reduction at same conditions. However, on the reduced Co(A+N)/SiO₂ sample, reduction degree of the cobalt species is still low [2]. To further increase the reduction degree, noble metal was added as promoter [3].

In this work, oxidized Co(N)/SiO₂ and Co(A+N)/SiO₂ samples, prepared by impregnation method with cobalt nitrate and the mixture of cobalt nitrate and cobalt acetate (mole ratio=1/1), respectively, are reduced by H₂ at 300-600°C and used for high pressure FT synthesis with fixed bed reactor. The reduced and used samples are characterized by XRD and EXAFS as well. Some results about the influences of reduction temperature of the oxidized samples and about the structural changes during FT synthesis are obtained.

Experimental

Sample preparation. The oxidized Co/SiO₂ samples were prepared by incipient-wetness impregnating cobalt nitrate or the mixture of cobalt nitrate and cobalt acetate (mole ratio=1/1) on a commercial SiO₂ (JRC-SIO-5), drying in air at 120°C for 12h. Then, the obtained samples were calcined in air at 450°C for 4h. Cobalt loadings of all samples, calculated as weight ratio of cobalt to silica, are 0.20.

Activity test. Catalytic activities of the cobalt catalyst samples for FT synthesis from syngas were measured with a fixed bed reactor. For each experiment, 0.4g of catalyst sample was placed into the reactor and in-situ reduced in 40ml/min flows of H₂ at 300-600°C for 6h. Thereafter the reaction was carried out in a 30ml/min flow of syngas with H₂/CO/Ar ratios of 62/33/5.0 at 1.0MPa and 220°C. Reaction temperatures were measured with a thermocouple inserted into the catalyst bed. Analyses of the gas-phase products were performed by an on-line gas chromatography, which were carried out every 20min during the reaction. The liquid products were collected

in an on-line trap at room temperature and analyzed by an off-line gas chromatograph after the reaction. Anderson-Schultz-Flory (A-S-F) distributions were plotted and the chain growth probability, α , was calculated using the C₉-C₂₂ data.

X-ray diffraction (XRD). Powder XRD patterns of the catalyst samples were obtained on a Miniflex diffractometer (Rigaku) using Cu K α radiation with a Ni filter. Cobalt phases were detected by comparing diffraction patterns with those in the standard powder XRD file compiled by the Joint Committee on Powder Diffraction Standards published by the International Center for Diffraction Data. The reduced and used samples were passivated in a stream of 1% O₂/He at room temperature before being transferred from the reactor for XRD measurements. The average sizes of the particles on the catalysts were calculated using the half-height width of the most intense peak of the diffraction pattern and the Scherrer equation.

Extended X-ray absorption fine structure (EXAFS). X-ray absorption spectra were measured using laboratory system equipped with double-crystal monochromator [4]. The reduced and used samples were passivated in a stream of 1% O₂/He at room temperature before being transferred from the reactor. Then the samples were pressed into pellets for the EXAFS measurements.

Results and Discussion

After the oxidized Co(A+N)/SiO₂ and Co(N)/SiO₂ samples were reduced by H₂ at 300-600°C, they were used for FT synthesis with fixed bed reactor at the conditions of 1.0MPa, 220°C and W/F=5.0g*h/mol, respectively. After FT synthesis for over 10h, the reaction becomes stable. The steady state activity data of the samples are shown in Table 1. Over the Co(A+N)/SiO₂ catalyst samples reduced by H₂ at 450-500°C, CO conversions are higher than over other samples. For Co(N)/SiO₂ catalyst, however, optimum reduction temperatures are 300-400°C. Over the samples reduced by H₂ at 500-600°C, CO conversions become obviously decreased. It is noticed that the Co(A+N)/SiO₂ samples reduced at 450-500°C show higher activities than the Co(N)/SiO₂ samples reduced at 300-400°C.

Table 1. Activity Data of the Co(N)/SiO₂ and Co(A+N)/SiO₂ Samples Reduced By H₂ at 300-600°C. H₂/CO=2.0, P=1.0MPa, W=0.4 g, V=30ml/min, W/F=5.0g*h/mol.

Sample	Reduction temp.	CO conv. (CO%)	CO ₂ (CO%)	CH ₄ (CO%)	α
Co(N)/SiO ₂	300°C	42.8	0.11	3.16	0.89
	400°C	42.3	0.12	2.86	0.88
	500°C	37.9	0.09	2.85	0.87
	600°C	29.2	0.08	2.92	0.87
Co(A+N)/SiO ₂	300°C	37.4	0.13	2.88	0.85
	400°C	54.2	0.18	4.62	0.86
	450°C	63.6	0.24	4.17	0.88
	500°C	64.9	0.24	4.80	0.88
	550°C	61.0	0.22	4.71	0.86
	600°C	57.7	0.19	5.18	0.86

Over the Co(N)/SiO₂ samples reduced at various temperatures, selectivity to methane and the chain growth probability, α , show very small changes. However, over the Co(A+N)/SiO₂ samples reduced at 450-500°C, selectivity to methane is relatively low and chain growth probability is high, while over the rest Co(A+N)/SiO₂ samples selectivity to methane is higher and chain growth probability is lower.

XRD patterns of both oxidized Co(A+N)/SiO₂ and Co(N)/SiO₂ samples show obvious peaks due to Co₃O₄ phase. However, the

intensities of the peaks for Co_3O_4 of the Co(N)/SiO_2 sample are significantly stronger than those of the Co(A+N)/SiO_2 sample. This result indicates that particle sizes of the cobalt species on the Co(A+N)/SiO_2 sample are obviously smaller than those on the Co(N)/SiO_2 sample. This is in agreement with that in the literature [2].

Table 2. Average sizes of the cobalt metal particles on reduced Co(N)/SiO_2 and Co(A+N)/SiO_2 catalysts determined by XRD data (nm)

Reduction Temperature	Co(A+N)/SiO_2	Co(N)/SiO_2
300°C	7.1	14.6
400°C	7.6	15.3
500°C	7.9	16.6
600°C	10.0	17.3

XRD patterns of the reduced samples show the peaks due to cobalt metal. But the particles on the Co(A+N)/SiO_2 samples are obviously smaller than those on the Co(N)/SiO_2 samples. It suggests that cobalt metal on the Co(A+N)/SiO_2 samples are well dispersed than that on the Co(N)/SiO_2 samples, which may be correlated to the fact that the Co(A+N)/SiO_2 samples show higher activities for FT synthesis than the Co(N)/SiO_2 samples.

Weak interaction between cobalt species with the silica support on the Co(N)/SiO_2 sample results in complete reduction of the cobalt species during H_2 reduction at 300-400°C. On the other hand, strong interaction between cobalt species and silica support on the Co(A+N)/SiO_2 sample results in incomplete reduction of the cobalt species under the same reduction conditions. To increase the reduction degree of the Co(A+N)/SiO_2 sample, higher reduction temperature is needed.

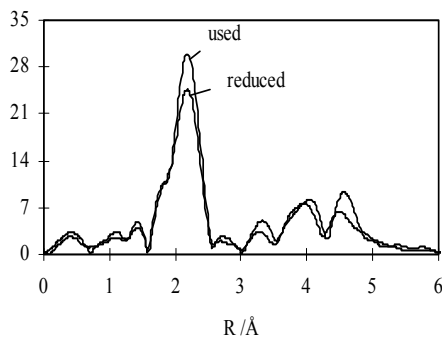


Figure 1. Radial distribution functions of Co atom for reduced and used Co(N)/SiO_2 catalysts from EXAFS data.

The Fourier transformations of Co K-edge EXAFS spectra (Radial distribution functions) of the reduced and used Co(N)/SiO_2 samples are shown in Figure 1. A strong peak at 2.1 Å clearly is observed, which is assigned to the Co-Co coordination shell in cobalt metal. Therefore, large particles of cobalt metal are formed on the Co(N)/SiO_2 sample after H_2 reduction at 400°C. During performing FT synthesis, the particles further aggregated.

Figure 2 shows the radial distribution functions of the reduced and used Co(A+N)/SiO_2 samples. For the reduced Co(N)/SiO_2 sample, the peak assigned to Co-Co coordination shell in cobalt metal is also observed. However, the intensity of the peak is obviously lower than that of the corresponding peak for Co(N)/SiO_2 catalyst. This result indicates that the metallic cobalt particles on the reduced Co(A+N)/SiO_2 catalyst are smaller than those on the reduced

Co(N)/SiO_2 catalyst, which is in agreement with the results from XRD measurements. The radial distribution function of the used Co(A+N)/SiO_2 catalyst is quite different from that of the freshly reduced sample. The peak assigned to Co-Co shell in cobalt metal becomes weaker and a new peak centered at 2.8 Å appears. The new peak can be assigned to Co-Co coordination shell in CoO . The above results indicate significant structural changes during performing FT synthesis. A part of the small metallic cobalt particles formed during H_2 reduction is oxidized to CoO .

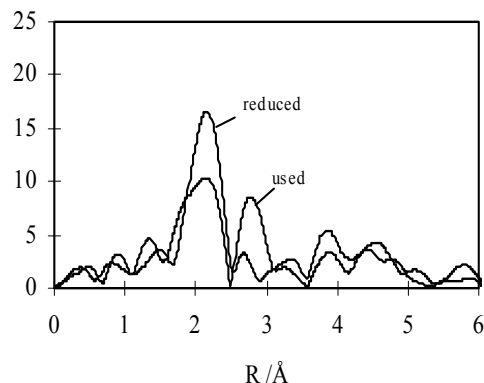


Figure 2. Radial distribution functions of Co atom for reduced and used Co(A+N)/SiO_2 catalysts from EXAFS data.

Conclusions

Co(A+N)/SiO_2 catalysts and Co(N)/SiO_2 catalysts are reduced by H_2 at 300-600°C and used for FT synthesis. Optimum reduction temperatures for Co(A+N)/SiO_2 samples are 450-500°C and optimum reduction temperatures for Co(N)/SiO_2 samples are 300-400°C. Co(A+N)/SiO_2 catalysts show higher activities for FT synthesis than Co(N)/SiO_2 catalysts, which may be due to that metallic cobalt particles on Co(A+N)/SiO_2 catalysts are smaller than those on Co(N)/SiO_2 catalysts. During performing FT synthesis, the small metallic cobalt particles on the Co(A+N)/SiO_2 catalysts are unstable and partly oxidized, while those large particles on the Co(N)/SiO_2 catalysts are rather stable and remain at metallic state.

Acknowledgement. This work was supported by Research for the Future Program of Japan Society for the Promotion of Science under the project "Synthesis of Ecological High Quality Transportation Fuels" (JSPS-RFTF98P01001).

References

- (1) Iglesia, E. *Applied Catalysis A: General*, **1997**, *161*, 59.
- (2) Sun, S.; Tsubaki, N.; Fujimoto, K. *Applied Catalysis A: General*, **2000**, *202*, 121.
- (3) Tsubaki, N.; Sun, S.; Fujimoto, K. *J. Catalysis*, **2001**, *199*, 236.
- (4) Tohji, K.; Udagawa, Y.; Kawasaki, K.; Mieno, A. *Rev. Sci. Instrum.* **1988**, *59*(7), 1127.

BIOCATALYTIC TREATMENT OF ORGANOSULFUR COMPOUNDS IN EMULSIONS IN SUPERCRITICAL FLUIDS

Marina A. Stanescu,^a Daniel M. Ginosar,^{*} Gregory A. Bala and Raymond P. Anderson

Idaho National Engineering and Environmental Laboratory
P.O. Box 1625
Idaho Falls, ID 83415-2208

Introduction

Sulfur levels in refinery crude oil feedstocks are increasing annually, while at the same time, federal and local regulators are requiring reductions in these levels for the finished transportation fuels. Sulfur moieties of concern are typically organosulfur complexes. Production and utilization of oils with appreciable sulfur content results in increased environmental pressures and costs to producers, refiners, and end users. Environmentally, utilization of high sulfur fuel products results in production of gaseous sulfoxide chemicals that are believed to be partially responsible for "acid rain," additionally, the sulfur in fuel has a detrimental affect on vehicle emission controls. In order to meet upcoming requirements and future ultraclean sulfur requirements for gasoline and diesel fuels, new economical sulfur removal processes must be developed.

Biological removal of sulfur from oil (biodesulfurization) is a potentially attractive alternative to conventional refinery processes such as hydrotreating.¹ Biodesulfurization processes offer the potential of lower capital and operating costs compared to traditional refinery processes and the potential to overcome many of the steric limitations of traditional catalytic methods. Biodesulfurization may occur via oxidative or reductive pathways. Oxidized products can be removed either by distillation or by heating above 300°C to eliminate sulfur dioxide.

Practical limitations for aqueous phase bioprocessing of organic constituents are well recognized and include bioavailability of substrates, relatively slow reaction kinetics, catalyst recycle, expensive separation processes to recover the desired products, and maintenance of biological integrity. Proteins and whole cells have been shown to be active in organic solvents;² however, organic solvents can be expensive, and separation or recycle from the reaction mixture can be difficult.

Supercritical fluids (SCFs) systems offer several advantages over conventional water and liquid organic solvents as reaction media.³ SCFs provide high solubility of organic compounds, enhanced mass-transfer due to the elimination of liquid/liquid interfaces, enhanced reaction kinetics, control of product solubility with minor variations in temperature and pressure, and a more energy efficient separation of final products. Enzymatic activity in SCFs has been proven and well documented.⁴ Limiting factors which may affect enzymatic activity in SCF solvent systems have been identified and are well characterized.

Reverse micelles and microemulsions consisting of water and SCFs can simultaneously disperse high concentrations of both hydrophilic molecules such as proteins and hydrophobic compounds. Larger amounts of water may be dispersed in SCFs by forming emulsions, allowing more hydrophilic materials to be solubilized in the fluid. Several research groups have demonstrated that stable

reverse micelles, microemulsions and emulsions based on perfluoropolyetherammonium carboxylate (PFPE) ($\text{CF}_3\text{O}(\text{CF}_2\text{CF}(\text{CF}_3)\text{O})_n\text{CF}_2\text{COO}^-\text{NH}_4^+$) surfactant can be formed in supercritical carbon dioxide.^{5,6} These emulsions are easily broken by decreasing pressure, allowing for simple catalyst recovery and energy efficient product separation.

We report the first biooxidation of organosulfur compounds in emulsions in supercritical fluids. Hemoproteins were chosen as biocatalysts for their ability to oxidize sulfides, thioanisoles, thiophenes and dibenzothiophenes (DBT) to their sulfoxide/sulfone products. DBT was chosen for the reaction studies as a compound typical of organosulfur compounds in crude oils and fuels. Oxidation of DBT is well known in aqueous buffer/organic solvents and organic solvents.⁷ Conversion up to 99% has been reported when the reaction was catalyzed by hemoglobin in aqueous buffer/organic solvents (75/25 vol.%) and 28% conversion when the reaction was performed in 99 vol.% ethanol. Protein catalysts used in the current study included horseradish peroxidase (HRP), hemoglobin (Hb), Cytochrome c (Cyt c), and soybean peroxidase (SBP). Supercritical fluids explored included carbon dioxide, methane, ethane and trifluoromethane. PFPE was selected as the surfactant for our CO_2 studies. The biooxidation of DBT is depicted in Figure 1.

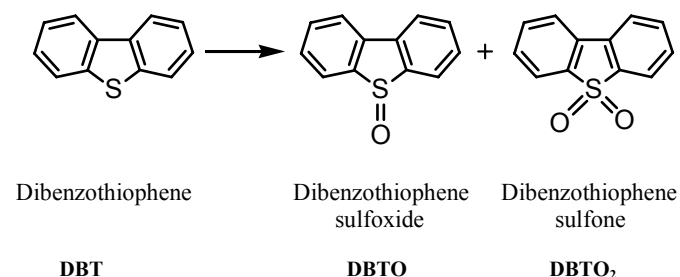


Figure 1. Biooxidation of DBT.

Experimental

Chemicals and reagents. DBT, DBTO₂, organic solvents and 30% H_2O_2 were purchased from Aldrich. Proteins, glycine, potassium phosphate, Tricine, and sodium acetate were purchased from Sigma. Carbon dioxide (SFE grade) was purchased from Matheson, and ethane (C.P.-grade, 99%) from Scott Specialty Gases. PFPE was prepared according to a literature procedure⁸ by reacting perfluoropolyether carboxylic acid (Fluorolink 7004, average MW = 615, Lot BL5420, Ausimont) with an excess of ammonium hydroxide solution, except for the final drying step. In this work, final drying was begun at 25°C and gradually increased to 60°C. The PFPE product was stored in a vacuum desiccator. All other chemicals were used as received.

Apparatus. The high-pressure apparatus used in this study, as shown in Figure 1, consisted of an ISCO pump (Model 260D), an HPLC injector, a pressure and temperature control system (Omega) and a stainless steel reaction vessel. Two types of reaction vessels were used, either a 100 ml autoclave (Autoclave Engineers) or a 4.1 ml optical cell equipped with quartz windows. Heat was supplied to the reaction vessel by a water bath or electrical resistance heating. The components of the system were connected via high pressure valves and fittings. A 5890 Series II HP gas chromatograph with a flame ionization detector (FID) and a 5890 Series II HP gas chromatograph/mass selective (MS) detector was used to analyze the product mixture.

General procedure for biooxidation of DBT in emulsions in supercritical fluids. DBT, surfactant, buffer and solid protein was loaded into the open reactor. The vessel was closed and sealed. The

^a Currently at U. S. Environmental Protection Agency, National Risk Management Research Laboratory, 6 West Martin Luther King Drive, MS 443, Cincinnati, Ohio 45268

^{*} Corresponding author. Fax: (208) 526-8541. E-mail: dmg@inel.gov

vessel and its contents were heated to 40°C for 1.5 hr and then pressurized to 1000 psi with the chosen SCF. The HPLC injector valve was used to add a 0.5 ml dilute solution of H₂O₂ with the final volume of SCF that was used to bring the reactor to its final pressure. Final concentrations were: 0.28 mM DBT, 1 – 25 μM protein, 1.4 wt% surfactant, and 4.48 mM hydrogen peroxide (H₂O₂). The contents of the vessel were stirred in the absence of light for 15 hours. Gas was slowly vented and bubbled through a solution of methylene chloride and methanol. The reactor was opened. Methylene chloride and methanol were used to wash and transfer the contents of the cell and the stirring shaft. The combined methylene chloride and methanol washes were evaporated by rotary evaporation at low temperature, followed by the evaporation of water at 60°C for 1.5-2 hours. The resulting mixture was then redissolved in a known volume of methylene chloride and analyzed by GC/FID or GC/MS.

General procedure for biooxidation of DBT in reverse micelles/microemulsions in supercritical fluids was the same as for biooxidation in emulsions, except for the following. The vessel was pressurized with the desired fluid to 90% of the final pressure. The contents of the vessel were stirred for 45 minutes to allow micelle formation. Micelles were visually detected by the appearance of a single phase. A buffered hydrogen peroxide solution was then added simultaneously with the remaining fluid via an HPLC injector.

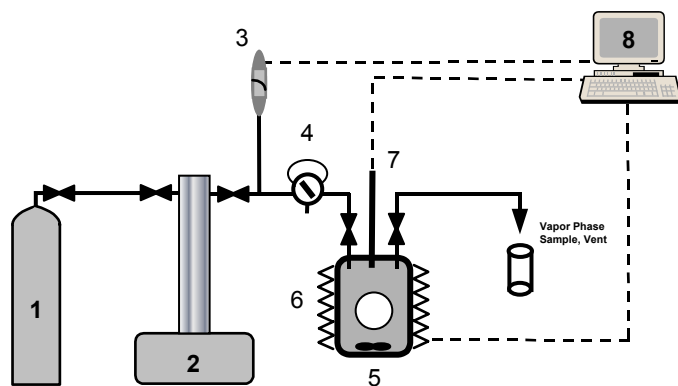


Figure 2. Schematic of the high-pressure reaction system. 1- SCF Supply, 2 - ISCO pump, 3 - pressure transducer, 4 - HPLC injection valve, 5 - high pressure reactor, 6 - heating element, 7- thermocouple, 8 - process control.

Results and Discussions

An aqueous phase buffer biooxidation reaction was run as a base case to compare results obtained in SCFs. The reaction was run using Hb in acetate buffer, pH=5.0, at concentrations of 3 μM DBT, 1 mM H₂O₂ and 12.6 mM enzyme. The mixture was stirred at 40°C for 2 hours. Conversion to product in the liquid buffer was 30.2 wt%. Due to the low solubility of DBT in the buffer solution, this conversion represents a product yield of 0.9 μM.

We previously studied the protein biooxidation of DBT in pure and modified SCFs. Hb and Cyt c were used in most of the cases since they are known to be more active towards the oxidation of DBT than HRP⁷. Proteins were studied in their free, lyophilized, PEG-conjugate forms, and immobilized on glass beads, alumina based support and agarose beads. In all cases, only very small amounts of product were formed (<1%). Control experiments showed that the low yield was due to protein inactivation caused by high localized concentrations of hydrogen peroxide and that a more hydrated environment was needed for the protein. The water pool of a reverse

micelle appeared to be a promising media to provide the desired environment.

Biooxidation of DBT in PFPE reverse micelles in carbon dioxide was explored as a potential desired reaction media. Since carbonic acid with a pH of about 3 forms when aqueous solutions are in contact with CO₂ at high pressures, 1M buffers (potassium phosphate, pH = 7, Tricine, pH = 8.5 and sodium acetate, pH = 6.83) were employed. When 8.4 μM Hb was added with a 1M potassium phosphate buffered solution, micelles were formed after 25 min. of stirring, as detected by the observation of a single phase. However no product was formed. Additional reverse micelle studies also failed to result in product formation.

It became clear that solution pH, driven by the presence of SC CO₂, negatively impacted enzyme activity and function. Therefore, buffer capacity played an important role. To explore this effect, control experiments were conducted using a 40 vol.% pool of liquid in the reactor exposed to an upper bed of SCF. Potassium phosphate buffer at 0.025 M and 1 M, pH = 7, were used in the hemoglobin-catalyzed oxidation of DBT in an aqueous buffer/ethanol (80/20 vol.%) solution exposed to CO₂ at 3,000 psi. Less than 1% product was formed at the high buffer concentration and no product was formed at lower buffer concentrations. When similar solutions were exposed to a 3,000 psi bed of ethane, the reaction resulted in a 26% product yield, even at the low buffer concentration. This data suggests that the acidity caused by presence of SC CO₂ negatively impacted the activity of the protein.

We chose to explore Soybean peroxidase (SBP), a commercially available, relatively inexpensive enzyme that exhibits high stability at acidic pHs and higher temperatures.⁹⁻¹⁰ SBP is known to be active towards oxidation of methyl phenyl sulfide in glycine buffer.¹¹ We found that SBP exhibited similar activity towards the oxidation of DBT in an ethanol/glycine buffer (20/80 vol.%) solution at pHs from 2.4 to 3.5. We carried out the SBP-catalyzed oxidation of DBT in a 50/50 wt.% CO₂/glycine buffer emulsion using 0.02 mM glycine buffer, pH = 2.4, at 3,000 psi and at two different temperatures, 45°C and 65°C, for 15 hours. The protein was more active at 65°C. At 45°C, product yield was less than 1 %, but increased to 4.1 % at 65°C. At the higher DBT solubility obtained in the emulsion, the 4.1% conversion represents a product yield of 11.4 μM; 12 fold higher than that obtained in the aqueous base case.

These results were consistent with SBP catalyzed biooxidation of methyl p-tolyl sulfide which showed an enhanced yield at the optimum temperature (65°C). Therefore, we studied the SBP-catalyzed oxidation of DBT in CO₂ – glycine buffer emulsions and microemulsions, pH = 2.4, at 2,000 and 3,000 psi and at various water contents present in the reaction. Results are presented in Table 1.

Table 1. SBP-Catalyzed Oxidation of DBT in CO₂/Glycine Buffer Emulsions at 65°C for 15 hours. (Reaction conditions: 0.02 mM glycine buffer, pH=2.4, 0.28 mM DBT, 1 mg/ml SBP, 1.4 wt% PFPE, and 4.48 mM H₂O₂.)

Buffer (wt.%)	CO ₂ (wt.%)	Pressure (psi)	Product yield (wt.%)
50	50	2000	Trace
50	50	3000	4.1
30	70	3000	2.8
0.75*	99.25	3000	0.5

*microemulsion

Product yield increased with the amount of aqueous buffer. In the

microemulsion, with less than 1 wt.% buffer solution, the hydrogen peroxide may be localized in the layer of hydration surrounding the protein. As aqueous buffer quantity increased, the concentrations of hydrogen peroxide decreased, providing a more suitable environment for protein activity. No product was formed in the absence of surfactant, or protein or hydrogen peroxide, suggesting that the reaction took place in the emulsion. However, the emulsion was not stable and required continual mechanical agitation. Even with constant stirring, the emulsion broke somewhat during the course of the reaction and by the end of the experiment, the cell contained a lower emulsion phase and an upper CO₂ phase. More aggressive stirring may have been necessary and may have increased conversion to product. Despite the modest conversions, total product yield was more than an order of magnitude greater in the SCF emulsion than in the aqueous phase reaction.

Conclusions

Biooxidation of DBT in emulsions in environmentally friendly carbon dioxide appears to be promising and can be extended to organosulfur compounds in general. We have found higher product yields in water/CO₂ emulsion systems compared to aqueous systems.

Acknowledgement. The authors gratefully acknowledge the analytical assistance provided by Catherine Rae and David B. Blackwelder. This work was supported by the U.S. Department of Energy, Office of Fossil Energy, National Energy Technology Laboratory, under contract number DE-AC07-99ID13727.

References

- (1) Monticello, D.J. *Curr. Opin. Biotech.* **2000**, *11*, 540.
- (2) Klibanov, A.M. *Nature*, **2001**, *409*, 241.
- (3) Hutchenson, K.W.; Foster, N.R. In *Innovations in Supercritical Fluids, ACS Symposium Series*; Hutchenson, K.W., Foster, N.R., Eds.; American Chemical Society: Washington, DC, 1995; Vol. 608, p 1.
- (4) Mesiano, A.J.; Beckman, E.J.; Russell, A.J. *Chem Rev.* **1999**, *99*, 623.
- (5) Johnston, K.P.; Harrison, K.L.; Clarke, M.J.; Howdle, S.M.; Heitz, M.P.; Bright, F.V.; Carlier, C.; Randolph, T.W.; *Science*, **1996**, *271*, 624.
- (6) Lee, C.T.; Psathas, P.A.; Johnston, K.P.; deGrazia, J.; Randolph, T.W. *Langmuir*, **1999**, *15*, 6781.
- (7) Klyachko, N.L.; Klibanov, A.M. *Appl. Biochem. Biotech.* **1992**, *37*, 53.
- (8) Chittofrati, A.; Lenti, D.; Sanguineti, A.; mVisca, M.; Gambi, C. M. C.; Senatra, D.; Zhou, Z. *Progr. Colloid Polym. Sci.* **1989**, *76*, 218.
- (9) Kraus, J.J.; Munir, I.Z.; McEldoon, J.P.; Clark, D.S.; Dordick, J.S. *Appl. Biochem. Biotech.* **1999**, *80*, 221.
- (10) McEldoon, J.P.; Dordick, J.S. *Biotechnol. Prog.* **1996**, *12*, 555.
- (11) Johnson, M.A.; Pokora, A.R.; Cyrus, J.; William, L. U.S. Patent 5,391,488, 1985.

COMBINATORIAL COMPUTATIONAL CHEMISTRY APPROACH TO THE DESIGN OF METAL SULFIDE CATALYSTS FOR CO HYDROGENATION PROCESS

Momoji Kubo¹⁾, Changho Jung¹⁾, Tsuguo Kubota¹⁾, Kotaro Seki¹⁾,
Seiichi Takami¹⁾, Naoto Koizumi²⁾, Kohji Omata²⁾,
Muneyoshi Yamada²⁾, and Akira Miyamoto¹⁾

¹⁾ Department of Materials Chemistry,
Graduate School of Engineering, Tohoku University,
Aoba-yama 07, Sendai 980-8579, Japan.

²⁾ Department of Applied Chemistry,
Graduate School of Engineering, Tohoku University,
Aoba-yama 07, Sendai 980-8579, Japan.

Introduction

Recently, computational chemistry made great impacts on the catalyst design and development. However, the computational chemistry is mainly employed to clarify the atomistic mechanism of the well-known catalytic reactions and to obtain the electronic information on the catalysts of which property and reactivity are well known experimentally. We suggested that such traditional computational chemistry can not contribute to the design and development of new catalysts at all. Hence, we recently introduced a concept of combinatorial chemistry used in the drug development to computational chemistry and proposed a new concept "Combinatorial Computational Chemistry"¹⁻³. In this concept, the computational chemistry is employed to perform a high-throughput screening of the catalysts including active metals, supports, and additives.

On the other hand, the synthesis of the high-quality transportation fuels is expected in terms of the high-efficient utilization of the energy and low environmental impact. The development of high-active and high-selective catalysts with high-resistance to sulfur for methanol synthesis and Fischer-Tropsch synthesis is strongly demanded in order to advance the industry of the high-quality transportation fuels. Recently Koizumi and co-workers reported that a lot of metal sulfide catalysts have high activity for the CO hydrogenation process⁴ and especially Rh sulfide has the highest activity and predominantly produces methanol⁵. Moreover, they found that the Rh sulfide catalyst is not deactivated by the H₂S, while regular methanol synthesis catalyst Cu/ZnO/Al₂O₃ is easily deactivated by the H₂S⁵. Moreover, they also reported that the products of the CO hydrogenation process are strongly depending on the metal species of the metal sulfide catalysts⁴. For example, Rh and Pd sulfides selectively produce methanol in the CO hydrogenation, while Re and Os sulfides predominantly produce hydrocarbons.

We have already applied our combinatorial computational chemistry approach to the design of the methanol synthesis catalysts based on the Cu/ZnO and the Fischer-Tropsch catalysts based on the supported Fe metals and have succeeded to propose new catalysts and additives⁶⁻¹⁰. Hence, we have confirmed the applicability of our combinatorial computational chemistry approach to the catalyst design.

In the present study, we applied our combinatorial computational chemistry based on the first-principles approach to the metal sulfide catalysts and investigated the dependency of the metal species in the metal sulfide catalysts to the CO hydrogenation process and its products on the electronic level.

Methods

Combinatorial computational chemistry based on the first-principles calculation¹¹ is performed by using ADF program¹²⁻¹⁴

developed in Vrije University, Netherlands. In this program, linear combination of Slater-type atomic orbitals are used in the Kohn-Sham formulation. The structure optimization is carried out by local density approximation (LDA) with Vosko-Wilk-Nusair (VWN) functional¹⁵. The energy of the optimized structure is calculated by generalized gradient approximation (GGA) with Becke 88 and Perdew-Wang 91 functionals¹⁶⁻¹⁷. The triple- ζ basis sets extended by polarization functions are used. The Mulliken method is employed to perform the atomic population analysis¹⁸.

Results and Discussion

Our combinatorial computational chemistry approach was applied to the CO adsorption on various metal sulfide catalysts. We also calculated the CO adsorption on various metal catalysts for the comparison, by using our combinatorial computational chemistry. The elongation of the C-O distance may lead to the formation of hydrocarbons, while the shrinkage of the C-O distance may lead to the formation of methanol. Hence, we paid attention to the C-O distance of the CO molecule adsorbed on the various metal and metal sulfide catalysts. The C-O distance of the CO molecule in the vapor phase is 0.113 nm. We found that the C-O distance of the CO molecule adsorbed on all the metal catalysts and metal sulfide catalysts is elongated, compared to the C-O distance in the vapor phase. It indicates that CO molecule on all the catalysts is activated by the adsorption. Moreover, the C-O distance was found to be strongly depending on the metal species. The C-O distance is shortened on the Co, Mo, Ru, Rh, and Ir sulfide catalysts compared to their metal catalysts. It indicates that these metal sulfide catalysts selectively produce methanol, which is in agreement with the experimental results by Koizumi and co-workers⁴. On the other hand, since the C-O distance is elongated on the Re and Os sulfide catalyst compared to their metal catalysts, these sulfides are suggested to be very effective catalysts to produce hydrocarbon selectively, which is also in good agreement with the experimental results by Koizumi and co-workers⁴.

Moreover, we clarified that the Pd sulfide catalysts have the specific characteristics compared to the other metal sulfide catalysts. We suggested that the Pd sulfide has the highest selectivity of the methanol synthesis among all the metal sulfide catalysts, which is in agreement with the experimental result by Koizumi and co-workers¹⁹. CO molecule has the plus charge on the Pd sulfide catalysts, while CO molecule has the minus charge on the other metal and metal sulfide catalysts, as shown in Fig. 1. It was suggested that this difference is due to the different adsorption structure of the CO molecule on the Pd sulfide and the other metal sulfide catalysts as shown in Fig. 2. CO molecule adsorbs on the on-top site of the metal species in the case of all the metal sulfide catalysts except the Pd sulfide catalyst. Hence, electrons transfer from metal species to the CO molecule and then CO gains minus charge on the most metal sulfide catalysts. Similarly, CO molecule surely adsorbs on the metal species in the case of all the metal catalysts, and then electrons transfer from metal to the CO molecule and CO molecule gains minus charge. On the other hand, CO molecule adsorbs on the bridge-site of the Pd sulfide catalyst and contacts with both the Pd and sulfur on the Pd sulfide catalyst. Hence, electrons transfer from the CO molecule to the sulfur atom and CO gains plus charge. Fig. 3 shows the molecular orbital of the CO molecule. The lowest unoccupied molecular orbital (LUMO) and the second LUMO of the CO molecule are anti-bonding orbitals, and the electron has to be transferred to the above two orbitals of the CO molecule from catalysts, in order to dissociate the CO molecule. However, the CO molecule on the Pd sulfide catalyst has plus charge and then a large number of electrons have to be transferred to the CO molecule from the catalysts after the adsorption, in order to dissociate the CO

molecule. Hence, the dissociation of the CO molecule is much difficult on the Pd sulfide compared to the other metal sulfide catalysts. We suggested that this is the reason why the Pd sulfide catalyst has the highest selectivity of the methanol. Moreover, we proposed that the catalysts which realize the bridge-site adsorption of the CO molecule has the high selectivity of the methanol. This proposed guidance to design the high-selective catalysts for methanol may be useful for the experiments.

In the previous papers⁶⁻¹⁰, we have proved that our combinatorial computational chemistry approach is very effective to design new catalysts with high-activity and high-resistance to poisons. Moreover, we indicated that our combinatorial computational chemistry is also applicable to predict the catalytic selectivity and to design new catalysts with high selectivity. Hence, we concluded that our combinatorial computational chemistry approach is a powerful tool to design new catalysts.

Model ^l @	Eads (kJ/mol)	CO Charge	CO Distance (nm)
Co-Co	-192.54	-0.115	0.1155
Co-S	-122.05	-0.064 ↓	0.1148 ↓
Mo-Mo	-111.48	-0.292	0.1172
Mo-S	-171.93	-0.204 ↓	0.1165 ↓
Ru-Ru	-216.94	-0.366	0.1183
Ru-S	-236.14	-0.122 ↓	0.1157 ↓
Rh-Rh	-253.55	-0.324	0.1176
Rh-S	-216.97	-0.115 ↓	0.1150 ↓
Ir-Ir	-187.79	-0.675	0.1181
Ir-S	-241.83	-0.396 ↓	0.1158 ↓
Pd-Pd	-314.23	-0.342	0.1172
Pd-S	-205.77	0.189 ↓	0.1178 ↑
Re-Re	-101.73	-0.315	0.1158
Re-S	-180.00	-0.322 ↑	0.1168 ↑
Os-Os	-172.36	-0.447	0.1161
Os-S	-237.84	-0.390 ↓	0.1164 ↑

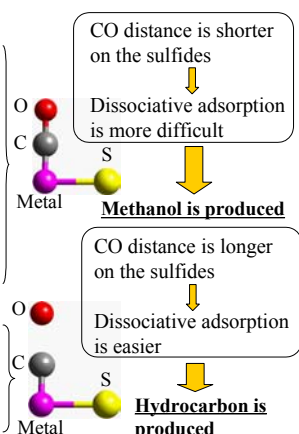


Figure 1 Adsorption energy, charge, and C-O distance of the CO molecule adsorbed on various metal catalysts and metal sulfide catalysts

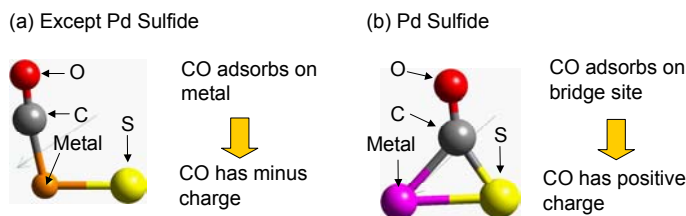


Figure 2 Adsorption structure of the CO molecule on the metal sulfide catalysts

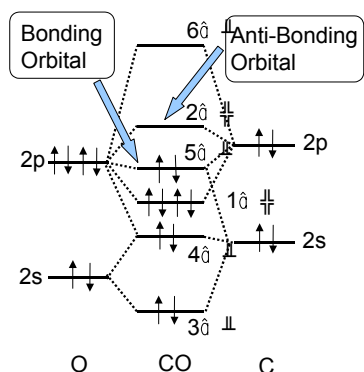


Figure 3 Molecular orbitals of the CO molecule

Conclusions

In the present paper, we have applied our combinatorial computational chemistry approach to the design of the metal sulfide catalysts for the CO hydrogenation process. We succeeded to clarify the dependence of the metal species in the metal sulfide catalysts to the products of the CO hydrogenation process. This result was in good agreement with the experimental results by Koizumi and co-workers. Moreover, we also propose that the Pd sulfide catalyst has the highest selectivity of the methanol from the CO hydrogenation process. This result strongly supports the experimental results by Koizumi and co-workers. Moreover, we propose that the catalysts which realize the bridge-site adsorption of the CO molecule have the high selectivity of the methanol. This proposed guidance to design the high-selective catalysts for methanol may be useful for the experiments.

Finally, we concluded that our combinatorial computational chemistry approach is effective and useful to design new catalysts with high activity and selectivity. We are going to expand the application of our combinatorial computational chemistry to various catalyst systems.

Acknowledgement

This work was supported by Research for the Future Program of Japan Society for the Promotion of Science under the Project "Synthesis of Ecological High Quality Transportation Fuels", (JSPS-RFTF98P01001).

References

- (1) Yajima, K.; Ueda, Y.; Tsuruya, H.; Kanougi, T.; Oumi, Y.; Ammal, S. S. C.; Takami, S.; Kubo, M.; and Miyamoto, A. *Appl. Catal. A* **2000**, 194/195, 183.
- (2) Yajima, K.; Sakahara, S.; Ueda, Y.; Belosludov, R.; Takami, S.; Kubo, M.; and Miyamoto, A. *Proc. SPIE* **2000**, 3941, 62.
- (3) Yajima, K.; Sakahara, S.; Ueda, Y.; Belosludov, R.; Takami, S.; Kubo, M.; Miyamoto, A.; Kawasaki, M.; Yoshimoto, M.; and Koinuma, H. *Proc. SPIE* **2000**, 3941, 2.
- (4) Koizumi, K.; Furukawa, T.; Miyazawa, A.; Ozaki, T.; Takahashi, Y.; and Yamada, M. *International Symposium on Synthesis of Ecological High Quality Transportation Fuels* **2000**, 53.
- (5) Yamada, M.; Koizumi, N.; Miyazawa, A.; and Furukawa, T. *Catal. Lett.* in press.
- (6) Belosludov, R.; Kubota, T.; Sakahara, S.; Yajima, K.; Takami, S.; Kubo, M.; and Miyamoto, A. *Proc. SPIE* **2001**, 4281, 87.
- (7) Sakahara, S.; Yajima, K.; Belosludov, R.; Takami, S.; Kubo, M.; and Miyamoto, A. *Proc. SPIE* **2001**, 4281, 97.
- (8) Belosludov, R. V.; Takami, S.; Kubo, M.; Miyamoto, A.; and Kawazoe, Y. *Mater. Trans.* **2001**, 40, 2180.
- (9) Sakahara, S.; Yajima, K.; Belosludov, R.; Takami, S.; Kubo, M.; and Miyamoto, A. *Appl. Surf. Sci.*, in press.
- (10) Belosludov, R. V.; Sakahara, S.; Yajima, K.; Takami, S.; Kubo, M.; and Miyamoto, A.; *Appl. Surf. Sci.*, in press.
- (11) Hohenberg, P.; and Kohn, W. *Phys. Rev. B* **1964**, 136, 865.
- (12) Baerends, E. J.; Ellis, D. E.; and Ros, D. P., *Chem. Phys.* **1973**, 2, 41.
- (13) Baerends, E. J.; and Ros, D. P. *Chem. Phys.* **1973**, 2, 51.
- (14) Boerring, P. M.; te Velde, G., and Baerends, E. J. *Int. J. Quantum Chem.* **1988**, 33, 87.
- (15) Vosko, S. H.; Wilk, L.; and Nusair, M. *Can. J. Phys.* **1980**, 58, 1200.
- (16) Becke, A. D. *Phys. Rev. A* **1988**, 38, 3098.
- (17) Perdew, J. P.; Chevary, J. A.; Vosko, S. H.; Jackson, K. A.; Pederson, M. R.; Singh, D. J.; and Fiolliais C. *Phys. Rev. B* **1992**, 46, 6671.
- (18) Mulliken, S. H. *J. Chem. Phys.* **1955**, 23, 1833.
- (19) Koizumi, N.; Miyazawa, A.; Furukawa, T.; and Yamada, M. *Chem. Lett.* **2001**, 1282.

DEEP DESULFURIZATION OF GASOLINE BY SARS PROCESS USING ADSORBENT FOR FUEL CELLS

Xiaoliang Ma, Michael Sprague, Lu Sun, and Chunshan Song*

Clean Fuels and Catalysis Program, The Energy Institute and
Department of Energy and Geo-Environmental Engineering,
The Pennsylvania State University, 209 Academic Projects Building,
University Park, PA 16802
*E-mail: csong@psu.edu

Introduction

Ultra-deep removal of sulfur from transportation fuels is becoming very important and is a very hot topic in R&D worldwide not only because the heightened interest for cleaner air and thus increasingly stringent environmental regulations for fuel sulfur content such as US EPA's tier II sulfur regulations for Yr. 2006, but also because the great need for making ultra-low-sulfur fuels for use in fuel cells as well as new vehicles that are much more efficient and environmentally friendly than existing cars and trucks today.

For the automotive fuel cells and micro-fuel cells, liquid hydrocarbons are promising candidate fuels due to their higher energy density and safety for transportation and storage. For the automotive fuel cells, especially for the current developing SOFC auxiliary power unit for automobile, gasoline is the important logistic fuel as it is readily available and the existing infrastructure in production, delivery and storage can be used. However, the current commercial gasoline usually contains significant amounts of sulfur up to 350 ppmw. The sulfur compounds in gasoline and H₂S produced from these sulfur compounds in the hydrocarbon reforming process are poisonous to both the catalysts in hydrocarbon fuel processor and the electrode catalysts in fuel cell stack. Thus, for fuel cell applications, the sulfur content in gasoline needs to be reduced to a very low level (< 0.1 ppmw).

In terms of technology availability, the current hydrotreating technology is difficult to reduce the sulfur content in gasoline to less than 10 ppmw, because the remaining sulfur compounds in current commercial gasoline are thiophene, 2-methylthiophene, 3-methylthiophene, 2,4-dimethylthiophene and benzothiophenes (1), which are difficult to remove. Consequently, development of new deep desulfurization processes of gasoline becomes one of the major challenges in hydrocarbon processing for the gasoline-based fuel cell applications. We are proposing and exploring a new process called SARS (selective adsorption for removing sulfur) (1-4). Our recent studies involved SARS-I (1-3) and SARS-II processes (2-4) by using adsorbent A-1 and adsorbent A-2, respectively, for ultra-deep desulfurization of liquid hydrocarbon fuels. The SARS-I and SARS-II differ from each other with respect to the type and nature of the adsorbent materials (A-1 for SARS-I and A-2 for SARS-II) and the optimum conditions of adsorption and desorption or regeneration. In one of our previous papers (4), we have reported our approaches in deep desulfurization of jet fuel (JP-8) by SARS-II process using adsorbent A-2. In the present paper, we will report our new approaches in deep desulfurization of gasoline by SARS-II process using adsorbent A-2 for fuel cell applications.

Experimental

For more quantitative analysis of sulfur compounds in treated liquid fuel, we used a model gasoline as a feed in the present study, which contains 400 ppmw (parts per million by weight) sulfur. The detailed composition of the model gasoline is listed in Table 1. The

sulfur compounds in the model gasoline are thiophene and benzothiophene, the corresponding sulfur concentration are 202 and 198 ppmw, respectively. The model gasoline contains 8 wt% of toluene as aromatic compound and contains 39.9 wt% of hexane and 59.5 wt% of decane as saturates. All chemicals contained in the model gasoline were purchased from Aldrich and were utilized without further purification. The adsorbent (A-2) used in this study was prepared from a transition metal with a surface area of 80-100 m²/g. The adsorption experiments were performed at ambient temperature and ambient pressure in a fixed adsorption bed, a stainless column with internal diameter of 4.6 mm and length of 150 mm. The adsorbent bed volume was 2.49 ml. The model gasoline was fed into the column and flowed up through the adsorption bed. The flow rate was 1.00 ml/min. Analysis of sulfur concentration in the samples was performed by using GC with a capillary column, XTI-5 (Restek) 30 m x 0.25 mm x 0.25 μm, and a flame ion detector (FID). Nonane was used as an internal standard for quantification.

Results and Discussion

Desulfurization of the model gasoline by adsorption was conducted at ambient temperature and ambient pressure by using adsorbent A-2. The sulfur concentration of the outlet model gasoline as a function of volume of the treated gasoline is shown in Figure 1. No detectable sulfur was found in the treated gasoline when the effluent volume is less than 160 ml, indicating that all sulfur in the model gasoline was removed by the selective adsorption. During this region, the sulfur concentration in the outlet model gasoline is less than 1 ppmw. The breakthrough point is around 160 ml. The corresponding breakthrough adsorption capacity of the adsorbent A-2 is 0.0191 g S per milliliter of the adsorbent. After this point, the sulfur concentration of the effluent increases with the increasing volume of the effluent. When the volume increases to around 220 ml, the adsorbent is saturated by sulfur. The saturated adsorption capacity is 0.0219 g sulfur per milliliter of the adsorbent. The preliminary desulfurization experiments show a very good performance of the adsorbent A-2 for selectively removing sulfur from the model gasoline. By comparison with the performance of the adsorbent A-2 for selectively removing sulfur from the JP-8 (4), the saturated adsorption capacity for the model gasoline is higher than that (0.015 g S/ml adsorbent) of the JP-8 by about 46%, indicating that the some coexisting compounds, for example, olefins and polycyclic aromatics, in the JP-8 influence probably the interaction between the sulfur compounds and the adsorption sites on the adsorbent surface.

By comparison of the adsorption profiles for thiophene and benzothiophene, as shown in Figure 1, we found that after the breakthrough point the concentration of thiophene in the effluent is slightly higher than that of benzothiophenes, implying that benzothiophene has a stronger interaction with the adsorbent than thiophene. In the future work, we will further examine the effect of alkyl substitutes at different positions on the adsorption of alkyl thiophenes and alkyl benzothiophenes as the commercial gasoline contains many alkyl thiophenes and alkyl benzothiophenes.

Table 1 Composition of model gasoline

nam	concentration wt %	S content wt
Sulfur compounds		
1 thiophene	0.0531	202
2 benzothiophene	0.0829	198
total	0.1360	400
Paraffin		
3 n-hexane	39.9	
4 n-decane	51.9	
total	91.9	
Aromatics		
5 toluene	8.0	

In comparison with other adsorption desulfurization processes, including Black & Veatch's IRVAD process (5,6), Phillips Petroleum's S Zorb process (7) and RTI's TRend process (8), the major potential advantages of our SARS-II process by using adsorbent A-2 for deep desulfurization of gasoline are that the adsorption process works at ambient temperature and ambient pressure without using hydrogen and the adsorbent A-2 has high selectivity to sulfur with high adsorption capacity.

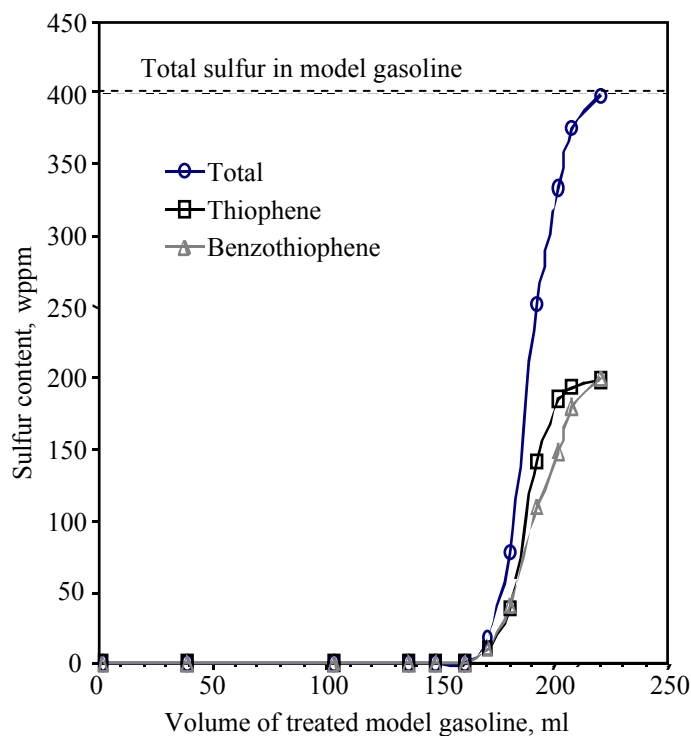


Figure 1 Adsorption profile of Adsorbent A-2 at ambient temperature and ambient pressure. Feed: model gasoline with total sulfur content of 400 ppmw.

Acknowledgments

This work was supported in part by US Department of Energy and US Department of Defense. We gratefully acknowledge the financial support.

References

1. Ma, X., Sun, Lu., Yin, Z. and Song, C. Am. Chem. Soc. Div. Fuel Chem. Prepr., **46** (2), 648-649 (2001).
2. Song, C. Keynote paper on desulfurization, Proceedings of the 5th International Conference on Refinery Processing, AIChE Spring 2002 National Meeting, New Orleans, LA, March 10-14, 2002.
3. Song, C., Ma, X. Appl. Catal. B, in submitting (2002)
4. Ma, X., Sprague, M., Sun, Lu., and Song, C. Am. Chem. Soc. Div. Petrol. Chem. Prepr., **47** (1), in press (2002).
5. Hydrocarbon Processing, May 1999, p. 39.
6. Irvine, R. L. U.S. Pat. No. 5,730,860, 1998.
7. Phillips Petroleum. <http://www.fuelstechnology.com/szorbdesiel.htm>. Viewed December 2001.
8. Turk, B. S., Gupta, R. P. Am. Chem. Soc. Div. Fuel Chem. Prepr., **46** (2), 392-393 (2001).

DEVELOPMENT OF A DIMETHYL ETHER-FUELED SHUTTLE BUS

Shirish Bhide, Elana Chapman, Jennifer Stefanik, Howard Glunt,
Louis I. Boehman and André L. Boehman

The Energy Institute
The Pennsylvania State University
405 Academic Activities Building
University Park, PA 16802

Francis J. Waller

Air Products and Chemicals, Inc.
Allentown, PA

Introduction

Dimethyl ether has been considered a potential ultra-clean replacement fuel for diesel engines [1]. Dimethyl ether (DME) burns “smokeless”, permits high levels of EGR for in-cylinder NO_x control and can be produced from synthesis gas derived from fossil fuel or biomass resources. These potential benefits of DME have motivated studies of the physical properties, the lubricity concerns and the combustion performance of DME [2,3]. In the present work, we seek to operate a laboratory engine and a campus shuttle bus on DME. To overcome the low lubricity and low viscosity of DME so as to be able to operate a conventional, common rail, DI diesel engine on DME, we have chosen to blend DME and diesel fuel. The conversion of the laboratory engine and the shuttle bus required development of a pressurized fuel delivery system to maintain the DME-diesel fuel blend above the vapor pressure of DME. This paper summarizes the outcomes from analyses of fuel properties, the laboratory engine studies and the conversion of the shuttle bus.

Experimental

Viscosity of DME-Diesel Blends. Quantitative measurements of the viscosity of blends of DME in a federal low sulfur fuel were obtained using a high pressure viscometer, using capillary tubes that provided optimal measurement accuracy depending on the viscosity of the fuel mixture [4]. Measurements were obtained over a range of pressures with the viscometer housing immersed in a constant temperature bath at 100°F (38°C). Results obtained at three different levels of chamber pressure are plotted in Figure 1 to show the impact of DME content on viscosity.

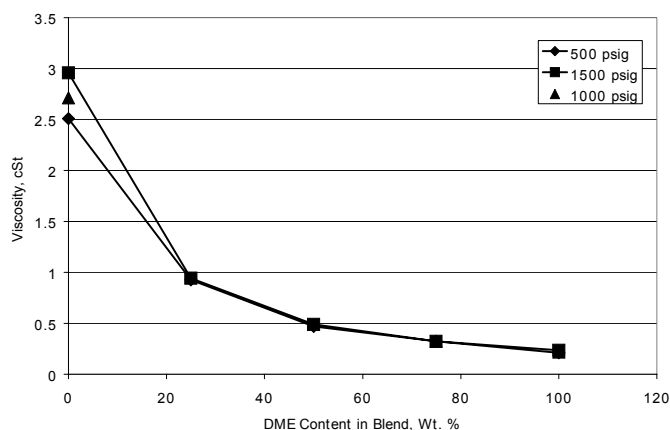


Figure 1. Blend response of viscosity to DME addition at various pressures [4].

Laboratory Engine Studies. The fuel system on the Navistar 7.3L V-8 “T444E” turbodiesel engine had to be modified to permit delivery of the fuel blend at elevated pressure [5]. The fuel rail in the cylinder head of the engine receives fuel at a pressure of about 70 psi. Fuel from this rail is then fed to the injectors.

A study was performed using #2 diesel fuel to measure the temperature rise of the fuel in the fuel rail. This measurement, coupled with the fuel consumption gave an approximate heat transfer rate between the cylinder head and the fuel in the gallery. A maximum target temperature was chosen for the diesel-DME blend based on the vapor pressure curve of DME and the pressure rating of the fuel rail. The required change in fuel recirculation flow rate was then calculated based on the above observations. This recirculated fuel was then cooled down using a water cooled heat exchanger. The fuel delivery pump was sized based on the above calculations.

Selecting a pump for DME was challenging due to the properties of DME. Gasket material for the pump had to be modified, as common materials such as Viton and buna-N have been found to be unsatisfactory. A fuel filter with a high filter surface area and high pressure capacity was needed. A modified propane filter was selected for the application. The fuel tank consisted of a modified 60 lb capacity LPG cylinder which was pressure tested at 120 psi prior to use.

From previous studies on this same engine for 2 wt.% oxygen in the diesel fuel, the cooling capacity of the heat exchanger and fuel circuit was found to be insufficient, based on the fuel temperatures recorded, as well as, observed engine instabilities. Therefore, the system shown in Figure 2 presents the modifications made, which included the addition of a second fuel coil in the cooled bath, and a larger chiller unit for cooling the bath. Additionally, the system was pressurized to 150 psi, which then increases the allowable fuel temperature before the DME becomes vapor.

Operation of the laboratory engine on blends of DME and diesel fuel resulted in reduction of particulate matter emissions. As shown in Figure 3, blending at up to 25 wt.% DME in diesel, corresponding to 10 wt.% oxygen addition resulted in significant reduction in particulate matter emissions.

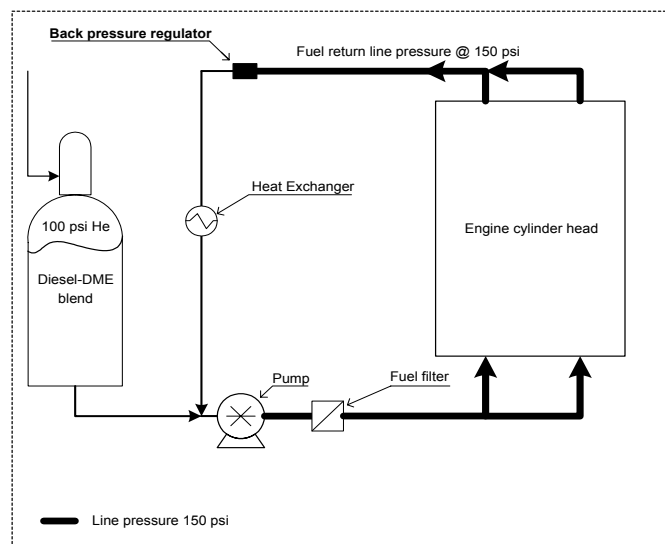


Figure 2. Diagram of the pressurized fuel system [5].

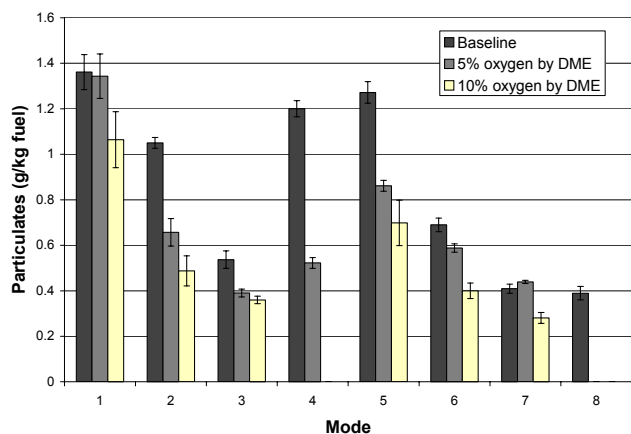


Figure 3. Particulate Matter Results per unit fuel consumed, g/kg fuel [5].

Shuttle Bus Conversion

The final stage of this project was the conversion of a campus shuttle bus and operation of the bus on the DME-diesel fuel blends. To accomplish this goal, the pressurized fuel system on the laboratory engine was adapted for application to a Champion Motorcoach “Defender” model bus with the same model engine (Navistar T444E) as was used in the laboratory study. To simplify the requirements for the fueling station for the shuttle bus, mixing of the DME and diesel fuel is performed onboard the bus. Figure 4 shows the shuttle bus used in this study. The final design and the operational procedures were reviewed and modified in a detailed “HAZOP” or failure modes effects analysis (FMEA). The outcome of the HAZOP analysis was to increase the number of check valves, manual valves and redundancy in the system.

The system on the bus consists of a transfer pump that delivers diesel fuel from the existing diesel fuel tank to the tank for the blended fuels, a propane tank for a recreational vehicle. This LPG tank was modified only by replacing o-ring materials with Kalrez™ o-rings. The connections on the LPG tank permit diesel fuel to be transferred to the tank, while the tank is vented to the atmosphere. Then, DME is transferred into the LPG tank. During the refueling processes, a handheld controller notifies the operator of the fill level in the LPG tank so that the desired proportions of fuel are transferred. Finally, a compressed cylinder of helium is connected to the LPG tank to provide a blanket of inert gas to maintain a minimum of 120 psig in the LPG tank and keep the DME in the liquid phase. A magnetically coupled gear pump serves to draw fuel from the LPG tank and transfer the fuel blend to the fuel rails in the cylinder heads of the engine. A backpressure regulator maintains the pressure in the fuel rails at a minimum of 150 psig, although during operation the rail pressure is typically near 200 psig. Fuel rejected from the rails passes through a pair of fuel coolers mounted in front of the radiator to keep the fuel temperature from rising above a bulk temperature of 50°C.

Upon completion of the majority of the conversion process, the bus was operated with the pressurized fueling system on diesel fuel but without DME blending. The bus was operated over several days at the Pennsylvania Transportation Institute’s test track near the Penn State University Park campus. During this shakedown process, emissions measurements were obtained in collaboration with Clean



Figure 4. Particulate Matter Results per unit fuel consumed, g/kg fuel.

Air Technologies (Buffalo, NY) using their portable diesel emissions analyzer (XXX). Among the chief challenges faced during the conversion and shakedown tasks was the power requirements and stability of operation of the gear pump. However, in-field adjustments and modifications resulted in consistent and stable operation of the components of the pressurized fueling system. The shuttle bus will operate on the DME-diesel fuel blend, at 25 wt.% DME, through Fall 2002 during which time periodic performance, emissions and system integrity tests will be performed.

Conclusions

Operation of a commercial diesel engine on DME-diesel blends has been accomplished with minimal modification to the engine, apart from addition of a pressurized fuel delivery system. This technique permits operation of vehicles, in part, on DME without jeopardizing the long term durability of the engine. Consistent with operation of diesel engines on oxygenated fuels, particulate emissions with the DME-diesel fuel blends are substantially reduced.

Acknowledgement. The authors wish to thank Air Products and Chemicals, Inc., the Pennsylvania Department of Environmental Protection, the National Energy Technology Laboratory of the US Department of Energy, Navistar International, Caterpillar, and DuPont Fluorochemicals for their support of this project. The authors also wish to thank Dr. James Hansel of Air Products for assistance with the HAZOP analysis, and David Klinikowski, Bruce Younken and Sam Entz of Penn State for their patient support.

References

- (1) Fleisch, T., McCarthy, C., Basu, A., Udovich, C., Charbonneau, P., Slodowske, W., Mikkelson, S.-E., and McCandless, J., **1995**, SAE Paper No. 950061.
- (2) Sivebaek, I. M., Sorenson, S. C., and Jakobsen, J., **2001**, SAE Paper No. 2001-01-2013.
- (3) Teng, H., McCandless, J.C. and Schneyer, J.B., **2002**, SAE Paper No. 2002-01-0862.
- (4) Bhide, S.V., Boehman, A.L. and Perez, J.M., Prepr. – *Am. Chem. Soc., Div. Fuel Chem.*, **2001**, 46(2), 400.
- (5) Chapman, E.M., Boehman, A.L., Tijm, P.J.A. and Waller, F.J., **2001**, SAE Paper No. 2001-01-3683.

Diffuse reflectance IR spectroscopic study on the role of promoters in the reactivity of carbon monoxide with hydrogen over novel Pd sulfide catalyst

Naoto Koizumi, Kazuhito Murai, Seiko Tamayama, Hiroyuki Kato, Toshihiko Ozaki, and Muneyoshi Yamada

Department of Applied Chemistry, Graduate School of Engineering, Tohoku University, 07 Aoba, Aramaki, Aoba-ku, Sendai 980-8579, Japan

Introduction

For an industrial methanol synthesis, Cu/Zn-type catalyst is currently employed using CO/H₂/CO₂ feed. This type of catalyst is usually operated at 523 K and 5 – 10 MPa and yields above 1000 g/kg-cat/h of methanol. However, due to thermodynamic limitations, a single-pass CO conversion is restricted below 60% (523 K and 5.0 MPa), which requires a gas-recycle system. Besides the Cu/Zn-type catalyst, reduced Pd catalysts are well known to show excellent activities at lower reaction temperatures and pressures. For example, a reduced Pd/CeO₂ yields 300 g/kg-cat/h of methanol from CO/H₂ feed at 443 K and 3.0 MPa, which is comparable with that obtained with the Cu/Zn catalyst at 503 K and 3.0 MPa from CO/H₂/CO₂ feed.¹

Many studies have shown that the methanol synthesis activity and selectivity of the reduced Pd catalyst changes sensitively depending on the natures of the supports^{1,2} and some metal additives such as Ca nitrate and Mg chloride improve a methanol synthesis activity of a reduced Pd/SiO₂.³⁻⁵ It is suggested that they change an electronic property of surface Pd sites and/or a morphology of Pd crystallites. Searching new type of methanol synthesis catalysts, the authors found that Rh sulfide (Rh₁₇S₁₅)⁶ and Pd sulfide (Pd₁₆S₇)⁷ yield methanol from CO/H₂ feed at a relatively higher reaction temperature and pressure (613 K and 5.1 MPa). These sulfide catalysts have a quite unique property, a sulfur tolerance. Pd₁₆S₇ shows a quite stable activity even in the presence of H₂S 100 ppm in concentration while a commercial Cu/Zn/Al catalyst is irreversibly poisoned by H₂S.⁷ In order to make clear the active site of the Pd₁₆S₇, we examined effects of supports⁸ and metal additives.⁹ It was found that a sulfided Pd/SiO₂ promoted with Ca nitrate shows a higher activity than the Pd₁₆S₇. STY of methanol obtained with the sulfided Ca-Pd/SiO₂ was 5 times higher than that obtained with the Pd₁₆S₇. At 593 K, 5.1 MPa and 30 m³ (STP)/kg-cat/h, STY of methanol obtained with the sulfided Ca-Pd/SiO₂ reached 730 g/kg-cat/h, which is about 50% of that obtained with the commercial Cu/Zn/Al catalyst from CO/H₂/CO₂ feed at the same reaction conditions.

As concerns reactive adsorbed species formed on the sulfided Ca-Pd/SiO₂, the authors found the formation of adsorbed CO species after the methanol synthesis by means of *in-situ* DRIFT spectroscopy.⁹ The adsorbed CO species was hydrogenated in a stream of H₂ to yield methanol. In this paper, to make clear the role of the Ca additive in the formation of such the reactive adsorbed species, the nature of adsorbed species formed on sulfided Ca-Pd/SiO₂, sulfided Pd/SiO₂, sulfided Ca/SiO₂ and sulfided SiO₂ were examined by *in-situ* DRIFT spectroscopy as well as CO uptake measurement.

Experimental

CO uptake measurements. CO uptake of the sulfided sample after CO hydrogenation reaction was measured by a pulse method. An oxidized sample was charged in a stainless steel reactor and then the reactor was connected with a gas-line for the sulfiding pretreatment and CO hydrogenation reaction. After sulfiding the sample in a stream of H₂S/H₂ at 673 K, the temperature was reached

down to room temperature. A feed composed of CO 33%/H₂ 62%/Ar was then continuously fed to the reactor at 5.1 MPa followed by heating of the sulfided sample up to 613 K. This temperature was held for 2 h and then the temperature was reached down to room temperature again. After flushing the syngas in the reactor with a helium flow at 573 K, CO 10%/He pulse was introduced into the reactor at 308 K. The amount of adsorbed CO was determined with a thermal conductivity detector.

DRIFT measurements. To obtain DRIFT spectra of adsorbed species formed on the sulfided sample during and/or after CO hydrogenation reaction, a high-pressure DRIFT chamber equipped with ZnSe window (Spectra-Tech Inc.) was employed here. Details of the procedures for DRIFT measurements can be referred to our preceding paper.⁹

Sample preparations. All the oxidized samples used here were prepared by the impregnation method. Details of the preparation methods can be also referred to our preceding paper.⁹

Results and Discussion

To make clear effects of the Ca additive on the number of adsorption sites for CO of sulfided Pd/SiO₂, CO uptakes of the sulfided Ca-Pd/SiO₂ with different Ca/Pd molar ratios were measured. In **Figure 1**, methanol yields normalized to moles of Pd atom in the sulfided Ca-Pd/SiO₂ with Ca/Pd molar ratios of 0, 0.1, 0.5 and 1.0 are plotted against amount of CO adsorbed on them. Slopes of dashed lines shown in the figure are TOF of each supported sulfide. The addition of small amount of Ca additive to the sulfided Pd/SiO₂ (Ca/Pd molar ratio = 0.1) increases the methanol yield substantially while it has little influence on the amount of adsorbed CO, which results in the increase of TOF from 0.06 sec⁻¹ to 0.20 sec⁻¹. It is worthy to note that both sulfided Ca/SiO₂ and sulfided SiO₂ yield no methanol and amount of CO adsorbed on them are negligible. Thus, it is suggested that the irreversible adsorption of CO predominantly occurs on coordinatively unsaturated Pd sites and the addition of the Ca additive significantly enhances a reactivity of the adsorbed CO species for the methanol formation.

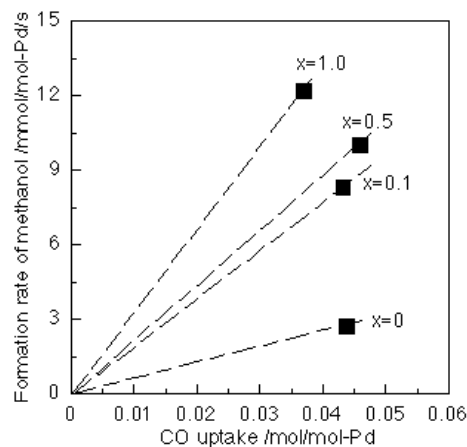
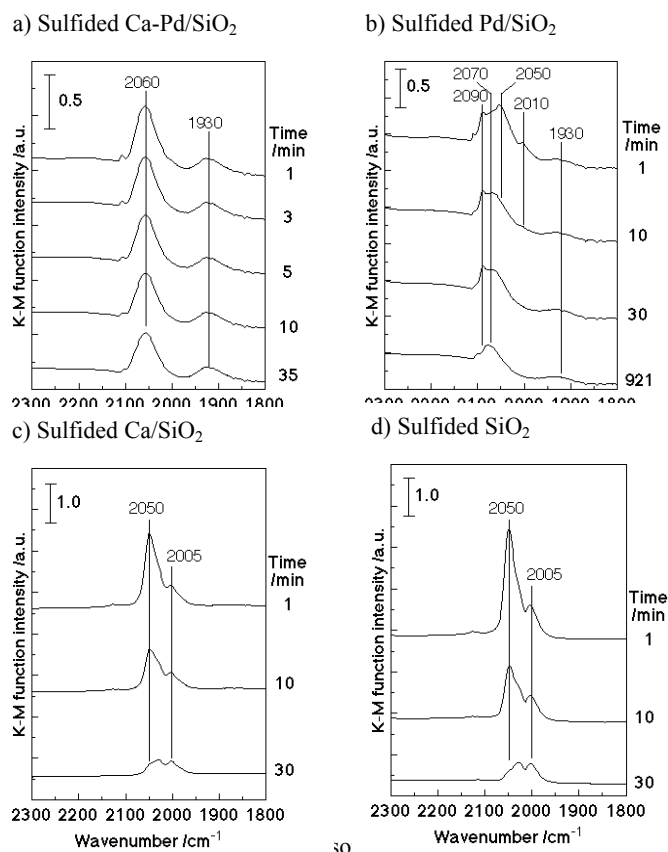


Figure 1 Relationship between yield of methanol normalized to moles of Pd atom in the sulfided Ca-Pd/SiO₂ with different Ca/Pd molar ratios (x ; $x = 0, 0.1, 0.5, 1.0$) and amount of CO adsorbed on them. CO hydrogenation reaction was carried out at 613 K, 5.1 MPa and 20 m³ (STP)/kg-cat/h using the feed composed of CO 33%/H₂ 62%/Ar.

To make clear differences of the nature of adsorbed CO species formed on the sulfided Ca-Pd/SiO₂ and sulfided Pd/SiO₂, DRIFT spectra were measured for both the sulfided samples during and/or

after CO hydrogenation reaction. DRIFT spectra of the sulfided Ca-Pd/SiO₂ (Ca/Pd molar ratio = 0.5) measured during the reaction showed IR bands at 1820, 1600, 1450, 1270, 1110, 1062, 1031, 1007 and 957 cm⁻¹. A shoulder band was also visible at 1304 cm⁻¹. The bands at 1062, 1031 and 1007 are assigned to C-O stretching vibration of the gas-phase methanol while the shoulder band at 1304 cm⁻¹ is assigned to C-H bending vibration of the gas-phase methane. On the contrary, very weak bands due to the gas-phase methanol were observed in the spectra of the sulfided Pd/SiO₂ during the reaction. Thus, the promoting effects of the Ca additive were clearly identified by DRIFT measurements. However, the intensity of the band due to the gas-phase CO was too strong to observe the adsorbed CO species.

Then, attentions were paid to the nature of adsorbed CO species remaining on the surface of sulfided samples after the reaction. The temperature was reached down to 298 K under the high-pressure syngas flow and then the pressure of the syngas flow was reached down to 0.3 MPa followed by the flushing with helium. DRIFT spectra of adsorbed CO species were recorded during the flushing as a function of time (**Figure 2**). DRIFT spectra of the sulfided Ca-Pd/SiO₂ show IR bands at 2060 and 1930 cm⁻¹. A weak band is also visible at around 2100 cm⁻¹. In a spectrum of the sulfided Pd/SiO₂, bands are visible at 2090, 2070, 2050, 2010 and 1930 cm⁻¹ at the beginning of the flushing while the bands at 2050 and 2010 cm⁻¹ disappear quickly. To assign these bands, DRIFT spectra of sulfided Ca/SiO₂ and sulfided SiO₂ were also measured. Both the spectra show bands at 2050 and 2005 cm⁻¹ at the beginning of the flushing. The intensities of these bands decrease quickly during the flushing. A weak band is also visible at 2030 cm⁻¹ in the both spectra of the sulfided Ca/SiO₂ and sulfided SiO₂ after the flushing of 30 min. These bands are assigned to CO species weakly interacted with SiO₂ surface (possible surface hydroxyl groups). From these spectra, we can assign the bands at 2050 and 2010 cm⁻¹ appeared in the spectrum of the sulfided Pd/SiO₂ to CO species interacted with SiO₂ surface. In other words, the bands at 2060 and 1930 cm⁻¹ in the spectra of the sulfided Ca-Pd/SiO₂, and those at 2090, 2070 and 1930 cm⁻¹ in the spectra of the sulfided Pd/SiO₂ can be assigned to CO species adsorbed on Pd sites (2090, 2070 and 2060 cm⁻¹: linear-type adsorbed species, 2030 cm⁻¹: bridge-type adsorbed species). Since the IR band positions of CO species adsorbed on Pd sites linearly in the spectra of the sulfided Pd/SiO₂ is higher than that of the sulfided Ca-Pd/SiO₂, surface Pd sites formed on sulfided Pd/SiO₂ are in a slightly electron deficient state compared with those on the sulfided Ca-Pd/SiO₂. As reported previously,⁹ the intensities of the bands of adsorbed CO species remaining on the surface of the sulfided Ca-Pd/SiO₂ after the methanol synthesis decreases during the heating of the sample in a stream of H₂. The decrease of the intensities of these bands is accompanied with the appearance of the bands due to the gas-phase methanol. On the contrary, no bands due to the gas-phase methanol were observed during the heating of the sulfided Pd/SiO₂ in the stream of H₂ while the intensities of the bands due to the adsorbed CO species decreases with increasing the temperature. Thus, the reactivity of adsorbed CO species remaining on the surface of sulfided Ca-Pd/SiO₂ for the methanol formation is much higher than that on the sulfided Pd/SiO₂. This is quite consistent with the notion suggested by the CO uptake measurements. Thus, it is concluded that the addition of the Ca additive to the sulfided Pd/SiO₂ slightly increase the electron density of the surface Pd sites, which results in the increase of the reactivity for the methanol formation of CO species adsorbed on them.



(a) Ca/Pd molar ratio = 0.5), sulfided Pd/SiO₂ (b), sulfided Ca/SiO₂ (c) and sulfided SiO₂ (d) after CO hydrogenation reaction at 613 K and 5.1 MPa using the feed composed of CO 33%/H₂ 62%/Ar. All the spectra shown here were measured during the helium flushing at 298 K and 0.3 MPa as a function of time.

Acknowledgement. This work was supported by Research for the Future Program of JSPS under the project “Synthesis of Ecological High Quality Transportation Fuels” (JSPS-RFTF98P01001).

References

- 1) Matsumura, Y.; Shen, W.-J.; Ichihashi, Y.; and Okumura, M., *J. Catal.*, **2001**, 197, 267.
- 2) Ichikawa, M.; and Shikakura, K., *Shokubai*, **1979**, 21, 253.
- 3) Kikuzono, Y.; Kagami, S.; Naito, S.; Onishi, T.; and Tamaru, K., *Chem. Lett.*, **1981**, p. 1249.
- 4) Gotti, A.; and Prins, R., *J. Catal.*, **1998**, 175, 302.
- 5) Gusovius, A. F.; Walting, T. C.; and Prins, R., *Appl. Catal. A: General*, **1999**, 188, 187.
- 6) Yamada, M.; Koizumi, N.; Miyazawa, A.; and Furukawa, T., *Catal. Lett.*, in print
- 7) Koizumi, N.; Miyazawa, A.; Furukawa, T.; and Yamada, M., *Chem. Lett.*, **2001**, p. 1282.
- 8) Koizumi, N.; Murai, K.; Takasaki, S.; and Yamada, M., *Pap. - Am. Chem. Soc., Div. Fuel Chem.*, **2001**, 46 (2), 437-438.
- 9) Koizumi, N.; Murai, K.; Takasaki, S.; Yamada, M. *Prepr. Pap. - Am. Chem. Soc., Div. Fuel Chem.*, **2002**, 47 (1), in-print

EFFECT OF N-CONTAINING MOLECULES ON THE HYDRODESULFURISATION OF DIBENZOTHIOPHENE

Marina Egorova and Roel Prins

Laboratory for Technical Chemistry
Federal Institute of Technology (ETH)
8093 Zurich-Hoenggerberg
Switzerland

Introduction

The oil industry is under increased pressure from the environmental legislation to limit the sulfur level in gasoline and diesel fuel with a view of reducing exhaust emissions. A sulfur specification of 350 ppm is currently practiced in the EEC and a sulfur content as low as 50 or even 10 ppm is being proposed for the year 2005. Nitrogen-containing molecules inhibit the hydrodesulfurization (HDS) of sulfur-containing molecules, but in normal HDS this is not a big problem because the amount of N-containing molecules in gasoil is much smaller than that of S-containing molecules. N-containing molecules will be harmful in deep HDS, however, because then the amounts of N- and S-containing compounds are comparable.

We have studied the influence of 2-methylpyridine and 2-methylpiperidine on the HDS of dibenzothiophene (DBT) over a sulfided NiMo/Al₂O₃ catalyst. DBT was chosen because it allows to study the removal of sulfur by the direct desulfurization pathway (hydrogenolysis) as well as by hydrogenation followed by desulfurization. Pyridine was believed to be the simplest model molecule to study hydrodenitrogenation (HDN). Although the network of reactions taking place in the HDN of pyridine is now well understood, the study of the kinetics of the HDN of pyridine proved to be extremely difficult. The reason for this difficulty is the occurrence of a side reaction of piperidine, the first intermediate in the HDN of pyridine. Two piperidine molecules disproportionate to N-pentylpiperidine and ammonia.¹ However, substitution of a hydrogen atom by a methyl group on the α carbon atom of pyridine hinders the disproportionation so much, that it is strongly suppressed and hardly interferes with the other reactions taking place during the HDN of pyridine and piperidine. Therefore we decided to use in our study 2-methylpyridine and 2-methylpiperidine as N-containing molecules.

2-Methylpyridine as well as 2-methylpiperidine suppressed the hydrogenation pathway of the DBT HDS. This indicates that N-containing molecules are harmful in deep HDS because in deep HDS 4,6-dialkyldibenzothiophene molecules must be desulfurized. For these molecules the direct pathway is weak² and HDS is mainly determined by the hydrogenation pathway. Although 2-methylpiperidine is a much stronger base than 2-methylpyridine, it hardly influenced the direct HDS of DBT, whereas 2-methylpyridine inhibited this pathway stronger. The difference in inhibition of the two HDS pathways indicates that they occur over different sites on the metal sulfide surface.

Experimental

Catalyst preparation. The NiMo/ γ -Al₂O₃ catalyst used in this work contained 8 wt% Mo and 3 wt% Ni and was prepared by successive incipient wetness impregnation of γ -Al₂O₃ (Condea, pore volume 0.5 cm³g⁻¹, specific surface area 230 m²g⁻¹) with an aqueous solution of (NH₄)₆Mo₇O₂₄·4H₂O (Aldrich), followed by an aqueous solution of Ni(NO₃)₂·6H₂O (Aldrich). The catalyst was dried in air at ambient temperature for 4 h, then dried in an oven at 120°C for 15 h, and finally calcined at 500°C for 4 h.

Reaction performance. A sample of catalyst (0.05 g) was diluted with 8 g SiC to achieve plug-flow conditions in the continuous-flow fixed-bed reactor. The catalyst was sulfided *in situ* with a mixture of 10% H₂S in H₂ at 400°C and 1.0 MPa for 4 h. After sulfidation, the pressure was increased to 5.0 MPa, and the liquid reactant was fed to the reactor by means of a high-pressure pump (Gilson 307). Experiments were carried out at 573 (HDS) and 613 K (HDN). The composition of the gas-phase feed in most experiments consisted of 1-6 kPa amine reactant, 1 kPa dibenzothiophene, 140 kPa decane (as solvent for the amine in HDN experiments) or 130 kPa toluene (as solvent for dibenzothiophene in HDS experiments), 11-18 kPa heptane and 8 kPa dodecane (as references for GC analysis), 36 kPa H₂S, and 4.8 MPa H₂.

Product analysis. The reaction products were analyzed by on- and off-line gas chromatography with a Varian 3800 GC instrument equipped with a PTA-5 fused silica capillary column (Supelco, 5% diphenylsiloxane/95% dimethylsiloxane, 30 m x 0.25 mm x 0.5 μ m). Detection was performed with a flame ionization detector as well as with a pulsed flame photometric detector, which is very useful for detecting small amounts of nitrogen- and sulfur-containing compounds. Weight time was defined as the ratio between the catalyst weight and the molar flow to the reactor. The weight time was changed by varying the flow rates of the liquid and the gaseous reactants, while keeping their ratio constant.

Results and Discussion

HDN network of 2-Methylpyridine. The HDNs of 2-methylpyridine and its intermediate products 2-methylpiperidine, 1-aminoheptane, and 2-aminoheptane were studied in order to clarify the reaction network of HDN.

2-Methylpiperidine is the only primary product in the 2-methylpyridine HDN, as expected, since the HDN of heterocyclic N-containing aromatic molecules can only occur after ring hydrogenation.^{1,3} The HDN of 2-methylpiperidine showed that four compounds such as 1-aminoheptane, 2-aminoheptane, 2-methylpyridine, and 2-methyl-3,4,5,6-tetrahydropyridine have non-zero selectivity at zero conversion of 2-methylpiperidine and thus might be considered to be primary products (Figure 1).

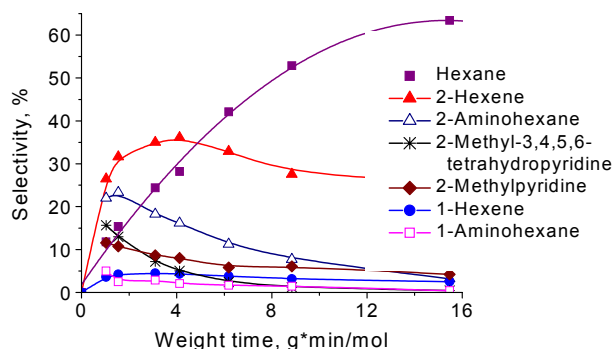


Figure 1. Product selectivities in the HDN of 2-methylpiperidine as a function of weight time.

The presence of most intermediates could be explained by a combination of pyridine ring hydrogenation, piperidine ring opening by elimination, and nitrogen removal by elimination as well as by nucleophilic substitution of the amino group by a sulfhydryl group, followed by elimination of H₂S or hydrogenolysis of the C-S bond. Aminoalkenes, which are expected to be the primary products of the

ring opening of alkylpiperidine, were not observed, probably because of fast hydrogenation to the corresponding amines.

Combining the results of the HDN of 2-methylpyridine, 2-methylpiperidine, 1-aminoheptane, and 2-aminoheptane, we arrive at the reaction scheme presented in **Figure 2**.

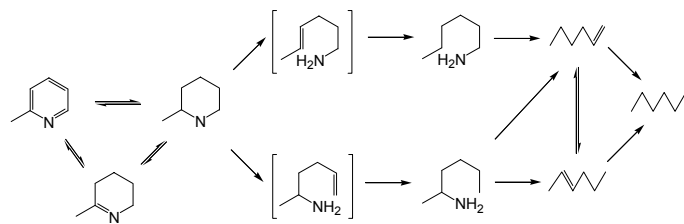


Figure 2. Scheme of the reaction network of the HDN of 2-methylpyridine and 2-methylpiperidine.

Comparison of the conversion of 2-aminoheptane and 1-aminoheptane showed that the reactivity of 2-aminoheptane is higher than that of 1-aminoheptane. Despite a higher reactivity, much more 2-aminoheptane than 1-aminoheptane was detected in the HDN of 2-methylpiperidine (**Figure 1**). This proves that the first C-N bond breaking in 2-methylpiperidine occurs predominantly between the nitrogen atom and the carbon atom of the methylene group. The fact that much more 2-aminoheptane than 1-aminoheptane is formed in the HDN of 2-methylpiperidine further indicates that the methyl group actually has a negative rather than a positive influence on the elimination and hinders the adsorption of 2-methylpiperidine in a conformation in which the nitrogen atom and the β H atom of the methylene group next to the $\text{CH}(\text{CH}_3)$ group approach the metal sulfide surface.

HDS of Dibenzothiophene and its inhibition by N-containing molecules. The product distribution obtained in the DBT HDS shows that the reaction goes through two parallel pathways (**Figure 3**): (i) direct desulfurization, which yields biphenyl, and (ii) hydrogenation followed by desulfurization, which gives first tetrahydrodibenzothiophene and then cyclohexylbenzene.²

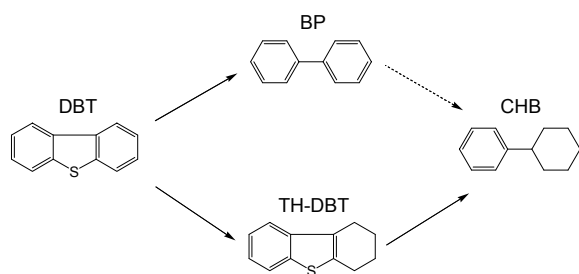


Figure 3. Scheme of the reaction network of the HDS of dibenzothiophene.

The product selectivities in the DBT HDS show that slow hydrogenation of biphenyl (BP) to cyclohexylbenzene (CHB) is also taking place, since the increase of the CHB selectivity with weight time is higher than the decrease of the tetrahydrodibenzothiophene selectivity. The DBT conversion showed first-order behavior when plotting $\ln[(C_{\text{DBT}})/(C_{\text{DBT}})_0]$ versus weight time.

Basic N-containing compounds have been characterized among the strongest inhibitors for HDS. Our experiments showed that the presence of any amount of N-containing molecule in the feed completely blocks the hydrogenation pathway of the DBT HDS, so that the only product observed is biphenyl. 2-Methylpiperidine is a

much stronger base than 2-methylpyridine. Nevertheless, the hydrogenolysis of DBT is inhibited noticeably only at high concentrations of 2-methylpiperidine (**Figure 4**). At 1:1 and 1:2 ratios of DBT to 2-methylpiperidine the conversion of DBT hardly changed. 2-Methylpiperidine did not convert to any products at 573 K and 5 MPa total pressure.

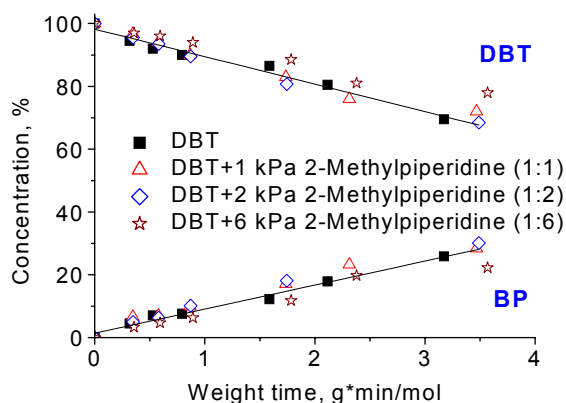


Figure 4. DBT HDS in the presence of different amounts of 2-methylpiperidine.

The experiments performed in the presence of the less basic 2-methylpyridine showed already an inhibition effect at lower concentration of the N-containing molecule (**Figure 5**). In these experiments 2-methylpyridine was partially converted to 2-methylpiperidine.

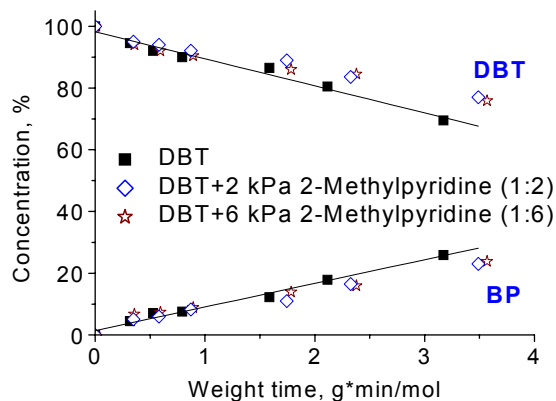


Figure 5. DBT HDS in the presence of different amounts of 2-methylpyridine.

References

- (1) Prins, R., *Adv. Catal.* **2002**, 46, 399.
- (2) Bataille, F., Lemberton, J. L., Michaud, P., Perot, G., Vrinat, M., Lemaire, M., Schulz, E., Breyse, M., Kasztelan, S., *J. Catal.*, **2000**, 191, 409.
- (3) Nelson, N., and Levy, R. B., *J. Catal.*, **1979**, 58, 485.

Evaluation Of Hydrocarbon Based Fuels In The Disintegrated Fuel Cell Power Train.

A. R. Khan, O.Y. Plevaya. C. Cioffi

Nuvera Fuel Cells
Acorn Park, Cambridge
MA-02140

Introduction

Growing interest in PEM fuel cells as a potential propulsion system for transportation vehicles initiated development of the advanced fuel-making technologies for improving environment and meeting future vehicle emission targets. These technologies will enable production of ultra-clean transportation fuels, alternative to Gasoline but utilizing it's infrastructure and being cost competitive at the same time. Strategic partnerships are created, including the fuel companies, to target at the development of alternative fuels and verification of their performance within the innovative fuel processing and fuel cell power systems. The current study was conducted within the Ultra Clean Transportation Fuels (UCTF) Program initiated by the U.S. Department of Energy (DOE).

Background

The insights of Autothermal Reforming (ATR) have been investigated in Nuvera Fuel Cells for a range of candidate fuels, including gasoline, methanol, ethanol, diesel and Naphtha (2). The previous efforts were concentrated on the parametric study of the syngas production efficiencies as a function of reformer operating conditions. The purpose of the current study was to evaluate fuels of interest in the full fuel-to-DC power train for their Hydrogen production efficiency through the ATR and following Water-Gas Shift and Carbon monoxide cleanup sections of the fuel processor. Another purpose of the study was to look at the profile of micro components in the processed reformat streams, which could potentially effect the fuel cell stack performance and compare the fuel reformat condensates as a part of system emissions and /or water recycling technology. Evaluation of power production data by the fuel cell stack operated on different fuel reformates concluded the scope of the study.

Fuels

Two fuels were selected for the current fuel-to-DC power studies. One fuel was a California Phase II certified Gasoline obtained from Chevron Phillips. This commercially available fuel meets the current strict emission standards of the state of California. The second fuel was a Fischer Tropsch naphtha obtained from the Sasol-Chevron joint venture. This is highly paraffin fuel with essentially no sulfur, nitrogen or aromatics, as presented in Table 1.

Table 1. Fuels specifications

Characteristics	Naphtha	California Phase II RFG
Hydrogen/Carbon ratio	2.25	1.8
Sulfur, ppm	<1	35
Aromatics, Vol. %	0.5	28.1
Olefins, Vol. %	0.5	7.5
Specific gravity	0.6906	0.7377
Lower Heating Value, Btu/lb	19130	18553

Experimental

Both fuels under study were processed into Hydrogen containing reformates in Nuvera's disintegrated Modular Pressurized facility (MPR), shown in Fig. 1.

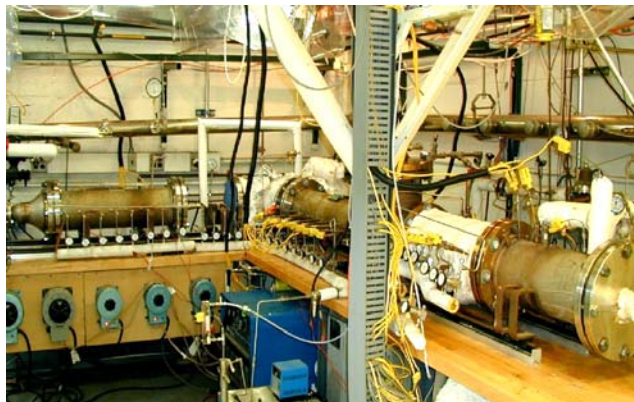


Figure 1. Modular Pressurized Reactor (MPR). The upstream section, including ATR and WGS sections.

This pilot plant facility comprises the totality of Fuel Cell based power-producing functionality, including temperature management modules, fuel reforming spool, high- and low-temperature Water-Gas-Shifts (WGS), optional sulfur capture module, two-stage preferential-oxidation based CO cleanup, and flexible PEM fuel cell test stand

The maximum firing rate for the front-end assembly, including preheat, ATR and WGS sections are 140 kWth (based on the Lower Heating Value (LHV) of the fuel; for the downstream assembly, they are 40 kWth of Hydrogen flow rate. Because of the differences in ratings between the upstream and downstream sections, provisions for bypassing the excess of Reformat flow to the exhaust manifold have been incorporated into the assembly.

The desulfurizer, external to the MPR, was installed to decrease the initial concentration of Sulfur in Gasoline from 35- 40 ppm to less than 1 ppm, which can be tolerated by the catalyst modules the fuel processing train comprises of. Sampling ports for sulfur analysis were located at the desulfurizer exit and at the exit of CO clean-up section. No sulfur was detected at the latter location with the analyzer sensitivity above 200 ppb.

Each fuel was mixed with the steam, preheated for the fuel to be vaporized and sent to the ATR section, containing Nuvera's proprietary catalytic module. The fuel thermal input has been maintained at 60 KW based on the lower heating value (LHV) with the fixed equivalence ratio of 3.65 and steam-to-carbon ratio of 3.4, where Equivalence ratio = (Fuel/Air)/(Fuel/Air)_Stoichiometric.

The reformat gas has been further processed in the WGS reactors followed by the cleanup from carbon monoxide. The operating pressure was maintained at 2.5 bar downstream of the cleanup section. All operating conditions were monitored for carbon formation using a differential pressure gauge across the reforming bed and an inline sample filter.

The sampling port for reformat stream was located at the exit of the clean-up section of the fuel processing train. Multiple samples were collected at the steady state to ensure repeatability. Collected samples were conditioned and sent to a specially configured gas chromatograph.

PEM Fuel Cell Stack

The fuel cell stack used in the study consisted of 30 cells and produced more than 3 KW of electrical DC power operating on pure Hydrogen and air at the cathode and anode pressure of 2.5 bar. The stack was maintained at temperature of 70°C measured at the cathode exhaust. Air flow entering the stack was humidified above 80% at 65°C. The cathode stoichiometry was maintained at 2, while reformat flow to anode was maintained constant and equivalent to 12 KW of the fuel thermal input.

Results And Discussion

Both fuels were successfully processed in Nuvera's MPR facility and the reformates were considered "clean" and contained no poisons to the fuel cell stack.

Equivalence ratio of air to fuel was originally planned to maintain at 3.65 for both fuels to maximize the hydrogen yield. In case of Naphtha processing we were able to maintain the equivalence ratio close to the designed value and satisfy the required temperature profile in the fuel processor at the same time. During gasoline fuel processing the air-to-fuel equivalence ratio had to be lowered to maintain the required temperature profile in the reactor and avoid skipping non-converted aromatics.

Maintaining designed temperature profile in multiple reactors, required to process sulfur containing gasoline, is a complicated task, and additional restrictions were imposed on the controls and operating strategy. Stability of the operating regime reflected consistency of the reformat composition data, recorded over the running time, through the wider deviation of bulk gas concentrations from the average values in case of gasoline reforming, shown in Table 2.

Hydrogen yield was slightly less during processing of gasoline in comparison with the Naphtha derived reformat and methane slip was also slightly higher in case of gasoline processing then in Naphtha reforming. Carbon monoxide concentration at the exit of clean-up reactor was oscillating below 20 ppm in both runs.

Table 2. Fuel Processing data of Naphtha vs. Gasoline.

Reformat bulk composition	Vol. %, Dry base,	Vol. %, Dry base,
Hydrogen	43.4 +/- 0.49	40.78 +/- 1.91
Nitrogen	35.8 +/- 0.68	36.87 +/- 2.32
Carbon dioxide	20 +/- 0.16	20.37 +/- 0.30
Methane	0.18 +/- 0.01	0.22 +/- 0.08

The different of both Hydrogen concentration in the product stream and Hydrogen production efficiency were theoretically predicted from the system analysis of both fuels due to the difference in their hydrogen-to-carbon ratio, presented in Figure 2 and 3.

Higher difference between experimental and theoretical values recorded in Naphtha processing versus Gasoline was attributed to operating strategy of the clean-up section purposed to decrease the concentration of carbon monoxide below 20 ppm, which could be sacrificial to the concentration of Hydrogen in the reformat stream. Since the current study was purposed on characterization of the entire power train, it was very important to balance all the subsystems within certain operating ranges, close to optimal to specific section but without sacrificing performance of another section of the power train at the same time, including the fuel cell stack.

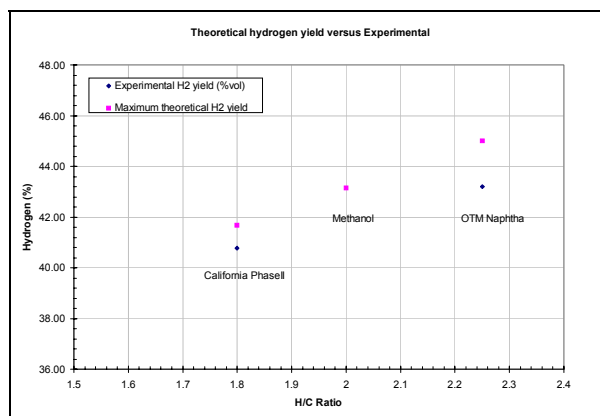


Figure 2. Hydrogen yield (experimental vs. theoretical) data in ATR fuel processing for fuels with different Hydrogen-to-carbon ratios. Oxygen concentration in the fuel is accounted if applicable.

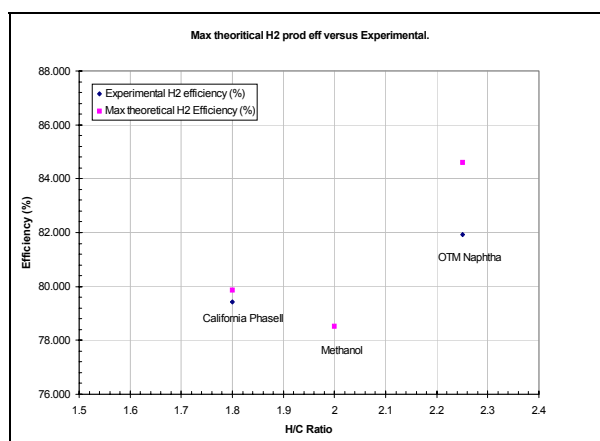


Figure 3. Hydrogen production efficiency (experimental vs. theoretical) in ATR fuel processing for fuels with different Hydrogen-to-carbon ratios.

The FTIR technique had been used to detect species at low concentrations in both fuel reformates. The FTIR had been calibrated for aromatic species and ammonia. In both fuel reformates no contaminants to the fuel cell stack had been detected under operating conditions specified above.

The process condensates have been sampled and analyzed for volatile organic compounds (VOC), metal ions and other contaminants.

The difference in Hydrogen concentration in gasoline and Naphtha reformates was insignificant to change the polarization characteristics of the fuel cell, shown in Figure 4.

The same stack was used for power generation on both Naphtha and Gasoline derived reformates. The base line Hydrogen polarization curve was recorded before introducing reformates to the stack and between the experiments with different fuels. There was no signs of performance degradation caused by feeding the stack anode with neither of the reformat streams. The reformat flow entering the stack was maintained constant and equivalent to 12 kW of the fuel thermal input.

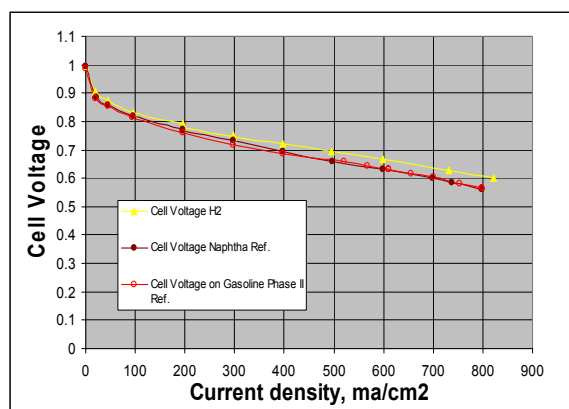


Figure 4. Polarization curves recorded on Naphtha and Gasoline Phase II ATR reformates vs. Hydrogen, cathode and anode pressure 2.5 bar, Cathode Stoichiometry 2, Fuel thermal input 12 kW.

Stack derating factor on both fuel reformates is estimated at 4.5% of power at 400 mA/cm² of current density and about 7% at 600 mA/cm² versus power production on pure Hydrogen at the corresponding current densities. The power production curves are shown in Fig.5.

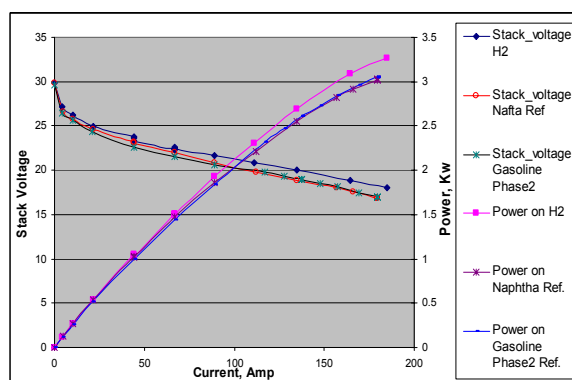


Figure 5. Power production of 30 cell stack on Naphtha ATR reformat vs. Gasoline Phase II reformat vs. pure Hydrogen, cathode and anode pressure is 2.5 bar, Cath. Stoich.=2, Fuel Thermal input 12 kW.

Cathode stoichiometry was maintained at 2 at all the points on polarization chart, while anode stoichiometry reached 1.5 only at the point of maximum power production. Maintaining high Hydrogen utilization at the fuel cell anode at the elevated current densities is a technical challenge associated with the decreased concentration of Hydrogen along it's consumption and increased dilutants – Nitrogen, Carbon Dioxide and water- at the exit of the stack. Maintaining

water balance to avoid stack flooding represent current state-of-the art technology along with the insights of the fuel cell stack, adding complexity to the issue of reformat utilization and, finally, efficiency. Mapping Hydrogen utilization by the fuel cell stack operating on fuel reformat to the current density would result in the stack sizing tradeoff issues versus operating efficiency and would be the subject of separate study.

Conclusion

Fischer Tropsch Naphtha and California Phase II RFG were successfully processed into fuel cell quality reformat using Nuvera's ATR based modular pressurized facility.

Both fuels were studied for Hydrogen production efficiency in the full fuel-to-DC power train and experimental data were compared to the theoretical simulation data. Hydrogen yield and reforming efficiency demonstrated in Naphtha processing were higher in comparison with gasoline Phase II, which had been predicted by system analysis of both fuels. Since gasoline contained sulfur, the power train configuration had an increased complexity and maintaining stable temperature profile became a challenging task in comparison to Naphtha processing.

The power production in the fuel cell stack was not effected by operating on different fuel reformates, since hydrogen partial pressure in the reformat streams varied insignificantly. The gross efficiency of the power production in Fuel Cell is estimated at 25%, considering 3 kW electrical output of the stack and the fuel thermal input of 12 kW.

Both fuel reformates were considered equivalent in terms of containing no poisons to the fuel cells, however, longevity of the fuel cell operation and effects of potential contaminants at micro levels should be the subject of the separate study.

Acknowledgements

This article was prepared with the support of the U.S. Department of Energy, under Award No. DE-FC26-01NT41096.

References

1. Development of OTM syngas process and testing of syngas-derived ultra-clean fuels in diesel engines and fuel cells. Report to DOE, October, **2001**.
2. Design, development and evaluation of hydrocarbon based fuels. B.O. Dabbousi et al. World Petroleum Congress, **2000**, Alberta, Canada
3. Future Wheels. NAVC Report to DARPA November 1, **2000**, Agreement No. NAVC1099-PG030044.

FISCHER-TROPSCH SYNTHESIS OVER COBALT CATALYSTS SUPPORTED ON MESOPOROUS MATERIALS

Kiyomi Okabe, Mingdeng Wei, and Hironori Arakawa

National Institute of Advanced Industrial Science and Technology,
Tsukuba Central #5, Ibaraki 305-8565, Japan

Introduction

Since the discovery of a series of mesoporous silicates (M41S), the materials have been used as the catalysts and support for many catalytic reactions, because of the uniform structure and the tunable mesopore diameters.¹⁻³ It is expected that the wide pores are advantageous to mass transfer of the products and to the chain growth in Fischer-Tropsch (F-T) synthesis. Several papers have been concerned with mesoporous materials as the support for F-T synthesis catalysts up to the present.⁴⁻⁵ However, most of them are supported on mesoporous silica, and the effect of metals incorporated into the silica framework has not been reported. In the present paper, mesoporous aluminosilicate (MPAS) was prepared by the rapid-room temperature preparation method,⁶ and Co-Ir catalysts supported on MPAS were used for F-T synthesis in slurry phase.

Experimental

Hexadecylpyridinium chloride (C_{16} -PyCl) was used as cationic surfactant in the preparation of mesoporous aluminosilicate (MPAS). C_{16} -PyCl (3.0 mmol) was dissolved in 50 cm³ of water. With vigorous stirring and optional heating, HCl was added to the surfactant solution in order to adjust the pH. The clear solutions of $Na_2O \cdot 2SiO_2 \cdot nH_2O$, $Al(NO_3)_3 \cdot 9H_2O$, and NaOH were added dropwise to the surfactant solution, in the molar ratio of (Si+Al)/ C_{16} -PyCl/NaOH/HCl/ H_2O = 1/0.12/1.06-1.27/0.61/141, at room temperature with vigorous stirring. After further stirring for 3 h, the precipitated product was filtered, washed thoroughly with water, dried in an oven at 373 K for 6 h, and calcined in air at 873 K for 6 h to remove the template. Mesoporous silica (MPS) was similarly prepared without adding $Al(NO_3)_3$. The MPS and MPAS thus prepared were impregnated with aqueous solutions of $Co(NO_3)_2 \cdot 6H_2O$ and $IrCl_4 \cdot H_2O$, dried and calcined at 573 K for 1 h, and then reduced in H_2 flow at 673 K for 15 h to form 20wt%Co-0.5wt%Ir/MPS and 20wt%Co-0.5wt%Ir/MPAS catalysts, respectively.

The catalyst powder (2 g) was slurried with 50 cm³ of *n*-hexadecane under an inert atmosphere. The F-T reaction was carried out with the catalyst slurry in an autoclave-type semi-batch reactor (flow type for gas phase). The feed gas ($H_2:CO:Ar = 60:30:10$) was bubbled into the slurry, and the dissolution of the gas was promoted by a specially designed stirring rod.⁷ The reaction conditions were as follows: $T = 503$ K, $P = 1$ MPa, $W/F = 10$ g-catal.h/mol. The effluent gas was periodically analyzed by on-line gas chromatography, and the contents of inorganic gases and C_{1-14} hydrocarbons were determined, with using Ar in the sample gas as the internal standard. The contents of C_{11+} hydrocarbons in the slurry were determined separately by gas chromatography after the reaction.

Results and Discussion

The XRD patterns of MPS and MPAS samples showed three peaks in the region $2\theta = 2-6^\circ$, corresponding to the (100), (110), and (200) reflections of a typical hexagonal lattice, indicating that they were structurally analogous to MCM-41. The N_2 adsorption measurements at 77 K, and the TEM images of MPS and MPAS confirmed the honeycomb structures with one-dimensional channels of ca. 3 nm in diameter. The pore size distribution of the catalysts

demonstrated that the uniform mesopore structure was retained after metal loading, as illustrated in Fig. 1. The MAS-²⁷Al-NMR result indicated that most of Al of MPAS was incorporated into the silica framework, as shown in Fig. 2.

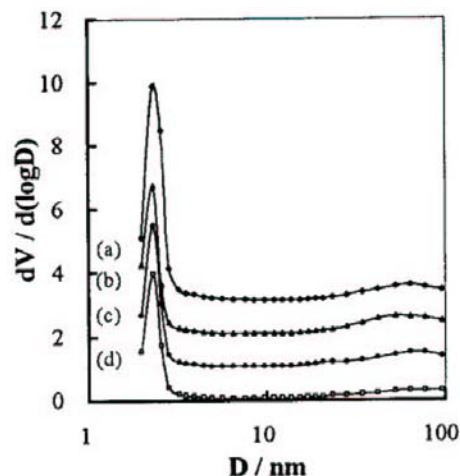


Figure 1. Pore size distribution of (a) MPAS (Si/Al = 29), (b) 5wt%Co/MPAS, (c) 10wt%Co/MPAS, and (d) 15wt%Co/MPAS.

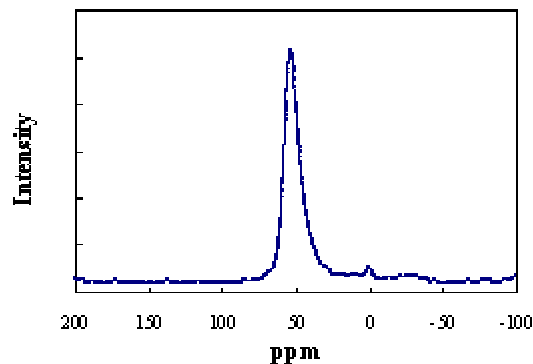


Figure 2. MAS-²⁷Al-NMR spectrum of MPAS (Si/Al = 19).

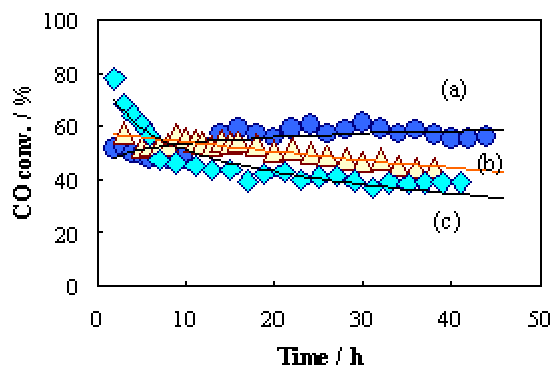


Figure 3. Time course of F-T reaction over (a) 20wt%Co-0.5wt%Ir/MPAS (Si/Al=19), (b) 20wt%Co-0.5wt%Ir/MPS, and (c) 20wt%Co-0.5wt%Ir-1.3wt%Al/MPS catalysts.

Figure 3 shows time course of F-T reaction over Co catalysts supported on MPAS (a), MPS (b), and MPS impregnated with Al (c).

The catalyst supported on MPAS (Si/Al = 19) was more stable than the catalyst supported on MPS, which was gradually deactivated during the reaction. The catalyst supported on MPS with Al-impregnation (Si/Al = 29) was also deactivated. The main difference between catalyst (a) and catalyst (c) is that Al of the former is incorporated into the silica framework, forming a tetrahedral coordination with O, while Al of the latter is in the form of Al₂O₃. Therefore, the framework Al is important for the stable activity of the catalyst.

Table 1. Effect of Catalyst Support on Fischer-Tropsch Reaction in Slurry Phase^{a)}

Catalyst support	CO conv. / %	Selectivity / C-%			α^b
		CH ₄	C ₂₋₄	C ₁₀₋₂₀	
MPAS ^{c)}	56.6	7.9	9.1	31.4	0.90
MPS	50.8	14.2	25.2	13.0	0.76
Al/MPS ^{d)}	42.0	13.0	18.9	20.5	0.77

a) Reaction results at the steady state (average values). b) Chain growth probability. c) Si/Al = 19. d) MPS impregnated with Al (Si/Al = 29).

Table 1 summarizes the F-T reaction results over the catalysts. The values listed are the average during 40 h of the reaction, since some of the catalysts were deactivated. Higher selectivity for C₁₀₋₂₀ hydrocarbons (diesel fuel fraction) and higher α -value (chain propagation probability of the CH_x intermediates of F-T reaction) were obtained over the catalyst supported on MPAS than the catalysts supported on MPS and Al-added MPS, with suppressing CH₄ formation below 8%.

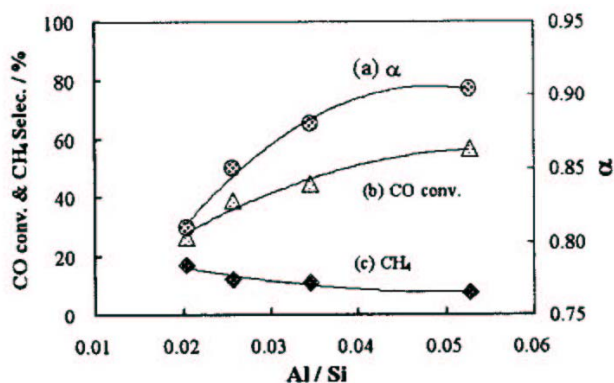


Figure 4. Effect of Al/Si of MPAS on F-T reaction over 20wt%Co/10wt%Ir/MPAS catalysts.

The effect of Al/Si of MPAS on the reaction is depicted in Fig. 4. The α -value and CO conversion increased and C_~ selectivity decreased with Al/Si of MPAS. It is generally accepted that Al incorporated into silica framework gives rise to an acid site. If Al of MPAS played a role of acidity in the F-T reaction, cracking of the products might take place, resulting in an increase of light hydrocarbon selectivity, as well as C_~ formation, and a decrease in the α -value. However, the reaction results were contradictory to the case. And no Brønsted acidity was detected by FT-IR measurement.

Since MPAS was prepared under basic conditions (pH = 10), it is possible that trace amount of Na may remain on the catalyst surface after washing, affecting the F-T reaction. However, neither catalytic activity nor selectivity were improved by adding trace amount of Na to the 20wt%Co-0.5wt%Ir/MPAS catalysts. Therefore, the improved catalytic properties are not ascribed to the impurity which might remain on the surface. The reason for such high catalytic properties has not been elucidated yet, and is now under investigation.

It was previously reported that the pore size of the catalysts affected F-T reaction, and that wide pores were preferable to higher hydrocarbon production.⁸⁾ In addition, the cost of MPAS is generally higher than the commercial silica. Thus, the surface of commercial wide pore silica (Fuji Silysia; Q-50, average pore diameter = 49 nm) was coated with MPAS, and utilized as the catalyst support, in order to reduce the cost of support and to improve the selectivity for higher hydrocarbons. The mixed support was prepared by adding Q-50 silica powder to the surfactant solution in the preparation step of MPAS (Si/Al = 19).

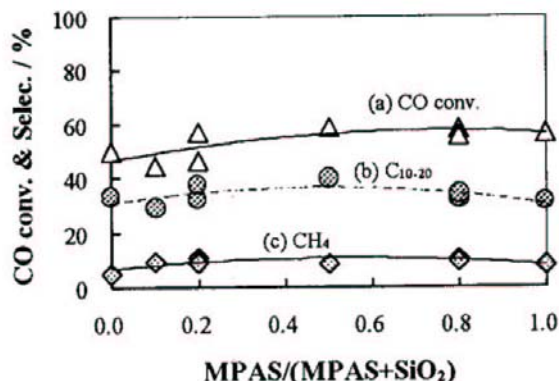


Figure 5. Effect of MPAS content in the support on F-T reaction.

When the mixed support MPAS-SiO₂ was used, a synergistic effect was observed, as illustrated in Fig. 5. The relatively low conversion over the catalyst supported on Q-50 silica was ascribed to the low surface area, although the α -value was high. Over the catalyst supported on MPAS alone, the pore size was so small that the chain growth of the reaction intermediates was limited in the catalyst pores, resulting in low C₁₀₋₂₀ selectivity. Consequently, the highest selectivity up to 40% was obtained over the catalyst supported on 1:1 mixture of MPAS-SiO₂, though the role of Al in the mixed support was not clear so far.

Conclusions

By using CJ6-PyCl as surfactant, mesoporous aluminosilicate (MPAS) was prepared under mild conditions. The Co-based catalyst supported on MPAS showed high and stable activity, and high selectivity for C₁₀₋₂₀ hydrocarbons in F-T synthesis. By using the mixed support of MPAS (Si/Al = 19) and wide pore SiO₂ (Q-50), the selectivity was improved up to 40% at CO conversion of 58.8%.

This investigation was financially supported by JSPS (Contract No. RFTF-98P01001).

References

- (1) Liepold, A.; Roos, K.; Reschetilowski, W.; Esculcas, A. P.; Rochia, J.; Philippou, A.; and Anderseon, M. W. *J. Chem. Soc., Faraday Trans.*, **1996**, *92*, 4623.
- (2) Chen, X.; Huang, L.; Ding, G.; and Li, Q. *Catal. Lett.*, **1997**, *44*, 123.
- (3) Zheng, S.; Gao, L.; Zhang, Q.; and Guo, J. *J. Mater. Chem.*, **2000**, *10*, 723.
- (4) Iwasaki, T.; Reinikainen, M.; Onodera, Y.; Hayashi, H.; Ebina, T.; Nagase, T.; Torii, K.; Kataya, K.; and Chatterjee, A. *Appl. Surf. Sci.*, **1998**, *130-132*, 845.
- (5) Yin, D.; Li, W.; Zhong, B.; and Peng, S. *Chin. J. Catal.*, **2000**, *21*, 221.
- (6) Setoguchi, Y. M.; Teraoka, Y.; Moriguchi, I.; and Kagawa, S. *J. Porous Mater.*, **1997**, *4*, 129.
- (7) Fan, L.; Han, Y.; Yokota, K.; and Fujimoto, K. *Sekiyu Gakkaishi*, **1996**, *39*, 111.
- (8) Okabe, K.; Li, X.; Matsuzaki, T.; Arakawa, H.; and Fujimoto, K. *Sekiyu Gakkaishi*, **2001**, *44*, 135.

Fuel requirements for fuel cell systems

John P. Kopasz, Theodore R. Krause, Shabbir Ahmed and Michael Krumpelt

Argonne National Laboratory, 9700 South Cass Avenue, Argonne, IL 60439

Introduction

Fuel cell vehicles offer the potential for obtaining very low emissions while achieving high fuel efficiency. The efficiency and emissions are related to the fuel choices made for the fuel cell vehicle. Hydrogen is the preferred fuel for fuel cells from the standpoint of onboard emissions and fuel cell performance. However, the hurdles to developing a hydrogen infrastructure have led many to conclude that on-board reforming of hydrocarbon fuels is a practical near-term solution which will allow for the introduction of fuel cell vehicles into the marketplace. Fuels considered for on-board reforming include methanol, gasoline, and diesel fuels. Gasoline has several advantages over methanol, including an existing infrastructure, consumer familiarity, lower costs, and higher hydrogen storage densities. The ability to use gasoline removes problems associated with market introduction of a fuel cell vehicle prior to full development of a new refueling infrastructure, avoiding the "chicken or the egg" problem of introducing a new drive train and fuel supply at the same time. It also reduces the costs for the fuel distributor. However, gasoline is a complex fuel that has been formulated to maximize its performance in internal combustion engines. Questions remain about the suitability of gasoline as a fuel for on-board reforming to hydrogen and whether a current gasoline blend can be utilized in a reformer. Some maintain a fuel-cell grade gasoline is needed, and that additional investments in the infrastructure will be required. The answers to these questions have a substantial impact on the economics for the fuel supplier, and the ease of introduction of a fuel cell vehicle into the market place.

The chemical environment, reaction conditions, and desired products from a fuel processor are quite different than those in an internal combustion engine (ICE), leading to different requirements for the fuels. A comparison of some of the conditions and relevant fuel characteristics are shown in Table I.

Table I. Comparison of ICE to Fuel Processor

	Reaction Phase	Reaction type	Important Fuel characteristics
ICE	Gas Phase	Free radical	Octane #, heat of combustion, flame propagation speed
Fuel Processor	Surface	Catalytic	Hydrogen content, reforming efficiency, Catalyst-fuel interactions, catalyst poisoning

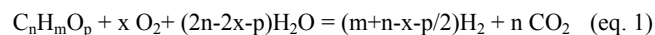
For ICE fuels, composition of the fuel helps control the combustion timing and prevent preignition of the fuel. In fuel processors, timing is not a concern. Of more importance is the hydrogen content of the fuel and the reforming efficiency one can obtain. The efficiency is

related to the fuel composition. For the fuel processor, since the reactions are all conducted catalytically, catalyst poisoning is a major concern. Sulfur impurities are expected to be a major problem. Sulfur is a well-known catalyst poison and may poison the autothermal reforming catalyst, the water gas shift catalyst, and the fuel cell anode catalyst. Evidence suggests that hydrogen sulfide at ppm levels will poison PEM fuel cells. However, sulfur is not the only potential poison. Detergents present in gasoline may result in the formation of ammonia in the processor, which will also poison the fuel cell anode catalyst. In addition, gasoline components such as xylene and mesitylene, which improve octane ratings, may have adverse effects for the fuel processor. In this paper we will review the tolerance of the different subsystems to sulfur and other potential problem components found in today's gasoline formulations

Fuel cell system components

To understand the effects of fuel composition and begin to develop some requirements for fuels for fuel cell systems, we must understand the components of the system. The system consists of the fuel processor, the fuel cell stack, and the radiator/condenser. The fuel processor consists of several subsystems that may be impacted by the fuel. These include the autothermal reformer (ATR), sulfur trap, water gas shift unit (WGS), and a preferential oxidation unit (PROX).

Depending on the catalysts and the fuel utilized, the ATR may be the first catalyst the fuel encounters. In the autothermal reformer the hydrocarbon fuel reacts with water and oxygen to produce hydrogen and carbon dioxide (eq. 1). However, due to equilibria between CO₂, H₂, CO and H₂O, carbon monoxide is also observed in the product gas.



The ATR utilizes precious metal or Ni based catalysts at temperatures on the order of 700-800°C. The exhaust from the ATR is directed to a sulfur removal unit to reduce the sulfur content. For catalysts that are not sulfur tolerant, such as Ni based catalysts, sulfur removal must be performed prior to the ATR. Sulfur removal at this point may be more complicated, since the sulfur can exist in several different forms, while after the ATR the sulfur will be present as H₂S. Generally, the sulfur removal unit proposed after an ATR is a ZnO based system. The operating temperature of this unit is in the range of 300°C. Recent advances suggest that sulfur levels can be decreased to sub ppm levels using this technology.^{1,2}

From the sulfur removal unit the product gas passes through the water gas shift catalysts, which reduce the CO concentrations from ~10% to less than 1%. Traditionally, the water gas shift catalyst is divided into a high-temperature bed and a low-temperature bed. The high temperature shift catalysts being iron-chrome based and operating at temperatures from ~350-400°C, while the low-temperature shift catalysts have been copper based and operated in the range of 200-250°C. After the water gas shift catalyst the CO concentration must be reduced further before entering the PEM fuel cell. Generally designs call for a preferential oxidation catalyst that selectively oxidizes CO in the presence of hydrogen and reduces the CO levels to less than 100 ppm. This is generally a low temperature catalyst.

Sulfur tolerance. Sulfur is a main concern in the fuel processor and in the fuel cell stack, however some advances have been made in improving the sulfur tolerance of fuel processor components. Traditionally, steam-reforming catalysts have been utilized in the ATR. These catalysts, which are generally nickel based, are readily

poisoned by sulfur. Recently, new catalysts based on noble metals on oxide-ion conductors have been developed. The Pt catalysts have demonstrated operation with a feed containing 50 wppm sulfur for >1000h with temperature cycling to simulate startup/shutdown without degradation of the catalyst.³ Non-precious metal based catalysts quickly degraded due to coke formation when sulfur was present in the fuel at these levels. The Pt catalyst operated for short periods of time with up to 1000 wppm sulfur without a significant decrease in performance.³

The downstream catalysts are much more susceptible to sulfur poisoning than the ATR catalysts, due to the lower operating temperature and increased adsorption of sulfur at the lower temperatures. In addition, the metals used in these catalysts (Ni, Fe, Cu) tend to have higher sulfur adsorption than Pt at a given temperature. Therefore, sulfur adsorption beds are needed to protect these catalysts and the fuel cell. Difficulties arise in sulfur adsorption after the ATR due to the high hydrogen and water content of the product gas stream. The high hydrogen and water concentrations in the gas phase drive the equilibria shown in eq. 2 toward H₂S(g). In addition, kinetics for H₂S adsorption have been slow. Addition of promoters, such as Ni, to the ZnO beds has provided for increased kinetics and improved operation under conditions with high H₂ and H₂O partial pressures. Utilizing these improved ZnO technologies, sulfur laden feed streams have been polished down to less than 0.03 ppm sulfur in the exit stream.^{1,2}

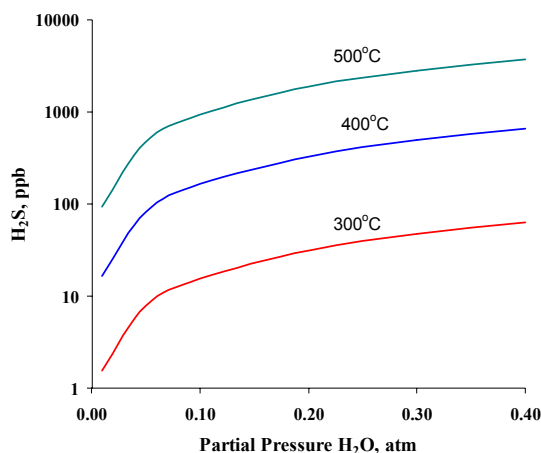
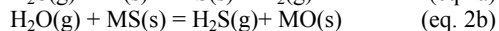
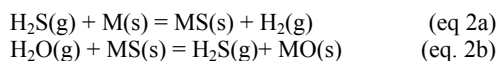


Figure 1. Effect of water concentration on equilibrium H₂S concentration above ZnO at 500, 400, and 300°C.

New shift catalysts and configurations are also being developed which show some sulfur resistance.⁴ Nobel metal based shift catalysts show potential for operation in simulated reformat containing sulfur at ppm levels without degradation in performance. While sulfur tolerant shift catalysts will not remove the need for a sulfur removal bed, it allows for further flexibility in the placement of the bed and may allow for operation at a more favorable temperature range for sulfur adsorption.

The anode catalyst is also susceptible to sulfur poisoning. The low temperature of operation for the anode catalyst leads to high sulfur coverage, poisoning the sites for reaction with hydrogen. The effects of ppm levels of H₂S on the cell performance have been demonstrated. After 5 h of operation with 1 ppm H₂S in the anode

feed Uribe et. al. observed a decrease in cell voltage of 50%.⁵ With 200 ppb H₂S, they observed a 50% decrease in cell voltage in less than 200h. The rate of the drop in cell performance varied linearly with H₂S concentration.⁵ The effects of sulfur poisoning of the anode are reversible, and cell performance after exposure to 30 wppm S could be returned to the same level of performance as without sulfur using potentiometric oxidation.⁵

Detergent additives. Detergent additives are needed for ICE to prevent clogging and fouling of fuel injectors, which leads to increased emissions. In a reforming environment, detergents may lead to poisoning of the fuel processor catalysts. Experiments utilizing n-secbutylamine as a surrogate for polyamine based detergents indicate that 50 wppm of the amine decreases the performance of the catalyst at temperatures below 750°C (fig. 2). However, at temperatures above 750°C, the performance appears to be unaffected. At these higher temperatures, the amine itself is reformed and the products from the reforming include ammonia. Equilibrium calculations indicate that the equilibrium ammonia concentration is in the ppm range. However, the catalysts downstream of the ATR reactor are susceptible to poisoning from ammonia at these levels. These catalysts operate at much lower temperatures than the ATR, and ammonia is expected to adsorb to the reactive sites of the water-gas shift, PROX, and anode catalysts. Ammonia is a known poison for copper based low-temperature shift catalysts. High-temperature shift catalysts have been developed which are resistant to ammonia poisoning.⁴

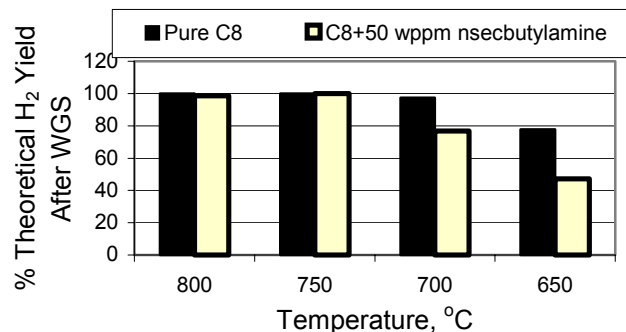


Figure 2. Comparison of hydrogen yield after taking credit for water-gas shift reactions for reforming pure isooctane and isooctane+50 wppm n-secbutylamine.

At the fuel cell stack, ammonia is an even greater problem. In addition to potentially poisoning the anode catalyst site, ammonia can also ion exchange with protons in the polymer electrolyte. Uribe and coworkers observed a substantial decrease in cell performance with ammonia content as low as 13 wppm.^{5,6} They observed a very slow recovery of the cell upon removal of ammonia after short term exposures and observed irreversible degradation after long-term exposure to 30 wppm NH₃. They attributed this to ion exchange in the anode catalyst layer for short-term exposures and ion-exchange with the bulk occurring for long-term exposures. After long-term exposure (15 h) to 30 ppm NH₃, the degradation was found to be irreversible.⁶ Ammonia can be effectively removed from the gas stream using ion-exchange resins to provide an ammonia free stream to the fuel cell.

Aromatics and naphthenes. Aromatics and naphthenes present in fuels can lead to decreased efficiencies. Aromatic components require higher temperatures to reform.³ The higher temperatures combined with lower hydrogen to carbon ratios lead to reduced

reforming efficiency. For example, the theoretical efficiency for autothermally reforming isooctane (defined as the lower heating value of the fuel in divided by the lower heating value of the theoretical amount of hydrogen out) is 90%, while that for toluene is 88%. In addition, aromatics and naphthenes have been found to decrease the conversion of paraffinic components in a multicomponent fuel.⁷

Water requirements. The fuel processor requires high-purity water. For utility applications, this water may be available on-site, but for transportation applications, the process water must be recovered from the fuel cell system exhaust gas. For such applications, it is critically important that the fuel cell system be a net water-producing device. A variety of environmental conditions (e.g., ambient temperature, pressure), fuel cell system design, and operating conditions determine whether the fuel cell system is water-producing or water-consuming. The fuel also has a substantial impact on the water balance. Aromatic components again are detrimental. Operating under atmospheric pressure at thermo-neutral conditions, with fuel utilization at the anode of 80% and an air stoichiometry at the cathode of 2.5, an exhaust gas temperature of 42.7°C is needed to obtain water balance for isooctane as a fuel. For the same conditions, an exhaust temperature of 34°C (only 93°F) or lower is needed to obtain water balance with toluene as the fuel. This exhaust gas temperature would be unobtainable over much of the United States during a substantial portion of the driving season. Water balance can be obtained by operating at higher pressures, lower fuel utilization, or lower air stoichiometries, however; these all decrease the system efficiency.⁸

Conclusion

The requirements for fuels for fuel cell systems are still evolving as improvements in catalysts designed for fuel cell systems continue. Catalyst poisons, such as sulfur and amines, can be dealt with on-board the vehicle, however; this adds complexity to the fuel processor and may impact overall efficiency due to added vehicle weight. Requirements for water self-sufficiency and high reforming efficiencies may also limit the aromatic content of fuels used for on-board reforming to hydrogen for fuel cell vehicles.

Acknowledgement. This work was supported by the U.S. department of Energy, Office of Advanced Automotive Technologies, in the Office of Transportation Technologies, under contract No. W-31-109-ENG-38.

References:

- (2) (1) Novochinskii, I.I.; Ma, C.; Song, C.; Lampert, J.K.; Shore, L. . Preprints of the AIChE Spring 2002 Meeting, New Orleans, LA, **2002**
- (3) Tawara, K.; Nishimura, T.; Iwanami, H.; Nishimoto, T.; and Hasuike, T. *Ind. Eng. Chem. Res.* **2001**, 40, 2367.
- (4) Kopasz, J.P.; Miller, L.E.; Ahmed, S.; Devlin, P.; Pacheco, M, **2001**, SAE Technical paper Series 2001-01-1915.
- (5) Carstensen, J.H.; Boglid-Hansen, J.; Pedersen, P.S. *Hydrocarbon Processing*, **1990**,57.
- (6) Uribe, F.A.; Gottesfeld, S.; Zawodzinski, T. 2001, presented at the 200th Meeting of the Electrochem. Soc., San Francisco, CA, **2001**.
- (7) Uribe, F.A.; Gottesfeld, S.; Zawodzinski, T. *J. Electrochem. Soc.* **2002**,149(3),A293.
- (8) Kopasz, J.P.; Miller, L.E.; Ahmed, S.; Devlin, P.; Pacheco, M. to be published in 2002, SAE Technical Paper Series
- (9) Kopasz, J.P.; Ahmed, S.; Kumar, R.; Krumpelt, M. Preprints of the AIChE Spring 2002 Meeting, New Orleans, LA., **2002**

Hydrodehalogenation with Mo₂C and W₂C

James D. Oxley, Millan M. Mdleleni and Kenneth S. Suslick

School of Chemical Sciences
University of Illinois at Urbana-Champaign
600 S. Mathews, Box 43-6
Urbana, IL 61801

Introduction

The environmental impact of chlorofluorocarbons (CFC's) and polychlorinated biphenyls (PCB's) has led to the strict regulation of halocarbons. Disposal of existing hydrocarbon contaminants and the prevention of future pollution is a serious problem that remains to be solved. Oxidative incineration of halocarbons can lead to more toxic secondary pollutants such as furans and dioxins. A promising solution is the hydrodehalogenation (HDH) of halogenated organic compounds to non-halogenated hydrocarbons.¹⁻³ Limited success has been achieved with various supported catalysts including Pd, Pt and Rh. However, these catalysts exhibit poor selectivity and are prone to attack by HCl produced during hydrodechlorination.⁴⁻⁹ Recently, our group reported the sonochemical synthesis and catalytic dehydrogenation activity of molybdenum carbide (Mo₂C).^{10,11} As part of ongoing studies in this laboratory concerned with heterogeneous catalysis over sonochemically prepared catalysts, the activity, selectivity and stability of sonochemically prepared Mo₂C and W₂C in HDH of several halogenated organics have been examined.

Experimental

The high purity (>99.5 %) halogenated hydrocarbons used in the present study were purchased from Aldrich and were used as received. Dichlorofluoromethane (CFC-12) was obtained from Mattex Service Company (Champaign, IL) and chlorodifluoromethane (CFC-22) was purchased from S.J. Smith. Organic solvents were purified, degassed and stored in an inert atmosphere (< 0.5 ppm O₂) glove box. Methane (99.99% purity), hydrogen (99.99% purity), and Helium (99.9% purity) were purchased from S.J. Smith and were further purified by passing through oxytraps prior to use.

Synthesis of Molybdenum and Tungsten Carbide. The sonochemical molybdenum carbide (Mo₂C) was prepared and characterized as previously described.¹⁰ Typically, a slurry of molybdenum hexacarbonyl (Mo(CO)₆, 2.5 g, 9.5 mmol) in 35 mL of hexadecane was irradiated with high intensity ultrasound (20 kHz, 80 W/cm², 1 cm² titanium horn; Sonics & Materials VCX600) for 3 h at 80°C under argon. The resulting black powder was filtered and washed several times with purified degassed pentane inside an argon-filled glove box. The washed powder was then heated to 80°C for 3 h under vacuum to sublime off the unreacted Mo(CO)₆. Oxygen contaminants were removed by heating the amorphous product to 500°C for 12 h under a flowing (30 cm³/min) CH₄/H₂ (1:1 ; v:v) atmosphere. The latter treatment also leads to crystallization of the initially amorphous carbide. Elemental analysis of the treated powder gives a Mo/C atomic ratio of 1.97, indicative of a stoichiometric Mo₂C. Tungsten carbide (W₂C) was prepared with tungsten hexacarbonyl using similar conditions. All parameters were the same except the sonication temperature of 90°C.

Catalysis. Fixed bed single-pass quartz and borosilicate microreactors operated at atmospheric pressure were used for all catalytic reactions. The vapors of the liquid substrates were carried from a thermally equilibrated saturator by a flow (flow rate = 27.5

cm³ (STP)/min) of purified hydrogen and helium. The flow rates were monitored with digital mass-flow controllers (MKS). The reaction products were analyzed with an on-line gas chromatograph (Hewlett-Packard 6890) mass spectrometer (Hewlett-Packard 5973) and a (35%-Phenyl)-methylpolysiloxane capillary column (Agilent DB-35MS).

Results and Discussion

The HDH activities of aryl halides with Mo₂C and W₂C are shown in Figure 1a. The HDH of aryl halides with Mo₂C leads exclusively to benzene, with activities following the unusual pattern of C₆H₅I < C₆H₅Br < C₆H₅Cl < C₆H₅F. With the exception of C₆H₅F, the activity of W₂C is greater than Mo₂C and follows a similar pattern. The catalysts are active at ambient pressure and low temperatures. Despite the high hydrogen to substrate ratio we observe *no* hydrogenation products. From figure 1b, the decrease in activity is less than 15% after 100 h and the calculated half-life of the sonochemically prepared Mo₂C catalyst is 350 h. Preliminary time-on-stream studies with chlorobenzene indicate W₂C has a longer half-life and greater stability than Mo₂C.

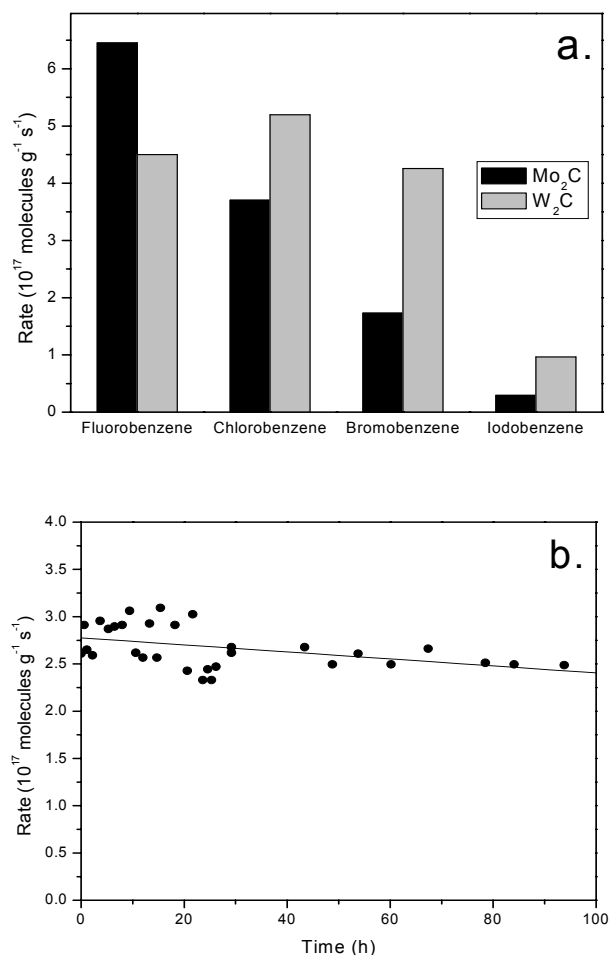


Figure 1: Catalytic activity of Mo₂C and W₂C for the HDH of halobenzenes with partial pressure = 7 mbar, P_{substrate}/P_{H₂} = 1:200, temperature at 300°C, and flow rate = 27 cm³ (STP)/min.; **a.** Activity for halobenzenes (P_{fluorobenzene}/P_{H₂} = 1:100); **b.** Activity for chlorobenzene with Mo₂C as a function of time-on-stream at 300°C.

The HDH of hexafluorobenzene with sonochemically prepared Mo₂C and W₂C is shown in Figure 2. After 12 hours, the activities for Mo₂C and W₂C at 300°C are 4.5x10¹⁷ and 2.2x10¹⁷ molecules g⁻¹ s⁻¹, respectively. The rates increase with temperature and the selectivities are temperature dependent. Above 400°C, benzene is the only product from the HDH of hexafluorobenzene with Mo₂C. The lower activity of W₂C with respect to Mo₂C is consistent with the trend observed for fluorobenzene.

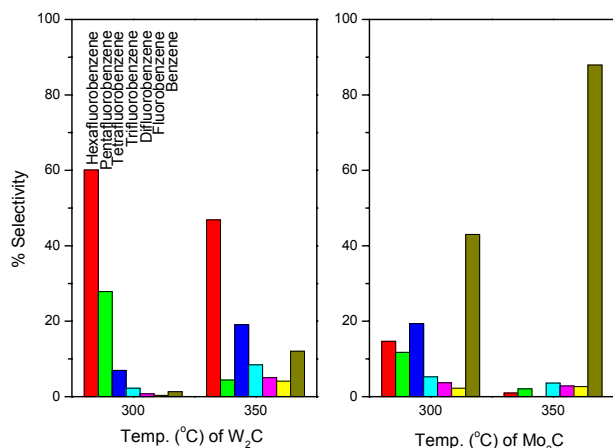


Figure 2. Catalytic selectivity of sonochemically prepared Mo₂C and W₂C for the HDH of hexafluorobenzene; Conditions: Substrate partial pressure = 29 mbar, P_{substrate}/P_{H₂} = 1:196, and flow rate = 27.5 cm³(STP)/min.

Several HDH studies were carried out with chlorocyclohexane, 1-chlorobutane, and 1-chloropropane under similar experimental conditions used for the halobenzenes. The hydrodechlorination (HDC) rate for chlorocyclohexane, 3.6x10¹⁸ molecules g⁻¹ s⁻¹ at 300°C, is at least an order of magnitude faster than the rate observed with chlorobenzene. Methylcyclopentane was the only product observed. The HDC of 1-chlorobutane and 1-chloropropane resulted in rates approximately five times greater than those observed with chlorobenzene. The majority of the products were dehydrogenated analogues of butane and propane. The higher rates of these substrates are consistent with the lower bond dissociation energy for the C_{aliphatic}-Cl versus the C_{arene}-Cl bond.¹²⁻¹⁴

The HDH of CFC's with sonochemically prepared Mo₂C results in methane as the major observed product. The activity at 300°C is 1.5x10¹⁹ molecules g⁻¹ s⁻¹. The rate increases with temperature and the selectivity is temperature independent. Figure 3 illustrates the distribution of products from the HDH of dichlorodifluoromethane (CFC-12). A similar activity and selectivity (> 75% methane) was observed with chlorodifluoromethane (CFC-22). The selectivity towards methane differs from the selectivity observed with a conventional W₂C catalyst.¹⁵ The HDH of CFC-22 with conventional W₂C gives CH₂F₂ (CFC-32) as the major product. No halogen-exchange products were detected during the HDH of either CFC.

Based on previous success with supported sonochemically prepared catalysts, we studied the HDH activity of sonochemically prepared Mo₂C supported on HZSM-5, activated carbon and Al₂O₃.^{16,17} The activities (per g of metal) of Mo₂C/ZSM-5 and Mo₂C/C_{activated} for the HDH of chlorobenzene were similar to the unsupported catalyst. No activity was observed with the Al₂O₃ supported catalyst.

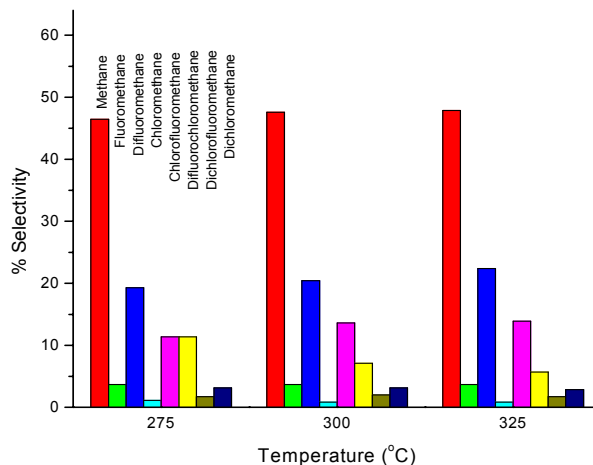


Figure 3: Catalytic selectivity of sonochemically prepared Mo₂C for HDH of CFC-12; Conditions: Substrate partial pressure = 100 mbar, P_{substrate}/P_{H₂} = 1:9, and flow rate = 27.5 cm³(STP)/min.

Conclusion

We have demonstrated that sonochemically prepared Mo₂C and W₂C are active, stable, and selective catalysts for the HDH of halocarbons. The activity of Mo₂C is greater towards fluorocarbons while the activity of W₂C is greater for chloro-, bromo-, and iodocarbons. Other halocarbons to be studied include chlorophenols, PCB's and polybromo diphenyl ethers (PBDE's).

Acknowledgement. This work is supported by the National Science Foundation under Grant CHE-00.

References

- Olie, K.; Vermeulen, P. L.; Hutzinger, O. *Chemosphere* **1977**, *6*, 455.
- Ahling, B.; Lindskog, A.; Jansson, B.; Sundstrom, G. *Chemosphere* **1977**, *6*, 461.
- Buser, H. R.; Bosshardt, H. P. *Chemosphere* **1978**, *7*, 165.
- Coq, B.; Farrat, G.; Fiqueras, F. *J. Catal.* **1986**, *101*, 434.
- Harper, R. J.; Kemball, C. *Trans. Faraday Soc.* **1969**, *65*, 2224.
- Coq, B.; Farrat, G.; Fiqueras, F. *React. Kinet. Catal. Lett.* **1985**, *27*, 157.
- Srinivaas, S. T.; Lakshmi, L. J.; Lingaiah, N.; Prasad, P. S. S.; Rao, P. K. *Appl. Catal. A* **1996**, *135*, L201.
- Creyghton, E. J.; Burgers, M. H. W.; Jansen, J. C.; Van Bekkum, H. *Appl. Catal. A* **1995**, *128*, 275.
- Choi, H. C.; Choi, S. H.; Lee, J. S.; Lee, K. H.; Kim, Y. G. *J. Catal.* **1997**, *166*, 284.
- Hyeon, T.; Fang, M.; Suslick, K. S. *J. Amer. Chem. Soc.* **1996**, *118*, 5492.
- Suslick, K. S.; Hyeon, T.; Fang, M. *Chem. Mat.* **1996**, *8*, 2172.
- Benson, S. W. *Thermochemical Kinetics*; 2nd ed.; Wiley and Sons: New York, 1976.
- Benson, S. W. *J. Chem. Phys.* **1958**, *29*, 546.
- Lide, D. R., Ed. *Handbook of Chemistry and Physics*; CRC Press: Boca Raton, 1993.
- Sherif, F. G. U.S. Patent 5426252, 1995
- Dhas, N. A.; Ekhtiarzadeh, A.; Suslick, K. S. *J. Amer. Chem. Soc.* **2001**, *123*, 8310.
- Danstin, G.; Suslick, K. S. *J. Amer. Chem. Soc.* **2000**, *122*, 5214.

Influence of Composition and Morphology on Photo and Electrocatalytic Activity of Electrodeposited Pt/WO₃

S. H. Baeck, T. Jaramillo, and E. W. McFarland

Department of Chemical Engineering
University of California
Santa Barbara, California 93106-5080

Introduction

Methanol oxidation, which is a multi-dehydrogenation process, has been strongly investigated for methanol-air fuel cells (DMFCs)[1-3]. However, the activities of commercial catalysts are still low. Platinum, a well-known catalyst for methanol oxidation, is easily poisoned by reaction intermediates. Intermediates such as CH_xO strongly adsorb on the platinum surface and permanently bind to the active site, thus preventing further reactions from taking place [4, 5]. To improve catalytic activity, platinum alloys, generally Pt-Ru, have been studied [6, 7]. Unfortunately, the alloy is electrochemically unstable because Ru dissolves at elevated potentials. In an attempt to increase the stability of methanol oxidation catalysts, a great number of researchers have investigated platinum or platinum alloys supported on metal oxides [8-10]. Shen and Tseung [11] reported that a Pt/WO₃ electrode showed promise as a catalyst for methanol oxidation – WO₃ can oxidize reaction intermediates, thus enhancing both the activity and stability of the catalyst. For this system, both the amount of platinum and the dispersion of platinum are of key importance.

WO₃ of several different crystal structures has been prepared by a variety of physical and chemical methods [12, 13]. Electrochemical deposition methods have also been used to synthesize WO₃ by dissolving Na₂WO₄ in sulfuric acid [14] or tungsten powder in hydrogen peroxide [15, 16]. The electrodeposition method has many advantages over other synthesis routes in terms of economics and flexibility for making large area WO₃ films. Pt and WO₃ can be electrochemically co-deposited using a hydrogen peroxide solution [17-19].

For the synthesis of Pt or Pt/WO₃ catalysts, we used four different methods: continuous electrochemical co-deposition, pulsed electrochemical co-deposition, serial electrochemical deposition (deposition of Pt on the surface of previously electrodeposited tungsten oxide), and electron beam evaporation of Pt on the surface of previously electrodeposited tungsten oxide. We addressed the following questions: 1) What is the role of tungsten oxide in methanol oxidation? 2) Can particle size and morphology of Pt/WO₃ be used to improve the catalytic activity for methanol oxidation? 3) What is the effect of the Pt/WO₃ ratio on the photocatalytic and electrocatalytic activity?

Experimental

E-beam evaporated Pt was fabricated in a Class 10,000 cleanroom environment. Electrodeposited tungsten oxides on Ti foil were placed in the high vacuum (~ 10⁻⁷ Torr) evaporation system and Pt was deposited at a rate of 1-1.5 Å/sec.

For the electrodeposition of tungsten oxide, the stabilized W-peroxo electrolyte was prepared by dissolving 1.83g of tungsten powder in 60ml of a 30% hydrogen peroxide solution. The excess hydrogen peroxide was subsequently decomposed with platinum black. The solution was diluted to 50mM with a 50:50 mixture of water and isopropanol. For the electrodeposition of platinum, 50mM chloroplatinic acid was used. For co-deposition of Pt/WO₃, the electrolyte consisted of 50 mM W-peroxo and various concentrations of chloroplatinic acid (1 mole % to 50 mole %), which allowed for control of the deposited Pt/WO₃ ratio. Both pulsed and continuous

electrodeposition were used; electrochemical pulses were 5 msec in duration, and for series deposition, the Pt/WO₃ ratio was controlled by varying the deposition time of Pt on WO₃ from 5 min to 30 min. The cathodic-potentiostatic deposition was performed using a conventional three electrode system (EG&G 273A) with Pt as a counter electrode and SCE as a reference electrode.

Following synthesis, samples underwent more detailed quantitative analysis. Scanning electron microscopy (Philips, XL-30 ESEM-FEG) and electron stimulated energy dispersed x-ray spectroscopy (Princeton Gamma Tech, IMIX) were performed to give surface morphology and composition. X-ray diffraction (Scintag, X2) was used to examine the crystal structures. The amount of platinum was calculated using the weight of deposits and the Pt/WO₃ ratio determined from EDS.

The electrocatalytic activity of Pt/WO₃ was measured in a solution of 0.5M MeOH and 0.5M H₂SO₄. The measurements were carried out from 0 to 0.8V vs SCE at room temperature. Testing for zero bias photocurrent utilized an electrochemical cell described in detail elsewhere [17]. Electrolytes, either 0.1M sodium acetate or 0.5M methanol, were pumped automatically into the cell and the electrical current was measured while the surface was illuminated with a chopped light source (Oriel, Xe 150W, chopped at 100 Hz). Due to losses through the optical fiber, the light intensity incident on the sample was approximately 25 mW/cm².

Results and Discussion

As-deposited tungsten oxide films were confirmed to be amorphous. XRD confirmed that crystalline films were obtained after 450°C calcination in air. Prior to testing, all samples were calcined as such immediately after deposition.

E-beam evaporated Pt exhibited a very smooth and dense surface, while electrodeposited Pt had a very rough morphology. Generally, e-beam evaporation of metals at slow rates and at low pressure is conducive to layer-by-layer growth, which accounts for the smooth and dense film.

Fig. 1 shows SEM photographs of Pt/WO₃ films prepared by various electrochemical methods: pulsed co-deposition (a), continuous co-deposition (b), and series deposition (c). In the case of the continuous co-deposited Pt/WO₃ film, large distinct clusters of platinum particles were easily seen on the tungsten oxide surface.

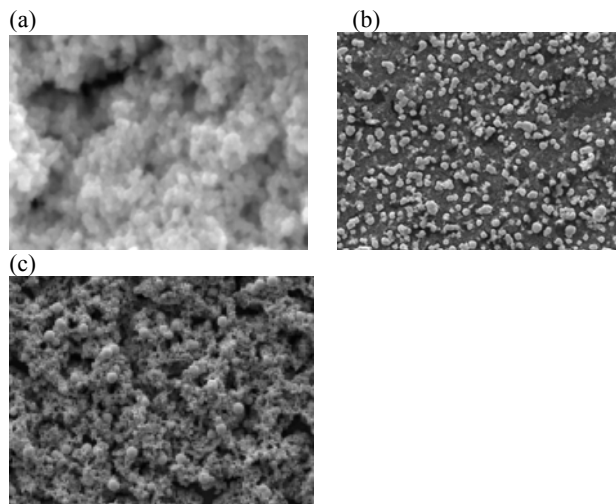


Figure 1. SEM photographs of (a)pulse electrocodeposited Pt/WO₃, (b)continuous codeposited Pt/WO₃, and (c) series deposited Pt/WO₃. In all cases substrate was Ti foil.

When Pt was electrodeposited on the tungsten oxide (series deposition), spheres of Pt were observed on the tungsten oxide surface and the particles were much larger than those of tungsten oxide. When we pulse co-deposited Pt with WO_3 , a very homogeneous phase was observed and the particle size was significantly smaller than that observed with the other two methods. Pulsed electrodeposition with short, high potential pulses can be used to nucleate particle growth at a higher number of sites than with lower voltage continuous deposition [20, 21].

Pt supported on different metal oxides has been studied for methanol oxidation, with certain catalysts showing higher activity than pure platinum [8, 9, 11]. However, in these references there was no mention of the absolute amount of platinum within the catalytic systems investigated. In each case, Pt is believed to be an active site for methanol oxidation, so the total platinum content of each catalyst must be known in order to accurately compare activities. To address this concern, we compared catalytic activities of Pt e-beam evaporated on WO_3 versus Pt evaporated on a Ti-foil substrate, Fig. 2.

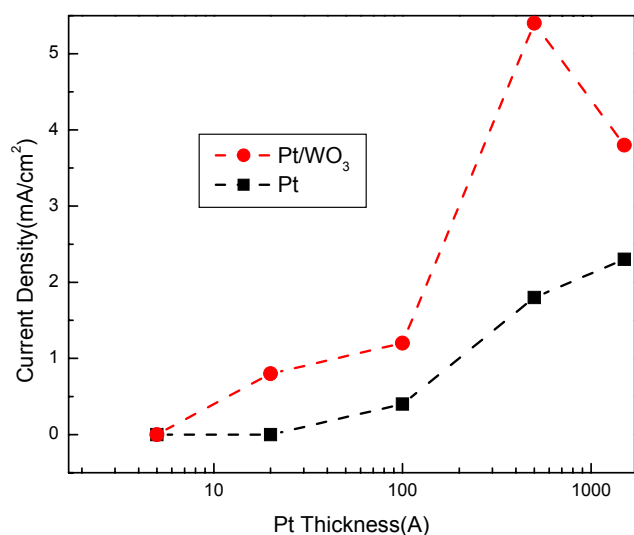


Figure 2. Current density for methanol oxidation of e-beam deposited Pt (square) and e-beam deposited Pt/ WO_3 (circle) as a function of thickness of Pt.

The two kinds of substrates were evaporated upon simultaneously to ensure the same Pt thickness, which was varied from 5 to 1500 Å. In case of Pt films on Ti foil, activity for methanol oxidation was observed only for Pt thickness of 100 Å or greater. Activity increased with thicker films, with a limit of 2.7 mA/cm² reached at a thickness of 1500 Å. Tungsten oxide itself has no activity for methanol oxidation. Methanol oxidation was observed with as little as 50 Å of Pt deposited on the tungsten oxide, and activity increased with increasing Pt thickness up to 500 Å, 5.4 mA/cm². The catalytic activity of 1500 Å Pt supported on WO_3 was lower than that of 500 Å Pt/ WO_3 , indicating that the thick Pt layer prevents exposure of WO_3 to the reactants, thus resulting in decreased catalytic activity. This reveals the importance of Pt- WO_3 interfaces for this reaction. One can observe that in every case, Pt deposited on tungsten oxide films showed higher current density for methanol oxidation than the same amount of Pt alone. We concluded that Pt/ WO_3 is a better catalyst for methanol oxidation than pure platinum.

Electrodeposited Pt showed 25 times higher current density for methanol oxidation than e-beam deposited Pt. This result can be explained by the great difference of surface morphologies between

the two samples. The surface of electrodeposited Pt was very rough and porous, while that of e-beam deposited Pt was smooth and dense. The rough morphology of electrodeposited films can be attributed to the mass transfer limitations of a solid-liquid interface during rapid deposition [22]. This yields a high surface area, leading to greater catalytic activity.

Table 1. Comparison of Catalytic Activities for Methanol Oxidation

Sample	Pt/ WO_3	Pt amount (mg)	Catalytic activity (mA/cm ² .mg Pt)
Electrodeposited Pt	-	2.6	14.1
Series deposited Pt/ WO_3	1.31	2.4	18.4
Continuous codeposited Pt/ WO_3	1.42	2.9	17.4
Pulse codeposited Pt/ WO_3	1.22	2.8	25.6

Catalytic activities for methanol oxidation were investigated for electrodeposited Pt/ WO_3 films, Table 1. We prepared Pt/ WO_3 films by three electrochemical methods: continuous co-deposition, pulsed co-deposition, and series deposition. The Pt/ WO_3 film prepared by pulsed co-deposition showed the highest activity for methanol oxidation, 25.6 mA/(cm² mg Pt), Table 1.

The differences in catalytic activity observed for the three electrochemical methods of preparation can be attributed to their differences in surface morphology, Fig. 1. Large clusters of Pt were found to exist on the surface of the WO_3 films prepared by series deposition or continuous co-deposition. Pulsed co-deposited Pt/ WO_3 films, meanwhile, exhibited great homogeneity and small particle size. These morphological features equate to a great number of Pt/ WO_3 interfaces, which makes for a very effective methanol oxidation catalyst.

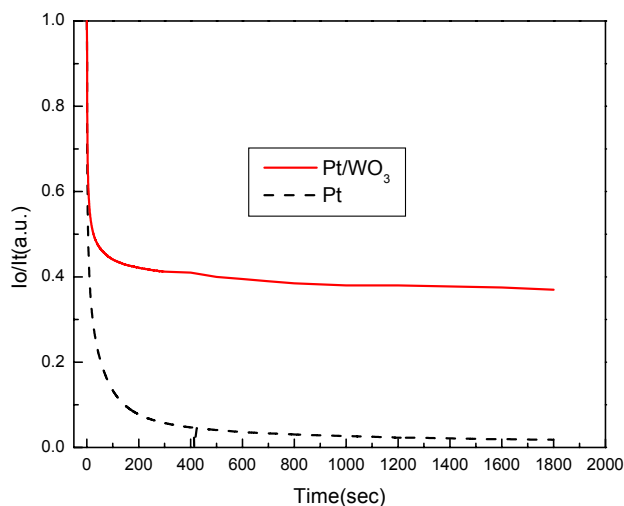


Figure 3. Current density with time on stream at 0.6V on Pt electrode (dashed line) and Pt/ WO_3 electrode (solid line)

Long-term oxidation of methanol was performed at a constant potential of 0.6V for both electrodeposited Pt and pulsed co-deposited Pt/WO₃. As shown in Fig. 3, the pure Pt electrode suffered from rapid deactivation to less than 2% of its initial current density within 10 minutes, most likely due to heavy poisoning. The Pt/WO₃, however, demonstrated a relatively high current density. Although it dropped to approximately 40% of its initial value after 5 minutes, it remained steady at that level for the next half-hour, showing little sign of decay. We can conclude that the Pt/WO₃ system is much more active and stable than the Pt electrode. It is well known that partially dehydrogenated intermediates may act as poisons [4, 5, 11]. The presence of WO₃, a known oxidizing material, can remove such intermediates by dehydrogenation, resulting in an increase of both activity and stability.

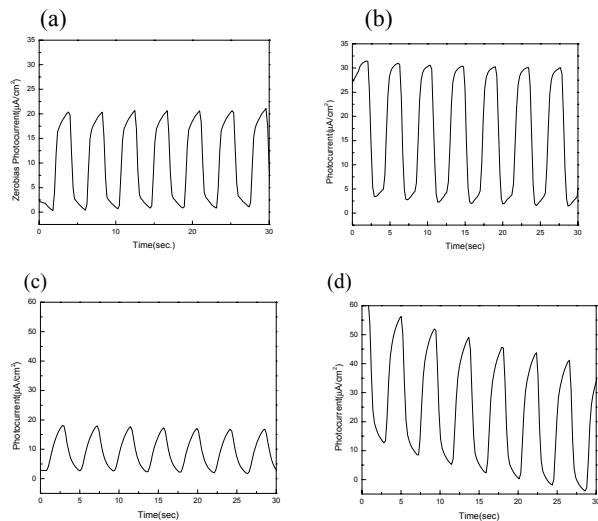


Figure 4. Zerobias photocurrents of WO₃(a, c) and 2.3% Pt/WO₃(b, d) in 0.1M sodium acetate electrolyte(a, b) or 0.5M methanol electrolyte(c, d).

Zerobias photocurrent was measured under chopped illumination for pure tungsten oxide and for 2.3% Pt doped tungsten oxide prepared by pulsed electrochemical co-deposition. Two different electrolytes were used – 0.1M sodium acetate solution (Fig. 8(a, b)) and 0.5M methanol (Fig. 8(c, d)). The measurement of zero bias photocurrent is an indirect means of screening for photocatalytic activity. Our previous work [19] showed that photoactive Pt/WO₃ could be obtained only when small amounts (below 5%) of highly dispersed platinum were added to tungsten oxide. Pt/WO₃ films with a large atomic ratio of platinum to tungsten tend to be photoinactive, presumably due to inhibited photon absorption. 2.3% Pt doped tungsten oxide showed higher photocurrent than pure tungsten oxide in both sodium acetate and methanol electrolytes.

Our results indicate that the requirements of an electrocatalyst are very different from those of a photocatalyst. A large atomic ratio of Pt to WO₃ yields a very effective electrocatalyst for methanol oxidation, whereas a low ratio of Pt to WO₃ is required for good photocatalysts.

Conclusions

Catalytic activity for methanol oxidation was investigated for different Pt doped tungsten oxide films synthesized by various methods based upon electrochemical deposition and electron beam evaporation. The electrocatalytic activity of these films depended significantly upon the method of preparation, which can be explained

by the vastly different morphologies of the films. The Pt/WO₃ film prepared by pulsed electrochemical co-deposition showed highest activity for methanol oxidation. This film exhibited a very homogeneous phase, which makes for a great number of Pt/WO₃ interfaces, thus explaining its effectiveness. Pt/WO₃ samples were compared to pure Pt samples (each sample contained the same weight Pt), and it was found that Pt/WO₃ is much more stable and active for methanol oxidation than pure platinum. It was also found that the requirements for an electrocatalyst are very different from those for a photocatalyst. A large atomic ratio of Pt to WO₃ improves the electrocatalytic properties of the material for methanol oxidation, while materials with low ratio of Pt to WO₃ are good photocatalysts.

Acknowledgement. Major funding was supported by the Hydrogen Program of the Department of Energy (DOE, Grant # DER-FC36-01G011092) and the Cycad Group (Santa Barbara, CA). Partial funding and facilities were provided by the NSF-MRSEC funded Materials Research Laboratory (UCSB); and the California Energy Commission, (CEC, Grant # 51539A/99-36).

References

- (1) Kelvin, L.; Liu, R. X.; Pu, C.; Fan, Q.; Leyarovskaya, N.; Segre, C.; and Smotkin, E. S., *J. Electrochem. Soc.*, **1997**, 144, 1543.
- (2) Lin, W.; Wang, J.; and Savinell, R., *J. Electrochem. Soc.*, **2001**, 144, 1917.
- (3) Lasch, K.; Jorissen, L.; and Garche, J., *J. Power Source*, **1999**, 84, 225.
- (4) Wang, K.; Gasteiger, H. A.; Marcovic, N.; and Ross, P. N.; *Electrochim. Acta*, **1996**, 141, 2587.
- (5) Marcovic, N.; Gasteiger, H. A.; Ross, P. N.; Jiang, X.; Villegas, I.; and M. J. Weaver, *Electrochim. Acta*, **1995**, 141, 91.
- (6) Watanabe, M.; Uchida, M.; and Motoo, S., *J. Electroanal. chem.*, **1987**, 229, 395.
- (7) Long, J. W.; Swider, K. E.; Merzbacher, C. I.; and Rolison, D. R., *Lanmuir*, **1999**, 15, 780.
- (8) Wang, Y.; Fachini, E. R.; Cruz, G.; Zhu, Y.; Ishikawa, Y.; Colucci, J. A.; and Cabrera, C. R., *J. Electrochem. Soc.*, **2001**, 148(3), C222.
- (9) Machida, K.; Enyo, M.; Adachi, G.; and Shiohara, J., *J. Electrochem. Soc.*, **1988**, 135, 1955.
- (10) Ermacov, Y. I. and Kuzvnetsov, B. N., *J. Mol. Catal.*, **1980**, 9, 13.
- (11) Shen, P. K. and Tseung, A. C. C., *J. Electrochem. Soc.*, **1994**, 141, 3082.
- (12) Le Bellac, D.; Azens, A.; and Granqvist C. G., *Appl. Phys. Lett.*, **1995**, 66, 1715.
- (13) Wang, H.; Lindgren, T.; He, J.; Hagfeldt, A.; and Lindquist, S. E., *J. Phys. Chem.*, **2000**, 104, 5686.
- (14) Su, L.; Zhang, L.; Fang, J.; Xu, Z.; and Lu, Z., *Solar energy Mater, Solar Cells*, **1999**, 58, 133.
- (15) Meulenkamp, E. A., *J. Electrochem. Soc.*, **1997**, 144, 1664.
- (16) Shen, P.; Chi, N.; and Chan, K. Y., *J. Mater. Chem.*, **2000**, 100, 697.
- (17) McFarland, E. W.; Baeck, S. H.; Brandli, C.; Ivanovskaya, A.; and Jaramillo, T. F., *Proc. 11th Canad. Hydro. Conf.*, **2001**.
- (18) Chen, Y.; Chen, K. Y.; and Tseung, A. C. C., *J. Electroanal. chem.*, **1999**, 471, 151.
- (19) Baeck, S. H.; Jaramillo, T. F.; Brandli, C.; and MaFarland, E. W., *J. Comb. Chem.*, submitted.
- (20) Pagotto Jr. Feire, C. M. A. and Ballester, M., *Surf. Coat. Tech.*, **1999**, 122, 10.
- (21) Nee, C. C.; Kim, W.; and Weil, R., *J. Electrochem. Soc.*, **1988**, 135(5), 1100.
- (22) Therese, G. H. A. and Kamath, P. V., *Chem. Mater.*, **2000**, 12, 1195.

LABORATORY EVALUATION OF PROMOTED ALUMINA ADSORBENT FOR FUEL DESULFURIZATION

Danna Leard Rehms

Alcoa World Chemicals
Adsorbents and Catalysts Division
109 Highway 131
Vidalia, LA 71373

Introduction

Naturally occurring fuel generally contains varying amounts of sulfur compounds. Refining processes like hydrodesulfurization (HDS) work to lower the sulfur content of these fuels to environmentally acceptable levels.^{1,2} The sulfur compounds in refined gasoline may include organic disulfides and polysulfides. Varying concentrations of aliphatic thiols, aromatic thiols, thiophenes and benzothiophenes are also present.³ Sulfur species in refined fuels such as gasoline, kerosene, diesel fuel, and jet fuel are objectionable because combustion of the fuel converts sulfur species to sulfur oxides that are released to the atmosphere. The U.S. Environmental Protection Agency has proposed new industry standards limiting the sulfur content of finished gasoline to 30 ppm. This limit is scheduled to be implemented in 2004.⁴ Besides the direct impact to the atmosphere, sulfur species are generally detrimental to automobile catalytic converter systems.⁵ Although the technology exists to produce ultra-low (<30 ppm) sulfur fuel using tried and true HDS systems, the extreme temperature and pressure conditions of such systems are often unfeasible or economically prohibitive. Adsorption may be useful in helping refineries to meet the lowest new sulfur standard if incorporated into, for example, a fixed bed system.

Even if gasoline leaves the refinery in an environmentally acceptable state, transport of "low-sulfur" hydrocarbons through a contaminated pipeline can also introduce elemental sulfur as an impurity. Sulfur species in liquid fuels have a corrosive effect on brass parts of valves, gauges, and fuel pumps. To avoid corrosion problems associated with elemental sulfur contamination, petroleum refiners may utilize processes to convert the elemental sulfur impurities to separable organic disulfides and polysulfides. Removal of the resulting disulfide and polysulfide species would then be necessarily performed "post-pipeline" where HDS technology is not often available. A fixed bed adsorption system may be useful in these applications.

Sulfur removal is also an issue in the field of fuel cell technology. Fuel processing units are generally placed upstream of the fuel cell catalyst to prevent poisoning by various impurities and to ensure good catalyst performance. A need exists for a compact, efficient and simple sulfur trap to prevent catalyst poisoning in fuel cell applications.⁶

We have developed a regenerable alumina-based adsorbent which is highly effective in removing sulfur compounds from hydrocarbon fluids.⁷ The adsorbent is macroporous promoted alumina with a surface area of approximately 200 m²/g. A laboratory evaluation of this novel adsorbent for removal of various sulfur species from finished gasoline is the subject of this paper.

Experimental

Adsorption capacity tests. The effectiveness of the new product for removing sulfur species was assessed through a series of laboratory screening tests. Initial tests were performed to establish static equilibrium capacities of the adsorbent for specific sulfur compounds. Further testing was performed to investigate efficiency

of removal from various solvents and from finished gasoline. A known weight of adsorbent spheres (1.4-2.4 mm diameter) was placed in a sealed container at ambient temperature and pressure along with a known weight of sulfur-containing hydrocarbon liquid (~100 ppmwS). Contact times were established to ensure equilibrium had been reached. Final sulfur concentrations in the liquid were measured to determine the capacity of the adsorbent for a given sulfur species.

Dynamic sulfur loadings were determined with a variation of the above test. The adsorbent was crushed and screened to a uniform size of 28x48 mesh (0.3-0.7 mm). A known weight of adsorbent (2-3 grams) was placed in a ½ inch diameter glass column. The column was mounted vertically and equipped with a metering valve at the bottom to control the rate of liquid flow. A 250 ml separatory funnel attached to the top of the column served as a reservoir to which a known weight of liquid was added. Specifically, we performed said experiments using a commercially available "sulfur-free" finished gasoline containing <1ppm sulfur. Individual gasoline samples were prepared by spiking the gasoline with known concentrations of common sulfur impurities.

Gasoline passed through the column of adsorbent at a rate of approximately 0.5 cm³/minute. Samples (~ 0.5 ml) were taken periodically and analyzed for sulfur content. Gasoline was continuously added to the reservoir until the contacted liquid's sulfur concentration reached that of the untreated gasoline. Chemiluminescence was used to determine the total sulfur concentration in all liquid samples (Antek model #9000NS).

For comparative purposes, all experiments were performed first with the promoted alumina adsorbent and then with unmodified activated alumina. In addition, comparative experiments were completed using an alumina-zeolite composite that is currently being offered commercially for removal of disulfides.

Regeneration Studies. Once the adsorbent column saturated, such that the sulfur content of the gasoline going in equaled the sulfur content of the gasoline coming out, the promoted alumina adsorbent was regenerated and the experiment repeated. A two-step regeneration process was employed. The adsorbent was transferred from the glass column to a ½ inch outer diameter stainless steel tube and placed in a programmable oven. In the first step, nitrogen gas (UHP grade) flowed through the adsorbent bed at approximately 1000 cm³/minute while the temperature was increased to a temperature ranging from 290-500°C and held for two hours. In the second step, air flowed across the hot adsorbent for two hours. The regenerated material was allowed to cool and returned to the glass column for subsequent adsorption cycles.

Results and Discussion

Sulfur loading capacities were established for a variety of typical fuel impurities: thiophene, 3-methylthiophene, benzothiophene, 2-methylbenzothiophene, ethyl mercaptan, and dimethyldisulfide (DMDS). Isooctane was chosen as the initial carrier in the testing. **Figure 1** indicates the promoted alumina's excellent performance in adsorptive capability for the sulfur species investigated. In all cases, initial equilibrium loading capacities of the new adsorbent were found to be much higher than those measured for the standard adsorbents. The promoted alumina showed performance enhancements ranging from 5 -75 times that of unmodified alumina and from 5 -50 times that of the composite alumina-zeolite adsorbent. Subsequent tests revealed that adsorptive capacities were extremely dependent on the carrier fluid of the sulfur species. Capacities were found to be much lower when sulfur-containing finished gasoline was tested using the above procedure. To determine the cause of this phenomenon, a set of experiments was performed using several different types of hydrocarbon fluids and comparing to the isooctane

results. Identical tests were performed with the various sulfur components in cyclohexane, hexane, and toluene.

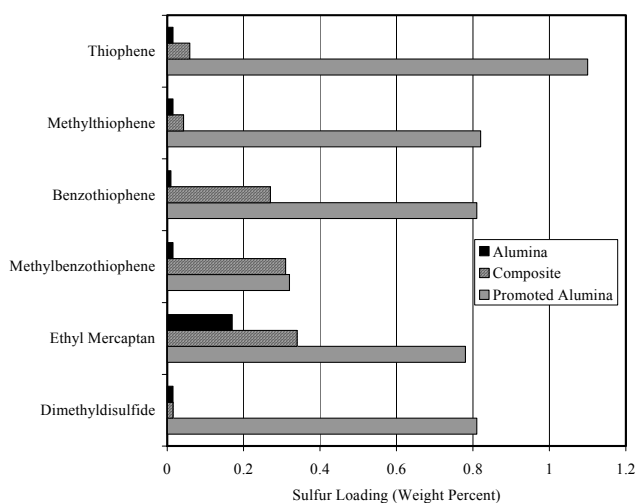


Figure 1. Sulfur loadings (weight percent) of various species on activated alumina, a composite zeolite-alumina, and promoted alumina.

Figure 2 shows equilibrium loading capacities for thiophene removal from the various hydrocarbons. Clearly, the adsorbent performs better when removing thiophene from saturated hydrocarbons than from unsaturated hydrocarbons. A typical experiment is shown in the figure below, but similar results were observed for the other sulfur species as well. Results indicate that the solvent can in some way inhibit sulfur removal by the promoted alumina. The mechanism behind this interference is not well understood. It should be noted that the interference is more pronounced for thiophene than any of the other species, and is almost negligible for ethyl mercaptan.

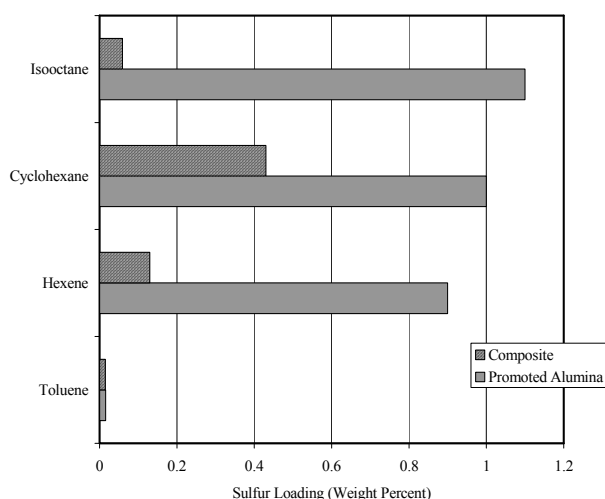


Figure 2. Sulfur loadings (weight percent) for thiophene removal from various hydrocarbons.

Dynamic adsorption tests described previously were performed on a finished gasoline stream to which known concentrations of the various sulfur species were added. At this point, the

regenerability of the adsorbent was also investigated. **Table 1** presents the actual regenerative loading capacities for the promoted alumina adsorbent for the various sulfur species. The adsorbent retains approximately 70% of its adsorptive capacity for ethyl mercaptan and 30% of its adsorptive capacity for DMDS upon regeneration at 290 C. Higher regenerative capacities can be achieved at higher temperatures. As expected, removal of thiophene and benzothiophene are more difficult given the aromatic nature of the carrier fluid.

Table 1. Dynamic Loading Capacities for Various Sulfur Components on Promoted Alumina

Sulfur Species	Adsorptive Capacity (Weight % Component)		
	Initial Adsorption	Oxidative Regeneration	
		290 C	340 C
Ethyl Mercaptan	2.5	1.9	2.0
Dimethyl disulfide	1.1	0.3	0.8
Thiophene	0.03	N/A	N/A
Benzothiophene	0.08	N/A	N/A

The regeneration process requires an oxidative step to re-oxidize the promoter on the alumina. **Figure 3** displays a breakthrough curve for the adsorption of DMDS from finished gasoline. The data is presented by plotting the liquid concentration as a function of grams of sulfur added per gram of adsorbent. Loading capacities were determined by integration of the curve. The graph demonstrates the need for the promoter to be in the oxidized state to be effective.

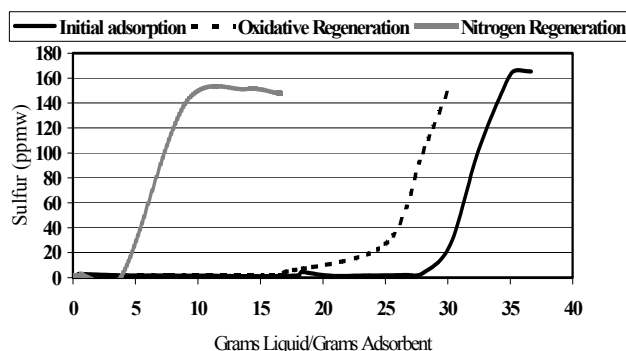


Figure 3. Breakthrough curves for DMDS adsorption by promoted alumina adsorbent. The Y-axis represents sulfur concentration in the effluent of the adsorption column.

Conclusions

Results presented here indicate the effectiveness of the promoted alumina adsorbent in removing sulfur compounds from hydrocarbon fluids. Clearly, adsorption capacities for sulfur contaminants vary greatly depending upon the hydrocarbon feedstream. This finding has serious implications given the nature of the sulfur adsorption market. As discussed previously, the applications that may benefit from a sulfur adsorbent such as this are numerous.

Additional test work is underway to quantitatively establish the adsorbent's effectiveness in removing sulfur compounds from other hydrocarbon streams. Further work is planned, which will allow us to better understand and overcome the problems of interference by unsaturated hydrocarbons on the adsorption process.

Acknowledgement. The author would like to thank John Novak and Elise Mophett of Alcoa for their guidance and support in the development of this adsorbent. Thanks also to Susan Cole for generating all of the dynamic adsorption testing data.

References

- ¹ Bartholomew, C.H. In *Catalytic Hydroprocessing of Petroleum and Distillates*; Oballa, M.C.; Shih, S.S., Ed.; Marcel Dekker: New York, 1994; pp. 1-32.
- ² Krenze, L.D.; Baron, K.; Paper AM-95-67; NPRA Annual Meeting, 1995.
- ³ Gates, B.C.; Katzer, J.R.; Schuit, G.C.A.; *Chemistry of Catalytic Processes*; McGraw-Hill: Chapters 3 and 5.
- ⁴ Greenwood, G.J.; Kidd, D.; Reed, L.; Paper AM-00-12; NPRA Annual Meeting, 2000.
- ⁵ Farrauto, R.J.; Bartholomew, C.H.; *Fundamentals of Industrial Catalytic Processes*; Blackie Academic and Professional: pp. 266-273.
- ⁶ *Chemical and Engineering News*, 1999, June 14, 1999, 31.
- ⁷ Rehms, D.L., *et al.*, Patent Pending.

MCM-41-Supported Co-Mo Catalysts for Deep Hydrodesulfurization of Light Cycle Oil-Based Real Feedstock

Uday T. Turaga and Chunshan Song*

Clean Fuels and Catalysis Program, The Energy Institute and Fuel Science Program, Dept. of Energy and Geo-Env. Engg., The Pennsylvania State University, University Park, PA 16802

*E-Mail: csong@psu.edu

Introduction

The increasing stringency of sulfur specifications has motivated intensive research in the hydrodesulfurization (HDS) of liquid hydrocarbon transportation fuels such as gasoline, diesel, and jet fuel. Most studies have, however, focused on mixtures of model compounds to simulate real feedstocks [1-5]. The few studies that have used real feedstocks to evaluate HDS catalysts have relied on hydrotreated [6-12] or low sulfur content feedstocks [13-15]. Previous work from our laboratory has established the superiority of MCM-41-supported catalysts for the HDS of a model compound [16] and a real feedstock [17]. This paper reports on further studies on HDS of real feedstocks; specifically a blend of light cycle oil (LCO) and refined chemical oil (RCO).

Light cycle oil is a by-product of the fluid catalytic cracking process (FCC) in a petroleum refinery. The FCC process enhances gasoline production and the increasing demand for gasoline translates into increased production of LCO. Traditionally, LCO has been used as a blendstock for home heating oil, industrial fuel oil, and diesel fuels. However, the increasing spread of natural gas in recent times for, both, heating homes and producing power has reduced demand for heating and fuel oils and, therefore, LCO [18]. Simultaneously, diesel demand is outpacing that of other transportation fuels [19]. Therefore, refiners are now using increasingly more LCO as a blendstock for the diesel pool.

Future military aircraft will require jet fuels capable of withstanding temperatures as high as 483°C. This will require that these fuels have high thermal stability. Research at the Energy Institute of the Pennsylvania State University has demonstrated that coal-derived jet fuel, because of their higher cycloalkane content, are more stable than paraffinic petroleum-derived jet fuels at temperatures higher than 400°C [20]. Refined chemical oil is a coal-derived liquid. More specifically, it is a distillate of coal tar which is a by-product of the process to carbonize coal to make metallurgical coke.

LCO has a low cetane index (typically 15-20), sulfur content as high as 3 wt.%, and 50-80 wt.% aromatics [21]. Its use in the diesel pool, therefore, requires extensive hydrotreating to meet existing diesel fuel combustion and environmental specifications. RCO is characterized by aromatics and high nitrogen contents. Thus, hydrotreating RCO is important for the production of jet fuels. Therefore, the HDS of a blendstock of LCO and RCO typifies a worst-case scenario for hydrotreating catalysts for clean diesel and jet fuel production. Nevertheless, using such a blendstock for evaluating HDS catalysts has the potential of yielding important information.

MCM-41—characterized by a hexagonal array of uniform mesopores, a narrow pore size distribution, and high surface area,

sorption capacity, and thermal stability—has distinct advantages as a catalytic support [22]. The mesopores of MCM-41 will, perhaps, facilitate easy diffusion of catalyst precursors and polyaromatic sulfur compounds (PASCs) during HDS reactions. Further, MCM-41, with its moderate and tailorable acidity when properly synthesized [23], could isomerize refractory PASCs such as 4,6-dimethylidibenzothiophene (4,6-DMDBT) to the more reactive variants such as 2,8- or 3,7-DMDBT without causing cracking as reported in the case of certain zeolite-based HDS catalysts [24].

Experimental

The LCO sample, produced in a fluid catalytic cracker, was obtained from United Refining Company, Warren, PA. Table 1 describes the key properties of the LCO sample used in this study. The RCO sample is a naphthalene fraction and was obtained from Koppers Industries, Pittsburgh, PA. The LCO-RCO blendstock was a 75%-25% mixture by weight, respectively. The catalytic activity for the HDS of the LCO-RCO blend was evaluated in a fixed-bed catalytic flow reactor. Table 2 presents a summary of the experimental conditions.

Table 1. Key Properties of LCO Sample.

Sulfur content	2.19 wt.%
API	10.2
Cetane index	17.6
ASTM distillation	
Initial boiling point	217.1°C
5%	246.6°C
50%	271.1°C
95%	325.9°C
Final boiling point	340.0°C

Table 2. Flow Reactor Experimental Conditions.

Catalyst Sulfidation	
Temperature	350°C
10% H ₂ S in H ₂ (vol.%) flow rate	200 ml/min
Time	4 hours
Deep HDS Reaction	
Temperature	300°C
Pressure	660 psi
Weight Hourly Space Velocity	4 h ⁻¹
Hydrogen/Hydrocarbon	300 ml/ml
Catalyst particle size	0.5-1.0 mm
Catalyst weight	1 g

The two catalysts evaluated for HDS activity were Co-Mo supported on mesoporous aluminosilicate molecular sieve of MCM-41 type and a commercial catalyst, Co-Mo supported on γ -Al₂O₃ (C-344 provided by Criterion Catalyst Company, Houston, TX). Aluminosilicate MCM-41 of SiO₂/Al₂O₃ ratio 50 was synthesized using previously reported recipes [16,23,25]. Both catalysts were sulfided using a uniform procedure as described in Table 2. The catalysts were evaluated for HDS activity over a period of 8 hours and the reactor effluents were collected at regular intervals. The reaction products were analyzed using a QP-5000 Shimadzu gas chromatograph equipped with a quadrupole (70eV) mass spectrometer. The sulfur

species of interest were identified on the basis of retention times obtained using model compounds.

Results and Discussion

The most refractory sulfur compounds in this blendstock originate in the LCO. Table 3 presents the distribution of sulfur in LCO between dibenzothiophene (DBT), 4-methyldibenzothiophene (4-MDBT), and 4,6-DMDBT. Depauw and Froment [26] also obtained a similar distribution of dibenzothiophenic sulfur in their molecular analysis of LCO. The other dominant sulfur species observed in this sample of LCO include benzothiophenes and naphthothiophenes which have not been analyzed quantitatively. Most of the sulfur in RCO is dibenzothiophene. RCO, however, contributes to the bulk of the nitrogen compounds, predominantly carbazole and quinoline.

Table 3. Dibenzothiophenic Sulfur Distribution.

Sulfur species	wppm	% of total sulfur
Total sulfur in LCO	21900	100.0
Dibenzothiophene	2625	11.9
Methyldibenzothiophenes	3518	16.0
4-Methyldibenzothiophene	1951	9.0
Dimethyldibenzothiophenes	3317	15.1
4,6-Dimethyldibenzothiophene	775	3.5
Total dibenzothiophenic sulfur	9460	43.2

Figure 1 presents the results of the activity of the two catalysts evaluated during this study. The activity of MCM-41-supported catalysts is comparable to that of the commercial catalyst. This is in contrast to the results for the HDS of LCO where the MCM-41-supported catalyst was consistently more active than the commercial catalyst [17]. The presence of organic nitrogen—from the RCO—in the blendstock apparently inhibits the activity of the MCM-41-supported catalyst.

The activities of, both, the MCM-41-supported and the commercial catalyst for the HDS of 4,6-DMDBT and 4-MDBT are significantly inhibited with time. This is attributed to the presence of organic nitrogen. Similar inhibiting influence of organic nitrogen on the HDS of 4,6-DMDBT has been reported [27]. Surprisingly, both catalysts seem oblivious to the presence of nitrogen so far as the HDS of DBT is concerned.

The substituted variants of DBT are known to undergo desulfurization, predominantly, through the hydrogenation pathway [28] since their adsorption on hydrogenolysis sites is sterically inhibited by the presence of the methyl groups. The sites responsible for hydrogenation activity are, however, known to be severely inhibited by organic nitrogen and aromatic compounds, in particular diaromatics like naphthalene [28]. LCO and RCO, both, contain significant amount of aromatics [21]. Based on the results presented in Figure 1, it seems plausible that the catalysts' activity for HDS of substituted DBTs is severely inhibited by organic nitrogen and aromatics. On the other hand, the adsorption of DBT on a catalyst surface is not sterically limited thus allowing its HDS via the hydrogenolysis route. This could, thus, explain organic nitrogen and aromatics' limited inhibition of the catalysts' activity for the HDS of DBT.

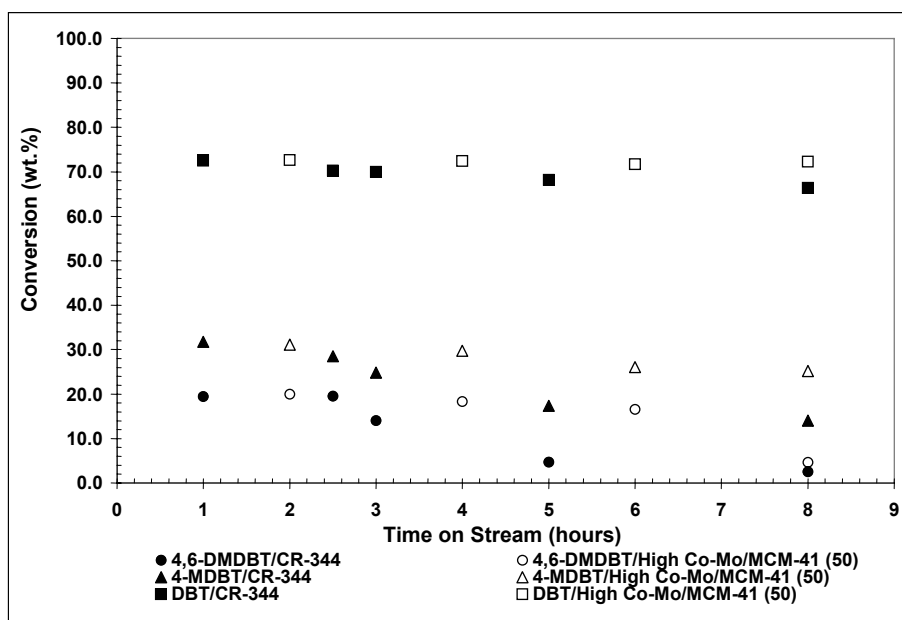


Figure 1. Activity of catalysts evaluated for the HDS of PASCs in LCO-RCO blendstock.

Conclusions

The HDS of a blendstock of LCO and RCO was comparatively studied over commercial γ -Al₂O₃- and MCM-41-supported Co-Mo catalysts. The HDS of DBT, 4-MDBT, and 4,6-DMDBT—PASCs present in LCO—and their relative reactivity in terms of conversion were examined as a function of time on stream. The MCM-41-supported catalyst demonstrates activity for the HDS of the refractory dibenzothiophenic sulfur compounds comparable to that of the commercial catalyst. Through comparative examination, the presence of organic nitrogen and aromatics in the blendstock appear to affect the HDS of the substituted DBTs extensively.

Acknowledgments. The authors are grateful to U.S. Air Force Office of Scientific Research for supporting this work, and to Prof. Harold H. Schobert and Dr. Xiaoliang Ma for helpful discussions.

References

- (1) Corma, A.; Gonzalez-Alfaro, V.; Orchilles, A.V. *J. Catal.* **2001**, *200*, 34-44.
- (2) Rollmann, L.D.; Howley, P.A.; Mazzone, D.N.; Timken, H.K.C. *Ind. Eng. Chem. Res.* **1995**, *34*, 3970-3973.
- (3) Bouchy, M.; Peureuxdenys, S.; Dufresne, P.; Kasztelan, S. *Ind. Eng. Chem. Res.* **1993**, *32*, 1592-1602.
- (4) Bouchy, M.; Dufresne, P.; Kasztelan, S. *Ind. Eng. Chem. Res.* **1992**, *31*, 2661-2669.
- (5) Rankel, L.A. *Energy & Fuels* **1992**, *6*, 826-830.
- (6) Corma, A.; Martinez, A.; Martinez-Soria, V. *J. Catal.* **2001**, *200*, 259-269.
- (7) Fujikawa, T.; Idei, K.; Ohki, K.; Mizuguchi, H.; Usui, K. *Appl. Catal. A: General* **2001**, *205*, 71-77.
- (8) Fujikawa, T.; Idei, K.; Ebihara, T.; Mizuguchi, H.; Usui, K. *Appl. Catal. A: General* **2000**, *192*, 253-261.
- (9) Lecrenay, E.; Sakanishi, K.; Mochida, I.; Suzuka, T. *Appl. Catal. A: General* **1998**, *175*, 237-243.
- (10) Lecrenay, E.; Sakanishi, K.; Nagamatsu, T.; Mochida, I.; Suzuka, T. *Appl. Catal. B: Environmental* **1998**, *18*, 325-330.
- (11) Lecrenay, E.; Sakanishi, K.; Mochida, I. *Catal. Today* **1997**, *39*, 13-20.
- (12) Corma, A.; Martinez, A.; Martinez-Soria, V. *J. Catal.* **1997**, *169*, 480-489.
- (13) Ancheyta-Juarez, J.; Aguilar-Rodriguez, E.; Salazar-Sotelo, D.; Marroquin-Sanchez, G. *Stud. Surf. Sci. Catal.* **1999**, *127*, 343-346.
- (14) Ancheyta-Juarez, J.; Aguilar-Rodriguez, E.; Salazar-Sotelo, D.; Betancourt-Rivera, G.; Quiroz-Sosa, G. *Stud. Surf. Sci. Catal.* **1999**, *127*, 347-350.
- (15) Ancheyta-Juarez, J.; Aguilar-Rodriguez, E.; Salazar-Sotelo, D.; Marroquin-Sanchez, G.; Quiroz-Sosa, G.; Leiva-Nuncio, M. *Appl. Catal. A: General* **1999**, *183*, 265-272.
- (16) Turaga, U.T.; Song, C. *Prepr. Pap. - Am. Chem. Soc., Div. Pet. Chem.* **2001**, *46*, 275.
- (17) Turaga, U.T.; Song, C. *Prepr. Pap. - Am. Chem. Soc., Div. Pet. Chem.* **2002**, *47*, 97.
- (18) UOP. *Diesel Fuel: Specifications and Demand for the 21st Century*, UOP; Des Plaines, IL, 1998.
- (19) DeCicco, J.; Mark, J. *Energy Policy* **1998**, *26*, 395.
- (20) Andréren, J. M.; Strohm, J.J.; Song, C. *Prepr. Pap. - Am. Chem. Soc., Div. Pet. Chem.* **1998**, *43*, 412.
- (21) Song, C. In *Chemistry of Diesel Fuels*, Song, C.; Hsu, C.S.; Mochida, I. Eds.; Taylor & Francis, New York, 2001, pp. 1-60.
- (22) Vartuli, J. C.; Roth, W.J.; Beck, J.S.; McCullen, S.B.; Kresge, C.T. In *Molecular Sieves: Science and Technology*, Karge, H.G.; Weitkamp, J. Eds.; Springer-Verlag, New York, 1998.
- (23) Reddy, K.M.; Song, C. *Stud. Surf. Sci. Catal.* **1998**, *117*, 291.
- (24) Isoda, T.; Nagao, S.; Korai, Y.; Mochida, I. *Prepr. Pap. - Am. Chem. Soc., Div. Pet. Chem.* **1996**, *40*, 563.
- (25) Reddy, K. M.; Song, C. *Catal. Lett.* **1996**, *36*, 103.
- (26) Depauw, G.A.; Froment, G.F. *J. Chromatography A* **1997**, *761*, 231-247.
- (27) Turaga, U.T.; Wang, G.; Ma, X.; Schobert, H.H.; Song, C. *Prepr. Pap. - Am. Chem. Soc., Div. Pet. Chem.* **2002**, *47*, 89.
- (28) Whitehurst, D.D.; Isoda, T.; Mochida, I. *Adv. Catal.* **1998**, *42*, 345.

A Microkinetic Model for the Water Gas Shift Reaction on Cu(111) and Fe(111)

Caitlin Callaghan, Ilie Fishtik and Ravindra Datta

Fuel Cell Center and Department of Chemical Engineering,
Worcester Polytechnic Institute
Worcester, MA 01609

Introduction

The development of lower temperature water-gas-shift (WGS) catalysts is of paramount importance. In particular, an efficient lower temperature WGS catalyst is crucial in improving the reforming process for developing a reformat-fed proton-exchange membrane fuel cell, as well as for the direct methanol fuel cell, intended for transportation and stationary applications. The approach so far has involved random or combinatorial screening of binary and tertiary catalysts of different compositions. Since there are infinite possibilities, not surprisingly, this approach so far has been met with only limited success.

The aim of the present work is to develop a microkinetic model for both lower and higher temperature WGS catalysts. The approach of microkinetics is appealing [1] since it is not based on any arbitrary assumptions regarding rate-determining step (RDS) and is, thus, not restricted to a particular set of conditions. In doing this we follow a novel approach developed recently by us [2] to *derive a complete* set of elementary reactions and reaction routes (RRs) for a given set of species, coupled with a reliable prediction of the elementary reaction energetics on a given catalyst based on the Unity Bond Index – Quadratic Exponential Potential (UBI-QEP) approach developed by Shustorovich [3] and the transition-state theory. This new approach allows us to develop *a priori* a complete microkinetic model for the WGS on a given catalyst and will also provide a rational approach for identifying the rate determining steps (RDS), if any, under different conditions, so that reduced models may also be developed.

Microkinetic Model and Simulation

The mechanism of the WGS reaction is assumed to proceed via a set of elementary reactions (ERs) comprising active sites (S) on the surface of the catalyst, surface intermediates (I_i), and terminal species (T_i). Generically the elementary reactions (s_j) may be written as

$$s_j = \alpha_{j0} S + \sum_{k=1}^q \alpha_{jk} I_k + \sum_{i=1}^n \beta_{ji} T_i = 0$$

where α and β represent the stoichiometric coefficients assumed to take positive values for products and negative values for reactants. The rate expressions of the elementary reactions are given by

$$r_j = \bar{A}_j \exp\left(-\frac{\bar{E}}{RT}\right) \theta_0^{\alpha_{j0}} \prod_{k=1}^q \theta_k^{\alpha_{jk}} \prod_{i=1}^n P_i^{\beta_{ji}} - \bar{A}_j \exp\left(-\frac{\bar{E}}{RT}\right) \theta_0^{\alpha_{j0}} \prod_{k=1}^q \theta_k^{\alpha_{jk}} \prod_{i=1}^n P_i^{\beta_{ji}}$$

where \bar{A}_j and \bar{E} are the pre-exponential factors and activation energies, respectively, and θ represents species coverage.

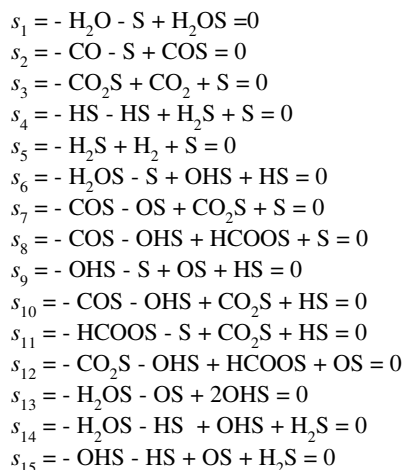
Our starting point in the development of the microkinetic model is the experimental evidence according to which the WGS reaction normally proceed via the following set of surface intermediates H₂O_s, COS, CO₂S, H₂S, HS, OHS, OS and HCOOS. Starting with these surface species, a plausible set of ERs may be generated using an appropriate chemical reaction generator. The stoichiometry of ERs is dictated further by the subsequent application of the UBI-QEP

method to calculate the energetic characteristics of these ERs. In other words, the ERs are limited to those 3 types for which the UBI-QEP method provides the necessary formulae:

1. AB(g) + S = ABS
2. AB(g) + S = AS + BS
3. AS + BCS = ABS + CS

The set of ERs generated under these stoichiometric constraints for the WGS reaction is presented in Table 1. Next, the UBI-QEP method is utilized to calculate the enthalpy changes as well as activation energies of each ER on both Cu(111) and Fe(111) (Table 2). Further, the pre-exponential factors are estimated using the conventional transition state theory [1]. Following Waugh [4], we assume an immobile transition state without rotation for all of the species that result in a pre-exponential factor of 10¹ Pa⁻¹s⁻¹ for adsorption/desorption reactions and 10¹³ s⁻¹ for surface reactions. The obtained microkinetic model for the WGS reaction is presented in Table 1. Fine-tuning of some of the pre-exponential factors of the adsorption/desorption reactions, however, is necessary in order to be consistent with the known thermodynamics of the overall reaction. Numerical simulations and analyses were performed for both CSTR and PFR.

Table 1. A microkinetic model for the WGS



Model Analysis and Reduction

Typical results of numerical simulations using the proposed microkinetic models for Cu(111) and Fe(111) are presented in Figures 1 and 2. As can be seen, the model can satisfactorily reproduce the main features of the WGS on both Cu LTS catalyst and Fe HTS catalyst without any further fine-tuning, e.g., coverage dependence of the activation energy, etc. Notice, for Cu(111) a much better description of the experimental data may be obtained if the last two elementary reactions, s_{14} and s_{15} , are dropped from the mechanism. The reason for this behavior is not yet clear. More detailed and exact kinetic measurements are necessary in order to discriminate among the full 15-elementary step and 13-elementary step microkinetic model on Cu.

To get a deeper insight into the nature of the WGS reaction mechanism we next use the RR formalism to reduce and simplify the microkinetic model. First, we enumerate a complete list of stoichiometrically distinct direct overall RRs (Table 3). The individual contributions of these overall RRs may be estimated by performing numerical simulations for each of the RRs separately. An example of such simulations in a CSTR for Cu(111) is presented in

Table 2. Preexponential factors ($\text{Pa}^{-1}\text{s}^{-1}$ for adsorption/desorption steps and s^{-1} for surface reaction) and activation energies (kcal/mol) microkinetic model for the WGSRs

ERs	\bar{A}_j	\bar{A}_j	Cu(111)		Fe(111)	
			\bar{E}_j	\bar{E}_j	\bar{E}_j	\bar{E}_j
s_1	10^1	10^{14}	0	13.6	0	17.2
s_2	10^1	10^{14}	0	12.0	0	32.0
s_3	$4 \cdot 10^{12}$	10^1	5.3	0	6.9	0
s_4	10^{13}	10^{13}	15.5	13.0	24.5	7.6
s_5	$6 \cdot 10^{12}$	10^1	5.5	0	7.1	0
s_6	10^{13}	10^{13}	25.4	1.6	19.9	12.0
s_7	10^{13}	10^{13}	0	17.3	20.6	4.5
s_8	10^{13}	10^{13}	0	20.4	9.0	12.2
s_9	10^{13}	10^{13}	15.5	20.7	12.4	29.1
s_{10}	10^{13}	10^{13}	0	22.5	10.3	10.9
s_{11}	10^{13}	10^{13}	1.3	3.5	4.4	1.8
s_{12}	10^{13}	10^{13}	4.0	0.9	19.3	0
s_{13}	10^{13}	10^{13}	29.2	0	24.6	0
s_{14}	10^{13}	10^{13}	26.3	0	24.8	0
s_{15}	10^{13}	10^{13}	1.3	4.0	3.4	3.2

Figure 3. From these simulations, we conclude that, for Cu(111), the main contributions come from four overall RRs, namely, RR_1 , RR_2 , RR_3 and RR_{18} . The first three RRs are the formate, redox and associative RRs, respectively. As can be seen from Figure 3, the formate and associative RRs are dominant at lower temperatures, while the redox RR is significant at higher temperatures. This result is of particular significance since it shows that both the formate and redox mechanisms may be important in different temperature ranges and for different feed compositions. RR_{18} represents a new RR and is due to the elementary reaction s_{15} . As already mentioned above, the prominence of this RR still needs to be proved. Similar evaluations for the WGS reaction on Fe(111) reveal that the dominant RRs are RR_1 , RR_3 , RR_{18} and RR_{19} , their contributions being equal. Further, when these dominant overall RRs are summed up, it is seen that the elementary reactions s_{13} and s_{14} drop out and, consequently, may be disregarded. We thus arrive at a simplified mechanism involving only the first 12 ERs and the elementary reaction s_{15} .

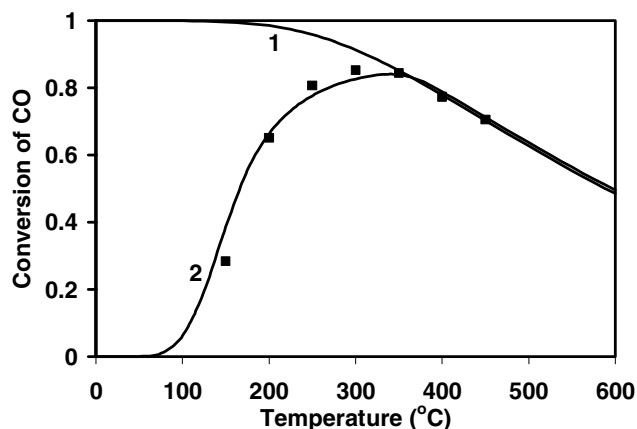


Figure 1. CO conversion vs. temperature on Cu(111). 1-equilibrium conversion; 2-microkinetic model; squares-experimental data from [5].

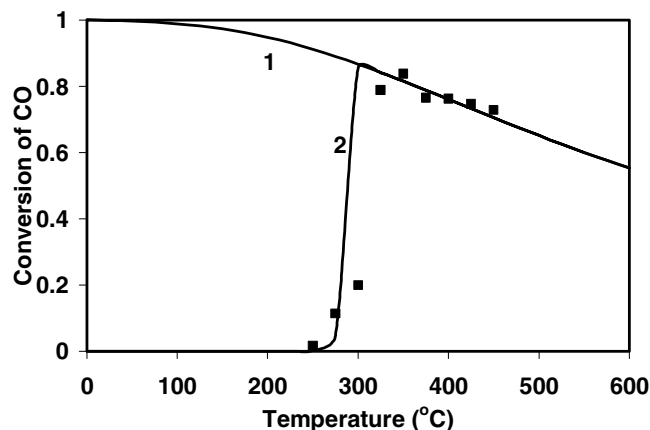


Figure 2. CO conversion vs. temperature on Fe(111). 1-equilibrium conversion; 2-microkinetic model; squares-experimental data from present work.

Table 3. A complete list of unique overall reaction routes for the 15-step microkinetic model of the WGS reaction microkinetic model.

- $RR_1 = s_1 + s_2 + s_3 + s_4 + s_5 + s_6 + s_8 + s_{11}$
- $RR_2 = s_1 + s_2 + s_3 + s_4 + s_5 + s_6 + s_7 + s_9$
- $RR_3 = s_1 + s_2 + s_3 + s_4 + s_5 + s_{10}$
- $RR_4 = s_1 + s_2 + s_3 + s_4 + s_5 + 2s_6 + s_7 - s_{13}$
- $RR_5 = s_1 + s_2 + s_3 + s_4 + s_5 + s_{10} + s_{11} - s_{12} + s_{13}$
- $RR_6 = s_1 + s_2 + s_3 + s_4 + s_5 + s_9 + s_{10} + s_{13}$
- $RR_7 = s_1 + s_2 + s_3 + s_4 + s_5 + s_8 + s_{11} - s_{12} + s_{13}$
- $RR_8 = s_1 + s_2 + s_3 + s_4 + s_5 - s_8 + 2s_{10} - s_{12} + s_{13}$
- $RR_9 = s_1 + s_2 + s_3 + s_4 + s_5 + s_8 + 2s_9 + s_{12} + s_{13}$
- $RR_{10} = s_1 + s_2 + s_3 + s_4 + s_5 + s_8 + s_9 + s_{11} + s_{13}$
- $RR_{11} = s_1 + s_2 + s_3 + s_4 + s_5 + s_7 + 2s_{11} - s_{12} + s_{13}$
- $RR_{12} = s_1 + s_2 + s_3 + s_4 + s_5 + s_7 + 2s_9 + s_{13}$
- $RR_{13} = s_1 + s_2 + s_3 + s_4 + s_5 - s_7 + 2s_{10} + s_{13}$
- $RR_{14} = s_1 + s_2 + s_3 + s_4 + s_5 - s_7 + 2s_8 + 2s_{11} + s_{13}$
- $RR_{15} = s_1 + s_2 + s_3 + s_4 + s_5 + 2s_6 + s_8 + s_{12} - s_{13}$
- $RR_{16} = s_1 + s_2 + s_3 + s_4 + s_5 + s_6 + s_8 + s_9 + s_{12}$
- $RR_{17} = s_1 + s_2 + s_3 + s_4 + s_5 + s_6 + s_7 + s_{11} - s_{12}$
- $RR_{18} = s_1 + s_2 + s_3 + s_5 + s_6 + s_7 + s_{15}$
- $RR_{19} = s_1 + s_2 + s_3 + s_5 + s_6 + s_8 + s_{12} + s_{15}$
- $RR_{20} = s_1 + s_2 + s_3 + s_5 + s_7 + s_9 + s_{14}$
- $RR_{21} = s_1 + s_2 + s_3 + s_5 + s_{10} + s_{14}$
- $RR_{22} = s_1 + s_2 + s_3 + s_5 + s_8 + s_{11} + s_{14}$
- $RR_{23} = s_1 + s_2 + s_3 - s_4 + s_5 + s_7 - s_{13} + 2s_{14}$
- $RR_{24} = s_1 + s_2 + s_3 - s_4 + s_5 + s_7 + s_{13} + 2s_{15}$
- $RR_{25} = s_1 + s_2 + s_3 - s_4 + s_5 + s_7 + s_{14} + s_{15}$
- $RR_{26} = s_1 + s_2 + s_3 + s_5 + s_7 + s_{11} - s_{12} + s_{14}$
- $RR_{27} = s_1 + s_2 + s_3 + s_5 + s_8 + s_9 + s_{12} + s_{14}$
- $RR_{28} = s_1 + s_2 + s_3 + s_5 + s_{10} + s_{13} + s_{15}$
- $RR_{29} = s_1 + s_2 + s_3 + s_5 + s_8 + s_{11} + s_{13} + s_{15}$
- $RR_{30} = s_1 + s_2 + s_3 - s_4 + s_5 + s_8 + s_{12} - s_{13} + 2s_{14}$
- $RR_{31} = s_1 + s_2 + s_3 - s_4 + s_5 + s_8 + s_{12} + s_{14} + s_{15}$

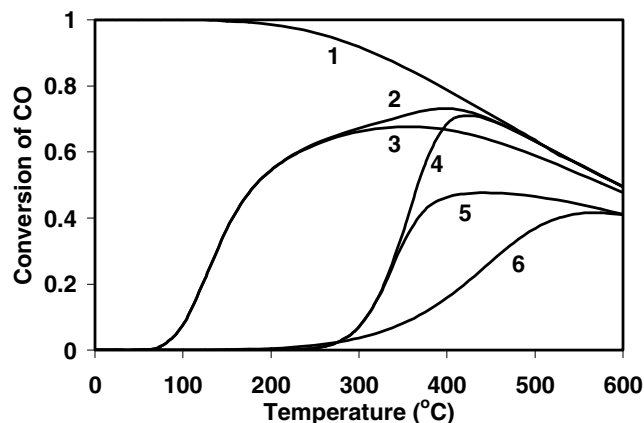


Figure 3. CO conversion vs. temperature for Cu(111) 1-equilibrium; 2-13-step mechanism; 3-RR₁ and RR₃, 4-RR₂; 5-RR₁₆; 6-RR₁₇.

Table 4. A 10-Step Reduced Mechanism for WGSR

s_1 :	$\text{H}_2\text{O} + \text{S} = \text{H}_2\text{OS}$	EQ
s_2 :	$\text{CO} + \text{S} = \text{COS}$	EQ
s_6 :	$\text{H}_2\text{OS} + \text{S} = \text{OHS} + \text{HS}$	RDS
s_8 :	$\text{COS} + \text{OHS} = \text{HCOOS} + \text{S}$	RDS
s_9 :	$\text{OHS} + \text{S} = \text{OS} + \text{HS}$	RDS
s_{10} :	$\text{COS} + \text{OHS} = \text{CO}_2\text{S} + \text{HS}$	RDS
s_{12} :	$\text{CO}_2\text{S} + \text{OHS} = \text{OS} + \text{HCOOS}$	RDS
s_{15} :	$\text{OHS} + \text{HS} = \text{OS} + \text{H}_2\text{S}$	RDS
$s_2 + s_3 + s_7$:	$\text{CO} + \text{OS} = \text{CO}_2 + \text{S}$	EQ
s_3 :	$\text{CO}_2\text{S} = \text{CO}_2 + \text{S}$	EQ
$1/2(s_4 + s_5)$:	$\text{HS} = 1/2\text{H}_2 + \text{S}$	EQ
$s_3 + 1/2s_4 + 1/2s_5 + s_{11}$:	$\text{HCOOS} = \text{CO}_2 + 1/2\text{H}_2 + \text{S}$	EQ

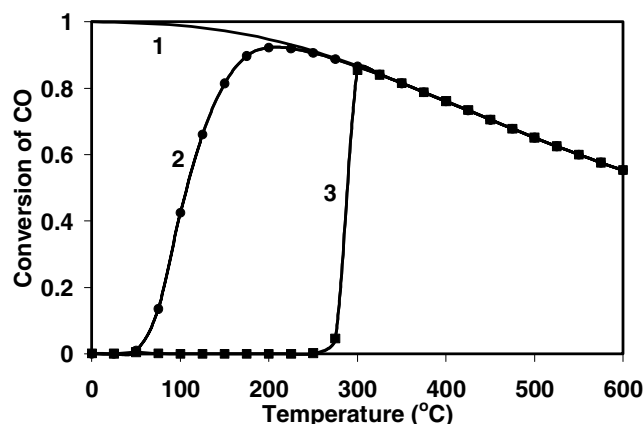


Figure 4. CO conversion vs. temperature for Cu(111) and Fe(111) 1-equilibrium; 2-13-step mechanism on Cu(111), dots-simplified microkinetic model for Cu(111); 3-15-step mechanism on Fe(111), squares-simplified microkinetic model for Fe(111).

The microkinetic model was further reduced using quasi-equilibrium and quasi-steady state approximations. Based on affinity

calculations, elementary reactions $s_1, s_2, s_3, s_4, s_5, s_7,$ and s_{11} were determined to be quasi-equilibrium (QE) reactions. Using the intermediate RRs formalism [2] one may next appropriately combine the QE elementary reactions into a set of intermediate reactions. Substituting the QE elementary reactions with the intermediate reactions result in an 12-step, 5-route and 5-RDSs simplified mechanism that is presented in Table 4.

The elementary reactions $s_6, s_8, s_9, s_{10}, s_{12}$ and s_{15} may therefore be considered rate determining steps. The next natural step in the reduction of the mechanism is to assume that the remaining surface intermediate OHS is a quasi-steady state (QSS) species. Under these conditions, the rates along the dominant RRs, i.e., $RR_1, RR_2, RR_3, RR_{19}$ and RR_{18} are equal to r_8, r_9, r_{10}, r_{12} and r_{15} and are given by

$$r_8 = \frac{\bar{k}_6 \bar{k}_8 K_1 K_2 P_{\text{H}_2\text{O}} P_{\text{CO}} \theta_0^2}{(\bar{k}_6 + \bar{k}_{15}) P_{\text{H}_2}^{1/2} + \bar{k}_9 + (\bar{k}_8 + \bar{k}_{10}) K_2 P_{\text{CO}} + \bar{k}_{12} K_3^{-1} P_{\text{CO}_2}} \left(1 - \frac{P_{\text{CO}_2} P_{\text{H}_2}}{K P_{\text{H}_2\text{O}} P_{\text{CO}}} \right)$$

$$r_9 = \frac{\bar{k}_6 \bar{k}_9 K_1 P_{\text{H}_2\text{O}} \theta_0^2}{(\bar{k}_6 + \bar{k}_{15}) P_{\text{H}_2}^{1/2} + \bar{k}_9 + (\bar{k}_8 + \bar{k}_{10}) K_2 P_{\text{CO}} + \bar{k}_{12} K_3^{-1} P_{\text{CO}_2}} \left(1 - \frac{P_{\text{CO}_2} P_{\text{H}_2}}{K P_{\text{H}_2\text{O}} P_{\text{CO}}} \right)$$

$$r_{10} = \frac{\bar{k}_6 \bar{k}_{10} K_1 K_2 P_{\text{H}_2\text{O}} P_{\text{CO}} \theta_0^2}{(\bar{k}_6 + \bar{k}_{15}) P_{\text{H}_2}^{1/2} + \bar{k}_9 + (\bar{k}_8 + \bar{k}_{10}) K_2 P_{\text{CO}} + \bar{k}_{12} K_3^{-1} P_{\text{CO}_2}} \left(1 - \frac{P_{\text{CO}_2} P_{\text{H}_2}}{K P_{\text{H}_2\text{O}} P_{\text{CO}}} \right)$$

$$r_{12} = \frac{\bar{k}_6 \bar{k}_{12} K_1 K_3^{-1} P_{\text{H}_2\text{O}} P_{\text{CO}_2} \theta_0^2}{(\bar{k}_6 + \bar{k}_{15}) P_{\text{H}_2}^{1/2} + \bar{k}_9 + (\bar{k}_8 + \bar{k}_{10}) K_2 P_{\text{CO}} + \bar{k}_{12} K_3^{-1} P_{\text{CO}_2}} \left(1 - \frac{P_{\text{CO}_2} P_{\text{H}_2}}{K P_{\text{H}_2\text{O}} P_{\text{CO}}} \right)$$

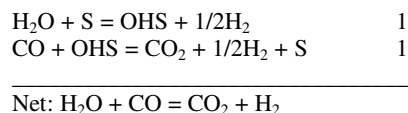
$$r_{15} = \frac{\bar{k}_6 \bar{k}_{15} K_1 (K_4 K_5)^{1/2} P_{\text{H}_2\text{O}} P_{\text{H}_2}^{1/2} \theta_0^2}{(\bar{k}_6 + \bar{k}_{15}) P_{\text{H}_2}^{1/2} + \bar{k}_9 + (\bar{k}_8 + \bar{k}_{10}) K_2 P_{\text{CO}} + \bar{k}_{12} K_3^{-1} P_{\text{CO}_2}} \left(1 - \frac{P_{\text{CO}_2} P_{\text{H}_2}}{K P_{\text{H}_2\text{O}} P_{\text{CO}}} \right)$$

The overall rate, r , is a sum of the rates along the dominant RRs:

$$r = r_8 + r_9 + r_{10} + r_{12} + r_{15}$$

Notice, for Cu(111) we neglected r_{12} and r_{15} while for Fe(111) we neglected r_9 . These simplified rate expressions are in perfect agreement with the full microkinetic model (Figure 4).

Also under the QSS condition for OHS, all of the dominant RRs may be combined into a final, two-step, one-route mechanism



This reduced mechanism could be compared to that proposed by Temkin, which is based on adsorbed O rather than OH.

Conclusions

In this work we have shown that a quite reliable microkinetic model for the WGS reaction on Cu(111) and Fe(111) may be developed based on a rather simplistic evaluation of the pre-exponential factors coupled with energetic estimations using the UBI-QEP method. The fact that these microkinetic models quantitatively describes the kinetics of the WGS reaction on a commercial Cu-Zn LTS and Fe HTS catalysts is quite surprising since some of the approximations involved are rather crude.

We further applied a simplification and reduction technique based on the RRs formalism. It was shown that only a very limited number of RRs dominate the kinetics of the process. This allows a dramatic simplification and reduction of the microkinetic model. The numerical performance of the final explicit rate expression is excellent when compared with the complete microkinetic model.

References

- [1] Dumesic, J. A., Rudd, D. F., Aparicio, L.M.; Rekoske, J.E., and Trevino, A. A. , *The Microkinetics of Heterogeneous Catalysis*, ACS, 1993.
- [2] Fishtik, I., and Datta R., *Ind. Eng. Chem. Res.* 40, 2416 (2001).
- [3] Shustorovich, E., and Sellers, H., *Surf. Sci. Reports*, **31**, 1 (1998).
- [4] Waugh, K. C., *Catalysis Today*, **53**, 161 (1999).
- [5] Xue, E., O’Keeffe, M. O., and Ross, J. R. H., *Catal. Today*, **30**, 107 (1996).

NETL's Ultra-Clean Fuels Focus Area: an Overview

Anthony V. Cugini, Bradley C. Bockrath, Bret H. Howard, Richard P. Killmeyer, Kurt S. Rothenburger, and Charles E. Taylor

U.S. Department of Energy
National Energy Technology Laboratory
P.O. Box 10940
Pittsburgh, PA 15236-0940

Introduction

The Ultra-Clean Fuels (UCF) focus area is involved in conducting the enabling science to provide the 21st century transportation systems with ultra-clean transportation fuels. The primary objectives of the UCF Focus Area are to take advantage of advances in computational chemistry, develop novel pathways to sulfur removal, develop advanced analytical techniques, develop improvements in separation science, and devise novel synthetic routes.

The following tasks are included in the UCF focus area: computational chemistry, advanced materials research, advanced analytical techniques, advanced hydrogen separations, and catalysis and reactor engineering.

The purpose of this paper is to present an overview of the UCF Focus Area.

Discussion

Computational Chemistry

Computational Chemistry utilizes advances in high speed computing to use simulation and modeling for understanding molecular processes and advancing technology. Molecular modeling is a powerful and rapidly developing suite of computational tools for understanding macroscopic phenomena in terms of molecular level events and properties. Molecular and materials modeling makes use of quantum chemical (electronic structure) and statistical mechanical methods to accurately describe the behavior of matter from a molecular viewpoint. The computational work of this group generates insight into the molecular level processes that control the outcome of experimental processes. Application of these methods to processes that use catalysts is particularly challenging, but has enormous promise.

In general, work will be conducted by both computations and complementary experimental efforts *i.e.* molecular modeling of hydrogen, hydrocarbon, and xenon adsorption on carbon nanotubes will be performed and comparison will be made with complementary experiments carried out at NETL. Simulations of chemisorption of hydrogen on carbon nanotubes will be performed and results will be compared with recent in-house experiments. Quantum mechanical electronic structure calculations will be carried out to model the formation of carbide deposits on iron and nickel surfaces and to elucidate the reaction mechanisms for hydrodesulfurization (HDS) of liquid fuels by heterogeneous catalysts.

The long-term goals of this work can be divided into two broad areas, the first being adsorption and reaction of gases on carbon nanotubes, and the second being chemisorption and reactions on metal surfaces. The fundamental difference between these two areas is in the nature of the surfaces under investigation. Other areas of research include F-T wax cracking, hydrogenation of aromatics, heteroatom removal, catalyst design, and carbonization reactions.

These goals can be achieved by employing optimized catalysts and procedures. The design of these catalysts and procedures would be based on a full understanding of the elementary chemical processes involved including both the control of the electronic

properties of various active sites and of the interactions of different molecular species with such sites assisted by various types of promoters.

Advanced Materials Research

The advent of new forms of carbon such as single- and multi-walled carbon nanotubes opens possibilities for fuels-related applications. These carbons are unique porous materials with properties that lend themselves to uses as adsorbents, gas storage media, and catalyst supports. Since their discovery in 1991 [1], there has been an explosion of interest in nanotubes, but their properties in relation to fuels applications have still not yet been well defined. For example, conflicting reports about their hydrogen storage capacity have been made; some optimistic, others pessimistic. (For a review see [2]). Their large potential to play a role in enabling technology for future fuels makes intense investigation of these materials wise. Past work on this project entailed the development of methodology for the use of a novel instrument, the pulse mass analyzer, to determine isotherms for hydrogen, methane, and other gases and liquids on nanotubes or other materials [3,4]. In addition to measuring adsorption isotherms, this versatile instrument opens the possibility to study the kinetics of carbon growth on catalysts [5]. Full exploitation of its capabilities can provide information of the growth, adsorption properties, and destruction of novel carbon forms. Theoretical studies [6,7] have been of considerable help in guiding these experiments and interpreting their results [8]. Other carbon products in addition to nanotubes will also be explored. Coal-derived pitches have been used as an inexpensive starting material for carbon fibers. Expanded use of carbon fibers would result if production costs could be reduced. Tailoring the reactive properties of coal-derived pitches presents a possible route to cheaper high-performance fibers, but this will require deeper knowledge of the chemistry of formation of isotropic and anisotropic mesophase. Complimentary experimental and theoretical studies are planned to improve the process.

Advanced Analytical Techniques

This research initiative supports the efforts toward the design of novel methods for removing sulfur from fuels by developing advanced analytical techniques for sulfur analysis as part of the ultra-clean fuels focus area. The presence of sulfur in petroleum products such as gasoline, diesel fuel, and jet fuel adversely affects the performance and lifetime of current automobile emission control catalysts. Sulfur in fuels is the main contributor to environmental acid rain products, and by-products of sulfur-containing fuels also pose human health threats because of their toxic and mutagenic properties. Sulfur compounds also have adverse effects on the performance and lifetime of catalysts designed to reduce emissions of particulate matter and oxides of nitrogen. These concerns have resulted in the legislative lowering of the allowable levels of sulfur in fuels. This lowering, in turn, has necessitated the development of removal strategies in order for the fuels produced from the refining process to meet these stringent requirements.

Traditional methods of desulfurization, such as hydrotreating, are not capable of removing those sulfur compounds that have lower reactivity [9-12]. To meet the removal efficiency desired, new methods and technologies for sulfur removal are being designed. By developing the capabilities for determining the presence and concentration of different classes of organo-sulfur compounds, or of individual compounds within the larger classes, these sulfur removal strategies can be evaluated, developed, and optimized toward more complete removal of sulfur from the fuels.

The removal of sulfur from fuels has been linked to other fuel properties, such as lubricity, thermal storage, and compatibility with

rings and seals currently used as engine components [13]. Many questions remain about the way that removing the sulfur-containing molecules affects the fuel quality and performance. Therefore, not only is the accurate determination of sulfur-containing compounds in fuels important for design and evaluation of desulfurization processes, but it is also a key in establishing functional relationships between sulfur compounds present and the fuel's performance. In this light, the analytical development component of this task will be developed to both identify individual sulfur components and determine their concentration, especially at the trace levels where their presence or removal may begin to affect other fuel properties.

Advanced Hydrogen Separations

The Advanced Hydrogen Separations Technologies effort investigates the development, modeling, and verification of novel hydrogen membrane reactor concepts.

Hydrogen can be produced from natural gas or other fossil fuel feedstocks. However, improving upon current methods for hydrogen separation from other gases remains a key issue, both for the large-scale production of hydrogen as in a refinery or Vision 21 plant environment, and for the small-scale purification of hydrogen as in fuel cell powered vehicles. Hydrogen separation membrane development, and its deployment in membrane reactor technology, has the potential for significant advances in hydrogen production and purification.

The development of advanced hydrogen separation membranes has the potential for profound improvements in efficiency for the separation and purification of hydrogen. The ideal membrane material would be low cost, highly selective, highly permeable, easily machined or formed, inert, and stable under severe operating conditions. Although such a membrane does not currently exist, there are materials and fabrication techniques that can produce membranes that possess several of these qualities. Hydrogen transport may take place through different types of materials--porous materials, diffusion-type membranes, and ion-transport membranes. Ceramic materials have the potential for low cost, high strength and chemical inertness, but are not easily formed, machined, and integrated into an otherwise metallic infrastructure. Some metals, such as palladium, possess both high selectivity and good permeability, but are easily poisoned and so expensive as to be impractical except in small, specialty applications. Composite materials offer some of the best qualities of their various component materials, but represent an increased manufacturing cost, complexity of fabrication, and potential for defects.

The long-term goal of this task is to produce novel prototypes for hydrogen separation membranes, either via collaboration or direct NETL in-house efforts. Specifically, two types of membranes are sought. One is a highly robust membrane capable of separating hydrogen from gasification feed streams at severe conditions of temperature (900°C) and pressure (up to 400 psi), while possessing chemical resistance to carbon monoxide, sulfur-containing compounds, ammonia, and other impurities. The second application is for membranes in "intermediate" severity conditions, such as those found in refinery processes. These include temperatures up to 500°C, with pressure drops and impurity tolerance dependent on the specific process.

Research efforts include:

- Hydrogen membrane development.
- Hydrogen membrane flux measurements
- Membrane reactor concepts.
- Sorption-based hydrogen separation concepts.
- Computational modeling.

Catalysis and Reactor Engineering

The objective of the Catalysis and Reactor Engineering Team is to explore experimental advancements in catalytic processes and reactor design for the production of fuels and chemicals from a variety of sources. Each Task investigates specific aspects of the advanced technologies for the production of ultra-clean fuels. Areas of interest will range from feedstock generation, reaction mechanisms, direct methane conversion, enhancements for improved Fischer-Tropsch (FT) performance, production of hydrogen and/or syngas from hydrocarbon feedstocks, fuels evaluation and upgrading, and the formation, dissociation, and conversion of methane hydrates.

One key area of research is the conversion of methane, the principle component of natural gas. It has been estimated that the world's supply of natural gas will be sufficient to supply the demand well into the next century [14]. Lately, most of the near-term projected use of natural gas is for replacement of other fossil fuels in the generation of electricity. However, the supplies of natural gas can also be used for conversion to chemicals and transportation fuels. At present, the most probable scenario for the conversion of natural gas, in remote areas such as Alaska, is by partial oxidation of the methane by an ion-transport membrane reactor to produce syngas followed by Fischer-Tropsch technology to produce liquids. Another possible route is the photocatalytic conversion of methane to methanol, under mild conditions, using light, water, and a semiconductor photocatalyst. Research is focusing on both the conversion of methane dissolved in water and methane contained within methane hydrates.

Another area of research is to overcome problems with current reforming processes. The reforming of fossil fuels (both liquid and gaseous) is an important process to help transform the transportation system from dependence on internal combustion engines to fuel cells. The problems with current reforming technologies are high operating temperatures and the quantity of carbon monoxide (CO) produced. Carbon monoxide acts as a poison upon contact with the proton exchange membrane (PEM) fuel cell (Pt based) catalyst. In an effort to reduce the CO produced, water is introduced with the fuel to convert the CO by the water-gas-shift (WGS) reaction. The objective of our research is to reduce the quantity of carbon monoxide produced during reforming to near-zero levels without the need for the water-gas-shift (WGS) reaction.

The conversion of natural gas into clean liquid fuels requires the use of cobalt-based Fischer Tropsch catalysts. Despite a great deal of research on these materials, the exact conditions to which the catalyst is exposed *after* reduction in hydrogen, and *before* it is fully on-line, have not been systematically studied in the open literature. These conditions include temperature, gas composition, and time. The specific relationships among these variables have a dramatic and irreversible effect on the activity, selectivity, and lifetime of the working catalyst. By conducting a systematic study of the activation of these catalysts, the changes in the cobalt metal that lead to optimal product yields and minimal deactivation rates can be identified.

Research into the physical properties and conversion of the methane contained within the methane hydrate molecule is an integral part of the Catalysis and Reactor Engineering Team. Methane hydrates have the potential of providing the U.S. with a supply of methane well into the next millennium. They occur naturally in deep-ocean and permafrost areas.

Many of the physical properties of methane hydrates are not well understood. One of these properties is the transport of methane within the hydrate [15]. Research planned in FY-02 will address this and other physical property issues with the aid of the larger hydrate reactor.

The photocatalytic conversion of the hydrates is based on research invented at NETL [16,17]. This research has applications in

the utilization of the methane contained in the vast hydrate deposits and as a solution to hydrate plugs that form in oil and gas pipelines.

Methane hydrates offer potential for the storage of natural gas. One volume of methane hydrates has the ability to store 180 volumes of methane at STP. [18] This ability of hydrates to contain vast quantities of methane opens the use of hydrates as a storage medium for natural gas. By use of methane hydrates, natural gas could be stored in a solid form at relatively moderate temperatures. Methane hydrates could also be used for the transport of stranded natural gas. By conversion of the natural gas into hydrates, transport to market of the solid hydrate is much more feasible than either pressurized liquefied natural gas tankers. In order to utilize hydrates as a storage medium for natural gas, the quantity of natural gas within the hydrate must be maximized.

Conclusions

The Ultra-Clean Fuels Focus Area at NETL has identified several issues that require advanced research to provide the 21st century transportation systems with ultra-clean transportation fuels. Specific Tasks were developed to address these issues and the research at NETL is striving to address the issues.

Acknowledgement

The authors would like to acknowledge the technical assistance from the members of the Ultra-Clean Fuels Focus Area.

Disclaimer

Reference in this report to any specific commercial product, process, or service is to facilitate understanding and does not necessarily imply its endorsement or favoring by the United States Department of Energy.

References

1. Iijima, S., "Helical Microtubules of Graphitic Carbon", *Nature*, **354**, (1991) 56-58.
2. Dillon, A. C.; Hebon, M. J., "Hydrogen Storage Using Carbon Adsorbents: Past, Present and Future", *Appl. Phys. A*, **72**, (2001) 133-42.
3. Bittner, E. W.; Smith, M. R.; Bockrath, B. C.; "Characterization of Adsorption on Carbon Nanotubes Using a Pulse Mass Analyzer", *Am. Chem. Soc. Div. Fuel Chem. Preprints*, **45(4)**, (2000), 898-902
4. Smith, M. R.; Bittner, E. W.; Bockrath, B. C., "Hydrogen Adsorption on Single-Walled Carbon Nanotubes", *Proceedings, Carbon '01, 25th Biennial Conference of the Amer. Carbon Soc.* (2001).
5. Armor, J. N.; Martenak, D. J., "Studying Carbon Formation at Elevated Pressure", *App. Cat. A: General*, **206**, (2001) 231-236.
6. Wang, Q.; Johnson, J. K., "Computer Simulations of Hydrogen Adsorption on Graphite Nanofibers", *J. Phys. Chem., B*, **103**, (1999), 277-281.
7. Wang, Q.; Johnson, J. K.; "Optimization of Carbon Nanotube Arrays for Hydrogen Adsorption", *J. Phys. Chem., B*, **103**, (1999), 4809-4813.
8. Johnson, K.; Smith, M.; Bittner, E.; Bockrath, B.; "Experimental and Simulation Study of Hydrogen Adsorption on Carbon Nanotubes", AIChE National Meeting, Reno NV, (2001).
9. Edwards, T.; Harrison III, W. E.; Maurice, L. Q. *American Institute of Aeronautics and Astronautics* **2001**, 1-10.
10. Lee, M. L.; Willey, C.; Castle, R. N.; White, C. M., Polynuclear Aromatic Hydrocarbons: Fourth International Symposium on Analysis, Chemistry, and Biology, Columbus, OH 1980; Battelle Press; 59-73.
11. Stumpf, A.; Tolvaj, K.; Juhasz, M. *J. Chromatogr. A* **1998**, *819*, 67-74.
12. Mossner, S. G.; Wise, S. A. *Anal. Chem.* **1999**, *71*, 58-69.
13. Shafi, R.; Hutchings, G. J. *Catalysis Today* **2000**, *59*, 423-442.
14. Energy Information Administration (EIA) report, *1998 Annual Energy Outlook*.
15. Hirohama, S.; Shimoyama, Y.; Wakabayashi, A. *J. Chem. Eng. Japan*, **29(6)**, 1014-1020, 1996.
16. U.S. Patent 5 720 858, February 24, 1998.
17. U.S. Patent 6,267,849, July 31, 2001.
18. Sloan, Jr., E.D. *Energy & Fuels*, **12** (1998) 191-196.

New Approaches to Deep Desulfurization for Ultra-Clean Gasoline and Diesel Fuels: An Overview

Chunshan Song*

Clean Fuels and Catalysis Program, The Energy Institute and Fuel Science Program, Dept. of Energy and Geo-Env. Engg.,
The Pennsylvania State University,
University Park, PA 16802

*E-Mail: csong@psu.edu

1. Introduction

The U.S. Clean Air Act Amendments of 1990 and new regulations by the U.S. EPA [EPA Gasoline-RIA, 1999; EPA Diesel-RIA, 2000; EPA RFG, 1999] and government regulations in many countries call for the production and use of more environmentally friendly transportation fuels with lower contents of sulfur and aromatics. In the mean time, the demand for transportation fuels has been increasing in most countries for the past two decades. The total U.S. consumption of petroleum products reached 18.68 million barrels per day (MBPD) in 1998. Of the petroleum consumed, 8.20 MBPD was used as motor gasoline, 3.44 MBPD as distillate fuels (including diesel fuels and industrial fuels), 1.57 MBPD as jet fuels, 0.82 MBPD as residual fuel oil, and 1.93 MBPD as liquefied petroleum gas (LPG), and 2.72—for other uses [EIA/AER, 1999].

Clean fuels research including desulfurization and dearomatization has become an important subject of environmental catalysis studies worldwide. Figure 1 presents a qualitative relationship between the size and type of sulfur molecules in various distillate fuel fractions and their relative reactivities. The reactivity ranking in Figure 1 is based on our experimental observations and a large amount of literature information [Knudsen et al., 1999; Whitehurst et al., 1998; Song et al., 2000]. With the new EPA Tier II regulations to cut the diesel sulfur from current 500 ppmw down to 15 ppmw by June 2006 and sulfur reduction from current 350 ppm to 30 ppm by 2005-2006, refineries are facing major challenges to meet the fuel sulfur specification along with the required reduction of aromatics contents.

The problem of deep removal of sulfur has become more serious due to the lower and lower limit of sulfur content in finished gasoline and diesel fuel products by regulatory specifications, and the higher and higher sulfur contents in the crude oils. A survey of the data on crude oil sulfur content and API gravity for the past two decades reveals a trend that U.S. refining crude slates continue towards higher sulfur contents and heavier feeds [Swain, 1991, 1998]. The average sulfur contents of all the crude oils refined in the five regions of the U.S. known as five Petroleum Administration for Defense Districts (PADDs) increased from 0.89 wt% in 1981 to 1.25 wt% in 1997, while the corresponding API gravity decreased from 33.74° in 1981 to 31.07° in 1997. In 2000, the average crude feeds to US refineries has 1.35 wt% sulfur and 31.0° API gravity, whereas European refinery feed by

comparison was sweeter at 1 wt% sulfur and 35 ° API gravity [Lawson, 2001].

2. Deep Desulfurization of Gasoline

Table 1 shows the typical gasoline pool compositions in the U.S. [Shorey et al., 1999] and in the Western Europe [Marcilly, 2001]. It is well known that naphtha from FCC makes up about 25-40% (average of 36% in the US) of gasoline blend stocks, but accounts for over 90% of the sulfur (up to 90-98%) and olefins in the entire gasoline pool. Therefore, the key to deep desulfurization of gasoline is sulfur removal from naphtha.

It is well known that sulfur removal from FCC naphtha can be achieved by catalytic hydrodesulfurization, but the accompanying decrease of octane number is a significant loss due to the saturation of olefins. Hydrotreating of FCC naphtha is an attractive process alternative, provided that octane losses are minimized. Because FCC naphtha also contains olefins which have higher octane number, selective sulfur removal without loss of octane number (loss of olefins) is desirable.

Approaches to reducing sulfur content in FCC naphtha include (1) post-treating product to remove sulfur from FCC naphtha [Sloley, 2001; O'Connor and Mayo, 2001]; (2) pretreating the FCC feed to remove sulfur [Shorey et al., 1999]; (3) increasing sulfur conversion in-situ to hydrogen sulfide during the FCC operation [O'Connor and Mayo, 2001].

There exist different active sites on hydrotreating catalysts (such as sulfided Co-Mo/Al₂O₃) for thiophene desulfurization and for olefin hydrogenation. Selective HDS could be achieved by passivating olefin hydrogenation sites. Some of the processes for gasoline desulfurization including selective HDS and alternate desulfurization options are briefly described below.

*Post treat FCC product to remove sulfur

- Apply conventional hydrodesulfurization without olefin preservation [Many companies]
- Convert organic sulfur to H₂S by selective hydrodesulfurization while preserving olefins [ExxonMobil's Scanfining; IFP Prime G+].
- Hydrodesulfurize organic sulfur, saturate olefins but convert paraffins for octane gain [ExxonMobil Octgain 125; UOP- INTEVEP ISAL].
- Catalytic distillation and hydrodesulfurization in the same vessel [CDTech's CDHydro + CDHDS].
- Sulfur adsorption and capture by solid adsorbent at elevated temperatures under low H₂ pressure [Phillips Petroleum S Zorb-Gasoline]
- Sulfur adsorption and capture by solid adsorbent at high temperatures [Research Triangle Institute TReND]
- Selective adsorption for removing sulfur (SARS) as organic compounds by solid adsorbent at ambient

temperature without using H₂ [Penn State University SARS process]

- Drop the organic sulfur to heavier fraction by alkylation of thiophenes [BP's OATS process].
- Remove the organic sulfur by using caustic treatment [Merichem's THIOLEX/REGEN process; EXOMER by Merichem and ExxonMobil] or extraction [GTC Technology's GT-DeSulf].

reduces sulfur in FCC naphtha and in Light cycle oil [Akzo Nobel, IFP, etc.]

***Increase sulfur conversion during FCC**

- Convert more organic sulfur into H₂S during FCC operation, which can moderately reduce sulfur in products [Akzo Nobel's Resolve; Grace Davison's Saturn (GSR-6.1)].

***Pretreat the FCC feed to remove sulfur**

- Deep hydrodesulfurization of FCC feed before catalytic cracking in FCC reactor, which greatly

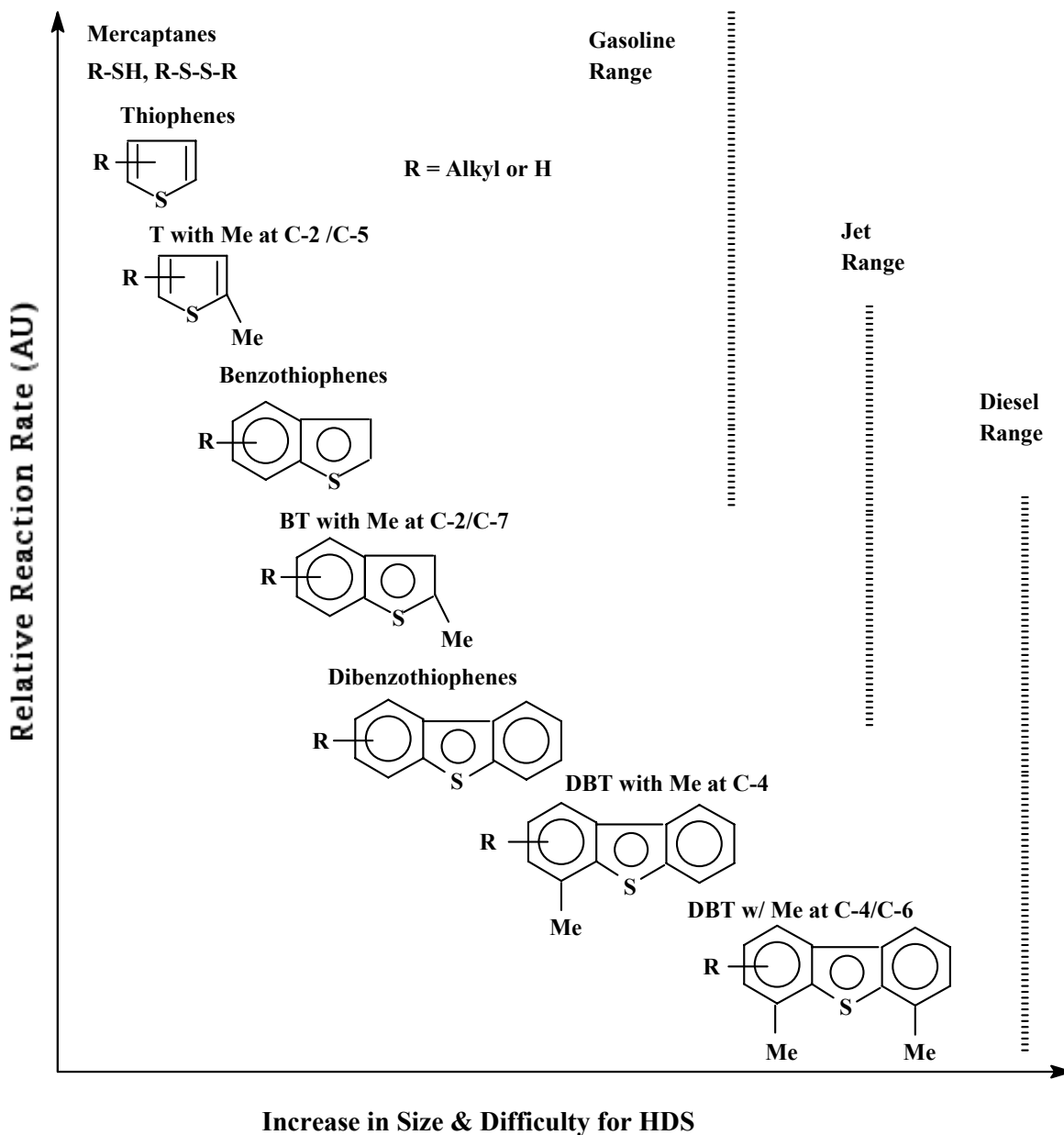


Figure 1. Reactivity of various organic sulfur compounds in hydrodesulfurization versus their ring sizes and positions of alkyl substitutions on the ring.

Compared to the diesel sulfur problem, it is not difficult to remove sulfur from gasoline. The challenges to the refinery for gasoline deep desulfurization are to meet the new EPA Tier-II regulations on sulfur contents and aromatic contents and still produce high-octane gasoline in a profitable manner.

In our laboratory, we are exploring a SARS (selective adsorption for removing sulfur) process for gasoline desulfurization at ambient temperatures without using H₂ [Ma

et al., 2001, 2002]. The SARS can be applied for on-site or on-board organic sulfur removal before the reformer for fuel cells, and for new desulfurization system for producing ultra-low-sulfur fuels in a future refinery. The SARS process is different from the Phillips S Zorb process that uses low-pressure H₂ at elevated temperatures [Gislason, 2001] and different from the TreND desulfurization process being developed by Research Triangle Institute that uses solid adsorbent at high temperatures [Turk and Gupta, 2001].

Table 1. Typical Gasoline Pool Composition in U.S. and W. Europe

Gasoline blend stocks	% Gasoline pool volume in US	% gasoline pool sulfur in US	% gasoline pool volume in W. Europe
FCC naphtha	36	98	27
Reformate	34	—	40
Alkylate	12	—	9
Light straight-run naphtha	3	1	7.5
Coker naphtha	1	1	~0
Hydrocracked naphtha	2	—	~0
Isomerate	5	—	10
Butanes	5	—	5.5
MTBE	2	—	1.0
Total	100 %	100 %	100 %

3. Deep Desulfurization of Diesel Fuels

The general chemistry of diesel fuel processing and hydrodesulfurization have been discussed in several recent reviews and books [Topsoe et al., 1996; Gates and Topsoe, 1997; Whitehurst et al., 1998; Knudson et al., 1999; Song et al., 2000]. Table 2 shows the volume fraction of U.S. highway diesel pool, and Table 3 shows the corresponding sulfur levels of U.S. highway diesel blendstocks [EPA Diesel-RIA, 2000]. Among the diesel blend stocks, the light cycle oil (LCO) from fluid catalytic cracking (FCC) contains highest amount of sulfur and aromatics, and the LCO also tends to have the highest contents of refractory sulfur compounds, especially 4methylthiophene and dibenzothiophene [EPA Diesel-RIA, 2000].

Deep desulfurization and ultra-deep desulfurization refers to processes to remove sulfur to below 500 ppmw and 15-50 ppmw, respectively. Described below are some of the processing approaches for ultra-deep desulfurization to produce ultra-low-sulfur (ultra-clean) diesel fuels. The key to ultra-deep desulfurization is the removal of refractory sulfur compounds, particularly 4,6-dimethyldibenzothiophene, from diesel fuels. In addition to straight-run gas oil, the light cycle oil (LCO) from FCC of heavy oils is a major blend stock for diesel fuels in the US. LCO has higher sulfur contents, in which the content of 4,6-dimethyldibenzothiophene is higher than other middle distillates in diesel pool. LCO also has higher aromatics contents, which makes the dearomatization necessary for producing low-aromatic diesel fuel.

The problem of deep hydrodesulfurization of diesel fuel is caused by the lower reactivity of 4,6-disubstituted dibenzothiophene, as represented by 4,6-dimethyldibenzothiophene (4,6-DMDBT) which has much lower reactivity than any other sulfur compounds [Ma et al., 1994] in diesel blend stocks. The methyl groups at 4- and 6-positions create steric hindrance for the interaction between sulfur and active sites on the catalysts. The problem is exacerbated by the inhibiting effects of polyaromatics and nitrogen compounds in some diesel blend stocks for diesel as well as H₂S that exist in reaction system on deep HDS. Based on experimental results, polyaromatics compete with sulfur compounds on the surface of hydrotreating catalyst, perhaps more for the flat chemisorption thereby influencing the hydrogenation and subsequent hydrodesulfurization, whereas H₂S compete with sulfur compounds, affecting more of the direct C-S hydrogenolysis route.

Approaches to ultra-deep desulfurization include (1) improving catalytic activity by new catalyst formulation for HDS of 4,6-DMDBT; (2) tailoring reaction and process conditions; (3) designing new reactor configurations; and (4) developing new processes. One or more approaches may be employed by a refinery to meet the challenges of producing ultra-clean fuels at affordable cost.

Design approaches for improving catalytic activity for ultra deep hydrodesulfurization focus on how to remove 4,6-DMDBT more effectively, by modifying catalyst formulations to (1) enhance hydrogenation of aromatic ring in 4,6-DMDBT by increasing hydrogenating ability of the catalyst; (2)

incorporate acidic feature in catalyst to induce isomerization of methyl groups away from 4- and 6-positions; and (3) remove inhibiting substances (such as H₂S) and tailoring the reaction conditions for specific catalytic functions. The catalytic materials formulations may be improved for better activity by using different supports (carbon, TiO₂, TiO₂-

Al₂O₃, HY, MCM-41, etc.) for conventional alumina-supported CoMo, NiMo and NiW catalysts; by increasing loading level of active metal (Mo, W, etc.); by adding one more base metal (e.g., Ni to CoMo or Co to NiMo); and by incorporating a noble metal (Pt, Pd, Ru, etc.).

Table 2 Volume Fraction of U.S. Highway Diesel Pool from each Feedstock Component

Diesel Blendstock	% of U.S. Highway Diesel Fuel Pool per Blendstock Boiling Fraction				
	Naphtha	Light Distillate	Heavy Distillate	Light Gas Oil	All Boiling Fractions Combined
Straight Run	0.1	6.4	4.9	1.0	12.4
Hydrotreated Straight Run	0.3	8.1	41.2	2.3	51.9
Cracked Stock	-	0.1	0.8	2.2	3.1
Hydrotreated Cracked Stock	-	2.1	15.6	1.7	19.4
Coker Gas Oil	-	-	1.0	-	1.0
Hydrotreated Coker Gas Oil	0.1	2.1	3.7	2.3	8.2
Hydrocrackate	-	1.3	2.7	-	4.0

Source: EPA, EPA420-R-00-026, 2000.

Described below are some of the processing approaches for ultra-deep desulfurization to produce ultra-low-sulfur diesel.

*** Approaches for deep desulfurization to produce ultra-low-sulfur diesel**

- Apply conventional hydrodesulfurization [Many companies can apply simple hydrotreating]
- Ultra-deep hydrodesulfurization of middle distillate [MAKFining premium Distillates technology (PDT) by Akzo Noble, Exxon Mobil, and Kellogg Brown]
- Ultra-deep hydrodesulfurization (SynHDS) and hydrodearomatization (SynSat) and cetane improvement by ring-opening (SynShift) of middle distillate [SynTechnology including new reactor design by SynAlliance including ABB Lummus, Criterion Catalyst, and Shell Global].
- Two-stage hydrotreating for ultra-low-sulfur diesel fuel using industrially proven high-activity TK catalysts [Haldor Topsoe]
- Ultra-deep hydrodesulfurization, hydrodenitrogenation and hydrogenation of distillate fuels [Unionfining by UOP]
- Hydrodearomatization (HDAR) of middle distillate in the second stage [MAKFining premium Distillates technology (PDT) by Akzo Noble, Exxon Mobil, and Kellogg Brown]
- Sulfur adsorption and capture by solid sorbent at elevated temperatures under low-pressure H₂ [Phillips Petroleum S Zorb Diesel]

- Selective adsorption of organic sulfur compounds in diesel fuels by solid adsorbent at ambient temperature without using H₂ [Penn State SARS process]
- Oxidative desulfurization by chemical oxidation in liquid phase [Ultrasonic desulfurization process by SulphCo using H₂O₂ under ultrasound irradiation; chemical oxidation by Petrostar using peroxyacetic acid]
- Biodesulfurization of distillate fuels using [microbial desulfurization process by Energy BioSystems Corp.]
- FCC feed deep hydrotreating to remove sulfur before catalytic cracking which produces naphtha and LCO [Some companies can apply deep hydrotreating for FCC feed]
- Undercutting of sulfur-rich narrow fraction of light cycle oil from FCC [to remove a narrow bp range that is rich in refractory sulfur compounds, and use it for off-road distillate fuels]

In our laboratory, we are developing new catalysts such as Co-Mo/MCM-41 and exploring effects of nitrogen on ultra-deep HDS for existing refinery processes [Song and Reddy, 1999; Reddy et al., 1998; Turaga and Song, 2001, 2002; Song et al., 2001]; exploring a novel SARS (selective adsorption for removing sulfur) process for ultra-deep desulfurization of diesel fuels at ambient temperatures without using H₂ [Ma et al., 2001, 2002; Sprague et al., 2002]; and further developing our proposed concept for design of sulfur-resistant noble metal catalyst for low-temperature hydrotreating [Song et al.,

1999a, 1999b; Reddy and Song, 1999; Sprague et al., 2002; Zheng et al., 2002] (see below).

Table 3 Sulfur levels of U.S. Highway Diesel Blendstocks (CA Excluded)

Diesel Blendstock	Sulfur Content (ppm) by Boiling Fraction				
	Naphtha	Light Distillate	Heavy Distillate	Light gas Oil	All Boiling Fractions Combined
Straight Run	827	1770	2269	4980	2218
Hydrotreated Straight Run	362	119	394	548	358
Cracked Stock	-	2219	2892	6347 ^a	5322
Hydrotreated Cracked Stock	18	37	939	1306 ^a	874
Coker Gas Oil	540	1800	3419	-	3419 (?)
Hydrotreated Coker Gas Oil	8	25	310	400	258
Hydrocrackate	-	1.3	2.7	-	4.0
	-	12	120	-	85

a: Indicate properties that were not reported in the refiner survey. These values were calculated by EPA using the reported sulfur contents of like boiling fractions in other diesel blend stocks by assuming the same relative sulfur levels between boiling fractions. Source: EPA, EPA420-R-00-026, 2000.

4. Deep Hydrogenation of Diesel Fuels

High aromatic content in distillate fuels lowers the fuel quality and contributes significantly to the formation of environmentally harmful emissions [Stanislaus and Cooper, 1994; Cooper and Donniss, 1996]. Reducing aromatic content along with sulfur content is generally desirable with respect to diesel fuel quality, as aromatic reductions increase cetane levels and generally improve combustion characteristics. California Air Resources Board (CARB) passed legislative measures to limit the sulfur and aromatic contents of diesel fuel to 0.05 wt% and 10 vol%, respectively, effective October 1993. However, reducing aromatics consumes hydrogen and increases the cost of desulfurization relative to a case where only sulfur was being removed.

Currently, conventional hydrotreating technology is adapted for dearomatization by aromatics saturation [Stanislaus and Cooper, 1994]. Typical conventional catalysts for fuel hydroprocessing are sulfided Co-Mo and Ni-Mo supported on alumina. Some studies have shown that complete hydrogenation of aromatics is not possible owing to equilibrium limitations under typical hydrotreating conditions. Conventional middle distillate hydrotreaters designed to reduce sulfur and nitrogen levels would lower the diesel aromatics only marginally [Stanislaus and Cooper, 1994; Cooper and Donniss, 1996]. For example, Ali and Siddiqui [1997] compared 3 types of hydrotreating catalysts, CoMo/Al₂O₃, NiMo/Al₂O₃ and NiW/Al₂O₃, for dearomatization of light cycle oil. They observed that the type of catalyst has a critical influence on the composition and properties of the product. Their data show that it was not

possible to obtain a diesel product that meets stringent specifications using one type of catalyst in a single-stage reactor even under severe operating conditions [Ali and Siddiqui, 1997].

While noble metals are active for hydrogenation at low temperatures, their use is limited because of their sensitivity to sulfur poison. In current processing schemes involving noble metal catalysts, two or more stages with multiple catalyst beds are used to achieve deep desulfurization and deep hydrogenation. Hydrodesulfurization occurs in the first stage over a Ni-Mo or Co-Mo catalyst, followed by intermediate byproduct gas removal. Finally, hydrogenation over the noble metal catalyst operates in the last stage or bottom bed where the concentrations of catalyst poisons (organosulfur and H₂S) are extremely low [Stork, 1996; Maxwell, 1997]. Commercial examples of two-stage or multi-stage hydroprocessing technology include the Shell Middle Distillate Hydrogenation process by Shell [Lucien et al., 1994; Stork, 1996], the Dual-Stage Process by Haldor-Topsoe [Cooper et al., 1994], and hydrotreating process by IFP [Marchal et al., 1994], and the SynSat process developed by Criterion/Lummus [Suchanek, 1996; Maxwell, 1997]. There are no reports of noble metal catalysts that can operate without such intermediate H₂S removal [Stork, 1996].

A New Approach for Catalyst Design.

Because of its importance, sulfur resistance of noble metal catalysts has been the subject of a number of studies [Cooper and Donniss, 1996; Absi-Halabi et al., 1997; Lin and Song, 1996; Schmitz and Song, 1997; Song et al., 1999a, 1999b]. More recently, a new approach has been proposed for the design of sulfur-resistant noble metal catalysts for low-temperature hydrotreating of sulfur-containing distillates to

produce clean distillate fuels [Song, 1998, 1999a] such as diesel fuels and jet fuels. The proposed design concept [Song, 1999b] invokes some unique zeolites as supports for noble metals and utilizes (1) shape-selective exclusion, (2) hydrogen spillover, and (3) two types of sulfur resistance. Unique zeolite supports can be used to prepare bimodal distributions of noble metal particles. Some metals are located in small pores (**Sm**: pore opening less than about 5 Å); whereas, others will be contained in large pores (**La**: pore opening larger than 6 Å). Preferably, the two pore systems inter-connect, or are at least uniformly distributed so that they are in close proximity. Diffusion of organosulfur compounds such as thiophenic molecules into the small-pores would be inhibited by size (shape-selective exclusion). The large pores (large micropore or mesopore range) would preferably allow fast diffusion and reaction of bulky polycyclic aromatic and sulfur compounds.

The thiophenic molecules could enter the large pores, but not the small pores. However, H₂ molecules can readily enter both types of pores, dissociatively adsorb on metal contained within, and be transported between pore systems by spillover. When the metal in the large pores becomes inactivated by adsorbed sulfur, spillover hydrogen could recover the poisoned metal sites by elimination of R-S-R and R-S-H. It is also of interest to classify sulfur resistance as either type I, resistance to organic sulfur compounds, or type II, resistance to inorganic H₂S (5). The metal species, particularly those in small pores, should have higher type II sulfur resistance. Figure 2 shows a simplified representation of the proposed new concept [Song 1999a, 1999b].

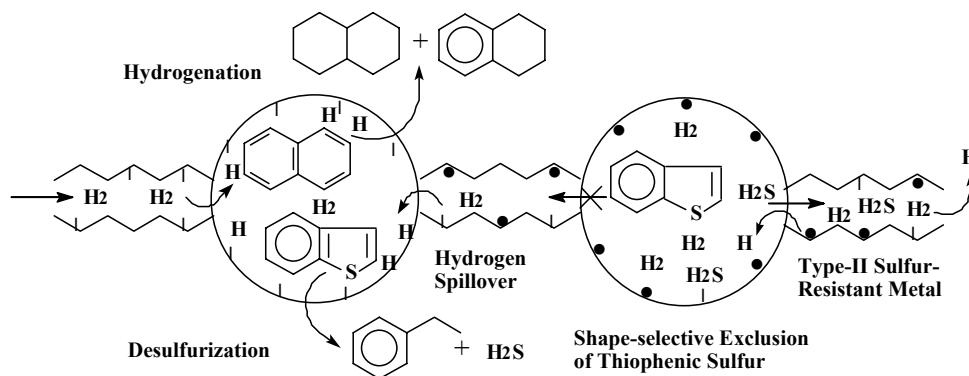


Figure 2. The proposed new concept for catalyst design based on shape-selective exclusion, hydrogen spillover, and two types of sulfur resistance. The black dots indicate metal particles on internal surface.

5. Conclusions

Heightened concerns for cleaner air and increasingly more stringent regulations on sulfur contents in transportation fuels will make desulfurization more and more important. The sulfur problem is becoming more serious in general, particularly for diesel fuels, as the regulated sulfur content is getting an order of magnitude lower, while the sulfur contents of crude oils refined in the U.S. are becoming higher.

The challenge for deep desulfurization of diesel fuels is the difficulty of removing refractory sulfur compounds, particularly 4,6-dimethyldibenzothiophene, with conventional hydrodesulfurization processes. The problem is exacerbated by the inhibiting effects of polyaromatics and nitrogen compounds as well as H₂S on deep HDS.

The challenge for gasoline deep desulfurization is the selective HDS of thiophenic compounds without a significant loss of octane number. Octane loss can be avoided by preserving olefinic components in FCC naphtha, or by isomerizing paraffinic components of naphtha.

The chemistries of gasoline and diesel fuel processing have evolved significantly around the central issue of how to produce cleaner fuels in a more efficient, environmentally friendly and affordable fashion. New design approaches are necessary for making affordable ultra-clean fuels.

Acknowledgments

I am grateful to Prof. Harold H. Schobert of PSU for many helpful general discussions on fuel chemistry, and to my coworkers including Dr. Xiaoliang Ma, Mr. Uday Turaga, Mr. Gang Wang and Mr. Michael Sprague of PSU for helpful discussions on diesel fuel desulfurization. I would like to acknowledge US Department of Energy, US Air Force Office of Scientific Research, and US Department of Defense for partial financial support of various portions of our research.

References

- Avidan, A., Klein, B. and Ragsdale, R. Improved Planning Can Optimize Solutions to Produce Clean Fuels. *Hydrocarbon Processing*, 2001, 80 (2), 47-53.

- Cooper, B. H. and Donnis, B. B. L. Aromatic Saturation of Distillates: An Overview. *Appl. Catal. A.*, 1996, 137, 203-223.
- EIA/AER. 1999. Annual Energy Review 1998. Energy Information Administration, U.S. Department of Energy, Washington D.C.
- EPA-Diesel RIA. Regulatory Impact Analysis: Heavy-Duty Engine and Vehicle Standards and Highway Diesel Fuel Sulfur Control Requirements. United States Environmental Protection Agency, Air and Radiation EPA420-R-00-026, December 2000
- EPA-Gasoline RIA. Regulatory Impact Analysis - Control of Air Pollution from New Motor Vehicles: Tier 2 Motor Vehicle Emissions Standards and Gasoline Sulfur Control Requirements. U.S. Environmental Protection Agency, Air and Radiation EPA420-R-99-023, December 1999
- EPA-RFG-II. Phase II RFG Report on Performance Testing. U.S. Environmental Protection Agency, Air and Radiation EPA420-R-99-025, April 1999.
- Gates, B. C.; H. Topsoe. Reactivities in Deep Catalytic Hydrodesulfurization: Challenges, Opportunities, and the Importance of 4-Methyldibenzothiophene and 4,6-Dimethyldibenzothiophene. *Polyhedron*. 1997, 16, 3213.
- Knudsen, K. G., Cooper, B. H. and Topsoe, H. Catalyst and Process Technologies for Ultra Low Sulfur Diesel. *Appl. Catal. A: Gen.*, 1999, 189 (2), 205-215.
- Lawson, W.F. Clean Transportation Fuels in the United States. Paper presented at the 3rd US-China Oil and Gas Industry Forum, Beijing, China, Sept 10-12, 2001.
- Ma, X., Sakanishi, K., and Mochida, I. 1994a. Hydrodesulfurization Reactivities of Various Sulfur Compounds in Diesel Fuel, *Ind. Eng. Chem.*, 33, 218-222.
- Ma, X., Sun, L., Yin, Z., and Song, C. New Approaches to Deep Desulfurization of Diesel Fuel, Jet Fuel, and Gasoline by Adsorption for Ultra-Clean Fuels and for Fuel Cell Applications. *Am. Chem. Soc. Div. Fuel Chem. Prepr.*, 2001, 46 (2), 648-649.
- Ma, X., Sprague, M.J., Sun, L., and Song, C. DEEP DESULFURIZATION OF LIQUID HYDROCARBONS BY SELECTIVE ADSORPTION FOR FUEL CELL APPLICATIONS. *Am. Chem. Soc. Div. Petrol. Chem. Prepr.*, 2002, 47, in press.
- Marcilly, C. Evolution of Refining and Petrochemicals. What Is the Place of Zeolites. *Stud. Surf. Sci. Catal.*, 2001, 135, 37-60.
- Maxwell, I. E. Innovation in Applied Catalysis. *Cattech*, 1997, 1, 5-13.
- News-OATS. Process Removes Sulfur, Octane Not Reduced. *Hydrocarbon Processing*, 2001, 80 (2), 33.
- News-THIOLEX. Taming Gasoline Sulfur. *Hydrocarbon Processing*, 2001, 80 (2), 129.
- O'Connor, P. and Mayo, S. Technology Opportunities for Clean Fuels. *Am. Chem. Soc. Div. Fuel Chem. Prepr.*, 2001, 46 (2), 381-386.
- Reddy, K. M., Wei, B., and Song, C. Mesoporous Molecular Sieve MCM-41 Supported Co-Mo Catalyst for Hydrodesulfurization of Petroleum Resids. *Catalysis Today*, 1998, 43 (3), 261-272.
- Reddy, K. M. and Song, C. Mesoporous Molecular Sieve MCM-41 Supported Pt and Pd Catalysts for Low-Temperature Hydrogenation of Aromatics in Distillate Fuels. Chapter 15 in *Designing Transportation Fuels for a Cleaner Environment*. J. G. Reynolds and M. R. Khan eds. Philadelphia: Taylor & Francis, 1999, pp. 173-185.
- Shorey, S. W., Lomas, D. A. and Keesom, W. H. Use FCC Feed Pretreating methods to Reduce Sulfur. *Hydrocarbon Processing*, 1999, 78 (11), 43-51.
- Sloley, A. W. Cat Naphtha Sulfur Management: Undercut or Not? *Hydrocarbon Processing*, 2001, 80 (2), 75-78.
- Song, C. Designing Sulfur-Resistant, Noble-Metal Hydrotreating Catalysts. *Chemtech*, 1999a, 29 (3), 26-30.
- Song, C. Sulfur-Resistant Noble Metal Catalysts Based on Shape-Selective Exclusion and Hydrogen Spillover. *Am. Chem. Soc. Symp. Ser.*, 1999b, 738, 381-390.
- Song, C., Reddy, K. M. Mesoporous Molecular Sieve MCM-41 Supported Co-Mo Catalyst for Hydrodesulfurization of Dibenzothiophene in Distillate Fuels. *Appl. Catal. A: Gen.*, 1999, 176, 1-10.
- Song, C., Hsu, C. S. and Mochida, I. *Chemistry of Diesel Fuels*. Taylor & Francis Publishing Company, New York, 2000, 294 pp. [ISBN 1-56032-845-2].
- Sprague, M. J.; Zheng, J.; Song, C. Effect of Sulfur Removal from Naphthalene on Its Hydrogenation over Mordenite-Supported Pd Catalysts. *Prepr. Pap. - Am. Chem. Soc., Div. Pet. Chem.* 2002, 47 (1), in press.
- Stanislaus, A. and Cooper, B. H. Aromatic Hydrogenation Catalysis: A Review. *Catal. Rev. - Sci. Eng.*, 1994, 36, 75-123.
- Stork, W. H. J. Performance Testing Of Hydroconversion Catalysts. *Am. Chem. Soc. Sym. Ser.*, 1996, 634, 379-400.
- Suchanek, A. How To Make Low-Sulfur, Low Aromatics, High Cetane Diesel Fuel. *ACS Div. Petrol. Chem. Preprints*, 1996, 41, 583-584.
- Swain E.J. US Crude Slate Gets Heavier, Higher in Sulfur. *Oil Gas J.*, 1991, 89 (36), 59-61.
- Swain E.J. US Refining Crude Slates Continue Towards Heavier Feeds, Higher Sulfur Contents. *Oil Gas J.*, 1998, 96 (40), 43-48.
- Topsoe, H., Clausen, B. S., Massoth, F. E. *Hydrotreating Catalysis. Science and Technology*. Springer-Verlag, Berlin, 1996, 310 pp.
- Turaga, U. and Song, C. Deep Hydrodesulfurization of Diesel and Jet Fuels Using Mesoporous Molecular Sieve-Supported Co-Mo/MCM-41 Catalysts. *Am. Chem. Soc. Div. Fuel Chem. Prepr.*, 2001, 46 (3), 275-279.
- Turaga, U.T., Wang, G., Ma, X., Song, C. and Schobert, H.H. Influence of Nitrogen on Deep Hydrodesulfurization of 4,6-Dimethyldibenzothiophene. *Prepr. Pap. - Am. Chem. Soc., Div. Pet. Chem.* 2002, 47(1), 89-92.
- Turk, B. S. and Gupta, R. P. RTI's TreND Process for Deep Desulfurization of Naphtha. *Am. Chem. Soc. Div. Fuel Chem. Prepr.*, 2001, 46 (2), 392-393.
- Whitehurst, D. D., Isoda, T., and Mochida, I. Present State of the Art and Future Challenges in the Hydrodesulfurization of Polyaromatic Sulfur Compounds. *Adv. Catal.* 1998, 42, 345.
- Zheng, J.; Sprague, M. J.; Song, C. Unique Sulfur-Resistance of Mordenite-Supported Pd Catalyst for Hydrogenation of Naphthalene in the Presence of Sulfur. *Prepr. Pap. - Am. Chem. Soc., Div. Petrol. Chem.* 2002, 47 (1), in press.

A New Method of Bimodal Support Preparation and Its Application in Fischer-Tropsch Synthesis

Noritatsu Tsubaki^{1*}, Yi Zhang², Shouli Sun², Yoshiharu Yoneyama¹, Xiaohong Li³, Kaoru Fujimoto³

*1. Department of Material System and Life Science, School of Engineering, Toyama University, Gofuku 3190, Toyama 930-8555, Japan

2. Department of Applied Chemistry, School of Engineering, The University of Tokyo, Hongo 7-3-1, Bunkyo-ku, Tokyo 113-8656, Japan

3. School of Engineering, Kita-kyushu University, Kita-kyushu, Fukuoka, Japan

Introduction

The reaction performance of the supported metal catalysts was controlled by a number of factors, such as support property, metal precursor identity and calcination temperature. Among these factors, support pore size has great effect on the mass transfer of reactants and products. The catalyst pore size affected not only catalytic activity but also product selectivity. On the other hand, the supported metal particle size has close relationship with the surface area of support. Generally, the metal dispersion is enhanced with the increased surface area of the support. But, if the support has large surface area, it usually has small pore size. Undoubtedly, the intrapellet diffusion efficiency is poor for small-pore catalyst, especially in the multi-phase reactor. The bimodal catalyst where both large pore and small pore coexist can guarantee high diffusion efficiency and large supported metal area meantime, as theoretically proved by Levenspiel [1].

Inui et al. developed a kind of bimodal Ni/SiO₂ catalyst utilizing very strong acidic corrosion function of *aqua regia*. This kind of catalyst showed high activity for methanation of CO₂ [2]. Inoue et al. found an alcohothermal treatment method of gibbsite to prepare bimodal alumina support, using various alcohols [3].

To find a simple preparation method and control pore size more easily, we here propose a new method, which made small pores formed on the inner walls of the support with large pores. Thus, this kind of support is estimated to realize not only higher diffusion efficiency of reactants and products by large pore, but also higher metal dispersion through the enlarged surface area; and can be expected to realize high catalytic activity. As an application of this kind of bimodal support, it was used for liquid-phase Fischer-Tropsch synthesis (FTS) where cobalt was supported.

Experimental

The bimodal support was prepared by incipient-wetness impregnation of commercially available silica gel (Cariact Q-50, Fuji Silysia Co., specific surface area: 70 m² g⁻¹, pore volume: 1 ml g⁻¹, pellet size: 74-590 μm and pore diameter: 50 nm) with silica sol (Snowtex XS, Nissan Chemicals Co.) of different concentration. After the impregnation, the support was dried in air at 393 K for 12 h, and then calcined in air at 673 K for 2 h. The properties of the silica sol were listed in Table 1.

Cobalt-supported catalyst with 10wt% metal loading was prepared by incipient-wetness impregnation of different supports, including the bimodal support, with cobalt nitrate aqueous solution. The catalyst precursors were dried in air at 393 K for 12 h, then calcined in air from room temperature to 673 K with a ramping rate of 2 K min⁻¹ and kept at 673K for 2 h. After calcination, the catalysts were activated in flowing hydrogen at 673 K for 10 h and at last, passivated by 1 % oxygen in nitrogen.

FTS reaction was carried out in a semi-batch autoclave (slurry-phase reactor, perfectly mixed flow reactor due to continuous stirring) with the inner volume of 80 ml. The passivated catalyst (1.0g, under 149 μm) and 20 ml liquid medium (n-hexadecane) were loaded in the reactor. During the reaction, effluent gas released from the reactor was analyzed by on-line gas chromatography. CO and CO₂ were analyzed by using an active charcoal column equipped with a thermal conductivity detector (TCD). The hydrocarbons were also analyzed on-line using capillary columns for C₁-C₅ (Porapak Q) and for C₆-C₂₀ (SE-30, uniport), respectively. The carbon balance was between 95% and 98% for all of reactions. Argon was employed as an internal standard with concentration of 3 % in the feed gas. The reaction conditions were P (total) = 1.0 MPa, CO/H₂ = 1/2, W/F (CO + H₂ + Ar) = 10 g h mol⁻¹, T = 513 K.

Pore size distribution, BET surface area and pore volume were determined by the measuring instrument for surface area and pore size of porous materials (Shimadzu ASAP 2000) where nitrogen was used as adsorbent. Supported cobalt crystalline size was detected by TEM (TOPCON EM-002B, Acc.Volt: 200kV, Point resolution: 0.18nm Line resolution: 0.14nm)

Results and Discussion

The pore distribution of the obtained bimodal support was shown in Fig. 1. It gave clear evidence that two kinds of pore existed. The two pore diameters of bimodal support prepared from Snowtex XS were 6 and 45 nm respectively. 45nm-pore was from the intrinsic pore of the used Cariact Q-50 pellet and 6nm-pore was the new pores formed from micro particle in silica sol Snowtex. Consequently, as compared in Table 2, BET surface area was enhanced from 70 m²/g of Cariact Q-50 to 106m²/g of the bimodal one, which was mainly the contribution from the newly-formed small pores. More importantly, the pore volume of the obtained bimodal support decreased from 1.0 ml/g of Cariact Q-50 to 0.4ml/g, indicating that silica sol indeed entered the uniformly distributed large pores of Cariact Q-50 as shown also in Fig. 1. If the silica sol did not enter the large pore, the observed pore volume would not change. Small silica particles from sol deposited onto inner walls of the large pore, via calcination and bond formation between surface silanol groups, to form small pores. If the large pore was blocked by the sol-derived silica structure, the BET surface area should be lowered remarkably. Considering the increased BET area and slightly decreased size of the large pore from original 50nm to 45nm, it is able to conclude that the obtained bimodal support formed according to the designed route.

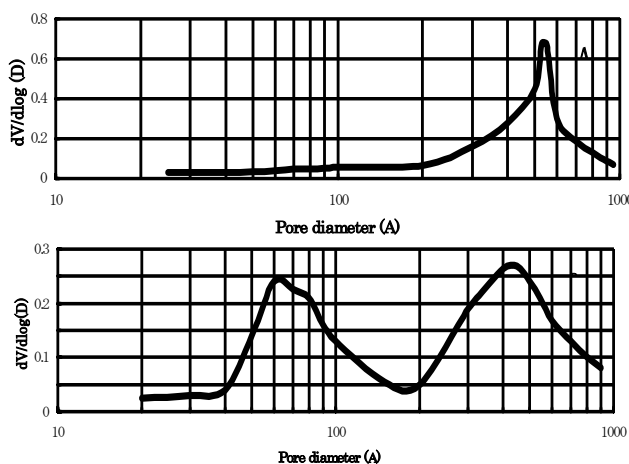


Figure 1. The pore size distributions of Q-50 and bimodal support A: Q-50. B: bimodal support.

Table 1 The properties of silica sol

Sol	pH	Content (wt%)	Solvent	Particle size nm
Silica	9.0-10.0	SiO ₂ 20%	Water	5.0

Table 2 The properties of various supports

Support	Surface area m ² /g	Pore Volume ml/g	Pore size nm
Q-50	70	1.0	50
Bimodal	106	0.4	6.0, 45
Q-3	546	0.3	3.0

To investigate the promotional role of the bimodal catalyst, it was applied to liquid-phase Fischer-Tropsch synthesis reaction. Liquid-phase Fischer-Tropsch synthesis reaction has advantages in temperature control, wax extraction and catalyst lifetime extension, compared to the common gas-phase reaction [4]. But the main drawback of the liquid-phase FTS reaction was the slow diffusion rate of the syngas as well as the formed hydrocarbons. To release the overall reaction from possible diffusion-controlled regime and obtain maximum hydrocarbon yield, bimodal Co/SiO₂ catalysts were tested.

The reaction performance of the catalysts prepared from the bimodal support or Cariact Q-50, Q-3 was compared in Fig. 3. The reaction rate of all of catalysts reached steady state from reaction running 1hr. Cariact Q-3 was an analogy to Q-50 but with average pore size of 3nm. Their property was shown in Table 2. Catalyst prepared from Q-3 support had the largest surface area but the smallest pore diameter. It exhibited low catalytic activity and the highest methane selectivity. For the catalyst prepared from Q-50 support, which had the lowest surface area and the largest pore size, the CO conversion, CH₄ and CO₂ selectivity were the lowest. For the catalyst prepared from bimodal support, the CO conversion was the highest, and meanwhile selectivities of CH₄ and CO₂ were as low as to those of the catalyst prepared from Q-50. Bimodal catalyst showed the best performances here.

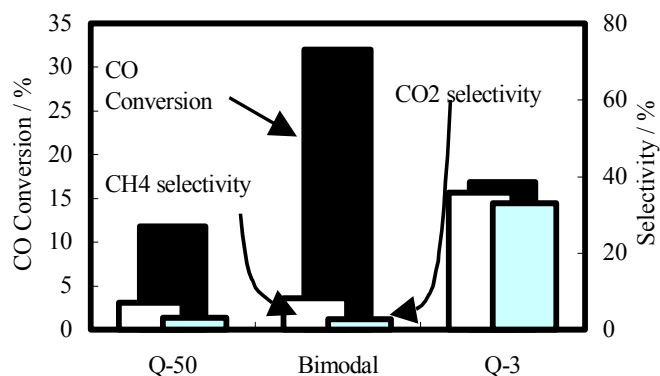


Figure 2. The reaction performance of cobalt catalysts prepared from different support

Reaction conditions: 513 K, 1.0MPa, W/F = 10 g h mol⁻¹, H₂/CO = 2, cobalt loading: 10wt%

The activities and selectivities of the FTS catalysts are markedly depending on their pore structure. The catalyst having a small pore size tended to produce lighter hydrocarbons. On the other hand, the product distribution of large-pore catalyst was wider and the proportion of the heavy hydrocarbon was high [5]. It has been

already pointed out that the propagation of the carbon-carbon chain occurred more easily on the catalyst with lower specific surface area where metallic particle size was larger [6, 7], which naturally decreased methane formation. Furthermore, 1-olefins are generally produced as primary products in FTS and are successively hydrogenated to paraffins [8]. But they can re-adsorb onto metallic sites to receive secondary hydrocracking, breaking the terminal double bond and releasing methane, especially in the liquid-phase FTS reaction [4]. When the pore size was larger, the transportation of the primary product was more effective and relevantly methane formation rate from secondary hydrocracking of olefins was lower. Also lower BET surface area of large-pore support determined larger metallic size and suppressed methane formation. Based on these reasons, the methane selectivity was the lowest for the catalyst prepared from Q-50. Due to the larger pore existing in the catalyst prepared from bimodal support, the CH₄ selectivity was also low. On the other hand, FT synthesis rates on cobalt catalyst can be improved by increasing the dispersion of supported cobalt crystalline. Generally, the metal dispersion is increased with the increased surface area and the decreased pore size of support. And the TEM data in Table 3 showed the supported cobalt crystalline size as 37nm for Q-50 catalyst, 22.6nm for bimodal catalyst and 1.4nm for Q-3 catalyst. For Q-3 derived catalyst, its small pore and slow diffusion efficiency determined high methane selectivity. But its CO conversion was not the highest, regardless of its highest metal dispersion in this study.

Table 3 The properties of Co/SiO₂ catalyst derived from various supports

Catalyst	BET m ² /g	Pore vol. ml/g	Pore size nm	TEM crystal size nm
Q-50 catalyst	52	0.82	54	37
Bimodal catalyst	82	0.28	8.0 47	22.6
Q-3 catalyst	513	0.16	3.7	1.4

Cobalt loading: 10%

The BET surface and pore volume decreased and average pore size increased very slightly for various Co/SiO₂ catalysts, since the supported cobalt crystalline blocked some smaller pore of support, but the bimodal catalyst still kept bimodal structure with two kinds of pore size of 8nm and 47nm, as in Table 3. Bimodal catalyst, having higher metal dispersion due to its larger BET surface area, and accelerated diffusion rate derived from the bimodal structure, exhibited the highest CO conversion and low methane selectivity.

The preparation method of introducing oxide sols other than silica into large-pore silica pellet is being developed.

References

- [1] O. Levenspiel, Chemical Reaction Engineering, 2nd ed., p. 496, Wiley, New York, 1972
- [2] T. Inui, M. Funabiki, M. Suehiro, T. Sezume, J. Chem. Soc. Faraday, I, 75(1979)787.
- [3] M. Inoue, K. Kitamura, T. Inui, J. Chem. Tech. Biotechnol., 46(1989)233..
- [4] L. Fan, K. Yokota, K. Fujimoto, Topics in Catalysis, 2(1995)267.
- [5] L. Fan, K. Yokota, K. Fujimoto, AIChE J. 38 (1992) 1639.
- [6] H. H. Nijs, P. A. Jacobs, J. Catal. 65 (1980) 328.
- [7] K. Fujimoto, T. Nobusawa, T. Fukushima, and H. Tominaga, Bull. Chem. Soc. Jpn. 58 (1985) 3164.
- [8] R. Madon, S. Reyes, E. Iglesia, J. Phys. Chem., 95(1991)7795.

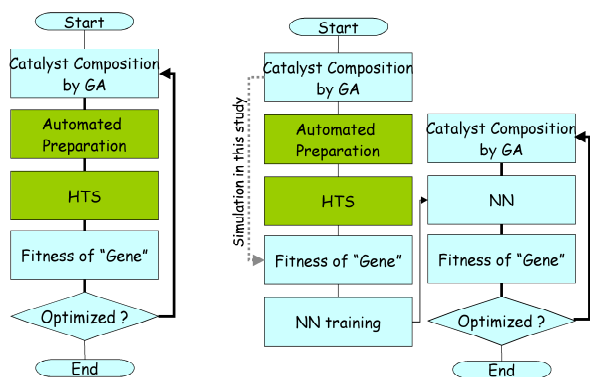
Optimization of Cu-Zn-Al-Sc Oxide Catalyst for Methanol Synthesis Using Genetic Algorithm and Neural Network

K. Omata, T. Umegaki, Y. Watanabe, N. Nukui and M. Yamada

Department of Applied Chemistry, Graduate School of Engineering, Tohoku University, Aoba 07, Aramaki, Aoba-ku, Sendai 980-8579, JAPAN

Introduction

Combinatorial catalysis (1) attracts much attention as an effective tool for catalyst development. The authors reported the tool consisting of high-pressure HTS reactor (2), automated catalyst preparation and genetic algorithm (GA) (3), which was applied successfully for optimization of copper base catalyst for methanol synthesis from syngas at 1MPa (4). Steps of catalyst composition specification by GA, automatic catalyst preparation, parallel activity test in high-pressure HTS reactor, and feedback to the GA program, are repeated in this method before satisfactory optimization (Figure 1(a)). Even though catalyst preparation is automated and activity-test is parallelized for large amount of catalyst sample to evaluate the large population of gene in GA program, these steps require much labor and time determining the rate of total screening. In order to replace these laborious experimental steps, evaluation by artificial neural network was introduced (Figure 1(b)).



(a) Conventional GA Process

(b) NN assisted GA Process

Figure 1. Flow chart of catalyst optimization using GA and NN for its evaluation function.

Among many type of a neural network, a back-propagation type neural network (NN) has been successfully applied to catalyst design. In their pioneering work, Hattroi and Kito applied NN to investigate the relationship between various properties of catalysts and both activity and selectivity of the catalyst (5). NN is also a promising tool to process and generalize experimental data. It facilitates approximation of catalytic activity under untested reaction conditions (6 - 9). The tool can be converted to optimization tool for catalyst composition (10). Hou et al reported the active catalyst for ammoxidation of propane optimized using NN trained by 23 experimental data showing the relation between catalyst component (P, K, Cr, Mo, V, Al₂O₃/SiO₂ ratio) and the activity

(10a). Cundari et al used GA as optimization tool to find better catalyst based on the identical data (11).

For better NN with high generalization ability, data dispersion is an important factor. From this point of view, the first generation in GA program is adequate for training data because it is determined randomly and dispersed. In the present study simulation of this method to replace experimental steps of catalyst preparation and activity test by NN was studied.

Experimental

Quaternary catalyst of Cu-Zn-Al-Sc was used. The activity for training should be determined by experiment but it was determined as a function of Cu/(Cu+Zn) ratio, (Cu+Zn)/(Cu+Zn+Al+Sc) ratio and Al/(Al+Sc) ratio (4) because the judgment for convergence is easier. The catalyst composition and its simulated activity for NN training are shown in Figure 2.

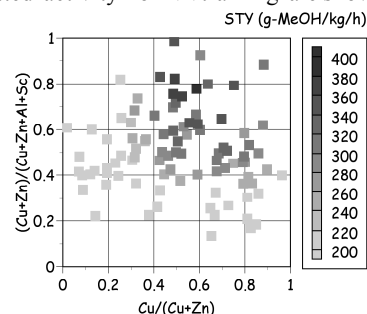


Figure 2. Catalyst composition and its simulated activity for training of neural network.

GA program for optimization was coded by Excel (3) and Neural Connection® (SPSS Inc.) was used as NN program for the activity evaluation. The number of nodes of input layer is 3, which accept Cu/(Cu+Zn) ratio, (Cu+Zn)/(Cu+Zn+Al+Sc) ratio and Al/(Al+Sc) ratio while the output layer of one node gives STY. The numbers of nodes of the hidden layers are 9 and 6, respectively. 92 dataset was used for training by back-propagation method. NN was suitably trained after 2000 epochs.

Results and Discussion

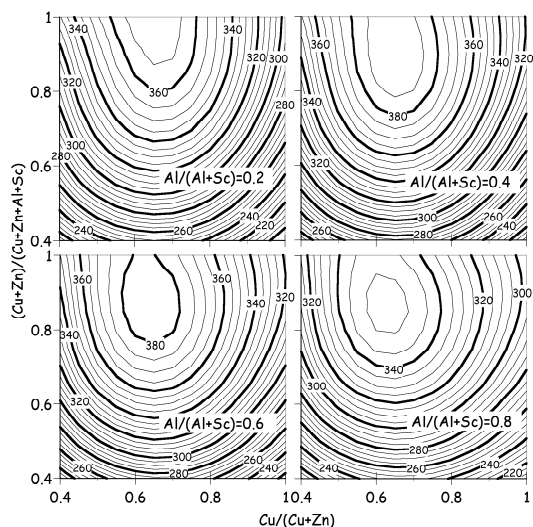


Figure 3. Activity by trained neural network.

The activity estimated by NN trained by back-propagation method is shown in **Figure 3**. The results suggest that the trained NN can be applied for minute evaluation of "gene" in GA program. The catalyst was optimized by the GA program using the NN as fitness of catalyst code. $\text{Cu}/(\text{Cu}+\text{Zn})$ and $(\text{Cu}+\text{Zn})/(\text{Cu}+\text{Zn}+\text{Al}+\text{Sc})$ of every catalyst in the 1st, 2nd, 5th, and 15th generation is plotted in **Figure 4**. The catalysts gradually converge to the optimum and the maximum activity at 15th generation is 391 of $\text{Cu}_{0.59}\text{Zn}_{0.32}\text{Al}_{0.04}\text{Sc}_{0.05}\text{O}_{1.05}$. Since the maximum activity of simulated STY is 400 of $\text{Cu}_{0.60}\text{Zn}_{0.30}\text{Al}_{0.05}\text{Sc}_{0.05}\text{O}_{1.05}$, the GA program assisted by NN succeeded to find the maximum.

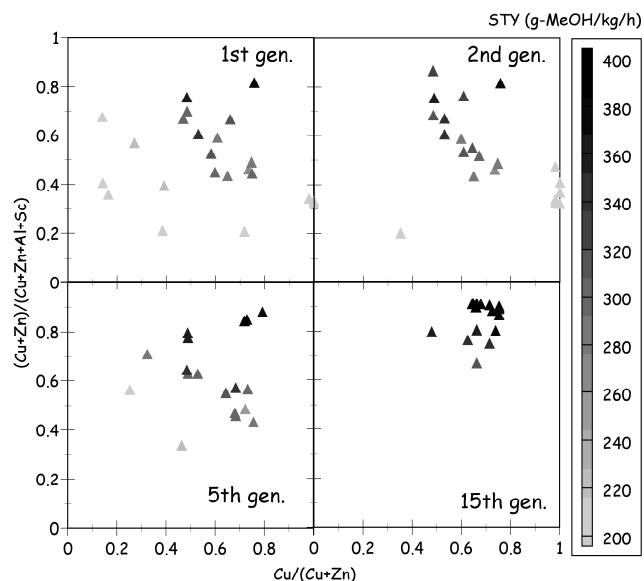


Figure 4 Convergence of Catalyst Component.

If NN can show the catalytic activity, GA program would be seemed worthless. Visualization for direct optimization is, however, only possible when the number of independent parameter is limited. In **Figure 3**, where the number of independent parameter is three, $\text{Cu}/(\text{Cu}+\text{Zn})$ ratio of every maximum point is 0.645. So mapping of the activity as a function of $(\text{Cu}+\text{Zn})/\text{all}$ and $\text{Al}/(\text{Al}+\text{Sc})$ is possible without the vague as shown in **Figure 5**. In such a lucky case optimum point can be directly found while optimization program is necessary when the number of independent parameter is more than four. As shown in **Figure 1**, GA and NN are complementary tools for catalyst optimization. The combination of combinatorial chemistry (parallel catalyst preparation), HTS (parallel activity test), GA and NN is certainly the robust tool.

Conclusions

Simple genetic algorithm assisted by neural network was applied successfully to optimize the catalyst of methanol synthesis from syngas at low pressure. The neural network trained by the initial experimental data from GA program gave good results because the dispersion of the initial data is high. The combination of parallel catalyst preparation, HTS reactor and GA with neural network should be promising to find the catalyst with higher activity.

Acknowledgement. This work was supported by Research for the Future Program of JSPS under the project "Synthesis of Ecological High Quality of Transportation Fuels" (JSPS-RFTF98P01001).

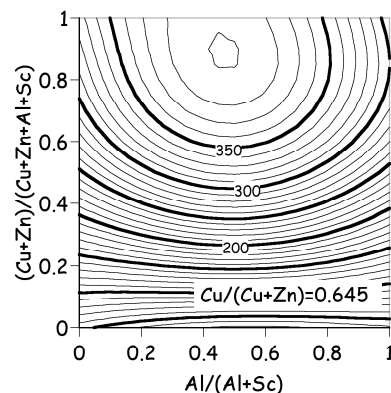


Figure 5. Mapping of the activity of Cu-Zn-Al-Sr oxide catalyst where $\text{Cu}/(\text{Cu}+\text{Zn})$ is fixed to 0.645 for optimization.

References

- (1) Senkan, S.; *Angew. Chem. Int. Ed.*, **2001**, 40, 312., (b) Jandeleit, B.; Schaefer, D. J.; Powers, T. S.; Turner, H. W.; Weinberg, W. H. *Angew. Chem. Int. Ed.*, **1999**, 38, 2494.
- (2) Omata, K.; Ishiguro, G.; Yamada, M. *Sekiyu Gakkaishi*, **2000**, 43(4), 317.
- (3) Omata, K.; Umegaki, T.; Ishiguro, G.; Yamada, M. *Sekiyu Gakkaishi*, **2001**, 44(5), 327.
- (4) Omata, K.; Umegaki, T.; Watanabe, Y.; Yamada, M. *Fuel Chem. Division Preprints*, **2001**, 46(2), 408
- (5) Hattori, T.; Kito, S. *Catalysis Today*, **1995**, 23, 347.
- (6) Sasaki, M.; Hamada, H.; Kintaichi, Y.; Ito, T. *Appl. Catal., A: General*, **1995**, 132, 261.
- (7) Kikukawa, N.; Makino, M. *Shigen-to Sozai*, **1994**, 110, 479.
- (8) Berger, D.; Landau, M.V.; Herskowitz, M.; Boger, Z. *Fuel*, **1996**, 75(7), 907.
- (9) Sharma, B.K.; Sharma, M.P.; Roy, S. K.; Kumar, S.; Tendulkar, S. B.; Tambe, S. S.; Kulkarni, B. D. *Fuel*, **1998**, 77(15), 1763.
- (10) (a) Hou, Z.-Y.; Dai, Q.; Wu, X.-Q.; Chen, G.-T.; *Appl. Catal., A: General*, **1997**, 161, 183, (b) Huang, K.; Chen, F.-Q.; Lü, D.-W.; *Appl. Catal., A: General*, **2001**, 219, 61.
- (11) Cundari, T.R.; Deng, J.; Zhao, Y.; *Ind. Eng. Chem. Res.*, **2001**, 40, 5475.

PRODUCTION OF OXYGEN CONTAINING FUELS FROM SYNTHESIS GAS

B.-T. Li, X.-H. Li, K. Asami and K. Fujimoto

Faculty of Environmental Engineering
University of Kitakyushu
Fukuoka, 808-0135, Japan

Introduction

It has been reported that, the emissions (smoke, particulate matter, CO, etc.) from diesel engine can be decreased by the addition of oxygen-containing compounds into fuel. Great efforts have been concentrated on the synthesis of oxygenates, such as higher alcohol synthesis and ether synthesis. One of the promising processes is the hydroformylation of α -olefins, which are the main product from the Fischer-Tropsch synthesis. At present, as traditionally representative homogeneous catalyst, cobalt and/or rhodium carbonyl, have been employed in the hydroformylation commercial process. In order to prevent the decomposition of the carbonyl intermediate, the high operation pressure of syn-gas (about 100 – 200 atm) has been necessary to apply to the system, but this will result in the extra economic investment for the high-pressure reactor and the operation cost for the gas compressor at the completion stage (about 20 – 30atm) of Fischer-Tropsch synthesis.

Considerable effort has been devoted and many attempts have been made to the hydroformylation process under lower pressure reaction conditions. M. E. Davis and his coworkers¹ studied the effects of toluene and methanol on the hydroformylation of 1-hexene over $\text{Rh}_6(\text{CO})_{16}$ at 20atm and 423K. However, the conversion of 1-hexene was as low as 1% in toluene, while no activity observed in methanol solvent. Thus it is likely to improve the catalytic activity by choosing a suitable solvent and reaction conditions.

In this work, hydroformylation of 1-hexene was studied over Co/active carbon in methanol solvent at lower pressure (30atm). The reason for cobalt catalyst was chosen due not only to its low cost, but also to its high activity in gas phase hydroformylation. The studies were performed in slurry liquid phase to examine the CO conversion versus time on stream and to determine the activity and stability of cobalt catalysts in terms of providing new possibilities in practical importance in the field of heterogeneous hydroformylation.

Experimental

Catalyst preparation. 10wt% cobalt loaded on active carbon was prepared by the conventional impregnation method. Active carbon (20 -- 40 mesh) was evacuated at 413K for 2h and then impregnated with aqueous solution of cobalt nitrate. The catalyst was dried in a rotary evaporator at 333K. It was heated in nitrogen at 673K for 4h and was reduced under hydrogen at 673K for 6h. The reduced catalyst was passivated at room temperature by 1% O_2/N_2 before use.

Hydroformylation reaction. Catalytic reactions were carried out in 85 ml semi-batch slurry-phase reactor equipped with a magnetic motor stirrer. A dry-ice cooled condenser was set after the reactor exit to prevent the loss of solvent. A dry-ice methanol trap was placed between the reactor exit and the pressure regulator to collect the solvent and products.

Catalyst, methanol and 1-hexene were charged into the autoclave. Reaction start-up by purging synthesis gas ($\text{CO}/\text{H}_2 = 1/1$) at 3.0MPa for pressure test. Then the autoclave was pressurized and heated to the reaction temperature. After reaction, the reactor was cooled down to room temperature and depressurized.

The liquid products remaining in the autoclave and collected in the cooling trap were combined and analyzed by GC-353 with a DB-1 capillary column. The gas phase products were analyzed by on-line

GC equipped with an active charcoal column. Argon was used as an internal standard with a concentration of 3.09% in the syngas.

Results and Discussion

In the blank test without catalyst, no 1-hexene conversion was observed under the reaction conditions. Also, without any solvents, Co/AC shows no activity even at the pressure of 50atm. The comparative effect of solvent on the hydroformylation of 1-hexene is shown in Table 1.

Table 1. Hydroformylation of 1-hexene in various solvents

Solvent	1-hexene Conv. %	Yield %				
		C7-al	C7-ol	ether	ester	isomer
Benzene	0.6	0.4	0.1	0	0	0.1
Octane	0.1	0	0	0	0	0.1
THF	0.1	0	0	0	0	0.1
Methanol	66.6...	16.7	0.6	32.7	0.5	16.1

Reaction conditions: catalyst: 0.2g; 1-hexene: 120mmol;
W/F=0.93g·h/mol; solvent/1-hexene= 2/1 (molar ratio); 3.0MPa;
403K.

In the solvents of benzene, octane and THF, only a small amount of 1-hexene was converted to 2-hexene. The enhanced 1-hexene conversion, 66.6%, was observed over Co/A.C. in methanol solvent, suggesting that methanol dramatically promotes hydroformylation of 1-hexene under the reaction conditions of 3.0MPa and 403K.

No n-hexane was detected, indicating that hydrogenation was completely inhibited. The promoting effect of methanol is not clarified, yet. Much information about products has been obtained by GC-MS. When methanol is applied as solvent, besides olefin isomers (trans-2-hexene, cis-2-hexene and 3-hexene), hexane, branched aldehydes (2-methylhexanal and 2-ethylpentanal), normal aldehyde and heptanol, a large amount of ether (1,1-dimethoxy heptane) and trace amount of ester (heptanoic acid methyl ester) are also detected. The role of methanol is not only as a solvent, but also as a reactant. The formations of ether and ester are shown as followings:

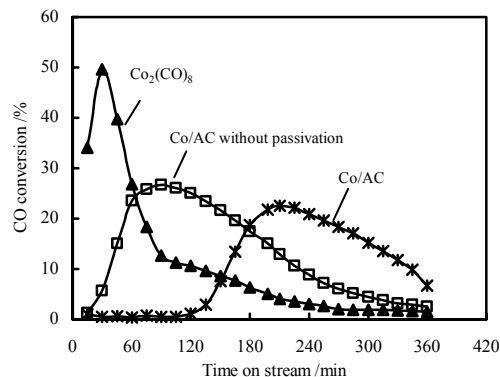
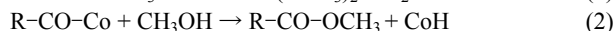


Figure 1. Comparison of CO conversion versus time on stream in methanol over $\text{Co}_2(\text{CO})_8$ and 10wt% Co/active carbon. 403K; 3.0MPa; 1-hexene: 120mmol.

The CO conversion dependence on time is presented in Figure 1. For the passivated Co/AC, an induction period exists at the beginning of the reaction, lasting for about two hours, but no such phenomenon was observed for $\text{Co}_2(\text{CO})_8$ and Co/AC without passivation. We

assumed that the induction period involves a reduction process, which provides more active metallic sites available for the hydroformylation.

For the homogenous catalyst, $\text{Co}_2(\text{CO})_8$, CO conversion decreased quickly within 30min after the reaction started, compared with heterogeneous catalyst. This suggests that in the heterogeneous system, the metallic sites are fixed on the solid surface, which makes the catalyst more stable than homogenous catalyst.

Figure 2 shows the activity of Co/AC and $\text{Co}_2(\text{CO})_8$ in methanol. With regard to the yield of oxygenates, there is no significant difference between the catalyst with and without passivation.

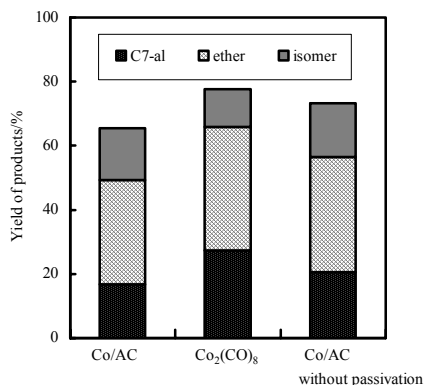


Figure 2. Comparison of yields of products over $\text{Co}_2(\text{CO})_8$ and 10wt% Co/active carbon. 403K; 3.0MPa; 1-hexene: 120mmol; methanol/1-hexene= 2/1 (molar ratio)

Even over the supported catalyst, the active metals still leach from the supports. The performance of filtered-off liquid phases and the recycled catalyst were also examined under the same conditions. The results showed that both of them showed good conversion of 1-hexene. Therefore, under our experiment conditions, it is difficult to distinguish clearly which part is from heterogeneous catalyst and which part is from leached metal.

It is normally believed that CO insertion is favorable under high CO pressure atmosphere. But at 403K and 30atm, 1-hexene shows no conversion without methanol, while by using methanol as solvent, Co/AC gives yield of oxygenates as high as 50%, a comparable result to its corresponding homogenous precursor.

In **Figure 1**, the decline in CO conversion from the peak value was observed. It is thought to be due to two aspects. One is the formation of inactive complexes. The water, formed in equation (1), might react with metallic cobalt as follow:



Here, CoO is an inactive species for the hydroformylation of 1-hexene. It is obvious that the cobalt metal instead of its oxide is favorable to this reaction. The additive of small amount of noble metal, Ru, Pd, Pt, is considered to be an effective method to reduce the formed CoO.

The other aspect of the declination in CO conversion maybe the decrease of the reactants, eg, 1-hexene and methanol. For Co/AC, after 6 hours, about 65% of 1-hexene is converted to oxygenates and isomer, which will decrease the rate of hydroformylation of 1-hexene. In order to verify this assumption, about 5g of 1-hexene and methanol were added to the solution at the end of 6-hour reaction. The variations in CO conversion with time on stream using 10wt%Co/AC as catalyst are displayed in **Figure 3**. With the liquid input after 2-hour, the increase in CO conversion was observed.

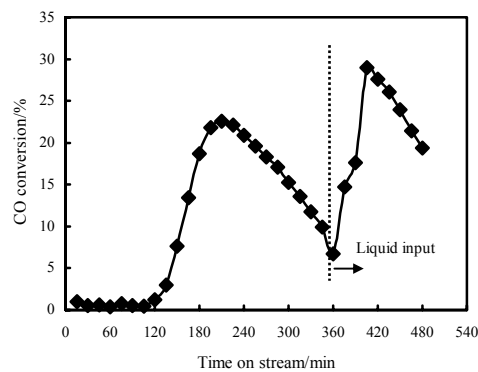


Figure 3. Hydroformylation of 1-hexene in methanol with 10wt% Co/AC. 403K; 3.0MPa; 1-hexene: 120mmol

The CO conversions at elevated pressures are shown in **Figure 4**. The induction period has no relation with the higher pressure. No conversion of 1-hexene was observed at 20atm, which shows that there is no cobalt carbonyl formed at this pressure. The higher the pressure, the higher CO conversion is. This suggests that at the same temperature, the higher pressure of syngas improved the formation of cobalt carbonyl species. In addition, the analysis of products shows the higher pressure, the higher the yield of oxygenates, the lower the yield of isomer.

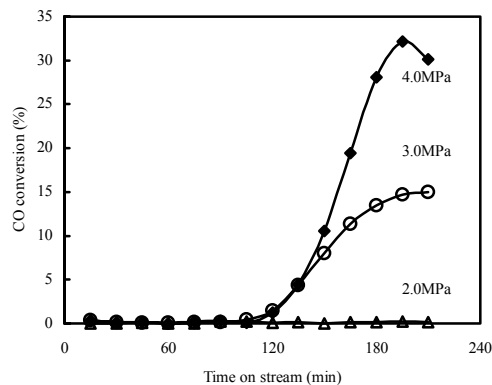


Figure 4. Elevated pressure effect on the hydroformylation of 1-hexene. 403K; 1-hexene: 120mmol; methanol/1-hexene= 2/1 (molar ratio)

Conclusion

In the gas flow semi-batch slurry phase, at lower reaction pressure (30 atm), by using methanol as solvent, the heterogeneous catalyst, Co/AC promotes the hydroformylation reaction, markedly giving di-ether and aldehydes. Moreover, it exhibits the similar yield of oxygenates to its homogenous counterpart.

The formation of the inactive cobalt species and the decrease in reactants are thought to be the two main reasons contributed to the declination in CO conversion.

Acknowledgement. This work was sponsored by NEDO grant (99GP2).

References

- (1) Robert J.D.; Joseph A. R. and Mark E.D. J. Catal., **1986**, 98,477-486.

Production of Syngas by Catalytic Gasification of Biomass at Low Temperature and Synthesis of Clean Transportation Fuels

Keiichi Tomishige and Mohammad Asadullah

Institute of Materials Science, University of Tsukuba, 1-1-1, Tennodai, Tsukuba, Ibaraki 305-8573, Japan, Tel + Fax: +81-298-53-5030

Introduction

To save ourselves and our new generation from air pollution, the future energy resources should be clean and offer large potential benefits to reduce emissions of pollutants and greenhouse gases.¹⁻⁴ In this sense, hydrogen is one of the most promising candidates for future energy demand. However, the traditional method of hydrogen production is the high temperature steam reforming or the partial oxidation of the fossil resources such as methane, light hydrocarbons, naphtha and heavy oils.⁵⁻⁹ To meet the growing demand of hydrogen and to prevent any energy-related problems, the alternative hydrogen sources, which should be renewable and sustainable, efficient and cost-effective, convenient and safe, must be developed and the production method also must be energy efficient.^{10,11} Biomass can be considered as such a feed-stock. However, the hydrogen production from biomass gasification is problematic because of the formation of tar (complex mixture of higher hydrocarbons) and char during the gasification even at high temperature. In order to get the higher energy efficiency, when the process is carried out at lower temperature (<1123 K) more tar and char are produced. Use of catalyst can reduce the tar amount in the product gas even at low temperature. However, the conventional Ni based catalyst hardly reduces the tar and conversely the catalyst is suddenly deactivated due to deposition of carbon on the catalyst surface.¹² Thus, a novel catalyst with high performance and a suitable reactor are necessary for a highly efficient low-temperature process. We have developed and described here such a process for the cellulose gasification using the Rh/CeO₂/SiO₂ catalyst in a continuous-feeding fluidized-bed reactor at as low as 773 K.

Experimental

The gasification of cellulose was performed in a continuous-feeding fluidized-bed reactor. The reactor system is almost the same as batch feeding system, which is previously published.¹³ However, the reactor dimension and feeding system have been modified for continuous-feeding gasification system. Here the gasification reactor is a quartz tube with the dimension of 66 cm high and 1.8 cm i.d. with a fluidized-bed section at the middle of the reactor. The cellulose feeder consisted of a glass vessel with a small pore at the bottom of about 0.5 mm diameter, allowing continuous feeding by vibrating the vessel with a vibrator. The vibration rate controlled the feeding rate. Cellulose particles (Merck, particle size 100–160 μm) were transported to the catalyst bed by the flow of N₂ gas through an inner tube of 5 mm i.d. Air and steam were introduced from the bottom of the reactor. Steam was supplied by using a microfeeder. The sample of the product gas was collected from the sampling port by micro-syringe and analyzed by Gas chromatograph (GC). The concentration of CO, CO₂, and CH₄ was determined by FID-GC and the concentration of hydrogen was determined by TCD-GC. The amount of char was determined by the amount of gas (mainly CO₂) formed after

stopping the feed of cellulose under the air flowing at the reaction temperature.

CeO₂/SiO₂ was prepared by the incipient wetness method using the aqueous solution of Ce(NH₄)₂(NO₃)₆ and SiO₂ (Aerosil, 380 m²/g). After drying at 393 K for 12 h, the catalyst was calcined at 773 K for 3 h under an air atmosphere. The Rh was loaded on CeO₂/SiO₂ by impregnation of the support with acetone solution of Rh(C₅H₇O₂)₃. The final catalyst was pressed, crushed and sieved to 150-250 μm particle size. Loading amount of CeO₂ is denoted in parenthesis using the weight percent. In each run, 3 g of catalyst was used and pretreated by a hydrogen flow at 773 K for 0.5 h. Composition of the commercial steam reforming catalyst (TOYO CCI, G-91) was 14 wt% Ni, 65-70 wt% Al₂O₃, 10-14 wt% CaO and 1.4-1.8 wt% K₂O. The composition of the dolomite was 21.0 wt% MgO, 30.0 wt% CaO, 0.7 wt% SiO₂, 0.1 wt% Fe₂O₃, and 0.5 wt% Al₂O₃. Before reaction the dolomite was calcined at 773 K for 3 h followed by a hydrogen treatment at 773 K for 0.5 h.

Results and Discussion

Initially, the gasification of cellulose was carried out on Rh/CeO₂/SiO₂ (35) and commercial steam reforming catalyst (G-91) at 773 K. The results are shown in Figure 1. The carbon conversion {C-conv = (formation rate of CO + CO₂ + CH₄) / (C-feeding rate in cellulose) × 100} to gas and formation of H₂, CO, CH₄, and CO₂ were stable on Rh/CeO₂/SiO₂ (35) (Figure 1a), however, on G-91 (Figure 1b) the C-conv decreased remarkably with time on stream. The rest of the carbon corresponds to the tar and char, which were deposited on the catalyst surface. When the cellulose feeding stopped after 25 min, the deposited carbon slowly converted to mainly CO₂ and this was much higher in the case of G-91 catalyst than that of Rh/CeO₂/SiO₂ (35). Here the total amount of CO₂ is assigned to the amount of char as listed in Table 1. On the lower active catalyst the char easily deposits and slowly takes part in the combustion reaction. So that the char can be build up on the lower active catalyst in the continuous feeding system and deactivates the catalyst as observed on G-91. In order to obtain a highly efficient catalyst, various kinds of Rh/CeO₂/M-type (M = SiO₂, Al₂O₃, and ZrO₂) catalysts with various loading of CeO₂ were prepared and tested in the gasification of cellulose in a continuous-feeding fluidized-bed reactor. As Table 1 shows, among the catalysts Rh/CeO₂/SiO₂ (35) exhibited the best performance with respect to the formation of syngas and/or hydrogen. As in the batch-feeding reaction,¹³ the Rh/CeO₂ catalyst exhibited considerably high C-conv; however, the BET surface area drastically decreased after the reaction because of CeO₂ aggregation.¹⁴ In the batch feeding gasification of cellulose, Pt, Ru, Pd, and Ni on CeO₂ and Rh on SiO₂, Al₂O₃, TiO₂, MgO, and ZrO₂ were also tested and the performance was lower than that of Rh/CeO₂. In the continuous feeding system, the Rh/CeO₂ catalyst suddenly deactivated due to decrease of surface area from 60 to 13 m² g⁻¹. The loading of CeO₂ on the high surface SiO₂ inhibited the aggregation of CeO₂ and maintained the catalytic activity of Rh/CeO₂/SiO₂ (35). The loading amount of CeO₂ plays a major role for C-conv and we found that the 35 mass% of CeO₂ on SiO₂ is the best. In addition, no decrease of the BET surface area of this catalyst was observed. As Table 1, at a particular temperature such as 823 K, Rh/CeO₂/SiO₂ (35) shows much higher C-conv and syngas formation. Furthermore, the tar and char are much lower than that of other systems. These results clearly represent the novelty of Rh/CeO₂/SiO₂ (35) catalyst for cellulose gasification.

The results of the effect of temperature on the gasification of cellulose on Rh/CeO₂/SiO₂ (35), G-91, and dolomite catalysts and on the non-catalytic gasification and pyrolysis are listed in Table 1. The C-conv as well as the CO and H₂ formation is the

Table 1. Performance of Various Catalysts in the Gasification of Cellulose^a

Catalyst	<i>T</i> /K	Formation rate / $\mu\text{mol min}^{-1}$				H_2/CO	C-conv /% ^b	Char /% ^c	Tar /% ^d
		CO	H_2	CH_4	CO_2				
Rh/CeO ₂ /SiO ₂ (35)	773	845	1077	676	1178	1.3	86	6	8
	823	1250	1286	653	1050	1.1	94	4	2
	873	1617	1666	470	966	1.1	97	3	0
	923	1910	1995	335	865	1.1	99	1	0
	973	2279	2357	211	615	1.1	99	1	0
G-91	823	798	1538	418	1261	1.9	79	18	3
	873	1289	1858	393	1114	1.5	87	10	3
	973	2053	2242	158	762	1.1	94	3	3
Dolomite	823	414	112	72	747	0.3	39	34	25
	973	1149	892	294	336	0.8	57	14	29
	1073	1383	1072	410	833	0.8	83	4	13
	1173	1656	1442	515	750	0.9	93	2	5
None	823	240	76	15	562	0.3	26	7	67
	1023	1536	456	357	457	0.3	65	4	31
	1073	1714	505	462	417	0.3	82	3	15
	1173	1943	592	499	455	0.3	92	2	6
None ^e	823	228	62	11	39	0.3	9	15	76

^aConditions: Cellulose, 85 mg min⁻¹ (C, 3148 $\mu\text{mol min}^{-1}$; H₂, 5245 $\mu\text{mol min}^{-1}$; O, 2623 $\mu\text{mol min}^{-1}$); Air, 50 cm³ min⁻¹; N₂, 50 cm³ min⁻¹; catalyst weight, 3 g; particle size of catalyst, 150-250 μm . ^bC conversion to gas = {(formation rate of CO + CO₂ + CH₄) / C-feeding rate} x 100. ^cChar% = (CO + CO₂ formation amount after stopping cellulose feeding / total C feeding) x 100. ^dTar% = 100 - (C conversion% + char%). ^eCellulose pyrolysis (N₂ flow, 50 cm³ min⁻¹ through distributor and 50 cm³ min⁻¹ with cellulose).

function of temperature and the catalyst activity. The increase of temperature favors the C-conv and syngas formation either in the catalytic or in the non-catalytic process. Thus, these are increased in all the systems with high temperature. On the other hand, the performance of the active catalyst also becomes higher with increasing temperature. Consequently the C-conv and syngas formation were improved drastically on Rh/CeO₂/SiO₂ (35) catalyst. About 94% carbon in the cellulose was converted to gas with a considerably high yield of CO and H₂ at as low as 823 K on Rh/CeO₂/SiO₂ (35) catalyst; however, this value was attained on G-91 catalyst at 973 K. Almost the complete C-conv was achieved at 923 K on Rh/CeO₂/SiO₂ (35). Methane was remarkably formed on the highly active Rh/CeO₂/SiO₂ (35) catalyst from the CO hydrogenation. On the other hand, the less C-conv was achieved on the dolomite and in non-catalyst system even at 1173 K. Especially, in the non-catalytic system, a very small amount of H₂ was formed. The reaction conditions of Table 1 were adjusted to the low temperature syngas production. In the hydrogen production system, the steam was introduced in order to proceed the steam reforming of tar and char and the water-gas shift reactions (H₂O + CO → CO₂ + H₂). The presence of steam in the reaction system facilitates the tar and char conversion to gas. Thus, in the next experiments, we added the various amounts of steam.

The C-conv as well as the selectivity of H₂ was dramatically improved by the steam addition (Figure 2) in the gasification of cellulose on Rh/CeO₂/SiO₂ (35) catalyst. In the

absence of steam, 86% C-conv with a less hydrogen was achieved at 773 K, whereas interestingly enough, the 100% C-conv with the higher hydrogen formation was found when the steam with H₂O/C = 0.35 was introduced. Furthermore, the formation of hydrogen and CO₂ expectedly increased with increasing the H₂O/C ratio. The limit of the temperature was 773 K for the complete conversion of cellulose to gas products. No successful report was found for the cellulosic biomass gasification at such a low temperature. This result indicates that the steam directly takes part in the gasification of the tar and char on the highly active catalyst even at low temperatures, and thus complete C-conv was achieved at 773 K. The biomass derived tar can be converted to gas on the Ni-based catalysts in the secondary-bed reactor at above 1073 K;¹⁵ however, in the primary-bed reactor the Ni-based catalysts suddenly deactivated by the carbon deposition,^{16,17} and the similar phenomenon was observed for G-91.

Finally, the combination of the high performance of the Rh/CeO₂/SiO₂ (35) with the fluidized-bed reactor will provide the novel system for the hydrogen and syngas production from biomass at low temperature with a high-energy efficiency.

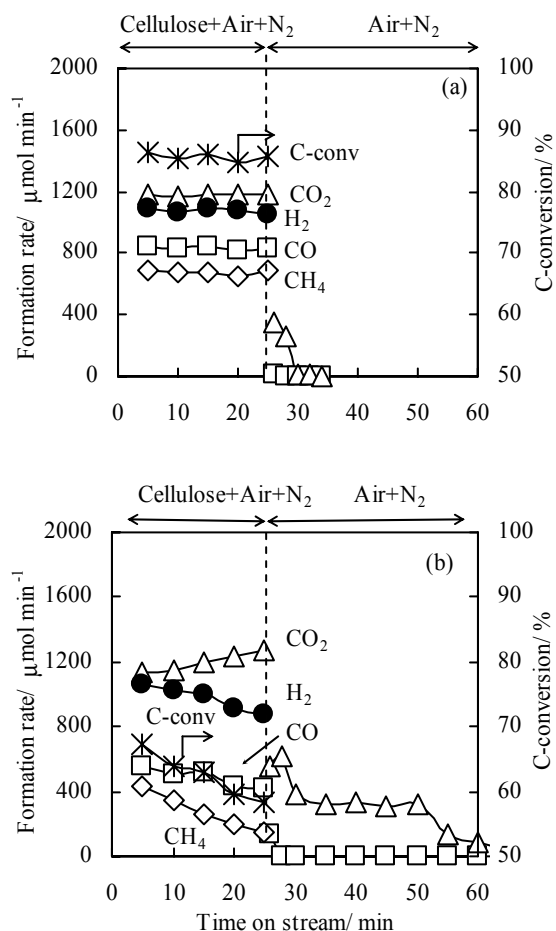


Figure 1. Dependence of time on stream on C-conversion and product distribution of cellulose gasification on (a) Rh/CeO₂/SiO₂ (35) and (b) G-91 at 773 K. Cellulose feeding rate, 85 mg min⁻¹ (C, 3148 μmol min⁻¹; H, 5245 μmol min⁻¹ and O, 2622 μmol min⁻¹); air flow, 51 cm³ min⁻¹ (O₂, 417 μmol min⁻¹); N₂ flow 51 cm³ min⁻¹.

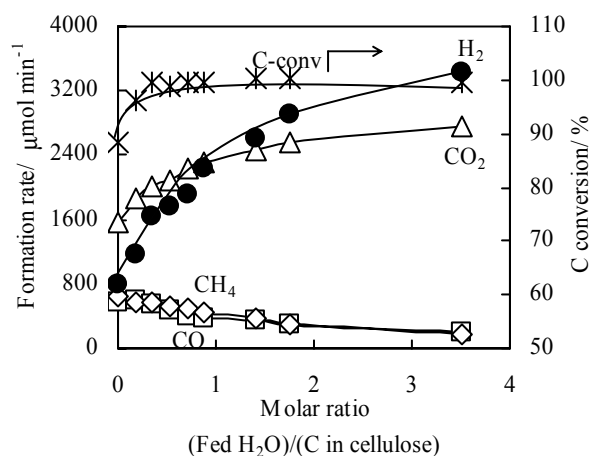


Figure 2. The influence of the steam to gas formation rate and C-conversion at 773 K over Rh/CeO₂/SiO₂ (35). Cellulose feeding rate, 85 mg min⁻¹ (C, 3148 μmol min⁻¹; H, 5245 μmol min⁻¹ and O, 2622 μmol min⁻¹); air flow, 100 cm³ min⁻¹ (O₂, 818 μmol min⁻¹); N₂ flow 50 cm³ min⁻¹ (2046 μmol min⁻¹); H₂O, 555 ~11110 μmol min⁻¹.

Acknowledgement. This research was supported by the Future Program of Japan Society for the Promotion of Sciences under the Project “Synthesis of Ecological High Quality of Transportation Fuels” (JSPS-RFTF98P01001).

References

- Ogden, J. M. *Annual Review of Energy and Environment* **1999**, *24*, 227.
- Steinberg, M., *Int. J. Hydrogen Energy* **1999**, *24*, 771.
- Pehr, K.; Sauermaun, P.; Traeger, O.; Bracha, M., *Int. J. of Hydrogen Energy* **2001**, *26*, 777.
- Dülger, Z.; Özçelik, K. R., *Int. J. of Hydrogen Energy* **2000**, *25*, 895.
- Pena, M. A.; Gomez, J. P.; Fierro, J. L. G., *Appl. Catal. A: General* **1996**, *144*, 7.
- Armor, J. N., *Appl. Catal. A: General* **1999**, *176*, 159.
- Saito, M., *Shokubai (Catalysis)* **1993**, *35*, 485.
- Kikuchi, E.; Uemiy, S.; Matsudo, T., *Stud. Surf. Sci. Catal.* **1991**, *61*, 509.
- Steinberg, M.; Cheng, C. H., *Int. J. Hydrogen Energy* **1989**, *14*, 797.
- Chum, H. L.; Overend, R. P., *Fuel Proc. Tech.* **2001**, *71*, 187.
- Scarpellini, S.; Romeo, L. M., *Energy Conv. & Management* **1999**, *40*, 1661.
- García, L.; Frence, R.; Czernik, S.; Chornet, E., *Appl. Catal. A: General* **2000**, *201*, 225.
- Asadullah, M.; Tomishige, K.; Fujimoto, K., *Catal. Commun.* **2001**, *2*, 63.
- Asadullah, M.; Fujimoto, K.; Tomishige, K., *Ind. Eng. Chem. Res.* **2001**, *40*, 5894.
- Corella, J.; Orío, A.; Toledo, J. -M., *Energy Fuel* **1999**, *13*, 702.
- Baker, E. G.; Mudge, L. K.; Brown, M. D., *Ind. Eng. Chem. Res.* **1987**, *26*, 1335.
- García, L.; Salvador, M. L.; Arauzo, J.; Bilbao, R., *Energy Fuel* **1999**, *13*, 851.

Promoting Effect of Water on Coal Hydrogenation - Synergistic Effect of Pyrite and Water-

Yoshiharu Yoneyama, Makoto Okamura, Maki Katoh,
Satoru Maekawa, Noritatsu Tsubaki, Yi Zhang

Faculty of Engineering,
Toyama University,
Toyama, Japan 930-8555

Introduction

Low-cost hydrogen sources are required for converting coals to liquid or gaseous fuels, and chemicals. Water is a promising candidate among hydrogen sources. Many researchers used water as hydrogen source through water-gas shift reaction or as an effective pretreatment method for hydrogenation and pyrolysis of coals.¹ Water at supercritical state or steam has been used as extraction or pretreatment vehicles of coals as well.²⁻⁵ On the other hand in the catalytic hydrogenation of coals, it is well known that water or steam deactivates hydrotreating catalyst.^{6,7} Even if it seems that water exhibited negative effect on coal hydrogenation with or without catalysts, addition of water increased the CO₂ formation and the contents of phenolic compounds in the obtained oils.³⁻⁵ These results strongly suggest that water interacts with coals under hydrogenation conditions.

In this study to clarify the role of water in the coal hydrogenation, Wandoan and Argonne premium coal were non-catalytically hydrogenated at 673 K with water addition. For comparison, experiments under nitrogen, and with addition of n-undecane (n-C₁₁) were also carried out. n-C₁₁ is thinking as an essentially unreactive organic medium with a critical temperature similar to that of water (estimated to be 636 K).

Experimental

Basic data of coals are listed in Table 1. The coals were dried at 333 K under vacuum for over 48 h to constant weight before use. Undecane (n-C₁₁) was used without further purification. Super high purity of hydrogen (over 99.999 %) and nitrogen (over 99.999 %) were used to minimize oxidization during the reaction.

Hydrogenation was carried out using coal of 1.5 g with or without adding water of 0.8 g, or adding n-C₁₁ of 0.8 g in a 25 ml horizontal microautoclave reactor at 673 K for 60 min under an initial hydrogen pressure of 6.9 MPa. For comparison, similar experiment under nitrogen was also conducted. The gaseous product was collected for analysis by gas chromatograph with thermal conductivity detector. The recovered products were placed into a thimble filter and separated to tetrahydrofuran (THF) soluble product by Soxhlet extraction with THF, followed by rotary-evaporation and drying in a vacuum oven at 333 K. The conversion was defined as the sum of the yields of gases and THF soluble products. When n-C₁₁ was used, the weight of n-C₁₁ was subtracted from the weight of THF soluble products. The experimental error range of the conversion and products yields was estimated from duplicate experiments to be within 3 wt%.

X-ray diffraction of THF insoluble product was measured on a Rigaku Rinto 2000 spectrometer to determine the structural changes of ash mineral.

Results and Discussion

Relationship between Carbon Content of Original Coal and the Conversion Figure 1 shows the relationship between the carbon content of original coals and the coal conversions using hydrogen or nitrogen, where water or n-C₁₁ was added. In the combination of

Table 1. Elemental Analysis of Coals (% daf)

Coal	C	H	N	O + S ^a	Pyrite ^b
Beulah-Zap	72.9	4.8	1.1	21.2	0.2
Wandoan	73.4	6.2	1.1	19.4	-
Wyodak	75.0	5.4	1.1	18.5	0.1
Illinois #6	77.7	5.0	1.4	16.0	5.0
Blind Canyon	80.7	5.8	1.6	12.0	0.4
Lewiston-Stockton	82.6	5.3	2.6	9.6	0.3
Pittsburgh #8	83.2	5.3	1.6	9.8	2.5
Upper Freeport	85.5	4.7	1.6	8.3	3.5

^a By difference ^bwt%, dry base

nitrogen and water, with the increasing the carbon content of original coals, the conversions of coals were enhanced, except for Upprt Freeport coal. Addition of n-C₁₁ did not enhance the coal conversion, however addition of water enhanced the coal conversion.

On the other hand, in the combination of hydrogen and water there existed no clear relationship between the carbon content of original coals and the coal conversions. Addition of water had promoting effect on coal conversion under hydrogen also. It was found that the conversions of both Illinois #6 and Pittsburgh #8 coals were irregularly large. The conversion of Illinois #6 coal increased about 20 % with added water, even though added water in nitrogen did not promote the coal conversion significantly. There existed synergistic effect between hydrogen and water on conversion of Illinois #6 and Pittsburgh #8 coals.

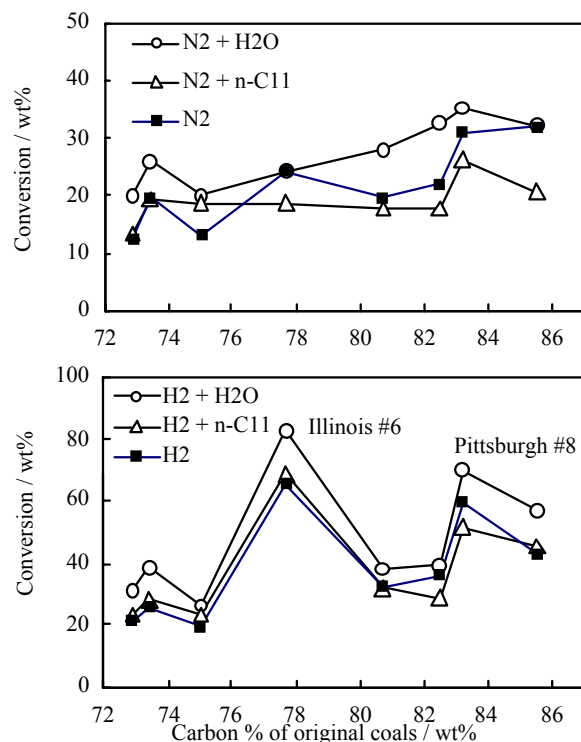


Figure 1. Relationship between carbon % of original coals and the conversion under nitrogen or hydrogen with added water or undecane (n-C₁₁). Temperature, 673 K; time, 60 min.

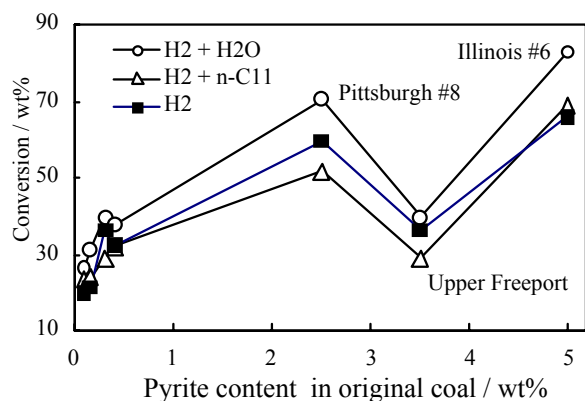


Figure 2. Relationship between pyrite content in original coal and the conversion.

Effect of Pyrite Content on Coal Conversion Since Illinois #6 and Pittsburgh #8 coals contain more pyrite than other coals as compared in Table 1, it is considered that pyrite plays an important role in the promoting effect of water on coal conversions using hydrogen. It is well known that pyrite in coals acts as catalyst in coal hydrogenation.⁷

Figure 2 exhibits the relationship between the pyrite contents of original coals and the conversions of coals in hydrogen. The conversions of coals containing larger amounts of pyrite were larger except for Upper Freeport coal, while the conversion of coals containing less amount of pyrite were lower. Because Illinois #6 and Pittsburgh #8 coals contain large amount of pyrite, synergistic effect between hydrogen and water is considered to be large. The conversion of Upper Freeport coal was low, though the content of pyrite was large. It is thinking that the strength of connecting linkages between aromatic moieties in coal becomes strong with increasing coal rank. Therefore, it seems that the conversion of Upper Freeport coal was low under the conditions we used. It is referred that pyrite plays an important role in the synergistic effect between water and hydrogen on coal conversion.

In order to examine the structural changes of pyrite, XRD of THF insoluble products from Illinois #6 coal were measured. Figure 3 shows XRD patterns of THF insoluble products from the reaction of Illinois #6 coal. It was found that all the THF insoluble products did not contain pyrite, but contained much amount of pyrrhotite. The THF insoluble products from H₂ and H₂ + n-C₁₁ contained significant amount of troilite, but that from H₂ + H₂O did not contained so much. It is well known that pyrite in coal ash decomposes to pyrrhotite under hydrogenation conditions and the pyrrhotite is an active catalyst for coal hydrogenation.⁷ Therefore these results indicate that pyrrhotite act as the catalyst in the hydrogenation. In addition because the amount of Troilite in the THF insoluble products from H₂ + H₂O was much smaller than those from H₂ alone and H₂ + n-C₁₁ and catalytic activity of pyrrhotite is higher than troilite, it is suggest that water addition is effective for maintaining catalyst activity of iron compounds higher.

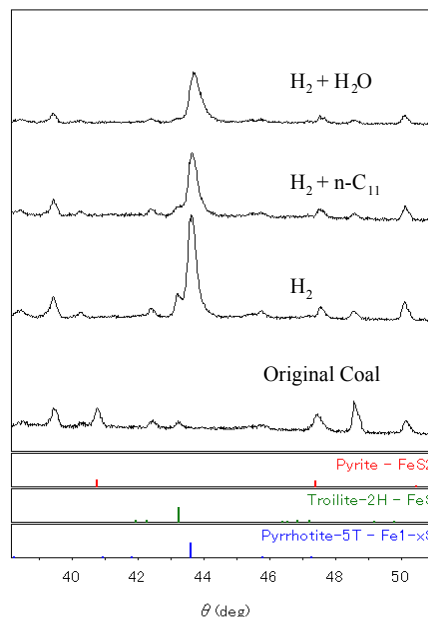


Figure 3. XRD patterns of THF insoluble products from Illinois #6 coal. 400 °C for 60 min

Conclusions

To investigate the effect of adding water on coal hydrogenations, several coals were hydrogenated with or without adding water under noncatalytic conditions. Addition of water enhanced the coal conversion under both nitrogen and hydrogen.

Synergism between water and hydrogen on coal conversion was found for the coals with large amount of pyrite. Illinois #6 and Pittsburgh #8 coals containing larger amount of pyrite exhibited irregularly large conversion. These results suggested that pyrite in coals acted as the catalyst and played an important role in the synergistic effect between hydrogen and water on coal conversion. It was indicated from the XRD patterns of THF insoluble product that pyrrhotite acted as the catalyst in the hydrogenation. Because the amount of troilite in the THF insoluble products from H₂ + H₂O was much smaller than those from H₂ alone and H₂ + n-C₁₁, added water seemed to be effective for maintaining catalyst activity of iron compounds higher.

Acknowledgements. This work was supported by the Research for the Future Program of the Japan Society for the Promotion of Science (JSPS) through the 148th Committee on Coal Utilization Technology of JSPS.

References

- Ross D. S., *Coal Science*, **3**, 301
- Graff R. A. and Brandes S. D., *Energy Fuels*, 1987, **1**, 84
- Desphande, G. V.; Holder, G. D.; Bishop, A. A.; Gopal, J.; Wender, I. *Fuel* **1984**, *63*, 956.
- Kershaw, J. R. *Fuel Process. Technol.* **1986**, *13*, 111.
- Artok, L.; Schobert, H. H.; Nomura, M.; Erbatur, O.; Kidena, K. *Energy Fuels* **1998**, *12*, 1200.
- Kamiya, Y.; Nobusawa, T.; Futamura S. *Fuel Process. Technol.* **1988**, *18*, 1.
- Ruether, J. A.; Mima, J. A.; Kornosky, R. M.; Ha, B. C. *Energy Fuels* **1987**, *1*, 198.
- Trewhella, M. Jr.; Grint, A. *Fuel* **1987**, *66*, 1315.

R&D Project of Ultra Clean Petroleum Fuel Refining in Japan

Takashi Hagiwara, Yoshihiro Mizutani and Kuniki Yoshitake

Technology department
Japan Petroleum Energy Center
4-3-9, Toranomon, Minato-ku
Tokyo 105-0001, Japan

Project Background

Petroleum fuels, such as gasoline, are in widespread use for automobiles, such as passenger vehicles and trucks, and are indispensable products in modern life and economic activities in Japan. On the other hand, improvement of atmospheric environment have been claimed consecutively. So, vehicle emission regulation for harmful substances such as CO, HC and NOx has become strict more and more. In addition, from the view point of global warming issue, reducing fuel consumption has also become demanded in recent years. Adapting these situation, technology development is conducted by both automobile and oil industries. Concerning technology development of oil industries, from 2002 fiscal year, R&D projects of producing clean petroleum fuel (for example sulfur free gasoline) and improving fuel quality for clean utilization of petroleum fuels have been launched. The former is R&D project of Ultra Clean Petroleum Fuel Refining and the latter is including JCAP2 (Japan Clean Air Program 2). Both projects are being conducted by Japan Petroleum Energy Center (JPEC) with the subsidy of Ministry of Economy, Trade and Industry (METI). In this talk, the outline of R&D project of Ultra Clean Petroleum Fuel Refining in Japan is introduced.

According to COP3, Japanese automobile manufacturers are required by regulation to reduce the fuel consumption of gasoline cars by 22.8% on average from the level in fiscal 1995 by the Government. To cope with this regulation, automobile manufacturers and related companies are working on improving the fuel consumption. In several technological options, spark ignition direct injection (SIDI) engines have the potential to reduce vehicle CO₂ emissions substantially (OEMs report up to 20%)¹. However, the NOx storage catalyst, used in SIDI engines is further more easily contaminated by fuel sulfur than conventional three-way catalysts². If the NOx adsorber dose not work sufficiently, the regulation of exhaust gas emission cannot be satisfied. At present, deactivated catalysts are periodically regenerated by raising the catalyst bed temperature at the sacrifice of fuel economy. Therefore, further reductions in the sulfur content of fuels are demanded. As shown in **Table 1**, regulations will likely require greater reductions in the sulfur content of fuels in the next few years.

Table 1. The gasoline Sulfur Regulation trend

	Regulation	Regulation trend
Japan	100ppm	Actual results (Average) of RG (Regular Gasoline): c.a.35ppm Actual results (Average) of PG (Premium Gasoline): c.a.8ppm <Ministry of the Environment> 2005 50ppm
US	1000ppm	<EPA> 2004 Refinery Cap: 300ppm 2005 30ppm (Refinery Cap: 300ppm) 2006 30ppm (Refinery Cap: 80ppm) <CARB> 2003 15ppm (Phase3-RFG (Reformulated Gasoline))
EU	150ppm	<EU standard> 2005 50ppm <Plan of introducing Zero Sulfur (S<10ppm) gasoline> 2005 Partial introduction 2011 overall introduction

Project Objectives

This project aims to help relieving global warming and atmospheric pollution by developing technology to minimize the sulfur content of fuels, especially motor gasoline. In addition, demand for heavy residual oil is rapidly declining in view of environmental pollution, in recent years. To match the oil products to the present demand structure, heavy residual oil should be converted to distillate such as gasoline and diesel fuel. And the technology for the effective and clean utilization of heavy residual oil needs to be developed. Thus, this project also aims to secure an inexpensive and stable supply of clean oil products by developing technology for removing sulfur (and other contaminant e.g. metals) not only from distillate converted from residual oil but also feed residual oil itself, which will help to promote the use of heavy residual oil.

Project structure

At present, gasoline is mainly produced by blending straight-run gasoline separated from atmospheric distillation unit, reformulated gasoline made by reforming of heavy naphtha, alkylated gasoline made by alkylation of light olefins, and cracked gasoline made by cracking of heavy oil in Fluid Catalytic Cracking unit (FCC). The cracked gasoline (FCC gasoline) includes a lot of olefins (high octane value), and it is blended to gasoline at the highest ratio. But the FCC gasoline contains much sulfur, and most of sulfur contained in the product gasoline is due to the FCC gasoline.

Unlike US and EU refineries, almost Japanese refineries had already equipped with FCC feed pretreater by SO_x regulation. So, FCC gasoline sulfur is already rather low in Japan, but further reduction is needed to produce sulfur free gasoline. Adapting this advantage of Japanese refineries, efficient desulfurization technology of the FCC (or RFCC) product with minimizing the octane value loss, either treating the FCC (or RFCC) products or its feed (residual oil and VGO) should be considered. In this project, following technologies shall be developed considering optimum integration design. 1) advanced hydrodesulfurization (HDS) technology for atmospheric residual oil and VGO, as feedstocks of Residue FCC (R-FCC) and FCC, respectively; 2) in-situ FCC desulfurization technology; 3) selective hydrodesulfurization technology for FCC gasoline; and 4) isomerization technology for gasoline stocks. The relationship among the respective technologies is shown in **Figure 1**. The details of Project elements are as follows.

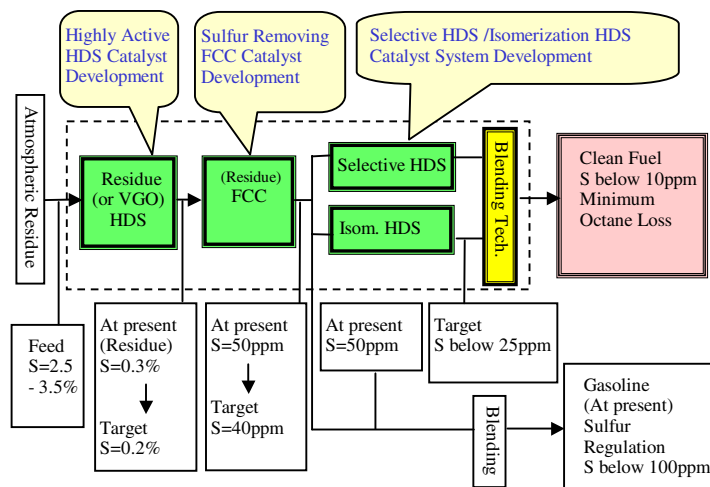


Figure 1. The R&D Project Structure of Ultra Clean Petroleum Fuel Refining in Japan

Project element

1)Advanced hydrodesulfurization technology for residual oil and VGO. In the present residue desulfurization catalyst system, catalyst for removing metals with high metal trapping ability is used in proper combination with desulfurization catalyst for avoiding activity deterioration caused by the reduction of diffusion properties of the reactants. Thus, efforts have been made to develop technologies to prolong the life of catalysts by improving the resistance against metals.

In this project, the desulfurization performances rather than the metal resistance of the catalyst are focused, and so new ideas shall be tested. Though existing catalysts are very active at the early stage of the desulfurization reaction, the performance quickly deteriorates sharply to less than 50% of initial activity. This early deterioration is caused by the coke formed in the reactions. Accordingly, if the formation of coke on the desulfurization catalyst can be reduced and early deterioration prevented, then a highly active catalyst can be obtained. This study aims to develop coke-resistant catalysts. The ordinary technique of controlling coke formation uses an active metal with high hydrogenation activity (Ni, W), but existing Ni catalysts have not been improved sufficiently. Consequently, this study will try to develop highly active catalysts by considering the coke formation mechanism at the acid point as an active site, and by introducing a new acidity control substance and its preparation technology. Existing catalysts have a service life of one year for residual oil containing 0.3% sulfur. This study aims to develop a highly active residue desulfurization catalyst capable of stably producing heavy oil containing 0.2% sulfur for one year, for the same quantity of feed processed by the present residue desulfurization and processing capacity.

2)In-situ desulfurization technology in fluid catalytic cracking unit (FCC). In-situ desulfurization technology of FCC catalysts is still at the test stage and has not been established industrially. These catalysts are given desulfurization properties by adding metals such as V, Zn and some kind of zeolites as inter-molecular hydrogen transfer and sulfur compounds cracking component.

This study targets not only FCC, but also residue FCC (RFCC), whose feed is residual oil, which requires more effective cracking and desulfurization functions of the heavier components than those of VGO. For the pore size distribution control and promotion of the hydrogen transfer reaction of zeolite and matrix for the rapid diffusion of the heavy components, optimization of support composition by the addition of metals as well as solid acidity control shall be performed. Catalysts having a shape-selective cracking desulfurization function are being developed, with a target of 20% less sulfur content in the product than that in the present FCC gasoline.

3)Selective hydrodesulfurization technology for FCC gasoline. The hydrodesulfurization of FCC gasoline causes the problems of hydrogenation of olefins and reduction of octane value. This study aims to develop a catalyst and a process for hydro-desulfurizing sulfur compounds without significantly hydrogenating the olefins. The coexistence of H₂S on the conventional CoMo desulfurization catalyst hinders the desulfurization and hydrogenation of n-olefins, but promotes the hydrogenation of iso-olefins. When the amount of Co is increased, the desulfurization reaction is promoted, but the hydrogenation reaction of olefins is hindered. Thus, the desulfurization active sites of the Co-Mo/Al₂O₃ catalysts are different from the hydrogenation active site of olefins³. It is expected that if the hydrogenation active sites of olefins are selectively reduced, catalysts with high desulfurization selectivity can be prepared. For example, covering the surface of the catalyst with some kind of coke can control the hydrogenation reaction of iso-olefins. It is known that the hydrogenation reaction of iso-olefins can be controlled by introducing the vapor of basic compounds such as pyridine. This study will

examine other practical catalyst modification methods, determine conditions that improve the desulfurizing properties and the process conditions. The target is to develop the catalyst and process to reduce the loss of octane value to 2.5 or less and the sulfur content to 10ppm or less when the sulfur content in the feed FCC gasoline (research octane number (RON) 90) is 50ppm.

4)Development of technology optimally combining isomerization technology for light ends. The other way to minimize the octane value loss in hydrodesulfurizing FCC gasoline, is converting produced paraffins into branched paraffins (i.e. isomerization). In the isomerization reaction of treated heavy FCC gasoline, for the C₇ and C₈ fractions, considerable paraffin cracking reactions are expected as side reactions unlike for the fractions C₅ and C₆. The isomerization reaction is more favorable in equilibrium at a lower temperature, while the cracking reaction proceeds further as the reaction temperature increases, and thus it is necessary to develop a catalyst and a process that show high activity at low temperature in order to secure the product yield. However, as the number of carbon atoms in the feed increases, the coking reaction on the catalysts may proceed rapidly.

Conventional isomerization catalysts, for example platinum supported zeolite or chlorinated alumina catalyst, is easily deactivated by small amount of sulfur compounds of the feed. Whereas, activity of the solid ultra-strong acid catalyst used in this study is hardly influenced up to a sulfur content of about 150ppm in the isomerization reaction of light naphtha. And active reaction temperature zone is much lower than the conventional one, especially reducing the water content of the feed to about 1ppm. Accordingly, reducing the water content to about 1ppm by adopting the dehydration pretreatment, applying this catalyst to the heavy FCC gasoline (mainly the fractions C₇ and C₈), the reaction temperature can be lowered and so cracking reaction can be mitigated. The targets are to achieve a sulfur content in the treated heavy FCC gasoline of 25ppm or less, and isomerized gasoline yield of 60% or more for feed C₇ to C₈.

Project Milestones

The scheduled duration of the project is five years from fiscal 2002 to fiscal 2006. At the end of fiscal 2004, the mid-term fiscal year, an assessment committee will be formed, consisting of outside experts in the field mainly from academic societies and industry. This committee will assess the degree of achievement of the research and development targets, the system of implementing the project, and plan the remainder of the project. A similar assessment committee will be set up in fiscal 2007 after the completion of the project to make a final assessment of the results of the technological development and of its position in the Japanese energy policy from technological and social aspects at that time. In addition, suggestions concerning the course of research and development toward practical application after the completion of the project will be made.

Acknowledgement

This work was conducted with the subsidy of the Ministry of Economy, Trade and Industry, Japan.

References

1. Enabling Fuel Requirement of Low Emissions Vehicle Technology in Europe. CONCAWE. 31 July, 2000.
2. ACEA data of the sulfur effect on advanced emission control technologies. July, 2000.
3. S. Hatanaka, M. Yamada and O. Sadakane, Ind. Eng. Chem. Res. 1997, 36, 5110.

RESEARCH ON NOVEL POLYISOBUTYLPHENOXY-ETHYL POLYAMINES AS GASOLINE DETERGENTS

Hejun Guo

Xi'an Research Institute of Hi-Tech, Hongqing Town, Xi'an 710025,
P.R.China

Zhizhong Liu Shenghua Li Shihai Xu

Department of Petroleum Chemistry, Logistical Engineering College,
Chongqing 400016, P.R.China

INTRODUCTION

At the present day, laborious researches are being carried out strenuously worldwide to develop high efficient and multifunctional gasoline detergents put into use required stringently to eliminate modern vehicle engine deposits which exert serious adverse effects on engine exhaust emissions and working performances (1,2). Based on the fact that the amino groups in detergent molecules can significantly promote deposit accumulation in engine combustion chamber(3), a new concept has been formed that gasoline detergents with relatively low thermal stability prepared based on polyisobutylene and amine could lead to much less CCD build-up. From this notion, more recently, a new family of gasoline detergents of 2-hydroxyl-3-parapolyisobutylphenoxy propyl amines were developed which not only possess very excellent performances for deterring and dispersing PFID, IVD and ISD, but also present lower CCD forming propensity due to relatively easy cracking of C—O—C bonds in their molecules. In the mean time, development of a novel kind of detergents of parapolyisobutylphenoxyethyl amines has also been advanced of which syntheses, performances, and thermal stability are presented in current paper.

EXPERIMENTAL

Synthetic Procedure

In present research, two polyisobutylenes of the number average molecular weight of 815 and 995 were utilized for current syntheses. Ethylenediamine, diethylenetriamine and 1,2-dibromoethane in their chemical purity were selected as synthetic materials. In the process of the production of the novel additives, analytically pure phenol was firstly alkylated with polyisobutylene using BF_3 as catalyst to produce polyisobutyl phenol as prepared in the previous study(4). The product of polyisobutyl phenol was then neutralized and followed by the reaction with three times of excess of 1,2-dibromoethane. Finally, the new intermediate product of bromoethyl polyisobutylphenyl ether was conducted to react with six times excess of amines to prepare the desired compounds. Detailed procedures of the new detergents preparations are presented as follows:

To a flask equipped with a stirrer, a thermometer, nitrogen inlet and addition funnel was added 69.0 grams of 79.2% weight percent as determined with chromatograph of crude polyisobutylene (Mw=815) alkylated phenol dissolved in 90 ml of toluene, or 85.0 grams of 76.7% weight percent of crude polyisobutylene (Mw=995) alkylated phenol dissolved in 90ml of toluene, and then was added dropwise a solution of 2.4 grams of NaOH dissolved in 25ml of distilled water. The mixture was stirred and maintained to $80^\circ\text{C}\sim 90^\circ\text{C}$ for 2 hours under N_2 atmosphere. After that, n-butanol was added to demulsify the mixture and phase separation made. Oil phase preserved was heated to completely evaporate toluene and then added 20ml of n-butanol and followed by 45.0 grams of neutral 1,2-dibromoethane washed with solution of 5% mass percent of NaHCO_3 beforehand. The reaction mixture was maintained between 105°C and 110°C until PH value of the mixture dropped to 8~9 and the reaction

was stopped. The product of NaBr was filtered, with solvents and unreacted 1,2-dibromoethane removed in vacuo.

To this new crude intermediate product was added 24.0 grams of ethylenediamine, or 40.0 grams of diethylenetriamine. Under N_2 atmosphere, the reaction mixture was heated and the reaction was conducted at $113^\circ\text{C}\sim 115^\circ\text{C}$ (for ethylenediamine) for 8 hours, or at 145°C (for diethylenetriamine) for 8 hours. Then in vacuo, unreacted amine was removed to give the final crude product.

The final crude product was chromatographed on silica gel, eluting firstly with toluene/cyclohexane/ ethyl ether (1:1:1), secondly with toluene/cyclohexane /ethyl ether/methanol (1:1:1:0.5) and finally with toluene/ cyclohexane/methanol/diethyl amine/ethylenediamine (1: 1:1:0.5:0~0.2) to gain the desired products as brown oils.

Four polyisobutylphenoxyethyl amines were prepared which were as follows: N-[2-parapolyisobutyl (Mw=815) phenoxy] ethyl ethylenediamine (G), N-[2-parapolyisobutyl (Mw=995) phenoxy] ethyl ethylenediamine (H), N-[2-parapolyisobutyl (Mw=815) phenoxy] ethyl diethylenetriamine (I), N-[2-parapolyisobutyl (Mw=995) phenoxy] ethyl diethylenetriamine (J).

Structure Characterization

A 1725X Perkin Elmer FT-IR spectrometer was adopted to conduct IR analyses. Its sample cell was KBr crystal. A Bruker AC-E200 superconductive NMR spectrometer was used to carry out ^1H NMR analyses. CDCl_3 was selected as solvent, and TMC as standard substance. The watched frequency was 200 MHz. GPC analyses were performed on an apparatus of Waters Associates Liquid Chromatograph, and elementary analyses were made with a tester of CHN-TMT type.

The absorption frequencies observed in IR spectra of the new products were as follows: 3300 cm^{-1} ($\nu_{\text{NH}_2}, \nu_{\text{NH}, \text{s}}$), 2930 cm^{-1} ($\nu_{\text{CH}_2}, \nu_{\text{CH}_3, \text{s}}$), 1640 cm^{-1} ($\delta_{\text{NH}_2, \text{m}}$), 1610 cm^{-1} ($\delta_{\text{NH}_2}, \nu_{\text{C}=\text{C}}, \text{s}$), 1513 cm^{-1} ($\nu_{\text{C}=\text{C}}, \text{s}$), 1467 cm^{-1} ($\nu_{\text{C}=\text{C}}, \delta_{\text{CH}_2, \text{s}}$), 1367 cm^{-1} (d, $\delta_{\text{CH}_3, \text{s}}$), 1250 cm^{-1} ($\nu_{\text{C}-\text{O}-\text{C}, \text{s}}$), 1140 cm^{-1} ($\nu_{\text{C}-\text{N}, \text{w}}$). In addition, 829 cm^{-1} (m) was confirmed as out-of-plane bending vibration of C=C-H of para-aromatic ring and 1185 cm^{-1} as stretching vibration of chain unit skeleton of polyisobutyl group.

The following were ^1H NMR spectra of the new products : $\delta 7.25$ (CDCl_3), 7.20 (d, 2H), 6.80 (d, 2H), 4.04 (t, 2H), 2.98 (t, 2H), 2.80(t, 2H), 2.75 (t, 2H), 1.86 (s, 3H for diamines), and $\delta 1.8\sim 0.6$ was acknowledged as chemical shifts of polyisobutyl protons. In Table 1 are displayed the elementary composition of compound G.

Table 1 Elemental Composition of Compound G

Element	C%	H%	N%	O%
Determined	82.18	12.89	2.95	1.98
Calculated	82.27	13.30	2.82	1.61

The number average molecular weights of 932.36 and 1192.05 for compound G and compound J respectively was measured by GPC as compared with 790.44 for polyisobutylene (Mw=815).

Performance Evaluation

Fuel oxidation reactor test which was developed by Kim et al to evaluate deposit-forming tendencies of liquid fuels on a metal surface in engines, especially in multiport fuel injection systems (5) was adopted for rating the PFID reducing performances of current new products. In present performance evaluation, tests were conducted on a set of apparatus of fuel oxidation reactor which was verified experimentally to be of good parallelism, repeatability and reproducibility(6,7). The reactor cylinder was 9.9 cm in diameter, 13.5 cm in height, and two kinds of stainless steel, cap-shaped coupons utilized in experiment were 1.99 cm and 2.78 cm

respectively in diameter.

In the experiment, a 90[#] gasoline to be tested was firstly distilled to cut off the range below 112°. 250 ml of the heavy fraction was taken as sample. The reaction temperature of fuel oxidation was maintained at 110° by a oil bath, and air flow rate was adjusted to 50 ml/min. After oxidation, the coupons were removed from the reactor to a well ventilated hood and cooled to room temperature. After that they were soaked in light gasoline fraction as gained above for 3 minutes and then in cyclohexane for another 2 minutes. The coupons were air dried in the hood and weighed to determine deposit amount.

In the tests of fuel oxidation reactor, additive dosage was selected as 200µg/g, and the samples were oxidized for 20 hours and 25 hours respectively.

Crankcase oil simulating test specified by SH/T0300-92 was introduced to determine performances of the new compounds to inhibit IVD formation derived from engine oil. In the present research, the working temperature of gum forming plate was set to 215° which is medium temperature of intake valve surface during engine working. Previous study showed that the results of this test could correlate well with those of engine dynamometer tests.

An ISD simulator developed by South West Research Institute (SwRI) was adopted for detergent performance evaluation. The tests were conducted in accordance with FTM791C 500.1 under conditions of air flow rate: 15±0.5 L/min, fuel flow rate: 2±0.1 L/min, deposit tube temperature: 190°, detergent dosage: 500µg/g, test duration: 50 minute.

Methanol solvable deposit (MSD) and methanol insoluble deposit (MID) prepared were sampled to investigate PFID dispersing performances of the new products. The two deposits were remarkably different in their IR spectra with the absorption strengths of ν_{OH} and ν_{C=O} of MID much greater, with their elemental compositions listed in Table 2.

Table 2 Elemental Composition of Deposits Prepared

Element	C%	H%	N%	O%
MSD	72.27	7.84	1.16	15.32
MID	59.34	4.96	3.14	26.52

The procedures of deposit dispersing experiments are as follows:

The solution of 15.0±0.3 mg of MSD and 100±0.5 mg of tested detergent dissolved in 3.0 ml of methanol were added to 20.0 g of a filtered kerosene and then heated to evaporate methanol completely. The mixture temperature was maintained at 70° and stirred for 3 hours. Then, the mixture was filtered through a piece of quantitative paper which had been washed with 20 g of the filtered kerosene firstly, 50 ml of above-gained light gasoline fraction secondly, 50 ml of cyclohexane finally before weighted. After the mixture was filtered, the paper was firstly washed with 50 ml of light gasoline fraction, and then with 50 ml of cyclohexane. The paper with deposit was dried and weighted.

15.0±0.3 mg of fined MID particle and 100±0.5 mg of tested detergent were added to 20.0 g of the filtered kerosene. The mixture was dispersed with ultrasonic of 20 kHz for 5 minutes. The mixture was heated to 45° and stirred for 3 hours, and then filtered, weighted through the same procedures as taken for MSD.

A Perkin Elmer TGA7 thermogravimetric analyzer was employed to determine the thermal stability of the new products under the conditions: 20.0 °/min of heating rate, 5.0 mg~12.0 mg of sample, and N₂ atmosphere.

RESULTS AND DISCUSSION

From the analytical results of IR, ¹HNMR, GPC and elementary composition presented above, it is easily inferred that the

chemical structures of the novel compounds of which chemical nomenclatures have been mentioned above are as follows :

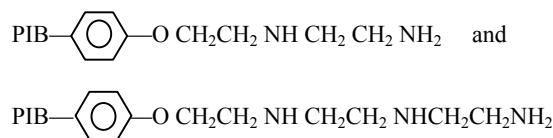


Figure 1 and Figure 2 exhibit the results of fuel oxidation

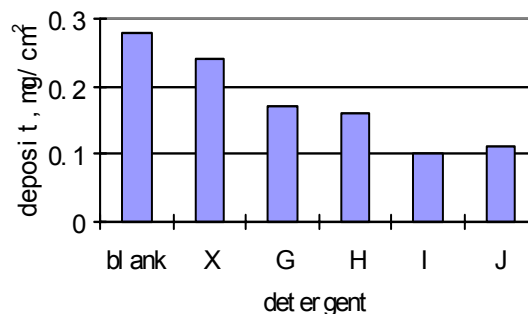


Figure 1 Results of deposit formation oxidized for 20 hours

reactor test. It is apparent that the new products can significantly inhibit PFID formation and their performances are far superior to that of paradyne 748(X), with their performances relatively strongly affected by amino groups and the influencing regularity being diethylenetriamine > ethylenediamine.

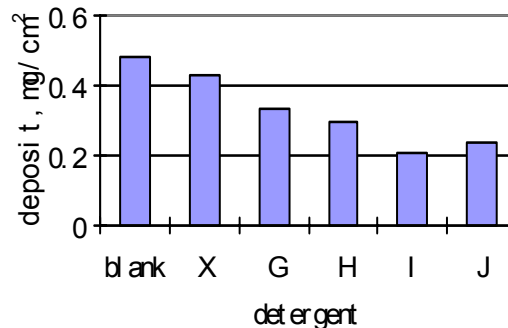


Figure 2 Results of deposit formation oxidized for 25 hours

In Figure 3 are displayed the results of crankcase oil simulating test. It is evident that the new synthesized detergents can also remarkably suppress IVD build-up derived from in-use engine oil, with similar influencing patterns of amino group to that recognized in fuel oxidation reactor test. In Figure 4 are illustrated the results of MSD dispersing test. It can be seen that the new compounds possess excellent capabilities of dispersing deposit suspending in gasoline to prevent MSD aggregating. The dispersancies of these new products are similar to that of paradyne 748 to disperse MID as observed from the results in Figure 5, although the performances are far inferior to those for dispersing MSD.

The results of ISD simulating test demonstrated that the amount of deposit formed 0.9 mg unadditized decreased to zero when 500 µg/g of compound J was added to a tested gasoline.

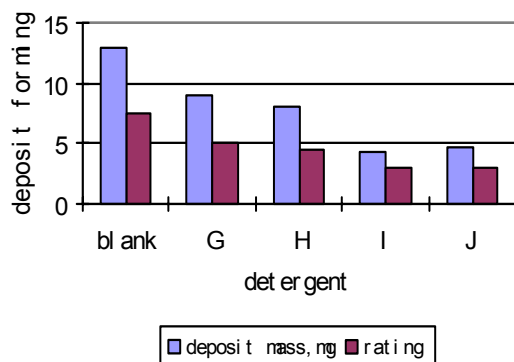


Figure 3 Results of crankcase oil simulating test with 0.6% detergent contained

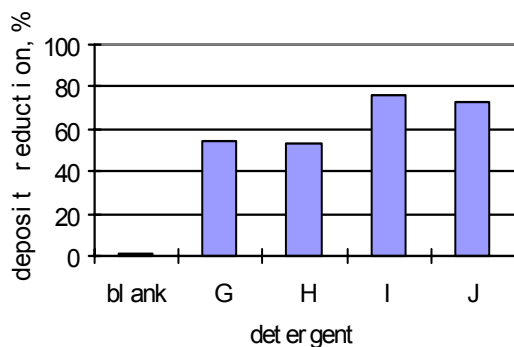


Figure 4 Results of MSD dispersing test

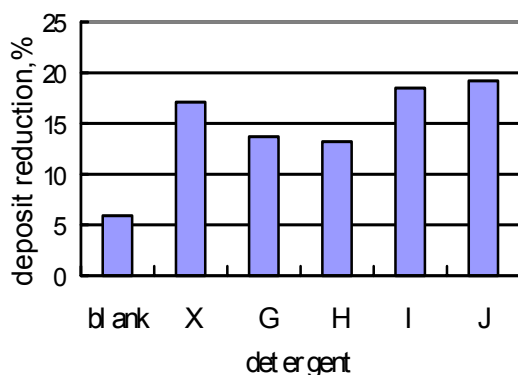


Figure 5 Results of MID dispersing test

TGA curve of compound J very similar to those of other three products is exhibited in Figure 6. It is clear that the novel compound begin to decompose and lose weight at about 250°C in response to thermal cracking of C-O-C bond in the detergent molecules.

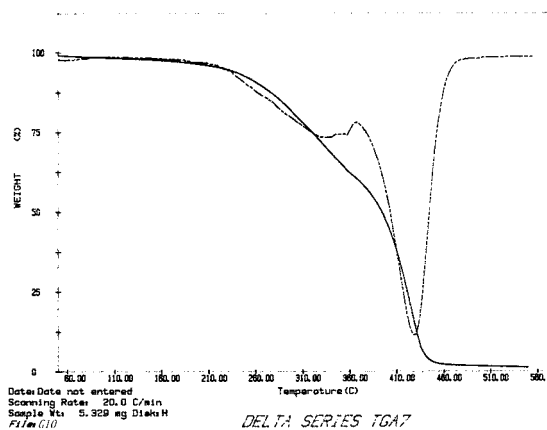


Figure 6 TGA curve of compound J

CONCLUSIONS

(1) A novel type of detergents of parapolyisobutylphenoxyethyl amines were synthesized using polyisobutyl (Mw=815,995) phenol, 1,2-dibromoethane, ethylenediamine and diethylenetriamine. The structures of the synthesized additives were identified by IR, ^1H NMR, GPC and elementary analyses.

(2) Detergent performances of the new products were evaluated with the methods of fuel oxidation reactor test, crankcase oil simulating test, deposit dispersing experiment, and ISD simulating test. The results showed that this novel type of compounds possess excellent capabilities to control PFID, ISD formations, and effectively suppress IVD growth derived from engine oil. These products exhibit outstanding performances for dispersing MSD compared with relatively weak abilities to disperse MID.

(3) The novel products decompose at about 250°C due to relatively easy thermal cracking of C-O-C bonds in their molecules, implying that they potentially possess comparatively low CCD forming characteristics.

REFERENCES

- (1) Gautam T. Kalghatgi, "Deposits in Gasoline Engines – A Literature Review", SAE Paper 902105 (1990)
- (2) Gautam T. Kalghatgi, "Combustion Chamber Deposits in Spark-Ignition Engines – A Literature Review", SAE Paper 952443 (1995)
- (3) Crema S, Schreyer P, and Miin T, "Effect of Thermal Stability of Detergents and Carrier Fluids on the Formation of Combustion Chamber Deposits", SAE Paper 961097 (1996)
- (4) Cherpeck R E, "Substituted Aromatic Polyalkyl Ethers and Fuel Compositions Containing the Same", USP 5637119, 1997, 1, 10
- (5) Kim C, Tseregounis S I, Scruggs B E, "Deposit Formation on a Metal Surface in Oxidized Gasolines", SAE Paper 872112 (1987)
- (6) Hejun Guo, Xiaochuan Guo, Zhizhong Liu, "Study on the Prevention of PFI Gasoline Engine Deposit Formation", Vehicle Engine (Chinese), 1999, 2
- (7) Hejun Guo, Xuanjun Wang, Xiao Liu, and Zhizhong Liu, Study on Evaluating techniques for Measuring Gasoline Detergent Performance, Vehicle Engine (Chinese), 2002, 1

Selective Sulfur Removal from Fuels Using Ionic Liquids at Room Temperature

Shuguang Zhang and Z. Conrad Zhang*

Akzo Nobel Chemicals Inc., 1 Livingstone Ave., Dobbs Derry, NY 10522

Introduction

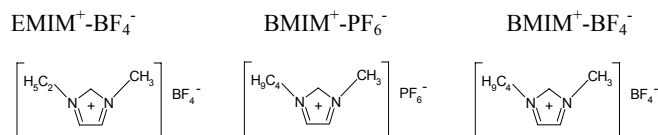
Sulfur removal from transportation fuels has become an increasing technical challenge as oil refineries face growing environmental pressures and strict regulatory requirements. In the United States, the Environment Protection Agency requires that the average concentration of sulfur in gasoline be lowered more than 90%, to 30 parts per million, phased in from by 2004 through 2006.¹ The new on-road diesel regulation specifies a per-gallon sulfur cap of 15 ppm effective mid-2006.² The European Union has stringent fuel quality rules that require maximum diesel sulfur content of 50 ppm in 2005 (350 ppm in 2000), and maximum petrol (gasoline) sulfur content of 50 ppm in 2005 (150 ppm in 2000).³

Refinery industry utilizes catalytic processes for desulfurization of transportation fuels through hydroprocessing. While the performance of conventional hydroprocessing catalysts have been highly effective for the reduction of sulfur levels, further removal of residual sulfur from the processed fuels is seen to largely increase the cost of hydroprocessing. The processes are highly energy intensive and consume large amount of hydrogen. For example, a study based on a typical Co-Mo catalyst shows that either about four times more active catalysts or an increase of 38°C in reaction temperature is needed to meet the required sulfur reduction of diesel products from 500 ppm to 50 ppm.⁴ Therefore, alternative technologies are of particular interest in providing potential solutions for S-free clean fuels.

Ionic liquids have been studied for possible applications related to green chemical processes, such as liquid/liquid extractions, gas separations, electrochemistry and catalysis.⁵⁻¹³ These liquids are easy to handle because of no-volatility, non-flammability, and high thermal stability. Therefore they pose little environmental harm.¹⁴ Many ionic liquids, except those composed of AlCl_4^- , are moisture tolerant.

In the present work, ionic liquids, 1-ethyl-3-methylimidazolium tetrafluoroborate ($\text{EMIM}^+\text{-BF}_4^-$), 1-butyl-3-methylhexafluorophosphate ($\text{BMIM}^+\text{-PF}_6^-$) and 1-butyl-3-methylimidazolium tetrafluoroborate ($\text{BMIM}^+\text{-BF}_4^-$), are investigated for sulfur removal from transportation fuels. The melting points of $\text{EMIM}^+\text{-BF}_4^-$ and $\text{BMIM}^+\text{-PF}_6^-$ are both close to 5°C. $\text{BMIM}^+\text{-BF}_4^-$ has a melting point about -80°C. $\text{EMIM}^+\text{-BF}_4^-$ is water miscible and $\text{BMIM}^+\text{-PF}_6^-$ is water immiscible.¹⁴ As liquids at room temperature, these compounds are also thermally stable up to above 300°C.¹⁵ Scheme 1 shows the structures of these three ionic liquids.

Even though AlCl_3 based ionic liquid is also effective for the removal of sulfur-containing compounds,¹⁶ it is limited to the absorption of certain aromatic compounds such as dibenzothiophene. Dark precipitate was formed when thiols are present.¹⁷ In this work, the absorption of various model components in typical gasoline and diesel fuels was studied using the neutral ionic liquids as shown in Scheme 1.



Scheme 1. Structures of ionic liquids

Experimental

Preparation of ionic liquids

Preparation of $\text{EMIM}^+\text{-BF}_4^-$ Equal moles of 1-ethyl-3-methyl-1H-imidazolium chloride (from Aldrich) and lithium tetrafluoroborate (from Aldrich) were dissolved in acetonitrile solution, respectively. These two solutions were gradually mixed together with active stirring. The precipitate, lithium chloride, was separated from the liquid by filtration. The liquid phase was distilled in a three-mouth flask at 100 °C to remove acetonitrile from ionic liquid.

Preparation of $\text{EMIM}^+\text{-PF}_6^-$ An $\text{EMIM}^+\text{PF}_6^-$ was prepared by mixing 1-butyl-3-methyl-imidazolium chloride and LiPF_6 (Aldrich) in acetonitrile followed by a filtration to remove LiCl precipitate and a distillation to remove acetonitrile. The 1-butyl-3-methyl-imidazolium chloride was obtained by refluxing equal molar amounts of 1-methylimidazole and 1-chlorobutane in a flask when heating and stirring at about 70°C for 48 h.¹⁸ Another sample was obtained from the laboratory of Professor Robin D. Rogers at the University of Alabama. It was prepared by the reaction of 1-butyl-3-methyl-imidazolium chloride and HPF_6 .¹⁶

Preparation of $\text{BMIM}^+\text{-BF}_4^-$ An $\text{BMIM}^+\text{BF}_4^-$ was prepared by mixing 1-butyl-3-methyl-imidazolium chloride and LiBF_4 (Aldrich) in acetonitrile followed by a filtration to remove LiCl precipitate and a distillation to remove acetonitrile. This sample contains about 10 mol% of impurity (dimer methylimidazole)

Varian Inova-500 MHz NMR spectrometer and Jeol GSX-270 MHz NMR spectrometer were used to verify the structures of the ionic liquids. NMR analysis was also conducted to obtain the sulfur content in the ionic liquid phase after absorption.

Measurement of absorption capacity and efficiency The model compounds, 2-methylpentane, 1-hexene, methylcyclopentane, toluene, trimethylbenzene, thiophene, 2-methylthiophene, and isobutyl mercaptan, were selected to represent typical molecules in gasoline and diesel fuel. The absorption capacity of an ionic liquid for a specific compound was measured at room temperature by adding 1 g of the ionic liquid and 2 g of a model compound to a glass vial. After shaking for a few minutes, two phases were formed and excess model compound in the upper phase was carefully removed. The absorbed amount of model compound in the ionic liquid phase is measured by weight.

The absorption selectivity of $\text{BMIM}^+\text{-PF}_6^-$ for thiophene from a mixture with toluene was measured by adding 1 g of the ionic liquid to a mixture of 2.12 g of thiophene and 2 g of toluene. After 15 min stirring, the weight loss of the mixture was measured. Concentrations of toluene and thiophene in the ionic liquid phase were measured by NMR after absorption. Similar procedure was applied to $\text{BMIM}^+\text{-PF}_6^-$ but with a mixture of 2.04 g of thiophene and 2 g of toluene.

The sulfur removal efficiencies of $\text{EMIM}^+\text{-BF}_4^-$ and $\text{BMIM}^+\text{-PF}_6^-$ for two gasoline samples were measured. In each case, 2 g of gasoline or diesel and 1 g of ionic liquid was mixed in a glass vial and shaken for 15 min. After settling down, the upper fuel phase was removed and analyzed. Quantitative elemental analysis of sulfur was conducted on a Bruker S4 Explorer wavelength dispersive X-ray fluorescence spectrometer. Aromatics analysis was carried out on HP

* email: zongchao.zhang@akzonobel.com

6890 GC/MS using an OV-1 column (30m x 0.32mm id x 5µm) for gasolines.

Recovery of used ionic liquids Used ionic liquids were recovered after adsorption either by washing with water followed by drying or by distillation.

Results and Discussion

Absorption capacity of the ionic liquids The absorption capacities of EMIM⁺-BF₄⁻, BMIM⁺-PF₆⁻ and BMIM⁺-BF₄⁻ for the eight model compounds are shown in Table 1, respectively. The three ionic liquids showed little absorption for paraffins and olefins, but absorbed a small amount of aromatics and a larger amount of thiophene and methylthiophene. In the used ionic liquids, the molar ratio of thiophene to ionic liquid was found to be 0.86/1, 3.5/1 and 2.2/1 for EMIM⁺-BF₄⁻, BMIM⁺-PF₆⁻ and BMIM⁺-BF₄⁻, respectively.

NMR analysis of the ionic liquid BMIM⁺-PF₆⁻ phase for absorbed toluene in a mole ratio of 0.86/1 and absorbed thiophene in a mole ratio of 3.5/1 are consistent with the measured weight loss from the organic phase. There was no ionic liquid found in the organic phase after absorption measurement.

Table 1. Absorption Capacity of EMIM⁺-BF₄⁻

Compound	mol/mol		
	EMIM ⁺ -BF ₄ ⁻	BMIM ⁺ -PF ₆ ⁻	BMIM ⁺ -BF ₄ ⁻
2-Methylpentane	0.093	0	0
1-Hexene	0.095	0	0.030
Methylcyclopentane	0.12	0	0.091
Toluene	0.15	0.78	0.30
Trimethylbenzene	0.12	0.071	0.15
Thiophene	0.86	3.5	2.4
2-Methylthiophene	0.16	1.2	0.73
(CH ₃) ₂ CHCH ₂ SH	0.089	0.19	0.056

The preferred absorption for thiophene, 2-methylthiophene and aromatics by the ionic liquids is likely resulted from the interaction of the aromatic ring with the cation of the ionic liquids. It is important to note, however, that methyl group on the aromatic compounds markedly reduced the absorption capacity. For example, the absorption capacity of BMIM⁺-PF₆⁻ for trimethylbenzene is only about 10% of that for toluene. The absorption capacities of BMIM⁺-PF₆⁻ and BMIM⁺-BF₄⁻ for 2-methylthiophene are about 1/3 of those for thiophene. Methylcyclopentane, a cycloparaffin without aromatic π charge density, and isobutylmercaptan, which contains sulfur but no ring, were only weakly absorbed.

For a specific aromatic compound, for example thiophene, BMIM⁺-PF₆⁻ and BMIM⁺-BF₄⁻ have higher absorption capacities than does EMIM⁺-BF₄⁻. The results suggest that the structure and the size of both cation and anion of an ionic liquid affect absorption. The local structure of the ionic liquids appears to have a significant effect on their interaction with the aromatic compounds. As shown in Table 1, the absorption capacity follows the general order: thiophene >> methylthiophene > toluene >> trimethylbenzene > isobutylthiol, hexene, 2-methylpentane, methylcyclopentane. It appears that absorption is favored for molecules with higher density of the aromatic π electrons. Clearly, those aromatics with 5-membered ring have stronger interaction with the ionic liquids. Sulfur in non-

aromatic molecules such as isobutylthiol has weak interaction with the ionic liquids. The specific local structures of the ionic liquids and the chemistry involved in their interaction with the model compounds are under further study.

Absorption of a mixture of thiophene and toluene When applied to a mixture of thiophene and toluene, BMIM⁺-PF₆⁻ and BMIM⁺-BF₄⁻ showed strong preference absorption for thiophene over toluene. The results of NMR analysis are shown in Table 2 and Table 3.

Table 2. Competitive Absorption of Thiophene and Toluene in BMIM⁺-PF₆⁻

Composition	Toluene/Thiophene/ BMIM ⁺ -PF ₆ ⁻ (mole ratio)
In whole mixture	6.0/7.2/1
Absorbed	0.65/1.07/1

Table 3. Competitive Absorption of Thiophene and Toluene in BMIM⁺-BF₄⁻

Composition	Toluene/Thiophene/ BMIM ⁺ -BF ₄ ⁻ (mole ratio)
In whole mixture	5.5/6.2/1
Absorbed	0.23/0.48/1

As compared with a single model compound, the amount of absorbed thiophene from a model mixture was reduced in both BMIM⁺-PF₆⁻ and BMIM⁺-BF₄⁻ in the presence of toluene. For the model mixture, BMIM⁺-PF₆⁻ again showed higher thiophene absorption than BMIM⁺-BF₄⁻. The higher thiophene absorption over toluene in both ionic liquids supports the observation that interaction with the ionic liquids is favored for molecules with higher π aromatic electronic density. The combined absorbed toluene and thiophene over the BMIM⁺-PF₆⁻ is at 1.72/1 in molar ratio.

Removal of sulfur compounds from gasoline samples Gasoline samples with low sulfur level (240 ppm) and high sulfur level (820 ppm) were treated with the ionic liquids. About 10-30 wt% of sulfur was preferentially removed from these samples with almost no noticeable change on aromatics content, which is important to octane number. The concentrations of total sulfur and aromatics in the untreated and the treated gasoline are shown in Table 4.

Table 4 Sulfur removal from gasolines

	Ionic liquid	EMIM ⁺ -BF ₄ ⁻		BMIM ⁺ -PF ₆ ⁻	
		S	Arom*	S	Arom.*
		(ppm)	(wt%)	(ppm)	(wt%)
Low S	Before treatment	240	33.2	240	33.2
	After treatment	200	33.5	170	33.1
High S	Before treatment	820	32.6	820	32.6
	After treatment	730	33.0	710	31.7

*toluene, ethylbenzene and xylene

It is evident that the ionic liquids showed remarkable selectivity for the removal of sulfur compounds over aromatics, particularly from the low sulfur gasoline sample. It should be noted that the absorptive removal of sulfur containing compounds from the gasoline sample represents mainly the removal of aromatic sulfur-containing molecules, even though various saturated sulfur compounds are also present.

Regeneration of ionic liquids and recovery of absorbed sulfur-containing compounds The ionic liquids saturated with sulfur containing compounds were readily regenerated by either direct distillation or by successive dissolution in water followed by vaporization of water. For a thiophene saturated EMIM⁺-BF₄⁻ phase, the absorbed thiophene was released into a separated phase upon addition of water, as EMIM⁺-BF₄⁻ is soluble in water. Water was then vaporized from the ionic liquid phase under a nitrogen flow at 110°C for about 3 h. The EMIM⁺-BF₄⁻ ionic liquid was nearly quantitatively recovered.

As BMIM⁺-PF₆⁻ is little miscible with water, its regeneration was carried out by direct distillation after saturated absorption of thiophene. Under nitrogen at 110°C for 3 h, the ionic liquid was full regenerated. The absorbed thiophene recovered from distillation corresponds to the amount absorbed. NMR analyses indicated that the ionic liquids maintained the original structures after the regeneration.

Conclusions

Ionic liquids, EMIM⁺-BF₄⁻, BMIM⁺-PF₆⁻, and BMIM⁺-BF₄⁻ showed remarkable selectivity for the absorption of aromatic sulfur-containing molecules from gasoline. These ionic liquids are moisture insensitive and thermally stable. The ionic liquids after saturated absorption of sulfur containing compounds were readily regenerated for reuse. The absorbed aromatics sulfur-containing compounds were quantitatively recovered during the regeneration. The preferential absorption of thiophene and methylthiophene over toluene suggests that higher aromatic π electron density in C₅ rings is favorably absorbed. Methyl group at the aromatic rings was found to reduce the absorption capacity, possibly due to steric effect. The cation and anion structure and size in the ionic liquids are important parameters affecting the absorption capacity for aromatic compounds.

Acknowledgement. We would like to thank Professor R. D. Rogers at the University of Alabama for kindly providing a sample of BMIM⁺-PF₆⁻. Analytical support by Drs. B. Su, B. Joyce, and G. Darsey at Akzo Nobel is appreciated.

Reference

1. <http://www.epa.gov/otaq/tr2home.html>.
2. <http://www.petroleumrefining.com/program19.html>.
3. <http://www.dieselnet.com/standards/eu/ld.html>.
4. Knudsen, K. G., Cooper, B. H., Topsoe, H., *Appl. Catal. A: General* **1999**, 189, 205.
5. Howard, K. A., Mitchell, H. L., Waghore, R. H., US Patent 4,359,596, **1982**.
6. Boate, D. R., Zaworotko, M. J., US Patent 5,220,106, **1993**.
7. Sherif, F. G., Shyu, L., Greco, C. C., US Patent 5,824,832, **1998**.
8. Koch, V. R., Nanjundiah, C., Carlin, R. T., US Patent 5,872,602 **1998**.
9. Silvu, S. M., Suarcz, P. A. Z., de Souza, R. F., Dupont, J., *Polymer Bulletin* **1998**, 40, 401-405.
10. Carmichael, A. J., Haddlettn, D. M., Bon, S. A. F., and Seddon, K. R., *Chem. Commun.* **2000**, 1237-1238.
11. Carlin, R. T., Wilkes, J. S., *J. of Mole. Catalysis*, 1990, 63, 125-129.
12. Golezdzinowski, M., Birss, V. I., and Galuszka, J., *Ind. Eng. Chem. Res.* **1993**, 32, 1795-1797.
13. Boon, J. A., Levisky, J. A., Pflug, J. L., and Wilkes, J. S., *J. Org. Chem.*, **1986**, 51, 480-483.
14. Professor Rogers, R. D., University of Alabama, <http://bama.ua.edu/~rdrogers/>.
15. Holbrey, J. D., and Seddon, K. R., *J. Chem. Soc., Dalton Trans.*, **1999**, 2133-2139.

16. Bösmann, A., Datsevich, L., Jess, A., Lauter, A., Schmitz, C. and Wasserschedl, P., *Chem. Commun.*, **2001**, 2494 - 2495
17. Zhang, Q., Zhang, C., in preparation for publication
18. Visser, A. E., Swatloski, R. P., and Rogers, R. D., *Green Chemistry*, February **2000**.

SHOULDN'T WE KNOW THE MOLECULAR COMPOSITION OF FISCHER-TROPSCH DIESEL FUELS

Attilio Bisio and Chris Atkinson

Atro Associates
Mountainside, NJ 07082
and
Atkinson & Associates
Morgantown, WV 26508

Introduction

In recent years there has been a movement towards significant reduction of emissions from diesel vehicles, particularly those which have heavy-duty diesel engines. Numerous studies have shown that the factors that govern how the properties of diesel fuels (which meet ASTM D975 requirements) influence emissions from diesel engines are both complex and interrelated. Moreover, interactions between the physical properties of a fuel and engine control system can result in changes to the settings for injection timing and exhaust gas recirculation (EGR) even when "sophisticated" electronic controls are used.

While the impact of fuel properties are strongly influenced by these interactions, there is general agreement that use of higher cetane and lower sulfur diesel fuels results in lower NO_x and particulate matter (PM) emissions that are largely engine technology, age and drive cycle independent. As a result, there is a growing interest in diesels produced by Fischer-Tropsch processes since they have a high cetane rating, contain no sulfur species and can contain very low levels of aromatics.

Discussion

To date, twenty six (26) studies comparing the engine out emissions of Fischer-Tropsch diesels to petroleum derived fuels, e.g. ASTM Low Sulfur 2D, CARB and Amoco EC-D and alternative fuels, e.g. Biodiesel and DME have been published. Significant reductions in NO_x and PM emissions have been shown for F/T diesels in all these studies. However, in some studies CO and HC emissions have been higher than for the comparative fuel studied.

The absence of sulfur species in Fischer-Tropsch diesel should facilitate the use (and retrofit) of continuously regenerating particulate traps or filters (such as the Johnson Matthey CRT) and improve their reliability significantly. The impact of using Fischer-Tropsch diesel on particulate traps and filters has not been studied. However, one study does attribute both lower engine-out NO_x emissions and a higher De NO_x efficiency to the use of Fischer-Tropsch diesels.

The higher cetane of Fischer-Tropsch diesel results in a shorter ignition delay and a more consistent rate of heat release. This translates into lower PM, NO_x , HC and CO emissions compared to petroleum derived diesels (although there are some inconsistencies in the available data). Whether in existing engines a cetane higher than 55 will have a significant an impact on engine-out emissions is not clear.

Only three (3) studies compare the performance of different Fischer-Tropsch diesels. Unfortunately, the properties of the overwhelming majority of the Fischer-Tropsch diesels studied to date do not differ significantly (Figure 1). However, there are suggestions that engine-out NO_x and PM emissions can be different

for Fischer-Tropsch diesels that have almost identical ASTM D975 properties. Often it is not appreciated that the properties of (and the

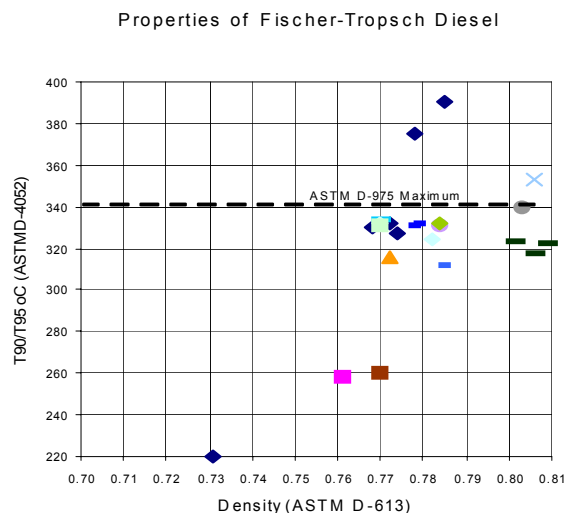


Figure 1. Properties of Fischer-Tropsch Diesel

nature and distribution of molecular species) in Fischer-Tropsch diesel are established in the downstream refinery processes (Figure 2) and not in the Fischer-Tropsch reactor. At present the limited

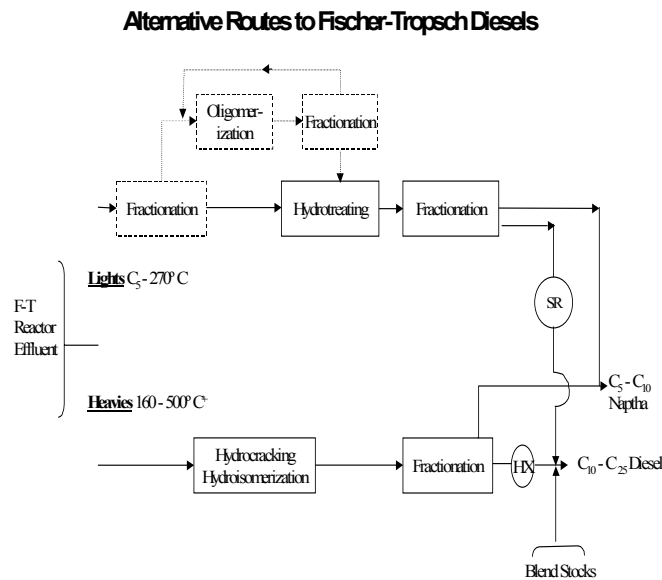


Figure 2. Alternative Routes to Fischer-Tropsch Diesels

information available about the number and types of molecular species in Fischer-Tropsch finished products is found largely in a growing number of patents. For typical Fischer-Tropsch diesels and gas oils we find the following:

- Boiling range 200-350 °C
- Carbon number range 10 – 24

- 500 measurable compounds that are homologous series of paraffins
- Absence of alcohols, aromatics, olefins or cyclic structures except for blends

GC-MS data can be used to establish the distribution of carbon isomers (**Figure 3**). Since this cut contains primarily monobranched isomers its cetane number is projected to be about 80 with a standard error of 6.

Conclusions

There is general agreement that a significant improvement in engine-out emissions and some improvement in after treatment emissions can be obtained by the use of Fischer-Tropsch diesels (regardless of the engines and testing protocols used). The improvements in engine-out emissions are largely attributed to the higher cetane of and zero sulfur of Fischer-Tropsch diesels. To date, the potential benefits of “zero sulfur” have not been fully captured. Moreover, differences in the distribution of isomeric structures in Fischer-Tropsch diesels may have an impact on engine out emissions. While, their impact is going to be smaller than that of higher cetane and zero sulfur information about the distribution of isomeric structures in Fischer-Tropsch diesel would be a first step in improving our understanding of their performance.

An improved understanding of the molecular chemistry of Fischer-Tropsch diesel fuels and gas oil is also essential if their full potential is to be realized in current and future engines. Since the production of Fischer-Tropsch fuels will be limited over the next decade, studies should be focused on its use in heavy-duty fleets operating in non-compliance urban environments.

References

An annotated bibliography is available from abisio@rcn.com.

		Relative Quantities
N-Hexadecane		
$\text{CH}_3 \text{CH}_2 (\text{CH}_2)_{12} \text{CH}_2 \text{CH}_3$		1.00
3-Methylpentadecane		
$\begin{array}{c} \text{CH}_3 \text{CH}_2 \text{CH} (\text{CH}_2)_{11} \text{CH}_3 \\ \\ \text{CH}_3 \end{array}$		0.60
3-Ethyltetradecane		
$\begin{array}{c} \text{CH}_3 \text{CH}_2 \text{CH} (\text{CH}_2)_{10} \text{CH}_3 \\ \\ \text{CH}_3 \text{CH}_2 \end{array}$		0.10
2,4-Dimethyltetradecane		
$\begin{array}{c} \text{CH}_3 \quad \text{CH}_3 \\ \quad \\ \text{CH}_3 \text{CH} \text{CH}_2 \text{CH} (\text{CH}_2)_9 \text{CH}_3 \end{array}$		0.50
2-methyl-4-ethyltridecane		
$\begin{array}{c} \text{CH}_3 \\ \\ \text{CH}_3 \text{CH}_2 \text{CH}_2 \text{CH} (\text{CH}_2)_8 \text{CH}_3 \\ \\ \text{CH}_3 \text{CH}_2 \end{array}$		0.08
2,3,4-trimethyltridecane		
$\begin{array}{c} \text{CH}_3 \quad \text{CH}_3 \\ \quad \\ \text{CH}_3 \text{CH}_2 \text{CH} \text{CH} (\text{CH}_2)_8 \text{CH}_3 \\ \\ \text{CH}_3 \end{array}$		0.20

Figure 3. Relative Quantities of C_{16} Isomers

SUPERCRITICAL PHASE FISCHER-TROPSCH SYNTHESIS: PRODUCT CONTROL

R. Prasert(a,b), N. Tsubaki(b),

X.-H. Li(a), K. Asami(a) and Kaoru Fujimoto(a)

- (a) Faculty of Environmental Engineering
University of Kitakyushu
Fukuoka, 808-0135, Japan
- (b) Faculty of Engineering
Toyama University
Gofuku, 630-8555, Japan

Introduction

The Fischer-Tropsch synthesis (F-T) reaction conducted in the solid-catalyzed gas phase reaction system, which has been commercially operated or will be operated in several countries, is inevitably accompanied by local overheating of catalyst surface as well as by production of heavy wax. Local overheating of catalyst may lead to the deactivation of catalyst and also to the increase in methane selectivity. Heavy wax may plug micropores of the catalyst and the catalyst bed itself, resulting in the catalyst deactivation.

The slurry phase F-T reaction process, on the other hand, in which a slurry, composed of fine powdery catalyst and mineral oil, is used as a reaction medium and has been developed to overcome defects of the gas phase process¹. The process has also some defect such as the diffusion of synthesis gas in the micropores of the catalyst.

It was known that a supercritical fluid has a unique characteristic in its molecular diffusion and its solubility parameter². The present authors developed F-T reaction in the supercritical phase and compared its reaction performance with those in the liquid and gas phases, both experimentally and theoretically. In summary, the supercritical phase F-T reaction shows unique characteristics such as quick diffusion of reactant gas, effective removal of reaction heat, and in situ extraction of high molecular weight hydrocarbons (wax). And these characteristics can be utilized to realize a new process where wax is selectively synthesized³.

Experimental

Reaction apparatus and product analysis. The configuration of reactor for the supercritical phase reaction was similar to that of a conventional, pressurized, fixed-bed flow reactor system. The only difference was that a vaporizer and an ice-cooled high-pressure trap were set upstream and downstream of the reactor, respectively. For the purpose to compare characteristic features of the gas phase, liquid phase and supercritical phase reactions, these three kinds of reactions were conducted in this fixed bed reactor. The liquid phase reaction was operated in down-flow-type trickle bed. The balance materials were nitrogen for the gas phase reaction, n-hexadecane and nitrogen for the liquid phase reaction. Reaction temperature was defined as the highest temperature of the catalyst bed, measured by a thermocouple placed along the center of the catalyst bed. Temperature profiles of the catalyst bed were distributed within 1-2°C in the supercritical phase reaction.

Supercritical fluid was selected under the criteria that follows:

1. Its critical temperature and pressure are slightly lower than the typical reaction temperature and pressure.
2. It should not poison the catalysts and should stable under the reaction conditions.
3. It has a high affinity for aliphatic hydrocarbons to extract wax from catalyst surface and reactor.

n-Hexane (C₆H₁₄), with critical temperature, *T_c*, and critical pressure, *P_c*, at 233.7°C and 29.7 bar, respectively, was chosen as the supercritical solvent. In wax synthesis experiments where reaction temperature was low, *n*-pentane (*T_c*, 196.6°C; *P_c*, 33.3 bar) was used alternatively as the supercritical fluid. The standard reaction conditions were *T*= 240°C, *P* (total) = 45 bar, *P* (CO+H₂) = 10 bar, *P* (balance gas) = 35 bar, CO/H₂ = 1:2, W/F (CO+H₂) = 10g of catalyst h/mol. Argon was used as internal standard with concentration of 3% in the feed gas.

Results and Discussion

Table 1 summarized the reaction behavior of Ru/Al₂O₃ catalyst. The rate of CO conversion in the supercritical phase reaction was higher than that in the liquid phase reaction, but lower than that in the gas phase reaction. This suggests that the diffusion of synthesis gas in the supercritical phase was faster than that in the liquid phase but slower than that in the gas phase. The amount of products extracted from the catalyst bed after the supercritical phase was much smaller than that in the gas phase reaction, but similar to that in the liquid phase reaction. Furthermore, the carbon chain growth probability in the supercritical phase or in the gas phase reaction was higher than that in the liquid phase⁴. This revealed that the CO/H₂ ratio inside the catalyst pores in the supercritical phase reaction was similar to that in the gas phase reaction, because of the effective molecular diffusion in the supercritical phase, which will be discussed later.

Table 1 Phase effect on Ru catalyst

Reaction phase	Gas	Supercritical	liquid
CO conversion (%)	44.7	39.0	28.0
Effluent products (a) (C-mol/g-cat.h)	10.8	12.8	8.82
Extracted products (b) (C-mol/g-cat.h)	3.0	0.2	0.5
Residual ratio [100b/(a+b)] (%)	22	2	5
Chain growth probability	0.94	0.95	0.85
Carbon balance (%)	90	99	96

Ru/Al₂O₃, standard reaction conditions; (a) the amount of total effluent products and (b) the amount of total extracted products after reaction.

It is well known that at the steady state of the gas phase reaction, catalyst micropores were filled with liquid hydrocarbons. But the average viscosity of this kind of liquid hydrocarbons was low due to the dilution effect of the co-existing nitrogen. High diffusion rates in the gas phase reaction could be realized.

Carbon balance was calculated as the percentage of the carbon amount of effluent and extracted products in the carbon amount of the inlet feed gas. From **Table 1**, it is clear that about 10% carbon stayed inside the catalyst pellet even after extraction by the supercritical extraction after reaction, indicating that these carbon species formed a coke-like structure at hot spots during gas phase reaction.

F-T wax, owing to its merits such as high melting point, high hardness value, low viscosity, as well as being nitrogen-, sulfur-, and aromatic-free, has been highly favored. It can be used, not only directly, in many fine chemical fields such as cosmetics, packing materials and adhesives, but also as feedstock for producing different-sized hydrocarbon products ranging from kerosene to aviation fuels. It is extremely difficult to selectively synthesize waxy hydrocarbons through T-T reaction. A main reason is that the F-T products fall in the Anderson-Schultz-Flory (ASF) distribution.

Development of a new type of F-T reaction, free from ASF constraint on its product selectivity, is of great importance for wax production, as modification of the F-T catalyst alone is not enough to increase wax selectivity significantly.

Here, we report that addition of a small amount of heavy 1-olefin into supercritical phase F-T reaction can significantly promote the chain growth and greatly enhance the selectivity of waxy products. As a matter of interest, this phenomenon does not occur in the gas phase reaction³. What was shown in **Figure 1** is the F-T product distribution profile for a 4 mol% (CO base) addition of 1-tetradecene or 1-hexadecene into the supercritical *n*-pentane fluid. It is clear from the figure that the product distributions in the olefin-added systems are very flat, in marked contrast with that in the supercritical phase F-T reaction without the addition of olefin. The selectivities for hydrocarbons lower than C₁₄ were higher in the F-T reaction without the addition of olefin. The reverse was true, however, for heavy products with carbon numbers higher than 14; the selectivity to waxy products was remarkably enhanced in the olefin-added reactions. Another remarkable phenomenon in the olefin-added F-T reactions was the suppression of methane formation. Similar behaviors were observed for the addition of 1-heptene.

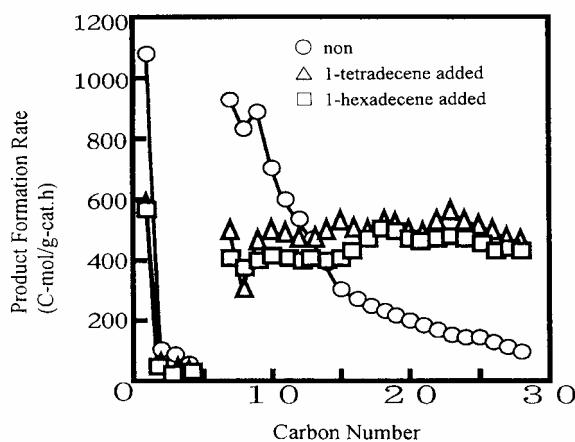


Figure 1. Addition of heavy olefins into supercritical phase F-T reactions: anti-ASF distribution Co-La/SiO₂ catalyst, $T=220^{\circ}\text{C}$, $P(n\text{-pentane})=3.5\text{ MPa}$, $P(\text{CO}+\text{H}_2)=1.0\text{ MPa}$, $W/F(\text{CO}+\text{H}_2)=9\text{ g-cat. h/mol}$; added olefin amount/4%(CO base) supercritical fluid/*n*-pentane.

The characteristics of the olefin-added reaction systems are listed in **Figure 2**. Methane selectivity in any olefin-added reaction was lower than half in the same reaction without addition of olefin. CO conversion was also higher in the 1-olefin added reactions except for 1,7-octadiene. On the other hand, CO₂ selectivity in all F-T reactions with heavy olefin addition was lower than that in the olefin-free reaction.

Compared with those in the common supercritical phase reaction, addition of olefins with long carbon chain into the accompanying fluid can accelerate the carbon chain growth. The essential prerequisites for the occurrence of this process are the rapid diffusion of these added olefins inside the catalyst pores to reach the metal sites and the effective diffusion of the produced heavy products from the interior active sites to the outer catalyst surface. Both of them can be realized only in the supercritical phase.

The added 1-olefins could arrive at metal sites by the aid of the accompanying supercritical fluid adsorb onto the active sites as alkyl

radicals to initiate the carbon chain growth; such chains should be indistinguishable from other carbon chains formed directly from synthesis gas. These new alkyl radicals would consume extra methylene to initiate new carbon chain propagation centers. Since methylene species are involved in the chain growth with the added 1-olefins as well, the selectivity of methane, which is formed mainly from methylene hydrogenation, decreases. Also, attributed to increased consumption of the adsorbed methylene species, adsorption and cleavage of CO to carbide on the metal site, as well as the hydrogenation of carbide to methylene species, are accelerated. Experimentally, the CO conversion increased with addition of 1-olefin. The acceleration in this direction may contribute to the suppressed CO₂ selectivity as well as in the olefin-added reaction, as CO₂ is the by-product from CO through the water-gas shift reaction.

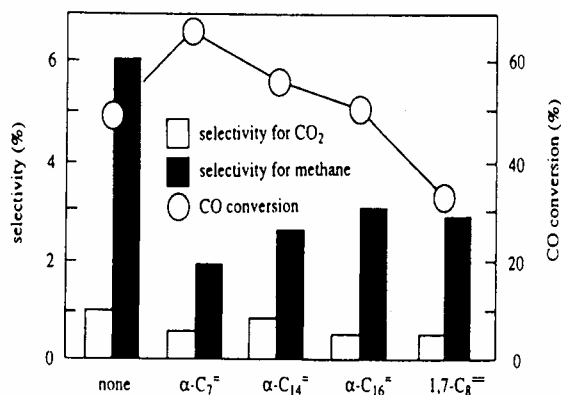


Figure 2. Reaction performance of the supercritical phase F-T reaction with addition of various long-chain olefins.

It should also be noted that the increase of CO conversion was more noticeable for addition of 1-olefin with shorter carbon chain (e.g., heptene); but enhanced chain growth occurred more effectively for addition of longer chain 1-olefins, as shown in **Figure 2**. We believe that if the added olefin had a rather long carbon chain, it would adsorb more strongly on the metal site and would cover a large active area of the catalyst, thereby inhibiting H₂ adsorption onto the metal site. This may be the reason for the lower CO conversion in the case of the addition of 1,7-octadiene and the relatively low CO conversion for the addition of 1-C₁₆H₃₂.

References

1. Koelbel H.; Ralek M., *Catal.Rev.-Sci. Eng.* **1980**, 21, 225
2. Debenedetti P.G.; Reid R.C., **1986**, 32, 2034
3. Fujimoto K.; Ohdan K.; Yoshii K. *Jpn. Kokai Tokkyo Koho* **1992**, 1992-181293, **1993**, 1993-138534, **1993**, 1993-138535
4. Yokota K.; Fujimoto K., *Fuel*, **1989**, 68, 255

Analysis

Sulfur content of product oil was determined by XRF. GC-SCD analysis was also conducted to determine DBT, 4-MDBT, and 4,6-DMDBT.

Results and Discussion

Concept of Two-Stage Process with Gas/Liquid Separation.

Conceptual diagram of the sulfur compound distribution in two-stage process with gas/liquid separation is shown in **Figure 2**. In the 1st-stage, HDS of "Reactive Sulfur Compounds" is perfectly carried out. As a result of the HDS and HDN reactions in the 1st-stage, a large amount of hydrogen sulfide and ammonia are produced. These compounds seriously inhibit HDS of "Refractory Sulfur Compounds" in the 2nd-stage. Removal of these inhibitors between the 1st-stage and the 2nd-stage accelerates HDS in the 2nd-stage. Based on the estimation of gas/liquid equilibrium, 86% of hydrogen sulfide can be removed, and more H₂S can be removed by application of stripping with H₂.

NiW catalyst can be applied to the 2nd-stage because the concentration of hydrogen sulfide and ammonia is comparatively low. NiW catalyst is superior to the CoMo catalyst and NiMo catalyst in the presence of low concentrations of hydrogen sulfide.

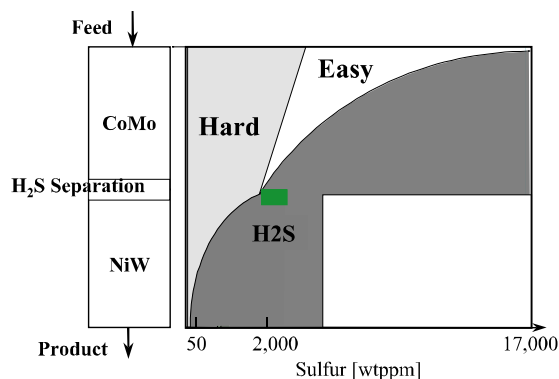


Figure 2. Conceptual diagram of the sulfur compound distribution in two-stage process with gas/liquid separation

Performance of Two-Stage Process with Gas/Liquid Separation. The performance of two-stage process with gas/liquid separation is shown in **Table 2**. In the base case, both the 1st-stage and 2nd-stage catalysts are CoMo catalyst and gas/liquid separation is not employed. The required reaction temperature for 50ppm product sulfur is 356°C.

In the case of only process improvement, both the 1st-stage and 2nd-stage catalysts are CoMo catalyst and gas/liquid separation is employed. The required reaction temperature for 50ppm product sulfur is 336°C. Simple application of the gas/liquid separation without modifying the catalyst improves 20°C of the required reaction temperature for 50ppm-sulfur diesel production.

In the case of both process and catalyst improvements, the 1st-stage and the 2nd-stage catalysts are CoMo catalyst and NiW catalyst, respectively. Gas/liquid separation is employed. The required reaction temperature for 50ppm product sulfur is 332°C. Application of the gas/liquid separation system and NiW catalyst for the 2nd-stage improves 24°C of the required reaction temperature for 50ppm-sulfur diesel production relative to the base case. (4°C lower reaction temperature than the case of only process improvement). **Figure 3** shows the potential to "sulfur free" diesel production.

In case of applying the NiW catalyst to the 2nd-stage, it is possible to produce 15ppm-sulfur diesel and 5ppm-sulfur diesel at 340°C and at 350°C, respectively.

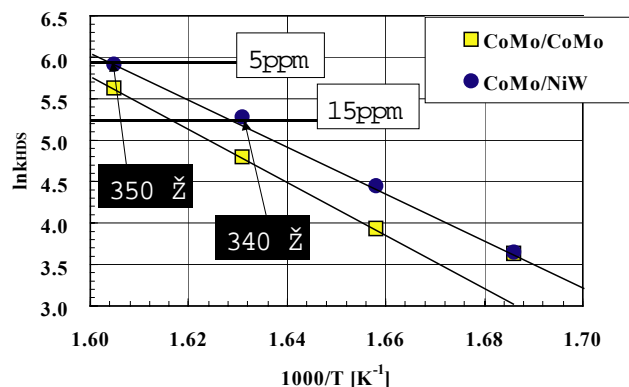


Figure 3. Potential to "sulfur free(S = 10 ppm or less)" diesel production by two-stage process with gas/liquid separation. (Feed 3, P(H₂): 5.0 MPa, H₂/Oil: 200 NL/L, Total LHSV: 2.0 h⁻¹) 1st-stage (50vol%) / Separator / H₂S Stripper / 2nd-stage (50vol%)

Table 2. Performance of Two-Stage Process with Gas/Liquid Separation

Improvement	Base	Process	Process & Catalyst
1st-stage catalyst	CoMo	CoMo	CoMo
Gas/Liquid Separation	No	Yes	Yes
2nd-stage catalyst	CoMo	CoMo	NiW
Required Reaction Temperature for 50 ppm Product Sulfur	356	336	332

Conclusions

The two-stage process with gas/liquid separation not only achieves ultra-low sulfur diesel production (S = 50ppm or less) under more beneficial conditions but also has great potential to sulfur-free diesel production (S = 10ppm or less). Removal of produced hydrogen sulfide and ammonia in the middle of the unit accelerates HDS of the following 2nd-stage. NiW catalyst can be applied to the 2nd-stage.

Acknowledgement. The Research of the two-stage process with gas/liquid separation has been entrusted by the New Energy and Industrial Technology Development Organization under a subsidy of the Ministry of Economy, Trade and Industry.

References

- 1) http://www.env.go.jp/press/file_view.php?serial=791&hou_id=1243.pdf (November 1, 2000, Japanese).
- 2) <http://www.epa.gov/fedrgstr/EPA-AIR/2000/June/Day-02/> (June 2, 2000).
- 3) <http://www.bmu.de/presse/2001/pm599.htm> (March 13, 2001).
- 4) http://europa.eu.int/rapid/start/cgi/guesten.ksh?p_action.gettxt=gt&doc=IP/01/6810|AGED&lg=EN (May 11, 2001).
- 5) Kabe, T.; Ishihara, A.; Qian, W. "Hydrodesulfurization and Hydrodenitrogenation Chemistry and Engineering", Kodansha, Tokyo (1999) and cited therein.
- 6) Koide, R.; Goto, Y.; Kawabata, M.; Ishida, K. Prepr. Div. Petrol. Chem., Am. Chem. Soc., 2001, 46, 398-401.

UTILIZATION OF COBALT CATALYSTS SUPPORTED ON MESOPOROUS SILICA FOR EFFICIENT PRODUCTION OF DIESEL FUELS BY FT SYNTHESIS

Yasuo Ohtsuka, Takashi Arai, Satoshi Takasaki, Naoto Tsubouchi

Institute of Multidisciplinary Research for Advanced Materials,
Tohoku University
Katahira, Aoba-ku, Sendai 980-8577, Japan

Introduction

Fischer-Tropsch (FT) synthesis has recently attracted increasing attention, since high quality diesel fuels without any sulfur and aromatic compounds can be produced directly from syngas derived from natural gas. A few processes have been commercialized for this purpose and some projects are in progress. Although many catalysts for FT synthesis have been proposed, a novel catalyst system that enables efficient production of C₁₀ – C₂₀ paraffin as diesel fraction may be developed.

The present authors have been working on the utilization of mesoporous silica materials with narrow pore size distribution, such as MCM-41¹⁾ and SBA-15²⁾, as catalyst supports in FT synthesis, since the mesopores may hold large amounts of catalyst components as nanoscale particles, enable ready diffusion of feed gas through liquid products condensed, and avoid blockage caused by carbon deposition. We have recently shown that, when 20 mass% Co is incorporated into SBA-15 with different pore diameters, Co/SBA-15 catalyst with average pore diameter of 8.4 nm has the highest activity at 523 K³⁾. This work focuses mainly on clarifying the effects of Co precursors and catalyst amount on CO conversion and space time yield (denoted as STY) of C₁₀ – C₂₀ hydrocarbons in FT synthesis at 503 K and 2.0 MPa with Co/SBA-15 catalysts.

Experimental

SBA-15 with average pore diameter of 8.6 nm was synthesized by heating an acidic aqueous mixture of triblock copolymer (EO₂₀PO₇₀EO₂₀), trimethylbenzene, and TEOS at 308 K for 24 h, followed by post-synthesis heat treatment at 370 K^{2),4)}. The material recovered after filtration and subsequent dryness at room temperature was air-calcined at 773 K for 6 h.

Co compounds were impregnated with SBA-15 support using an ethanolic solution of Co(CH₃COO)₂, Co(NO₃)₂ or the equimolar mixture, denoted as Co(A), Co(N) or Co(A+N) respectively, Co loading being 20 mass% as the metal, unless otherwise stated. The resulting samples were again air-calcined at 773 K. All of Co/SBA-15 catalysts were subjected to N₂ adsorption and X-ray diffraction (XRD) measurements. The pore size distribution and specific surface area were determined by the BJH and BET methods, respectively. The temperature programmed reduction (TPR) runs of these catalysts were also carried out under flowing H₂ at a heating rate of 10 K/min up to 1273 K in order to examine the reducibility of Co species.

FT synthesis was performed with a high-pressure gas-phase reaction system including a stainless flow reactor. About 0.1 – 0.5 g of the catalyst charged into the reactor was first pretreated with atmospheric H₂ for 12 h at 673 K, then cooled down to 373 K, and finally heated up to 503 K in a stream of H₂/CO with a molar ratio of 2:1 at 2.0 MPa, reaction time and W/F being 6 h and 4.0 g h/mol, respectively, unless otherwise stated. With product analysis, C₁ – C₅ hydrocarbons were on-line analyzed with a high-speed micro GC, and C₆ – C₂₈ hydrocarbons in liquid products recovered were determined with a capillary GC-MS. The carbon in waxy materials remaining in the catalyst after solvent washing was detected by the conventional elemental analyzer.

Results and Discussion

Properties and Structures of Co/SBA-15 Catalysts. Table 1 summarizes some properties of Co/SBA-15 catalysts. The SBA-15 support with average pore diameter of 8.6 nm provided pore volume of 1.9 cm³/g and BET surface area of 880 m²/g. When 20 mass% Co in total was impregnated, the volume and surface area decreased remarkably to 1.3 – 1.4 cm³/g and 460 – 590 m²/g, respectively, irrespective of kind of precursor salt. These observations show that Co particles are held inside the mesopores.

Table 1. Properties of Co/SBA-15 Catalysts

Co (A) (mass%)	Co(N) (mass%)	D _p ¹⁾ (nm)	V _p ²⁾ (cm ³ /g)	S _{BET} ³⁾ (m ² /g)	D(Co ₃ O ₄) ⁴⁾ (nm)
0	0	8.6	1.9	880	-
0	10	8.6	1.6	720	12
0	20	8.5	1.3	590	20
10	10	8.2	1.4	530	9.1
20	0	8.3	1.3	460	n.d.

¹⁾Average pore diameter determined by the BJH method.

²⁾Pore volume determined by the BJH method.

³⁾BET surface area.

⁴⁾Average crystalline size of Co₃O₄ calculated by the Debye-Scherrer method.

With the XRD profiles for Co/SBA-15 catalysts, the weak peaks of Co₃O₄ appeared with the Co(10N), Co(10A+10N) and Co(20N), whereas any diffraction lines of Co species were not detectable with the Co(20A). As shown in Table 1, the average crystalline sizes of Co₃O₄ were estimated to be 9 – 20 nm, which were slightly larger than the corresponding average pore diameters, suggesting that some of Co₃O₄ particles are present outside the mesopores.

Performances of Co/SBA-15 Catalysts. CO conversion and STY of C₁₀ – C₂₀ fraction are plotted against the composition of Co precursor in Figure 1, where the former is provided as the value at a steady state and the latter is calculated from the average selectivity. The Co(20A) was almost inactive, and CO conversion was thus only 1%. In contrast, the Co(10A+10N) and Co(20N) promoted FT synthesis dramatically, and the conversion reached 85 – 90% after 6 h. Since the conversion with the Co(10N) was as small as 20%, it is evident that there is a synergy in the catalysis by the Co(10A+10N).

When the activity of the Co(20N)/SBA-15 was compared with that of Co(20N) catalyst supported on commercial SiO₂ with average pore diameter of 8.7 nm³⁾, CO conversion at 503 K with the present catalyst was three times higher, though the Co(20N)/SiO₂ was used in a slurry phase reactor at a lower pressure of 1.0 MPa. Since it has generally been reported that the pressure dependency of CO conversion in FT synthesis with Co catalyst is small, the comparison mentioned above strongly suggests that not only uniform mesopores of the Co(20N)/SBA-15 but also the larger pore volume and higher surface area suitable for supporting 20 mass% Co account for very high conversion of 90% observed in this work.

For the average hydrocarbon distribution with the Co (20N) and Co(10A+10N) catalysts during 6 h reaction, the proportion of C₅+ fraction exceeded 70 C-mol% in both cases, and selectivity to C₁₀ – C₂₀ hydrocarbons ranged 30 – 32 C-mol%, the probability of chain grown being 0.92 – 0.93 though the linearity for the Anderson-Schulz-Flory distribution was not good. Any significant amounts of CO₂ were not detectable. The elemental analysis revealed the retention of about 10 C-mol% of waxy materials in the Co (20N) and Co(10A+10N) catalysts after FT reaction and subsequent solvent washing. As is seen in Figure 1, the STY of C₁₀ – C₂₀ paraffin was as large as 260 – 270 C-g/kg h with these catalysts.

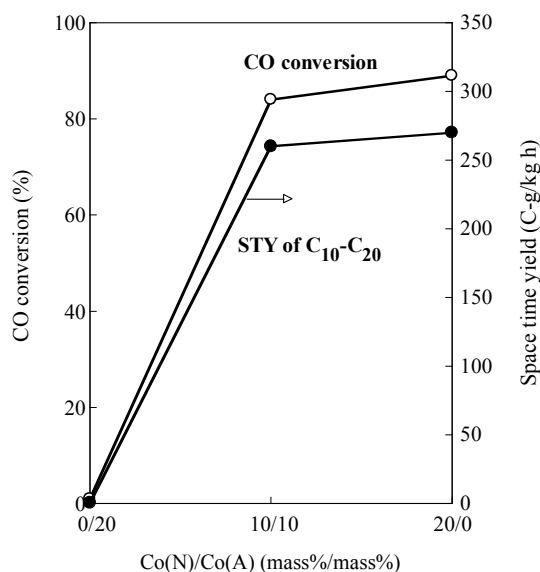


Figure 1. Performances of 20 mass% Co/SBA-15 catalysts

When the effect of W/F on catalytic performance of the Co(20N) was examined by changing only the amount charged into the reactor in the range of 0.1 – 0.5 g, CO conversion after 6 h increased monotonously with increasing W/F, as is expectable, whereas the STY of C₁₀ – C₂₀ paraffin showed a maximal value of 350 C-g/kg h at W/F of 2.4 g h/mol. Under these conditions, the productivity of C₅ – C₂₀ hydrocarbons reached 710 C-g/kg h.

Structural Stability of Co/SBA-15 Catalysts. Catalyst life is one of the key factors for development of the practically feasible Co/SBA-15. In order to obtain some information for this purpose, the structural stability after reaction was investigated.

Figure 2 shows the pore distribution of the Co(20N) catalyst after reaction and subsequent solvent washing. The height of the peak observed around 9 nm decreased to be one third of that of the fresh catalyst before reaction, which resulted in the considerable reduction in pore volume. Almost the same distribution was observed with the Co(10A+10N) used. Such a reduction was caused by the retention of significant amounts of waxy materials inside the mesopores, as mentioned above. In fact, the XRD measurements confirmed the presence of very sharp diffraction lines attributable to higher saturated hydrocarbons, that is, paraffin wax, with the Co(20N) and Co(10A+10N) used. When these samples were air-calcined at 773 K to burn the wax up, the XRD peaks disappeared. As shown in Figure 2, the removal of the wax restored the pore distribution of the re-calcined catalyst to almost the same state as before reaction.

With the XRD profiles for the re-calcined Co(10A+10N) and Co(20N) catalysts, the peaks of Co₃O₄ appeared, and the average crystalline sizes were estimated to be 12 – 13 nm, which were nearly equal to those (9 – 20 nm) for the corresponding fresh catalysts (Table 1). When the TPR runs were carried out, H₂ consumption observed up to 800 K was identified to the reduction of Co₃O₄ to CoO and subsequently to metallic Co. Such TPR profiles were not changed significantly after reaction followed by air calcination, regardless of type of catalyst.

These observations indicate that not only pore structures of the Co(10A+10N) and Co(20N) with high catalytic performances but also the dispersion and reducibility of Co₃O₄ particles are almost unchanged before and after reaction. In other words, the reuse of the Co/SBA-15 catalysts would be possible.

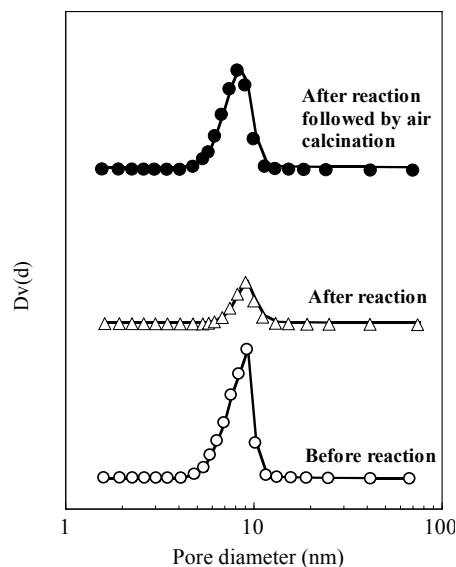


Figure 2. Changes in pore distribution of Co(20N)/SBA-15 catalyst

Conclusions

FT synthesis with Co catalysts supported on mesoporous silica (SBA-15) with average pore diameter of 8.6 nm has been carried out at 503 K and 2.0 MPa for the purpose of producing diesel fuels efficiently. The conclusions are summarized as follows:

- (1) Impregnation of 20 mass% Co with SBA-15, followed by air calcination, decreases pore volume and surface area remarkably, showing that Co particles are held mostly inside the mesopores.
- (2) Co acetate is almost inactive, whereas the catalyst from the nitrate or an equimolar mixture of both compounds is quite active, and CO conversions reach 85 – 90% at a steady state.
- (3) The active catalysts achieve high space time yields of 260 – 270 C-g/kg h for C₁₀ – C₂₀ hydrocarbons as the main fraction of diesel fuels. The yield further increases to 350 C-g/kg h at the optimum value of W/F.
- (4) Pore structures of the Co/SBA-15 catalysts and the dispersion and reducibility of Co species are not changed significantly even after FT synthesis and subsequent air calcination at 773 K.

Acknowledgement. The present work has been supported by Research for the Future Program of Japan Society for the Promotion of Science (JSPS) under the Project “Synthesis of Ecological High Quality Transportation Fuels” (JSPS-RFTF98P01001). The authors gratefully acknowledge Professors Muneyoshi Yamada (Tohoku University) and Kaoru Fujimoto (The University of Kitakyushu) for their helpful suggestions and discussion.

References

- (1) Beck, J. S.; Vartuli, J. C.; Roth, W. J.; Leonowicz, M. E.; Kresge, C. T.; Schmitt, K. D.; Chu, C. T.-W.; Olson, D. H.; Sheppard, E. W.; McCullen, J. B.; Higgins, J. B.; Schlenker, J. L. *J. Am. Chem. Soc.* **1992**, *114*, 10834.
- (2) Zhao, E.; Feng, J.; Huo, Q.; Melosh, N.; Fredrickson, G.; Chmelka, B.; Stucky, G.; *Science* **1998**, *279*, 548.
- (3) Wang, Y.; Takahashi, Y.; Noguchi, M.; Ohtsuka, Y. *Proc., 7th China-Japan Symposium on Coal and C₁ Chemistry* (Hainan Island, China), pp. 65-68 (2001).
- (4) Wang, Y.; Noguchi, M.; Takahashi, Y.; Ohtsuka, Y. *Catal. Today* **2001**, *68*, 3.
- (5) Sun, S.; Tsubaki, N.; Fujimoto, K. *Appl. Catal. A: General* **2000**, *202*, 121.

ZEOLITE-BASED ADSORBENTS FOR DESULFURIZATION OF JET FUEL BY SELECTIVE ADSORPTION

S. Velu, Xiaoliang Ma and Chunshan Song*

Clean Fuels and Catalysis Program, The Energy Institute and
Department of Energy and Geo-Environmental Engineering
The Pennsylvania State University
209 Academic Projects Building, University Park, PA 16802
E-mail: csong@psu.edu

Introduction

Gasoline, jet fuel and diesel are the three major types of transportation fuels. Currently, these fuels contain significant amounts of sulfur, up to 300 ppmw in gasoline, 500 ppmw in diesel and 3000 ppmw in Jet fuel¹. Combustion of these fuels in IC engines emits SO_x, a major air pollutant. Owing to the stringent environmental regulations imposed in recent years, the removal of sulfur compounds from transportation fuel is becoming more and more important issue. In addition, the possibility that these fuels can be reformed catalytically onboard or onsite to produce H₂ for fuel cells to drive automobiles or residential uses in the near future, demands reduction of sulfur content to near-zero level.²

Hydrodesulfurization (HDS) is the conventional method being employed to remove the sulfur compounds. However, this method is incapable of removing some of refractory sulfur compounds present in jet fuels and diesel.¹ Furthermore, the HDS process is operated at high temperature and pressure. Under these conditions, a part of olefines and aromatics contained in the fuels are saturated and as a consequence the octane number decreases substantially.

On the other hand, adsorptive desulfurization is a new challenge to remove sulfur compounds from the transportation fuels, because adsorption would be accomplished relatively at lower temperature and pressure.³ The success in this method, however, depends on the development of highly selective adsorbents, because the commercial adsorbents are not desirable for this application.

Several kinds of adsorbents have been reported for the removal of H₂S from the flue gas, natural gas and coal-derived gas.⁴ However, the development of a selective adsorbent for the removal of organic sulfur compounds from the transportation fuels is still in its infancy. There are only a few reports on the use of transition metals such as Ni, Cu, Co or in some cases noble metals (Pt and Pd) supported on Al₂O₃, SiO₂, ZnO or mixture thereof.¹ These metal and metal oxide components bind organic sulfur compounds, which results in metal sulfide formation. One disadvantage is that they must be used with expensive components (metal or support) in significant quantities. Further, they are relatively more difficult to regenerate for subsequent runs. On the other hand, adsorption by zeolites could offer a powerful means for the development of methods for super purification, as they possess "size-selective" sorption property.

We are exploring SARS (selective adsorption for removing sulfur) process concept in our laboratory. The objective of the present investigation is to explore some selective zeolite-based adsorbents for the removal of organic sulfur compounds from transportation fuels. We present here some of our preliminary results on the desulfurization of JP-8 jet fuel over transition metal ion-exchanged Y-zeolites.

Experimental

Commercially available NH₄ Y-zeolite (Aldrich; SiO₂/Al₂O₃ molar ratio = 5) was ion-exchanged with various transition metal ions using 3 to 5 fold excess amounts of 0.1 M metal nitrates at 80°C for 24 h. After ion-exchange, the zeolite suspension

was filtered, washed with copious amount of deionized water and dried at 80°C overnight and then calcined at 450°C for 6h in air atmosphere employing a temperature ramp of 2°C/min. Adsorption experiments were performed in a batch reactor. A JP-8 jet fuel sample was supplied by the Wright Laboratory of the US Air Force. About 6 g of the JP-8 jet fuel and 1g of the ion-exchanged Zeolite in a 100 ml round-bottom flask were stirred at 80°C for 4-5 h.⁵ The treated jet fuel was then separated from the adsorbent and analyzed by a GC equipped with a pulsed flame photometric detector (PFPD) using benzothiophene as an internal standard.

Results and Discussion

The PFPD gas chromatogram of the JP-8 jet fuel untreated and treated using CeY-zeolite and PdY-zeolite are shown in Figure 1, while the sulfur adsorption data are gathered in Table 1. The major sulfur compounds present in the JP-8 jet fuel are 2,3-DMBT, 2,3,7-TMBT, 2,3,5/6-TMBT with a net sulfur content of 736 ppm. The intensity of these peaks decreases significantly after treatment with ion-exchanged zeolite. Among the adsorbents tested, the Ce-exchanged and Pd-exchanged zeolites exhibit a better sulfur adsorption capacity (50 to 60 %). The HY-zeolite, without a metal also exhibits some sulfur adsorption capacity of about 30 %. On the other hand, the adsorption capacity of Cu-exchanged and Zn-exchanged zeolite is negligibly low under the present experimental conditions.

Table 1 Desulfurization of JP-8 jet fuel over Zeolite-based adsorbents

Adsorbent	Amount of Sulfur removed (Weight %)	Adsorption capacity x 10 ⁴ (g of sulfur / g of adsorbent)
NiY-Zeolite	45	20
CuY-Zeolite	7	3
ZnY-Zeolite	0	0
CeY-Zeolite	60	27
PdY-Zeolite	58	26
HY-Zeolite	29	13

It is also interesting to note from Figure 1 that the relative concentration (peak intensity) of 2,3-DMBT and 2,3,7-TMBT (2,3-DMBT/ 2,3,7-TMBT ratio) is around 2.4 in the untreated jet fuel as well as in the fuel treated with CeY-zeolite. Similar results were also observed in the chromatograms of fuel treated with NiY-zeolite and HY-zeolite. On the other hand, this ratio is close to unity in the fuel treated with PdY-zeolite. This indicates that the PdY-zeolite is more selective towards 2,3-DMBT. The difference in the selectivity of sulfur adsorption between Ce-exchanged and Pd-exchanged zeolites indicates that the mode of adsorption of sulfur compounds over PdY-zeolite is probably different from that of others. The methyl group in the 7-position of the 2,3,7-TMBT would cause a steric hindrance thereby inhibiting the interaction between the sulfur atom and the adsorbent. A systematic study is currently underway in order to understand the mechanism of sulfur adsorption over zeolite-based adsorbents. The study will also be extended to gasoline and diesel fuels and detailed results will be presented.

Conclusions

Zeolite Y exchanged with Ce and Pd exhibits a higher sulfur adsorption capacity compared to other transition metal ion -exchanged zeolites in the desulfurization of Jet fuel containing around 736 ppm of sulfur. The PdY-zeolite exhibits a higher selectivity for the adsorption of 2,3-DMBT. As Ce is less expensive

than Pd, the Ce-exchanged zeolite may be considered a more promising candidate for deep desulfurization of transportation fuels.

Acknowledgments. This work was supported in part by US Department of Energy and in part by the US Department of Defense. We gratefully acknowledge the financial support.

References

- 1 Song, C, and Ma, X, *Appl.Catal.B Environ.* (Submitted); Song, C. Am. Chem. Soc. Div. Fuel Chem. Prepr., **2001**, 46 (1), 8.
- 2 Brown, L.F., *Intl.J.Hydrogen Energy*, **2001**, 26, 381.
- 3 Yang, R.T., Takahashi, A., and Yang, F.H., *Ind.Eng.Chem.Res.* **2001**, 40, 6236.
- 4 Slimane, R.B., and Abbsasian, J. *Ind.Eng.Chem.Res.* **2000**, 39, 1338.
- 5 Kulprathipanja, S., Nemeth, L.T. and Holmgren, J.S. **1998**, *U.S.Patent*: 5,807,475.

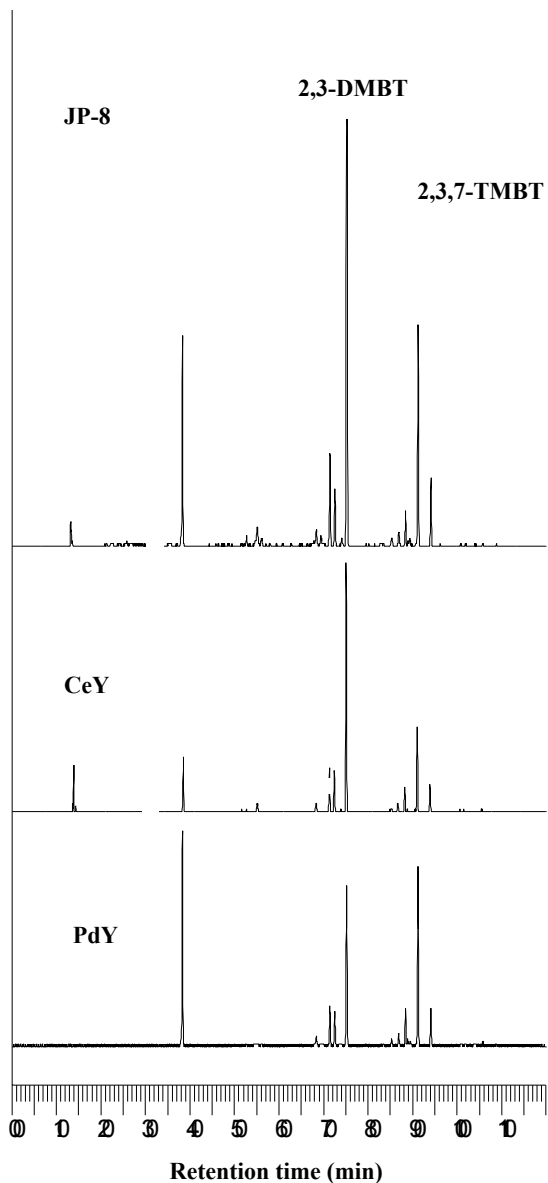


Figure 1 PFPD Chromatograms of untreated JP-8 jet fuel and that treated with CeY-, and PdY-zeolites